Dissertation zur Erlangung des Doktorgrades
der Fakultät für Chemie und Pharmazie
der Ludwig-Maximilians-Universität München

Virus-Host Interactions: Novel Actions in an Ancient Battle

Cathleen Holze

aus
Potsdam, Deutschland

2016

Erklärung

Diese Dissertation wurde im Sinne von § 7 der Promotionsordnung vom 28. November 2011 von Herrn Professor Dr. Matthias Mann betreut.

Eidesstattliche Versicherung

Diese Dissertation wurde eigenständig und ohne unerlaubte Hilfe erarbeitet.

München, den 02.05.2016

Cathleen Holze

Dissertation eingereicht am 03.05.2016

1. Gutachter: Prof. Dr. Matthias Mann

2. Gutachter: Prof. Dr. Karl-Peter Hopfner

Mündliche Prüfung am 20.06.2016

We keep moving forward,
opening up new doors and doing new things,
because we're curious...
and curiosity keeps leading us down new paths.

Walter Elias 'Walt' Disney

(1901-1966, American entrepreneur, film producer, voice actor, and animator)

Abstract

Virus-host interactions play a pivotal role within the ancient battle between viruses and host. Viruses modulate a wide range of host signaling pathways, such as cell survival and programmed cell death. Both pathways play prominent roles as part of the innate immune system. Thus, the regulation of cell survival and programmed cell death is essential during antiviral activities. Several cell death pathways are well studied, including their inducers and involved proteins. The induction of reactive oxygen species (ROS) by viruses leads to cell death as well, but detailed mechanisms are widely unknown.

In the main project of my thesis I describe the identification of a new programmed cell death pathway, which is independent of caspases and induced by ROS. This pathway includes the cytoplasmic ROS sensor KEAP1, the mitochondrial phosphatase PGAM5 and the mitochondrial cell death execution protein AIFM1. Further analysis revealed that KEAP1 releases PGAM5 upon stimulation with high amounts of ROS. Subsequently, PGAM5 dephosphorylates AIFM1 at position serine 116. Besides its role in this cell death pathway, KEAP1 is known to induce cell survival by releasing NRF2. This would highlight the role of KEAP1 as a switch between cell survival and cell death in response to virus induced ROS. All proteins involved in this pathway are targeted by viral proteins, belonging to different viral classes, emphasizing the co-evolution of this cell death pathway and these viral proteins. I applied affinity purification coupled to mass spectrometry as well as functional assays to identify and characterize this pathway. In conclusion, the innate immune system requires control of ROS to execute cell survival and cell death pathways by which the innate immune system copes with viral infections.

In the two additional projects of my thesis as well concerning virus-host interactions I contributed to a large story that investigated strategies of viral perturbations of the host and interactions of viral RNA with host proteins.

Contents

Abbreviations

2'-5'-OAS 2'-5'-Oligoadenylate synthetase

5'PPP 5'-triphosphorylated

AE-MS affinity enrichment coupled to MS

AIFM1 Apoptosis-inducing factor, mitochondrial 1

AIM2 Absent in melanoma 2

ALR AIM2-like receptor

AP-1 Activator protein 1

AP-MS affinity purification coupled to MS

Apaf1 Apoptotis protease-activating factor 1

ARE antioxidant response element

BAD BCL-2-associated agonist of cell death

BAX BCL-2 associated X protein

BCL-2 B-cell lymphoma-2

BH3 BCL-2 homology 3

BID BH3-interacting domain death agonist

CARD caspase activation and recruitment domain

cGAMP cyclic GMP-AMP

cGAS cGAMP synthetase

CICD caspase-independent cell death

CID collision induced dissociation

CLR C-type lectin receptor

CREB cAMP response element-binding protein

DAI DNA-dependent activator of IFN regulatory factor

DAMP damage associated molecular pattern

DCs dendritic cells

ds double strand

eIF Eukaryotic translation initiation factor

ER endoplasmatic reticulum

ESI electrospray ionization

ETD electron transfer dissociation

EThcD electron-transfer and higher-energy collision dissociation

FADD Fas-associated death domain

$FADH_2$ reduced flavin-adenin-dinucleotid

FluAV Influenza A virus

GAS IFNγ activated sequence

GSH Gluthation

H_2O_2 hydrogen peroxide

HCD higher-energy collision dissociation

HCV Hepatitis C virus

HPLC high pressure liquid chromatography

HSV-1 Herpes simplex virus 1

IκB Inhibitor of κB

ICAM Intercellular adhesion molecule

IFI16 IFNγ inducible protein 16

IFIT IFN-induced proteins with tetratricopeptide repeats

IFITM IFN-induced transmembrane protein

IFN Interferon

IFNAR IFNα receptor

IFNGR IFNγ receptor

IKK Inhibitor of NF-κB kinase

IL Interleukin

IMM inner mitochondrial membrane

IMS intermembrane space

IRAK IL-1 receptor-associated kinase

IRES internal ribosome entry site

IRF IFN regulatory factor

ISG IFN stimulated gene

ISGF IFN stimulated gene factor

ITAF IRES trans-acting factor

JAK1 Janus kinase 1

KEAP1 Kelch-like ECH-associated protein 1

KSHV Kaposi's sarcoma-associated herpesvirus

LaCV La Crosse virus

LFQ intensity based quantification

LGP2 Laboratory of genetics and physiology 2

LPS lipopolysaccharides

LRR leucine rich repeats

M mitochondrial matrix

m/z mass to charge ratio

MALDI matrix assisted laser desorption ionization

MAM mitochondria-associated membranes

MAPK Mitogen-activated protein kinase

MAVS Mitochondrial-associated adaptor protein

MDA5 Melanoma differentiation associated gene 5

MLKL Mixed lineage kinase domain-like protein

MOMP mitochondrial outer membrane permeabilization

MS mass spectrometry

mtDNA mitochondrial DNA

Mx Myxovirus resistance

MyD88 Myeloid differentiation primary response protein

NADH reduced nicotinamid-adenin-dinucleotid

NEMO NF-κB essential modulator

NF-κB Nuclear factor kappa B

NLR Nod-like receptor

NRF2 Nuclear factor (erythroid-derived 2)-like 2

NS Non-structural

OMM outer mitochondrial membrane

OxPhos oxidative phosphorylation

PAMP pathogen associated molecular pattern

PAR Poly(ADP-ribose)

PARP1 Poly(ADP-ribose) polymerase 1

PCD programmed cell death

PIAS Protein inhibitor of activated STAT

PKR RNA-dependent protein kinase

PRR pattern recognition receptor

PTM post-translational modification

RD repressor domain

RIG-I Retinoic acid-inducible gene 1

RIPK Receptor-interacting protein kinase

RLR RIG-I-like receptor

RNA Pol II RNA Polymerase II

ROS reactive oxygen species

Rota Rotavirus A

RSV Respiratory syncytial virus

SARM Sterile alpha and TIR motif-containing protein 1

SILAC Stable Isotope Labeling by Amino Acids in Cell Culture

SOCS Suppressor of cytokine signaling

SOD Superoxide anion dismutase

ss single strand

STAT Signal transducer and activator of transcription

STING Stimulator of interferon genes protein

TBK1 TANK-binding kinase

TCA tricarboxylic acid

TICAM TIR domain-containing adapter molecule

TIM Translocase of the inner membrane

TIR Toll/interleukin-1 receptor

TIRAP Toll/interleukin-1 receptor domain-containing adapter protein

TLR Toll-like receptor

TNF Tumor necrosis factor

TOM Translocase of the outer membrane

TRAF TNF receptor-associated factor

TRIM Tripartite-motif

TYK2 Tyrosine kinase 2

VDAC1 Voltage-dependent anion channel 1

XIAP X-linked inhibitor-of-apoptosis protein

1 Introduction

Infections of hosts occur regularly, but only few result in pathogenic disease. Due to the host's defense system, particular the innate and adaptive immune system, most pathogens can be kept in check. Additionally, scientific research on pharmaceutical remedies already allows treating and eliminating of many pathogens, especially fungi and bacteria. However, compared to fungi and bacteria, there are only few pharmaceutical treatments to eliminate viral pathogens from the host. Particularly persistent virus infections are difficult to treat. In case of virus infections the host has to fight the battle against pathogens, which frequently find ways to escape detection and elimination by the immune system. Therefore, the immune system developed more radical ways to eliminate intruders, such as inducing death of infected cells. In this context mitochondria, essential cellular organelles, play an important role in the connection of the immune system with cell death. To support the immune system and mitochondria in this task, it is our keen interest to elucidate cellular mechanisms that are involved in virus sensing and elimination. These new findings will support the discovery of new approaches for treatments against viral pathogens. In the following four chapters I will introduce

(1) the innate immune system, as essential part of the host's antiviral defense

(2) mitochondria, as essential organelle of the cell to regulate antiviral immunity

(3) viruses, hijacking pathogens that need to be eliminated by the immune system

(4) mass spectrometry, as meaningful high throughput method for analysis of cellular system and mechanisms

The first chapter 'the immune system' discusses especially the innate immune system with focus on the human immune system. I describe the components as well as signaling and execution processes as steps of the innate immune system, particularly in the context of virus infections. The following chapter describes functions of mitochondria being important for the immune defense, such as reactive oxygen species (ROS) synthesis and signaling as well as cell death mechanisms. The third chapter deals mainly with the mechanisms how viral pathogens use the cell for themselves and avoid detection by the innate immune system. The last chapter focuses on mass spectrometry as method to study the innate immune system and more generally focuses on the use of mass spectrometry in the field of protein-protein interaction studies to elucidate signaling pathways and virus-protein interactions.

1.1 The innate immune system

The immune system of vertebrates is divided in two parts: the innate immune system as a first line of defense against invading pathogens and the adaptive immune system which enable to long lasting memory and protection from re-infection by similar pathogens. Both systems consist of cells, molecules and processes that link these molecular machines and cells in organisms to protect against invading pathogens (figure 1.1). The innate immune system encompasses non-specific physical barriers such as mucus and cornea, as well as a set of germ-line encoded receptors, which are partly expressed in a cell-type specific manner. Particularly cells of the innate immune system, including macrophages and dendritic cells (DCs), express a wide repertoire of immune receptors [1, 2]. The adaptive immune system of humans includes T- and B-cells, which have the ability to

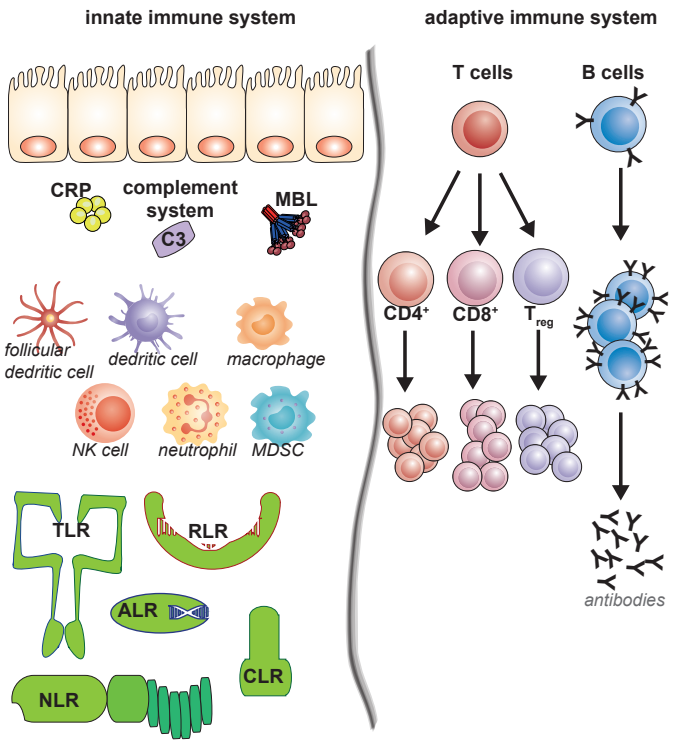

Figure 1.1: Comparison of innate and adaptive immune system (adapted from [4]). The innate immune system as first line of defense composes of the endothelia barrier as first defense, soluble factors (e.g. CRP, complement system, MBL) in the blood and a subset of germ line encoded receptors mainly localized on innate immune cells. These receptors are classified in five groups: TLR, NLR, RLR, ALR and CLR. The adaptive immune system as long lasting defense is activated some days after the innate immune system. It composes mainly of two cell types: T cells and B cells. T-cells differentiate depending on the innate immune system signals to various T cell types having regulatory or helping functions. B cells instead produce antibodies from an antibody stock continuously generated by recombination.

generate B- and T-cell receptors by somatic recombination, allowing generation of receptors with almost unlimited specificity [3].

Despite its complexity, the immune system has to distinguish correctly between molecules derived from pathogens (non-self) and healthy tissue (self). Inability to correctly identify infected vs. non infected cells can lead to detrimental side effects such as autoimmune diseases [5]. As the focus of this thesis is to contribute to our understanding of basic function of the innate immune system, the following chapter focuses on three functional parts of the innate immune system. Firstly, the activation of the innate immune system by invading pathogens; secondly, the intra- and intercellular signaling that alerts the organismal immune system and thirdly, the execution of the immune response to perturb the pathogen. A part of these final execution processes is the activation of the adaptive immune system, which involves inflammatory processes. Here it is of critical importance that organisms control these inflammatory processes since malfunction can culminate in detrimental effects such as immunopathology or insufficient clearance of pathogens.

1.1.1 Pattern recognition receptors - Activation of the innate immune system

The innate immune system is widely known as the first line of defense and reacts quickly to infections or tissue damage [6]. Historically, it was thought to act in an unspecific manner on pathogens [1]. However, more recent development revealed a higher specificity than expected, mostly due to the discovery of a wide range of pattern recognition receptors (PRRs) (figure 1.1) [1]. There are two kinds of PRRs: endocytic and signaling PRRs [7]. Endocytic PRRs are either membrane bound on phagocytes, called scavenging receptors, or distributed freely in extracellular compartments, called soluble receptors [6]. Scavenging receptors enable direct sensing and phagocytosis of

detected invading microorganisms [6]. Soluble receptors sequester molecules of the complement system, resulting as well in destruction of invading pathogens [6]. This section focuses on signaling PRRs, which activate pathways resulting in transcriptional changes, subsequent release of signaling molecules, such as cytokines, and activation of the innate and adaptive immune system.

Activation of the innate immune system occurs after detection of a molecular signature (called 'pattern') that is associated with a pathogen or injury [8]. Patterns derived from pathogens, such as bacteria, yeast, viruses, parasites, worms are called pathogen associated molecular patterns (PAMPs) [8]. Patterns of injuries and non-pathogenic stimuli are named damage associated molecular patterns (DAMPs) [9]. DAMPs are in many cases proteins or nucleic acids which are present in non-physiological cellular compartments (e.g. nucleic acids in endosomes) or chemically modified, for instance through oxidation in the extracellular milieu [9]. Many diverse PAMPs have been described and include bacteria cell wall components, such as lipopolysaccharides (LPS), carbohydrate structures and proteins in various modified forms [8]. Furthermore, non-processed viral nucleic acids can serve as PAMPs [10]. Binding of PAMPs to PRRs activates the innate immune system and sets off cascades of events that culminate in the 'arming' of the organism against invading pathogens [10]. Therefore, pattern recognition is a key function that is relatively well studied.

Currently, five families of PRRs are known: membrane-bound Toll-like receptors (TLRs) and C-type lectin receptors (CLRs) and cytoplasmic Nod-like receptors (NLRs), RIG-I-like receptors (RLRs) and recently discovered AIM2-like receptors (ALRs) [11, 12]. After detection of pathogens, PRRs initiate various PRR-specific signaling cascades resulting in production of Interferons (IFNs), pro-inflammatory cytokines (e.g. Tumor necrosis factor (TNF), Interleukin (IL)-1β, IL6) and chemokines (e.g. CXCL, CCL) [12]. Furthermore, PRR activation can lead to modulation of cellular machineries (e.g. modulation of translation) and induction of cell death [13]. The next sections focus only on TLRs, RLRs and ALRs as they are involved in virus sensing.

Toll-like receptors

TLRs were the first PRRs being discovered. A protein named Toll was first identified in Drosophila [14], and eleven years later the conserved signaling function in immunity was revealed in Drosophila, plants and humans [15, 16]. Later, ten other proteins of the human TLR family were identified. TLRs are transmembrane proteins with extracellular leucine rich repeats (LRR), forming horseshoe shape structures as binding sites for PAMPs, a linker region (LR), for subcellular localization and an intracellular Toll/interleukin-1 receptors (TIR) domain, for downstream signaling [17]. Except of four TLRs (3, 7, 8 and 9), which are located to the endosome, all TLRs are plasma membrane bound [18]. The TLRs and their activating PAMPs are displayed in (table 1). Focusing on viruses, DNA as well as single (ss) and double (ds) stranded RNAs, are detected by TLRs during the virus infection process in endosomal compartments [17]. After PAMP binding in most cases dimerization of TLRs occur which results in recruitment of adaptor proteins to the TIR domain and subsequent signaling [19]. Stimulation of TLRs leads via a signaling cascade to activation and nuclear translocation of IFN regulatory factors (IRFs), Nuclear factor κB (NF-κB) and Activator protein-1 (AP-1), which regulate transcription of IFNs, pro-inflammatory cytokines (TNFα, IL-1β, IL-6) and effector cytokines to activate the adaptive immune system [1].

RIG-I-like receptors

Compared to TLRs, which sample the extracellular environment and endocytosed material, several viruses enter the cytosol without being detected by these receptors. A distinct set of receptors,

Table 1: **Ligands of TLRs [17, 20–22])**

Receptors	Ligand	Origin of ligand
TLR1	triacylated lipopeptides	Bacteria and mycobacteria
TLR2	Lipoprotein/ Lipopeptides	Various pathogens
	Peptidoglycan (PGN)	Gram-positive bacteria
	Lipoteichoic acid	Gram-positive bacteria
	Lipoarabinomannan	Mycobacteria
	Phospholipomannan	Fungi
	Glycoinositolphospholipids (GPI anchor)	Trypanosoma cruzi
	Zymosan	Fungi
	Heat-shock protein 70	Host
	envelope proteins	Measles virus, hCMV, HSV-1
TLR3	double-stranded RNA	Viruses
TLR4	Lipopolysaccharid (LPS)	Gram-negative bacteria
	Fusion protein	RSV
	Heat-shock protein 60 and 70	Host
	Type II repeat extra domain A of fibronectin	Host
	Oligosaccharides of hyaluronic acid	Host
	Polysaccharide fragments of heparin sulphate	Host
	Fibrinogen	Host
TLR5	Flagellin	Bacteria
TLR6	diacylated lipopeptides	Mycoplasma
TLR7	single-stranded RNA guanine nucleoside analog[1]	Viruses
TLR8	single-stranded RNA	Viruses
TLR9	CpG-containing DNA	Bacteria and viruses
TLR10	N.D.	N.D.

[1] 7-Thia-8-oxo-guanosine, 7-deazaguanosine, and related guanosine analogs

named RIG-I-like receptors (RLRs), were identified which screen the cytosol and also nuclear environment for virus-derived nucleic acids in order to stimulate the innate inmmune system [23]. RLRs are cytoplasmic PRRs and have three known members: Retinoic acid-inducible gene 1 (RIG-I), Melanoma differentiation associated gene 5 (MDA5) and Laboratory of genetics and physiology 2 (LGP2) [23]. RLRs can contain tandem N-terminal caspase activation and recruitment domains (CARDs), Asp-Glu-X-His/Asp (DExD/H) helicase domain and *C*-terminal repressor domain (RD) (figure 1.2) [23].

Although RIG-I and MDA5 can recognize RNA viruses, they differ in the type of virus they sense. Whereas RIG-I detects paramyxovirus, influenza virus and Japanese encephalitis virus, MDA5 is required for picornavirus detection [24]. RIG-I has been shown to bind dsRNA bearing a 5'-triphosphorylated (5'PPP) overhang or diphosphates [25–28]. MDA5 interacts with dsRNA which exceeds 100 nt [29] and LGP2 binds diverse dsRNAs [30, 31] (table 2). The RD seems to be the do-

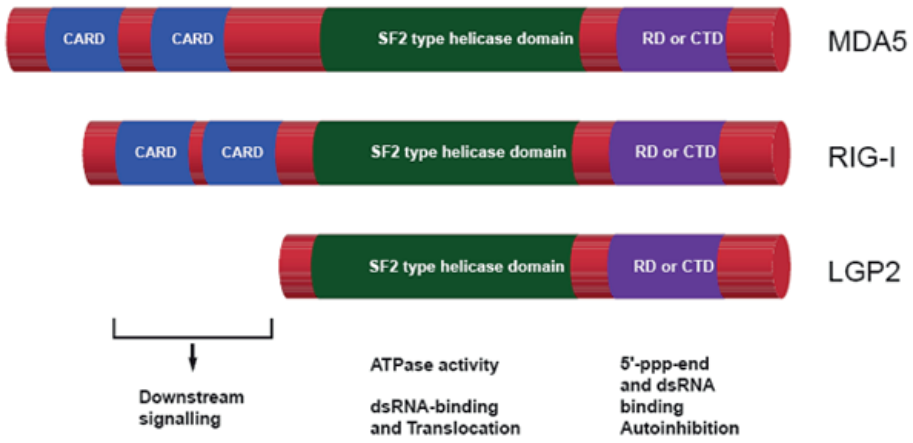

Figure 1.2: Domain structure of RLRs [23].
All three RLRs compose of a SF2 type helicase domain and a RD or CTD. Only RIG-I and MDA5 can signal further downstream via their tandem CARD.

main responsible for distinction between various ligands for these receptors, as the key residue in the RD differs in all three receptors [32]. These types of RNA are usually not present in the cytosol but produced in vast amounts by virus replication. Further described signaling mechanisms focus on RIG-I. By interaction of the RD with triphosphates, conformational changes of RIG-I occur, resulting in tetramer formation [33]. This releases the CARDs from the DExD/H helicase domain. Now other RNA structures, such as dsRNA, can bind within the DExD/H helicase domain and finally activate RIG-I [25, 32, 34]. Upon activation, RIG-I initiates NF-κB and IRF3 and -7 translocation to the nucleus, resulting in expression of type I IFN and subsequent activation of IFN stimulated genes (ISGs), also called IFN regulated genes (IRG) [34, 35]. LGP2 seems to control RIG-I and MDA5 by different mechanisms [36]. This is probably due to LGP2 lacking CARDs which are critical for downstream signaling [37]. LGP2 was proposed to be a negative feedback regulator for RIG-I [36]. The LGP2 RD has the highest dsRNA binding affinity of all three receptors and could thus compete for binding to downregulate the signal [38]. This function could be upstream of RIG-I and MDA5 such as facilitating ligand detection [36]. Additionally, LGP2 has been suggested to participate in anti-microbial signaling of DNA viruses and cytosolic DNA [39].

Table 2: Ligands of RLRs [10, 21]

Receptors	Ligand	Origin of ligand
RIG-I	5'PPP ssRNA (base pairing) short dsRNA sequences specific to viral genomes (poly-U region)	Viruses
MDA5	long dsRNA with >100 nt long poly I:C	Viruses
LGP2[1]	dsRNA	Viruses

[1] LGP2 an inhibitor and modifier of RIG-I and MDA5, respectively

Apart from cytosolic virus-derived RNA also cytosolic DNA is a signature for infection with a pathogen. Thus devoted receptors that constantly assay the cytoplasm for presence of DNA have evolved and are a critical part of the innate immune system.

AIM2-like receptors

The first cytoplasmic DNA sensor that was identified is called Absent in melanoma 2 (AIM2). AIM2 can bind DNA and activates the inflammasome, a macromolecular complex that has the ability to mature pro-cytokines into their biologically active versions. AIM2 was thus coining a new family of receptors called AIM2-like receptors (ALRs). This family now comprises various cytoplasmic and nuclear receptors (table 3) that are involved in cytokine induction as well as inflammasome activation. In 2006 Stetson proposed a TLR9 a cytosolic DNA sensing pathway that is independent of TLR9 [40]. A year later DNA-dependent activator of IFN regulatory factors (DAI) was the first proposed cytosolic DNA sensor activating IRF-3 and IRF-7 [41]. However, even at this time it was already evident that it cannot be the only sensor and that DNA sensing in the cytoplasm is much more complex than sensing of specific RNAs [42]. Indeed, several other DNA receptors where identified, among them absent in melanoma 2 (AIM2), IFN gamma inducible protein 16 (IFI16) and cGAMP synthetase (cGAS) [11, 43–47]. The latter three receptors are at the moment the most widely accepted PRRs sensing DNA [12, 48]. AIM2 and IFI16 compose of two domains: two DNA-binding HIN-200 domains and a protein-protein interaction Pyrin domain [12]. AIM2 is a cytosolic protein and initiates formation of an inflammasome [44], resulting in cytokine maturation and cell death. IFI16 is a nuclear localized protein, which shuttles to cytosol [44, 46], where it has been reported to result in both, inflammasome and IFN induction [11, 46]. IFI16 mainly recognizes foreign DNA from viruses replicating in the nucleus, such as viruses of the herpesvirus family (HSV-1, KSHV and EBV) [11, 46, 49]. Additionally, IFI16 requires association of Breast cancer type 1 susceptibility protein (BRCA1) (a DNA damage indicator) to distinguish between self and non-self DNA [50]. cGAS is a cytosolic protein, which signals compared to the other two receptors via a second messenger, called cyclic GMP-AMP (cGAMP) [51–53]. cGAS leads to IFN and cytokine induction, upon detection of dsDNA and RNA:DNA hybrids [51, 53, 54].

Table 3: Ligands and localizations of ALRs [21, 55]

Receptors	Ligand	Localization	Origin of ligand
AIM2	dsDNA	cytoplasmic	Viruses
DAI	DNA sequences specific to viral genomes (poly-U region)	cytoplasmic	Viruses
IFI16	dsDNA oligonucleotides poly(dA-dT) poly(dG-dC)	nuclear	Viruses
cGAS	DNA poly(dA-dT) poly(dG-dC)	cytoplasmic	Viruses

After detection of pathogens by PRRs the innate immune system is activated. The signals which are transmitted vary based on the PRR which is activated as well as on the activation strength. Many of

the receptors result in activation of the NF-κB signaling pathway and in induction of IFN expression. The next chapter elucidates details of these signaling pathways, roles of second messengers in signaling and of organelles as signaling hubs.

1.1.2 Signaling pathways of the innate immune system

After activation of PRRs, they mostly assemble to large signaling complexes including adaptor proteins. These complexes activate signaling cascades, which subsequently activate transcription factors. This results in expression of IFNs, cytokines and chemokines, which lead to expression or activation of execution proteins, leukocytes and is needed for the full activation of the adaptive immune system. The signaling cascades differ between the different receptors (or receptor classes). TLRs for example signal through distinct proteins, namely Myeloid differentiation primary response protein (MyD88) and/or TIR domain-containing adapter molecule 1 (TICAM1, or TRIF). Signaling downstream of RLRs and ALRs involves proteins that are physically linked to organelles, such as mitochondria, peroxisomes, mitochondria-associated membranes (MAM) and endoplasmic reticulum (ER) (second part of this section) [56] and second messengers that have to be bound by adaptor proteins which further transmit the signal. Thus, the before mentioned receptors utilize these diverse pathways which eventually results in similar but also diverse transcriptional responses that are translate in distinct outcomes. Importantly, the receptors and their downstream pathways also cross talk with each other to enhance and specify the immune answer [57].

TLR3 and TLR7 signaling starting at endosomes

TLRs signal through their intracellular TIR domain. TLRs dimerize after binding of appropriate PAMPs to the extracellular/ endosomal LRR domain, which leads to a conformational change of the TIR domain of some TLRs, such as TLR9 [58]. Subsequently, adaptor proteins, possessing as well a TIR domain, bind to the TLR's TIR domain. Several adaptor proteins are known to be involved in TLR signaling: MyD88, Toll/interleukin-1 receptor domain-containing adapter protein (TIRAP, or MAL) , TICAM1, TICAM2 (or TRAM) and Sterile alpha and TIR motif-containing protein 1 (SARM) [59]. Except of SARM, all proteins mediate downstream signaling. SARM has a TIR domain but it has been shown to block the activity of TICAM1, but not of MyD88 [60, 61]. All TLRs, except TLR3, bind MyD88 or a complex with MyD88 and TIRAP [59]. After adaptor protein activation, kinases are bound and activated. These kinases initiated gene expression by phosphorylation of distinct transcription factors, including NF-κB, IRF3, IRF5 and IRF7 [62]. These transcription factors translocate to the nucleus and regulate expression of antiviral and pro-inflammatory genes.

The following two pathways describe TLR3 and TLR7 signaling as examples for the two distinct pathways involved in recognition of viral dsRNA or ssRNA, respectively (figure 1.3). The adaptor proteins involved in TLR3 and TLR7 signaling are TICAM1 and MyD88, respectively. Compared to other TLRs, the endosomal TLRs (3, 7, 8, 9) are cleaved at the ectodomain in the endolysosomal compartment before activation [63, 64]. This is essential to avoid recognition of self while regular protein processing at the ER [65]. However, this is controversially discussed.

TLR3 signals only through the adaptor protein TRIF [66, 67]. TLR3 binding to dsRNA results in phosphorylation of several tyrosine residues by protein tyrosine kinases, namely Epidermal growth factor receptor (EGFR) and Src [68]. TRIF oligomerizes upon binding to phosphorylated TLR3 and subsequently distributes the signal to three different pathways: IFN induction, cytokine induction

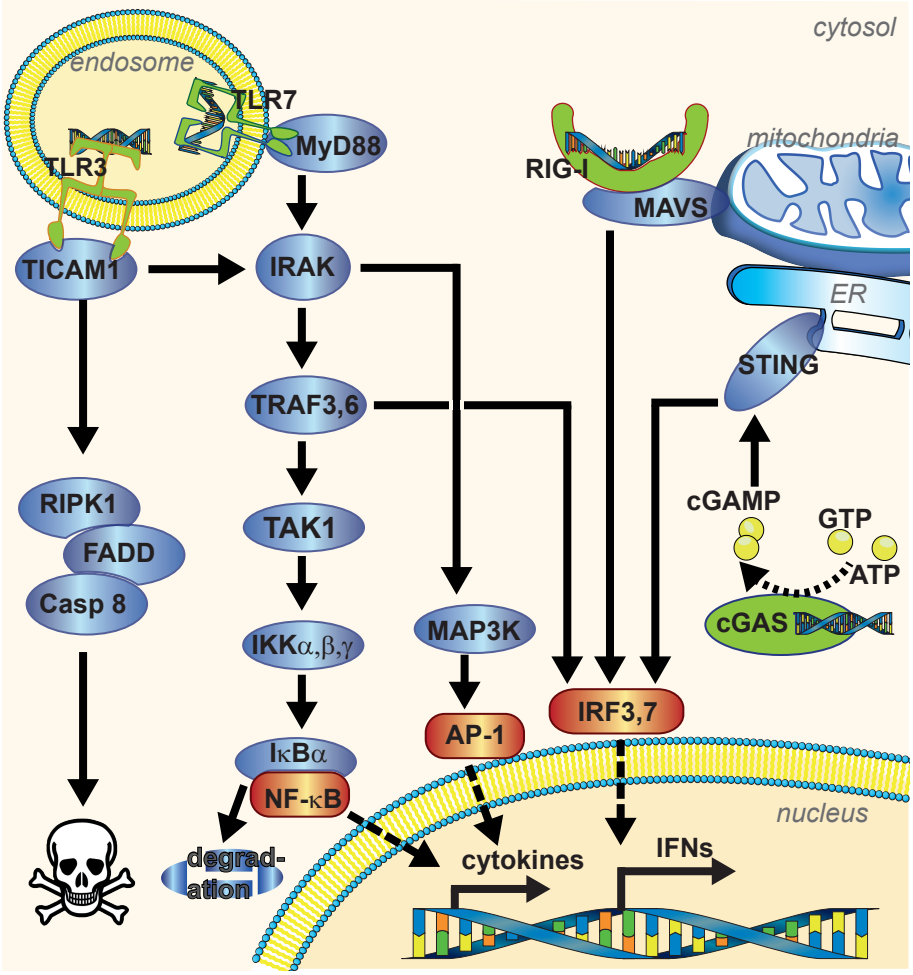

Figure 1.3: Downstream signaling of PRRs upon viral infection to activate gene expression.
The schema shows exemplarily PRRs recognizing viral nucleic acids: endosomal TLR3 and 7, RIG-I and cGAS as examples for TLRs, RLRs and ALRs, respectively.

and cell death induction. To induce IFN expression, TRIF employs TNF receptor-associated factor 3 (TRAF3) [69]. TRAF3 binds Inhibitor of NF-κB kinase (IKK)ε, which subsequently either recruits TANK-binding kinase 1 (TBK1) or IL-1 receptor-associated kinase 1 (IRAK1) for phosphorylation and thereby activation of IRF3 or IRF7, respectively [70–72]. Both transcription factors induce type I IFN. IRF3 is responsible for IFN-β gene regulation [35, 73, 74]. For induction of cytokine expression, TRIF employs TRAF6 [75]. TRAF6 engagement leads to binding of Mitogen-activated protein kinase kinase kinase 7 (MAP3K7 or TAK1), TGF-beta-activated kinase 1, MAP3K7-binding protein 2 (TAB2) and dsRNA-activated protein kinase (PKR) [76]. Subsequently, this whole complex is released to the cytosol and activates Mitogen-activated protein kinase (MAPK) pathways and the IKK complex. Both pathways lead to activation of transcription factors, such as cAMP response element-binding protein (CREB), AP-1 and NF-κB [72]. NF-κB, which is phosphorylated by various kinases, translocates upon dimerization into the nucleus and activates gene transcription of pro-inflammatory cytokines, such as IL-1β, IL-6 and TNFα, as well as of IFNγ [77, 78]. NF-κB transcription factors are a family of five different proteins: NFκB2 p52/p100, NF-κB1 p50/p105, c-Rel, RelA/p65, and RelB. To act as transcription factors they dimerize and initiate transcription of genes

involved in a broad spectrum of biological processes, among them innate and adaptive immunity, inflammation, stress response [1]. To induce cell death, TRIF binds to Receptor-interacting protein kinase 1 (RIPK1) [79]. Hereby, RIPK1 recruits FAS-associated death domain (FADD), which interacts with caspase-8 and subsequently activates caspase-8-dependent apoptosis [79]. However, recent studies have shown that RIPK1 can also induce caspase-8 dependent apoptosis without FADD [80]. Further, RIPK1 can induce necroptosis, a caspase-independent cell death pathway (see chapter 1.2.2) [81]. TLR3 signaling can be blocked by SARM and Disintegrin and metalloproteinase domain-containing protein 15 (ADAM-15); both impair binding to TRIF by their own TIR domain [60, 82].

TLR7 signals via adaptor protein MyD88. After binding to TLR7, MyD88 interacts with IRAK1 and 4 via their death domain (DD) [59]. Subsequently, TRAF6 binds this complex. As mentioned above, TRAF6 activates the IKK complex and MAPK pathway. TRAF6 ubiquitinylates IKKβ and subsequently phosphorylates inhibitor of κB (IκB) proteins. This phosphorylation leads to poly-ubiquitinylation and proteasomal degradation of these inhibiting proteins releasing the transcription factor NF-κB. The MAPK pathway involves a cascade of MAP kinases [83]. First, MAP3K7 phosphorylates MAP2K this kinase further phosphorylates MAPK which can be one of these three kinases: ERK, JNK or p38. The final MAPK subsequently phosphorylates and activates the transcription factors AP-1 (all three MAPK) and CREB (only by p38) [84, 85].

RIG-I signaling via mitochondria signaling hub

Cytosolic recognition of viral RNA is accomplished by RLRs. The described signaling pathway in the following section elucidates the downstream signaling of RIG-I after binding viral RNA (figure 1.3). After ligand binding and the before full activation, Tripartite motif protein (TRIM)25 binds to the first CARD of RIG-I [86]. Subsequently, TRIM25 ubiquitinylates the second CARD of RIG-I [86]. The ubiquitinylated RIG-I interacts with 14-3-3ε protein to form a 'RIG-I translocon' complex, consisting of RIG-I, TRIM25 and 14-3-3ε protein [87]. This complex is guided by 14-3-3ε to mitochondria and associated structures. Here, RIG-I binds to mitochondrial associated adaptor protein (MAVS), also called IPS-1, VISA and CARDIF [88–91]. MAVS is located at the outer mitochondrial membrane, peroxisome or MAM [88, 92, 93]. MAVS has an *N*-terminal CARD, which interacts with the CARDs of RIG-I. This process initiates polymerization of MAVS via its transmembrane domain [94, 95]. Further, adaptor proteins of the TRAF family, including TRAF3, TRAF5 and TRAF6 [94, 96–100], are recruited to MAVS filament and ubiquitinylate MAVS at Lys63. This ubiquitinylation results in binding of NF-κB essential modulator (NEMO) [101]. NEMO is an adaptor protein which can recruit proteins leading to IFN production as well as proteins leading to pro-inflammatory cytokine induction [101]. To induce IFN NEMO binds TBK1. After formation of this NEMO-TBK1 complex, MAVS is ubiquitinylated by TRIM25 resulting in degradation of MAVS. Without MAVS the NEMO-TBK1 complex is released to the cytosol where TBK1 phosphorylates IRF3 which dimerizes and translocates to the nucleus activating IFN transcription [102]. To induce pro-inflammatory cytokines, NEMO recruits IKK, which results in IκB degradation and release of NF-κB [88]. Additionally to these pro-survival pathways, apoptosis, a cell death pathway (chapter 1.2.2), induction is described for MAVS [103]. This is supported by the finding that MAVS activates caspases, cellular proteases involved in programmed cell death, which subsequently cleave MAVS [104–106]. Additionally to the activation of caspases, MAVS influences the ubiquitinylation of Voltage-dependent anion channel 1 (VDAC1). Upon ubiquitinylation VDAC1 is degraded, resulting in decreased outer mitochondrial membrane potential and subsequently cell death [107].

cGAS signaling by generation of cGAMP as second messenger

Compared to intracellular RNA signaling via MAVS which is locally acting within the cells, intracellular DNA signaling has the potential to cross cell-cell borders. In addition to the organelle localized protein STING, a second messenger, called cGAMP, is part of the DNA signaling (figure 1.3). The *N*-terminal region of cGAS binds the backbone of canonical B-DNA [108, 109]. Upon DNA binding, cGAS dimerizes and catalyzes the dinucleotide formation of ATP and GTP to cGAMP [47, 53, 110]. This produced second messenger has a 2'-5'-linkage which is different from the known 3'-5'-linkage in the prokaryotic second messenger cGAMP [52]. After synthesis, cGAMP binds to ER localized Stimulator of interferon genes protein (STING) [111]. Thus, the ER is a signaling hub in DNA sensing. After cGAMP binding, STING translocates to the Golgi where it initiates innate immune response [111–114]. Similarly to MAVS, STING can signal through two different pathways. One pathway involves binding of TBK1 which subsequently phosphorylates IRF3 resulting in IFN induction [112, 115]. The other pathway involves the IKK complex resulting in NF-κB activation [116]. Upon DNA sensing by cGAS not only in the infected cell but in neighboring cells as well IFNs are produced. This is due to the fact that cGAMP can pass through gap junctions [117]. This allows a fast response of the whole cellular environment with the aim to reduce the infectibility of cells and by that reduce the viral load.

All those examples show that the site of signal detection is not the site of signaling. It is currently not clear why this happens, but an interesting hypothesis is that this local separation of detection and signaling may raise the threshold required to induce potent antiviral signaling. This could be important to minimize accidental signaling that could induce autoimmunity [56]. After ligand binding by various PRRs they initiate different signaling pathways, resulting in activation of transcription factors, like NF-κB, AP-1, IRF3 and -7 and CREB. After activation of transcription factors, cellular machinery starts transcription of type I IFNs, pro-inflammatory cytokines and chemokines. These different proteins are translated in the cytosol and released via the ER-Golgi apparatus and endosomes to the extracellular environment. The releasing cell as well as the neighboring cells detect these proteins with appropriate receptors and start subsequent signaling to protect from spreading pathogens. The next chapter will elucidate further these different execution proteins, their downstream signaling and resulting effects on the host and pathogen.

1.1.3 Execution of signaling

Pro-inflammatory cytokines, chemokines and IFNs are a subset of small proteins which are secreted upon the before mentioned induction of the innate immune system. As PRRs are mainly located on innate immune cells, these immune cells warn other cells of the organism by appropriate small proteins to become protect from the invading pathogen [118]. The secreted proteins can act in an autocrine and paracrine way on target cells, where they stimulate further cytokine production and in the case of IFNs also activate expression of IFN stimulated genes (ISGs) which have antiviral activity. The following section gives an overview on secreted proteins, the second part describes IFN induced cellular pathways and finally focuses on the activity of some ISGs.

IFNs, cytokines and chemokines

IFN was discovered by Issacs and Lindenmann nearly 60 years ago [119]. They applied supernatant of chicken membranes treated with an inactivated influenza virus to other membranes which were subsequently protected from viral infection [119]. Biochemical analysis showed that the transferred activity was due to an acid stable protein which they called IFN. It is now known that many different

types of IFN proteins exist, that can broadly be separated in three types (type I, II and III) depending on their gene and protein sequence and the receptor that is activated by the respective IFN.

Type I IFNs are expressed in all cells and contain five different protein groups: IFNα, β, ω, τ and δ. However, only the first three are present in humans, the latter two were detected only in giraffes and ruminants and in pigs, respectively [120, 121]. IFNα contains a family of 14 genes, encoding for distinct isoforms, whereas IFNβ names only one protein [122]. Type I IFNs have no introns. The isoforms of IFNα are responsible for the outcome of the immune response with respect to antiviral, antiproliferation and immunomodulatory activity. Above mentioned signaling events results in IRF3 and -7 activation, which subsequently induces transcription of type I IFNs in infected cells [123, 124]. An exception to this activation procedure are plasmacytoid dendritic cells (pDCs), which have the ability to utilize a fast track pathway, involving TLR signaling via MyD88 followed by direct activation of IRF7 [123]. This results in very fast and prominent induction of IFNα gene and protein expression [123]. Type I IFNs are expressed quickly after virus detection but only for a short period of time.

The only member of type II IFNs is IFNγ. IFNγ is a secondary cytokine, as it is not directly induced by PRR signaling, but by the cytokine IL-12 as well as in response to activation of specific receptors present on NK cells and primed T-cells. IL-12 is regulated through NF-κB signaling and secreted exclusively from immune cells [125], such as DCs. After release, IFNγ forms homodimers, which bind to IFNγ receptor (IFNGR), composing of four subunits [126]. IFNγ is one of the major molecules, besides TNFα and other immunoregulatory cytokines, such as IL-12 and IL-18, to enable crosstalk between innate and adaptive immune system [127–129]. Additionally, its expression appears to be more sustained than expression of type I IFNs.

Type III IFNs compose of IFNλ with at the moment four known family members, IFNλ 1-4 [130–133]. IFNλ signal via the IFNλ receptor 1 (IFNLR1 or IL-28R), which is mostly localized on epithelial cells and mediate antiviral immunity similar to type I IFNs [130, 134]. Type I and II IFNs have in common that they promote an antiviral state in cells for defense against pathogens by inducing expression of ISGs, described in more detail in part three of this chapter.

Pro-inflammatory cytokines are mainly induced through activation of NF-κB. They are composed of around 40 genes, such as IL-1β, IL-6 and TNFα, encoding for proteins with a molecular weight between 8-40 kDa [135–137]. Among other functions, these cytokines are involved in the maturation of T-helper (Th) cells into Th1, Th2 and Th17 cells.

Finally, also chemokines are secreted upon activation of the innate immune system. These are cytokines which induce chemotaxis. Currently, around 50 chemokines are described and divided in two groups based on the position of their cysteine residues in their *N*-terminus: CC (both cysteines together) and CXC (cysteines divided by one other amino acid) [138]. Chemokines induce activation and migration of leukocytes to their sites of action. These locations can be either sites of infection or lymphatic organs that are involved in activation of the adaptive immune system.

IFN signaling pathway

Intracellular signaling cascades triggered by type I and III IFNs are identical and exemplified based on IFNα signaling in figure 1.4 [130, 134]. IFNAR is a heterodimeric receptor consisting of two chains, namley IFNAR1 and 2. The cytoplasmic tail of IFNAR1 binds Tyrosine kinase 2 (TYK2) and the cytoplasmic tail of IFANR2 binds Janus kinase 1 (JAK1). Both kinases subsequently activate two different signaling pathways, a third is mediated by the IFNAR heterodimer itself. The

first signaling pathway results in tyrosine phosphorylation of Signal transducer and activator of transcription (STAT)1 and 2 by both kinases. STAT heteromers interact in the nucleus with IRF9. This trimeric complex is called IFN stimulated gene factor 3 (ISGF3) and binds to IFN-stimulated response element (ISRE) promoter to induce ISG expression [139]. The second signaling pathway results in phosphorylation of IRS 1/2 by both kinases which subsequently activate Phosphoinositide 3-kinase (PI3K) [140]. PI3K can phosphorylate AKT which regulates Mammalian target of rapamycin (mTOR). mTOR positively influencing mRNA translation and is particularly involved in translation of ISG proteins. PI3K can as well phosphorylate Protein kinase Cδ (PKCδ) which regulates ISG transcription and apoptosis [141]. This signaling through PI3K can regulate the biological activity of ISGF3. The third signaling pathway, mediated by IFNAR1/2 itself, activates MAPK signaling cascade for activation of p38. Upon activation by MAPK, Mitogen- and stress-activated protein kinase 1 and 2 (MSK 1/2) phosphorylated p38, which translocates to the nucleus and modifies histones for ISG expression [142, 143].

There are various cellular mechanisms that inhibit the IFN system to control the immune response in order to avoid its overreaction. Among other proteins, Suppressor of cytokine signaling (SOCS) and Protein inhibitor of activated STAT (PIAS) as inhibitors of the JAK-STAT pathway are dampening IFN and cytokine related signaling. SOCS inhibits STAT activation, by binding to JAK [144, 145], whereas PIAS inhibits STAT protein translocation [146].

IFNγ binds to the cell surface heterodimeric IFNγ receptor (IFNGR) 1/2. It induces via JAK2 the phosphorylation and homodimerization of STAT1, which translocates to the nucleus and activates transcription of genes controlled by IFNγ activated sequence (GAS) promoter [147]. Nuclear phosphatases dephosphorylate STAT1, which translocates out of the nucleus to reenter the signaling pathway. Genes that are regulated by GAS promoters are also controlled by type I IFN signaling. However, a specific subset of genes regulated by type I and II IFNs exist.

IFN stimulated genes

In this introduction I refer to type I IFN stimulated genes as ISGs. ISGs are proteins which act intracellularly and often have the potential to inhibit various steps of the viral life cycle, such as entry, translation and replication [148]. However, ISGs do not always protect individual cells from cell death but rather prevent the viruses to spread and infect neighboring cells or tissues. ISGs can also target non-viral intracellular pathogens and regulate activity of type I and II IFNs. Among the known around 2000 genes regulated by the ISRE promoter [149] are known antiviral proteins including: RNA-dependent protein kinase (PKR), 2'-5'-oligoadenylate synthetase (2'-5'-OAS), Myxovirus resistance (Mx) proteins, IFN-induced proteins with tetratricopeptide repeats (IFIT) proteins, IFN-induced transmembrane (IFITM) protein, Intercellular adhesion molecule (ICAM), TRIM proteins [141]. The defect of individual ISGs can result in severely impaired antiviral defense against particular pathogens, illustrating the complexity and specificity of certain ISGs. In this section I will describe two extensively studied ISGs, namely PKR and IFIT family, in more detail.

PKR has two *N*-terminal dsRNA binding motifs which bind dsRNA generated during viral infections, and two kinase domains for autophosphorylation and phosphorylation of targeted substrates [150, 151]. Upon dsRNA binding PKR dimerizes and is activated by autophosphorylation [152]. Activated PKR influences cellular protein translation, various signal transduction pathways and apoptosis (see chapter 1.2.2) [150, 153, 154]. PKR controls protein synthesis by phosphorylation of the α subunit of Eukaryotic translation initiation factor (eIF)2, which subsequently inhibits eIF2 and arrests protein translation of capped mRNAs [150]. As example for signal transduction pathways

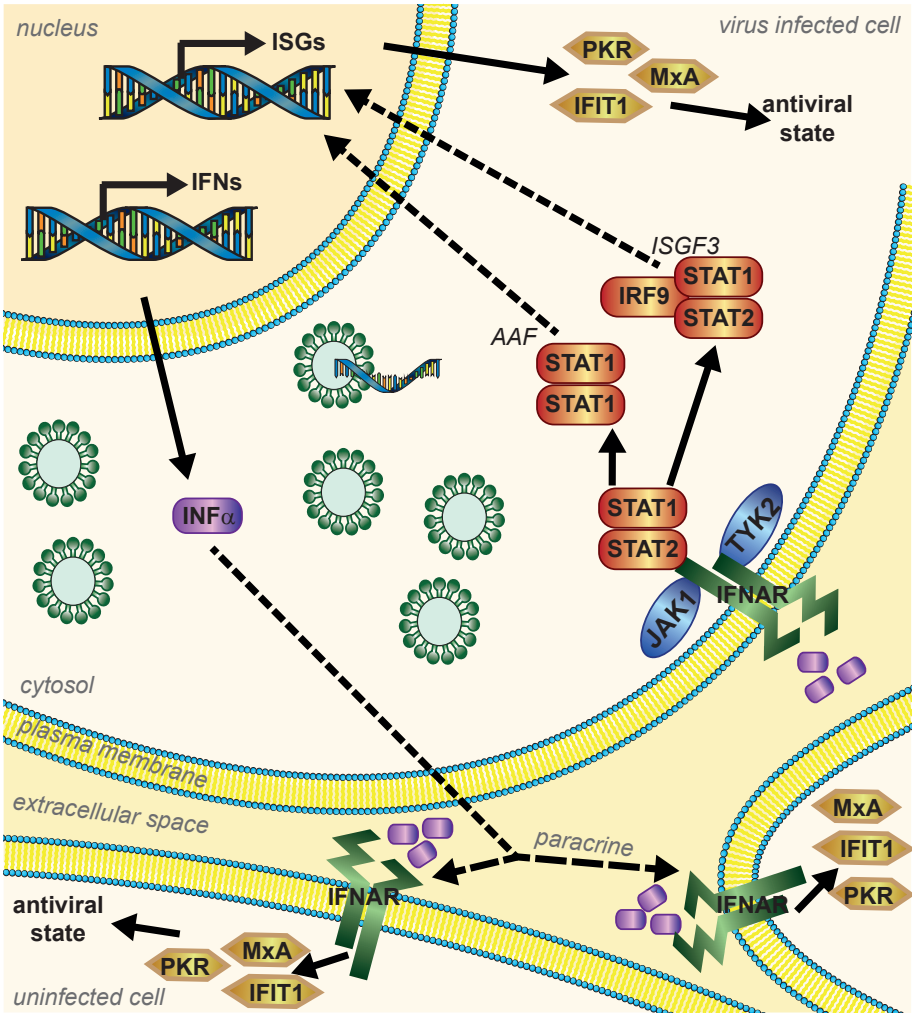

Figure 1.4: Interferon stimulated execution signals of the innate immune system.
After transcription initiation by IRF3 and 7, IFNα is produced and secreted from a virus infected cell. Extracellular IFN binds in an autocrine (same cell) or paracrine (neighboring cells) fashion to IFNAR and induces oligomerization of the transcription factors STAT1 and 2 and IRF9. These transcription complexes translocate to the nucleus and initiate transcription of ISGs. Cells express ISGs to achieve an antiviral state within cells, either to eliminate already replicating virus or be prepared to eliminate invading virus in the neighboring cells.

NF-κB signaling is described. To control NF-κB signaling, PKR phosphorylates IκB, which subsequently leads to release of NF-κB and its translocation to the nucleus [155]. Activation of NF-κB is independent of eIF2 phosphorylation [156]. Finally, PKR induces apoptosis through activation of Fas-associated death domain (FADD) and caspase-8 [157]. Apoptosis induction through PKR is triggered by various stimuli, such as eIF2 phosphorylation [158] and NF-κB activation [158], mostly depending on the viral infection.

IFIT proteins have four members in humans, IFIT1, 2, 3 and 5 [159]. IFIT proteins are expressed at very low level and are induced upon viral infection or IFN treatment. All IFITs are cytoplasmic proteins without reported enzymatic activity. However, IFIT proteins form large protein complexes, consisting of IFIT proteins and additional cellular factors [160–162]. Formation of such complexes may influence the spectrum of viruses target by individual IFIT proteins [163]. IFIT proteins have

been shown to bind to viral nucleic acids within a positive charged pocket, such as 5'PPP-RNA and 2'Ounmethylated RNA [160, 162, 164–166], both common nucleic acids associated with viral infection [167, 168]. By binding of 2'O unmethylated RNA, IFIT1 blocks translation of this RNAs [162].

1.2 Involvement of mitochondria in innate immunity

An important feature of the innate immune system is the utilization of cellular organelles, such as mitochondria and ER, as signaling hubs. Besides their participation in IFN induction, mitochondria are also involved in cell death and ROS production. The next chapter will elucidate the last two mentioned tasks in more detail.

Mitochondria are essential cellular organelles which differ in their composition from all other cellular organelles. Based on the endosymbiotic theory, mitochondria are suggested to be leftovers from a symbiotic relationship with prokaryotic cells. Major hints are the existence of mitochondrial DNA (mtDNA) and the remarkable similarity of the mitochondrial membrane ATPase and mitochondrial membrane composition compared to bacteria derived counterparts [169]. Additionally, unlike other organelles which have one surrounding membrane, mitochondria have two membranes. Mitochondria can be divided in four compartments, the outer mitochondrial membrane (OMM), the intermembrane space (IMS), the inner mitochondrial membrane (IMM) and the matrix (M) (figure 1.5). Both membranes consists of lipid bilayers that differ in their protein and lipid content [170].

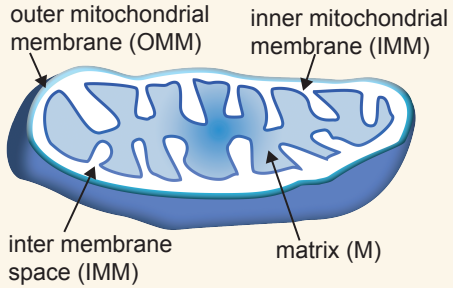

Figure 1.5: Structure of mitochondrion. Mitochondria consist of four compartments divided by two lipid bilayer membranes: outer mitochondrial membrane and inner mitochondrial membrane. The space between the membranes is called intermembrane space. The compartment within the inner mitochondrial membrane is called matrix.

In humans, mitochondrial DNA only encodes for 13 mitochondrial proteins, 22 tRNAs and two ribosomal RNAs [171]. The additional 1000 proteins annotated to localize to mitochondria are encoded by nuclear DNA [172]. Mitochondria are present in several copies within each cell harboring several copies of mtDNA. Energy production is a major task of mitochondria [173] and the copy number of mtDNA scales with the energy demand of the cell. Mitochondrial fusion and fission processes adjust the number of mitochondria per cell as well as the mtDNA copy numbers [174]. Some cell types, particular neuronal and muscle cells have a higher energy demand [173].

Mitochondria are involved in multiple cellular functions, such as transport and import of biomolecules, energy metabolism, ROS metabolism, Calcium homeostasis, cell death and innate immunity. The most prominent function is the generation of energy in form of ATP synthesis. Other metabolic functions are the synthesis of amino acids and lipids as well as synthesis of heme and iron-sulfur clusters. Additionally, mitochondria take part in regulation of the cellular stress response, cell proliferation and play a central role in programmed cell death [175]. Accordingly, mitochondria have a major influence on aging and cancer processes as well as on neurodegenerative diseases, such as Alzheimer's and Parkinson's disease [175]. In addition, mitochondria are also a major hub for immune signaling.

The following sections shortly describe mitochondrial energy metabolism and will focus on ROS synthesis and functions as well as on various cell death pathways acting via mitochondria.

ATP synthesis with the oxidative phosphorylation (OxPhos) system

Adenosine triphosphate (ATP) is the most important molecule for storage and transmission of energy within the cell. To generate energy the cell has to metabolize incoming nutrients, such as carbohydrates, lipids and proteins, by glycolysis, β-oxidation and proteolysis, respectively. The products of these three catabolic processe, pyruvate, acetyl-CoA and several other metabolites, are used in the tricarboxylic acid (TCA) cycle. The TCA cycle takes place in the mitochondrial matrix and generates reduced nicotinamid-adenin-dinucleotid (NADH) and reduced flavin-adenin-dinucleotid ($FADH_2$). NADH and $FADH_2$ are substrates for the oxidative phosphorylation (OxPhos) system located on the IMM. The OxPhos system consists of five protein complexes (I-V). Electrons from NADH and $FADH_2$ are passed along the first four complexes and the resulting energy is used to pump protons to the IMS. The last complex, complex V, is an ATP synthetase which uses this proton gradient (IMS to matrix) to bind free phosphate to ADP, generating ATP [176]. A side product of the OxPhos system are ROS which can be used as second messenger to control physiological functions, but also result in detrimental effects if their intracellular concentration is raising above a critical level.

1.2.1 Synthesis and effects of reactive oxygen species

Reactive oxygen species (ROS) and reactive nitrogen species (RNS) are comprised of different highly reactive molecules, based on oxygen or nitrogen, respectively (figure 1.6) This section focuses only on ROS as major player in immunity.

oxygen	O_2	O=O
peroxide	$\bullet O_2^{-2}$	$\bullet$-O=O-$\bullet$
superoxide anion	$\bullet O_2^{-}$	$^{-}$O=O$\bullet$
hydroxyl radical	$\bullet OH$	H-O$\bullet$
hydroxyl ion	OH^-	H-O$^-$
hydrogen peroxide	H_2O_2	H-O-O-H

Figure 1.6: Types of reactive oxygen species. Common reactive oxygen species with name, chemical formula and simplified electron structures. The dots designate an unpaired electron, which is chemically named radical.

There are eight known sites for ROS production at the IMM. Two of them are located in complex I and III of the OxPhos system (figure 1.7) [177]. A side product of the establishment of the proton gradient are electrons, which leak out of the redox centers and react with oxygen in the matrix to generate superoxide anions [178]. Superoxide anions re reduced by Superoxide dismutases (SODs) to hydrogen peroxide (H_2O_2). These reactions also take place in the IMS and cytosol. Here different SODs are involved. In total, humans encode for three SODs: SOD1 (a Cu/Zn-SOD), SOD2 (a MnSOD) and SOD3 (a Cu/Zn-SOD) [179]. They differ in their cellular localization and the metal ions in their catalytic center [179]. SOD1 is mainly localized in the cytosol and partly in the mitochondrial IMS. It convertes mainly cytosolic ROS produced by NOX enzymes on ER and plasma membrane as well as leaking ROS from mitochondria. SOD2 is localized in the mitochondrial matrix and responsible for ROS leaking from the OxPhos system. SOD3 was detected in all extracellular liquids and quenches free radicals [180–182]. Mutations of SOD enzymes are commonly found in neurodegenerative disease, such as amyotrophic lateral sclerosis (ALS), and result in increased cell death [183, 184]. Since H_2O_2 is detrimental to cells when transformed to hydroxyl radicals, catalase reduces H_2O_2 to water and oxygen or the Gluthation (GSH) scavening system scavenges H_2O_2 by generating water.

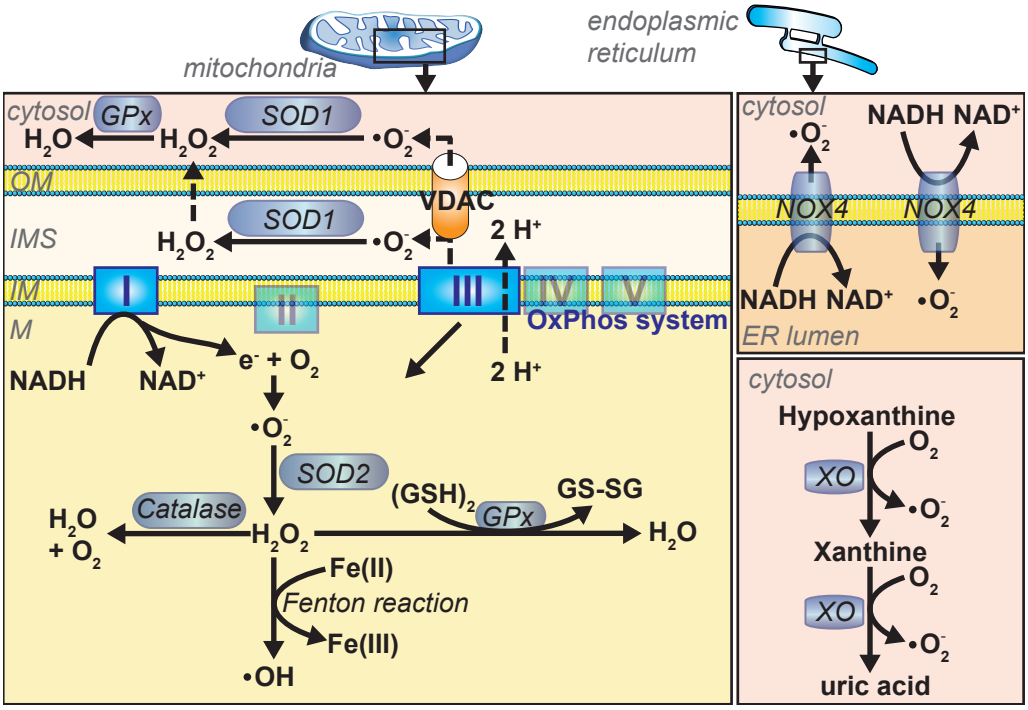

Figure 1.7: Cellular synthesis of reactive oxygen species.
Cellular ROS are synthesized mainly on three different places in the cell: [a] at Complex I and III of the OxPhos system in the mitochondrial inner membrane, [b] at the ER membrane by NADPH oxidase (NOX)4 and [c] in the cytosol during transformation of hypoxanthine to uric acid catalyzed by Xanthine oxidase (XO). In all cases superoxide anion is produced which can be detoxified by Superoxide dismutases (SODs) to hydrogen peroxide. Hydrogen peroxide can be reduced to water by enzymatic reactions including Catalase or Glutathione peroxidase (GPx). Hydrogen peroxide can freely diffuse through the mitochondrial membranes. The Fenton reaction generates hydroxyl radicals from hydrogen peroxide which is highly reactive.

If the H_2O_2 amount is too high to be controlled by catalytic or scavenging proteins, it transforms to hydroxyl radicals by an oxidation reaction that involves iron. Hydroxyl radicals are highly reactive molecules which target lipids, DNA and proteins. Such targeting can cause detrimental effects in the cell. Oxidation of lipids (figure 1.8 a) results in disintegration of membranes. If the IMM is affected, the proton gradient is lost, which leads to decrease of ATP synthesis. Oxidation of DNA bases (figure 1.8 b) effects base pairing due to changes of hydrogen bonds and ultimately induce mutations. Finally, the uncontrolled oxidation of protein backbones (figure 1.8 c) can lead to peptide bond breaks and malfunctional or non-functional proteins. If these oxidation processes either accumulate or actively increase above a critical threshold, cells initiate a cell death program.

Despite having the above described detrimental effects, ROS can be also used in a controlled manner as second messenger. As such it is involved in the regulation of several biological processes, such as epigenetics, autophagy, immunity, cell proliferation and differentiation, hormone signaling and cell death [185]. These cellular processes are controlled by defined oxidation reactions between ROS and cysteine residues of proteins, which modulate the function of targeted proteins as shown in figure 1.9. As with other cellular second messengers, like Ca^{2+}, the ROS concentration is relevant for downstream signaling. Low intracellular levels of ROS (pico- to nanomolar) are required for general homeostasis [185]. Slightly elevated levels initiate ROS scavenging pathways [185]. These pathways can include Catalase, Glutathione or Kelch-like ECH-associated protein 1 (KEAP1) and

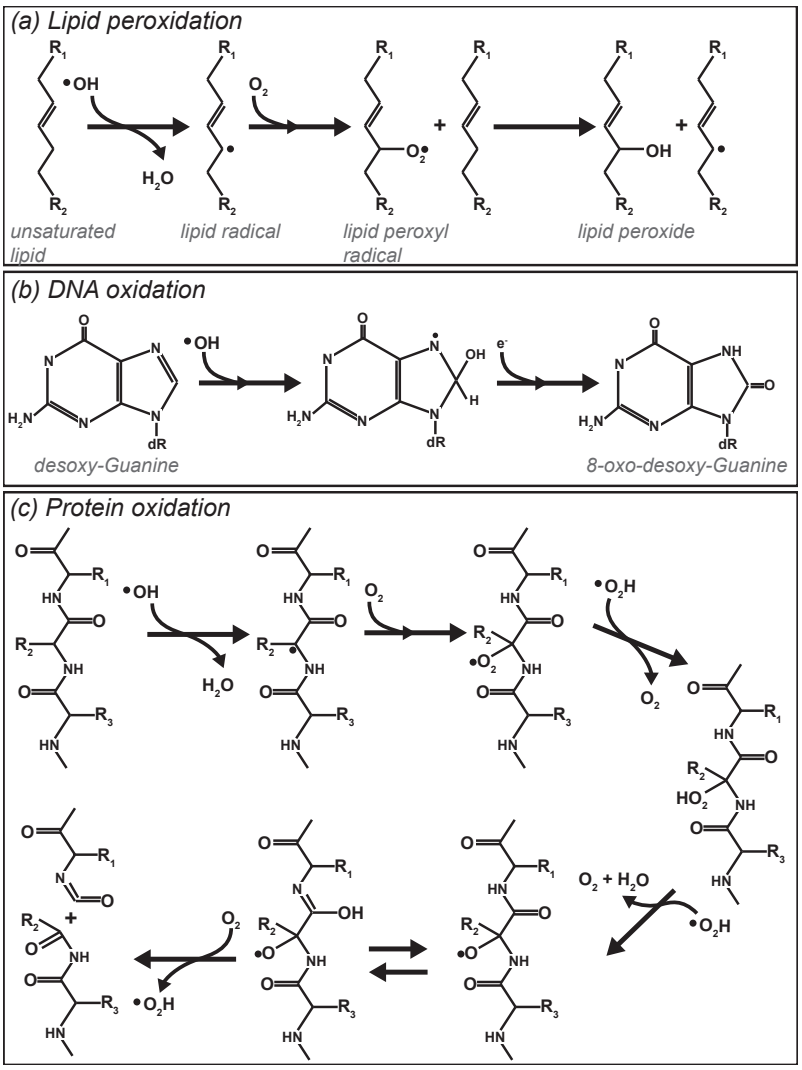

Figure 1.8: Oxidation reactions on cellular macromolecules by reactive oxygen species.
Hydroxyl radicals can react with cellular macromolecules molecules (lipids, DNA and proteins) and induce irreversible damage. (a) lipid peroxidation (b) DNA oxidation (c) protein oxidation

Nuclear factor (erythroid-derived 2)-like 2 (NRF2) [185–188]. The latter pathway sense ROS via KEAP1 which results in activation of a transcriptional program [186–188]. In homeostatic conditions, KEAP1 acts as a scaffold protein for substrates of E3 ligase Cullin 3 (CUL3) [189]. One of these substrates is NRF2. NRF2 binds directly upon translation KEAP1 [186]. This interactions mediates ubiquitin dependent proteasomal degradation of NRF2 through CUL3 [189, 190]. KEAP1 is a cysteine-rich protein [191], which changes its conformation upon high oxidative stress by formation of disulfide bridges [191]. These conformational changes result in release of NRF2 and translocation of NRF2 to the nucleus [191]. In the nucleus NRF2 binds to antioxidant response elements (ARE) on the DNA and activates transcription of cytoprotective genes, such as NAD(P)H:quinone reductase (NQO1), Glutathione S-transferase (GST), Heme oxygenase 1 (HMOX1) and Thioredoxin (TXN) [192–195]. Highly increased levels of ROS, as described before, result in oxidative stress and subsequently cell death [185].

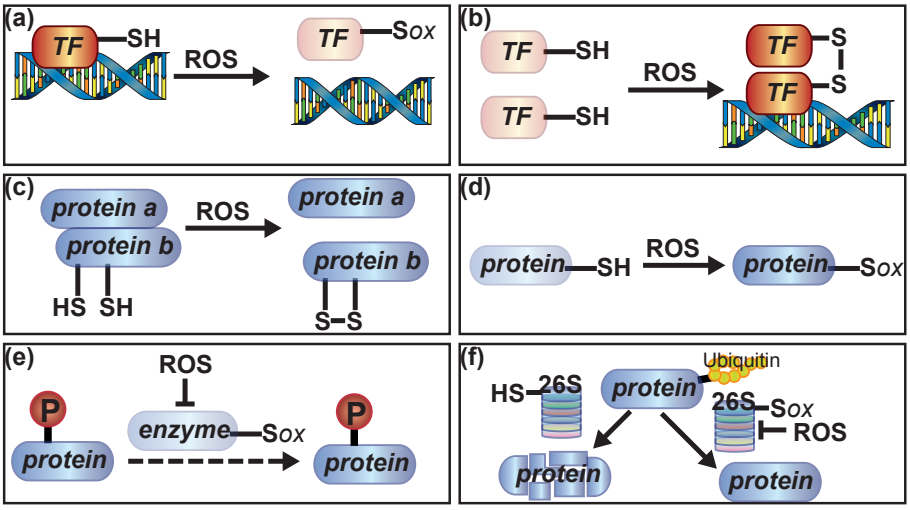

Figure 1.9: ROS acting as a second messenger influence protein functions (adapted from [196, 197]).
Proteins can be activated (darker color) or inactivated (faint color) by small amounts of ROS. [a] Transcription factors (TF) can be deactivated by oxidation, resulting in impaired DNA binding e.g. NF-κB, AP-1, HIF-1α. [b] TF can also be activated by forming heterodimers via disulfide bonds e.g. FOXO binding to p300/CBP acetyltransferase. [c] Proteins can interact via disulfide bonds and dissociate upon forming disulfide bonds, due to conformational changes e.g. KEAP1-NRF2, ASK1-TRX, p53-JNK. [d] Oxidation of proteins can result in activation e.g. disulfide bond-mediated homodimers of ATM kinase phosphorylate HSP27 and activate G6PD which contributes to maintenance of cellular redox homeostasis. [e] Proteins can be inhibited by ROS such as Protein tyrosine phosphatase, resulting in elevated protein phosphorylation of their target proteins. [f] Stability of proteins can be influences by ROS e.g. proteasome subunit 26S can be inactivated through oxidation, resulting in less degradation of ubiquitinylated proteins.

1.2.2 Cell death pathways

Mitochondria are involved in several cell death signaling pathways. Cell death in general is a natural process required during development or regeneration of cells or tissue [198]. In addition, cell death can also be caused by injury or be a consequence of pathogen encounter [198]. There are various forms of cell death. They differ in their induction, by the morphological changes on the cell and partly their localization in the organism. The main cell death pathways are programmed cell death (PCD), including apoptosis and necroptosis, as well as uncontrolled cell death such as necrosis. Apoptosis and necrosis can be clearly distinguished by their morphological changes on the cell (table 4).

Table 4: Morphological characteristics of apoptosis and necrosis (adapted from [199])

Morphological characteristics of cellular organelles	apoptosis	necrosis
cytoplasm	shrinking	swelling
membrane	blebbing	loss of integrity
mitochondria	become leaky	swelling
nucleus	condensation	no changes
chromatin	aggregation at nuclear membrane	no changes
vesicle formation	yes, cell fragmented into small vesicles	no, complete cell lysis

Table 5: **Comparison of various forms of programmed cell death [202–204]**

	Programmed cell death					
	Caspase-dependent			**Caspase-independent**		
	intrinsic apoptosis	**extrinsic apoptosis**	**pyroptosis**	**parthanatos**	**necroptosis**	**necrosis**
involved proteins	Bcl-2 family members, caspases, cytochrome c	Bcl-2 family members, caspases, TNF receptor family, cytochrome c	caspase-1, IL-1β	PARP1, Calpains, AIFM1	RIPK1, RIPK3, MLKL	
inflammatory	no	no	yes	no	yes	yes

1.2.2.1 Programmed cell death

Programmed cell death (PCD) comprises various forms of cell death including, apoptosis, parthanatos and necroptosis [200]. PCD is essential for cell homeostasis of multicellular organisms. A well-studied example is apoptosis, which is required for successful development [201]. Malfunctions of PCD can result in pathological disorders, like cancer, neurodegenerative diseases or failures during embryogenesis [198]. The various forms of PCD differ both in their involved proteins and their biochemical outcome (table 5).

The following section will only focus on intrinsic and extrinsic apoptosis, parthanatos and necroptosis. The most studies PCD pathway until now is apoptosis. There are two mechanistically distinct apoptotic signaling pathways: an intrinsic and an extrinsic signaling pathway. They vary in the inducing trigger coming from inside the cell or outside the cell, respectively. Both of these pathways require caspases, cell death specific cysteine proteases [205], although caspase-independent cell death pathways, involving cathepsin, calpains and serine proteases exist [206, 207]. Caspase-independent cell death pathways pathways involve different triggers and execution proteins and can be activated also in the presence of caspases in the cell [198, 208].

Intrinsic apoptosis

Intrinsic apoptosis (figure 1.10) is also called mitochondrial apoptosis since the apoptotic signals are transmitted through mitochondria. It can be triggered by damage of cellular macromolecules (proteins, DNA) or organelles, upon ultraviolet irradiation, exposure to toxic chemicals or withdrawal of essential proteins like growth factors [209]. All triggers result in the release of mitochondrial resident molecules which activate caspases. The major players of intrinsic apoptosis are members of the B-cell lymphoma-2 (BCL-2) family, released mitochondrial IMS proteins, such as cytochrom c, and caspases. The BCL-2 family comprises three groups of proteins: the inhibitory or anti-apoptotic

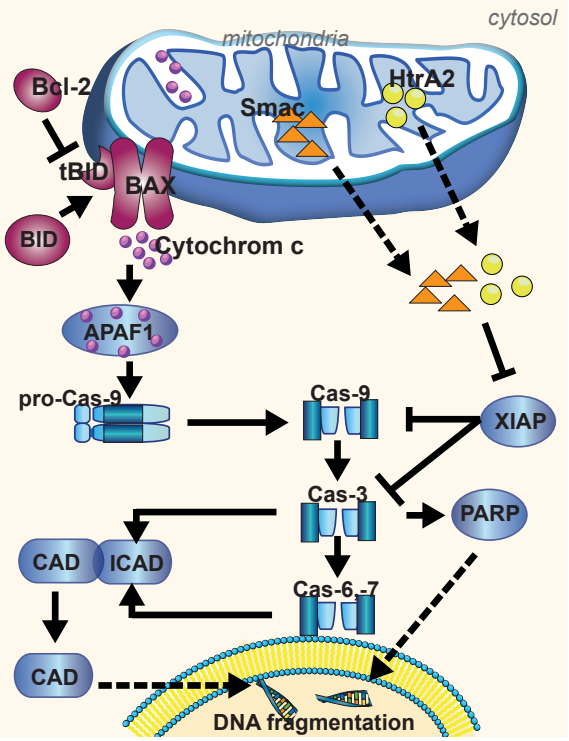

Figure 1.10: Intrinsic apoptosis pathway.
Upon intracellular stimuli, such as damaged proteins or UV irradiation, pro-apoptotic proteins of the BCL-2 family are activated, like BAX and BID. BAX forms homooligomers which translocate to mitochondria and with the help of tBID form pores in the mitochondrial outer membrane resulting in the release of cytochrom c, SMAC and HtrA2. The latter two inhibit XIAP, which inhibits caspases under normal conditions. Cytochrom c binds APAF1, which oligomerizes and subsequently interacts with pro-caspase-9. Caspase-9 is fully active upon release of XIAP and cleaves caspase-3, which cleaves targeted substrates and resulting in DNA fragmentation. Bax can be inhibited by pro-survival proteins, such as Bcl-2 and Bcl-xL.

proteins (e.g. Bcl-2, BCL-xL), the pro-apoptotic proteins (e.g. BAX, BAK) and the regulating Bcl-2 homology 3 (BH3)-only proteins (e.g. BAD, BID, NOXA and PUMA) [210–213]. Caspases are assigned to three groups: the initiator caspases, responsible for starting the signaling process, the effector caspases, executing the death signal by cleaving cellular substrates, and inflammatory caspases, which mediate inflammatory responses [198].

Regulatory BH3-only proteins are activated upon stress signals [211, 214]. One example is the transcriptional regulation of NOXA and PUMA by p53 after DNA damage [215]. PUMA binds to the pro-apoptotic protein BAX [216] upon which BAX forms homooligomers, translocates from the cytosol to mitochondria and inhibits by binding anti-apoptotic protein Bcl-2 [217, 218]. It was recently shown by Grosse et al. and Salvador-Gallego et al. that BAX forms ring and arc like structures on OMM [219, 220], the so-called mitochondrial outer membrane permeabilization (MOMP) pores [219, 220]. MOMP formation leads to releaso of several IMS proteins, including cytochrome c, Diablo homolog mitochondrial (DIABLO or Smac) and Serine protease HTRA2 mitochondrial (HtrA2 or Omi) [221–223]. Cytochrom c is normally involved in the energy metabolism at the electron transport chain. After an apoptotic stimuli cytochrome c is released and binds the scaffold protein Apoptotic protease-activating factor 1 (Apaf-1) [224]. Apaf-1 subsequently oligomerizes and interacts with the initiator caspase-9 via their CARD, forming the activated caspase-9-Apaf-1 holoenzyme complex [225]. The complex is still inhibited by X-linked inhibitor-of-apoptosis protein (XIAP) to avoid false activation of cell death. Smac and Omi support the apoptosis inducing function of cytochrome c by binding to XIAP [223]. When the interaction of XIAP to caspase-9-Apaf-1 holoenzyme complex is released, the complex is fully activated and is called apoptosome [225, 226]. Caspase-9 can now cleave effector pro-caspases-3, -6 and -7. After cleavage, these effector caspases cleave their substrates at the appropriate recognition sequence [227]. Slee at al. showed that caspase-3 is the most important effector caspase responsible for cleavage of various

substrates involved in cytoskeleton structure and DNA repair [228], such as actin, nuclear lamins, Receptor-interacting protein (RIP), XIAP, Poly(ADP-ribose) polymerase 1 (PARP1) and Inhibitor of caspase-activated DNase (ICAD) [228]. ICAD inhibits caspase-activated DNase (CAD), which amongst others is responsible DNA fragmentation and chromatin condensation [229]. The results of caspase cleavage is membrane blebbing and cell shrinkage, chromatin condensation and nucleosomal fragmentation, which are the aforementioned morphological characteristics of apoptosis [230]. Another hallmark of apoptosis is the exposure of a plasma membrane lipid called phosphatidylserine to the outer surface of apoptotic cells [231]. Phosphatidlyserine marks the apoptotic cell for phagocytosis, the end of the cell death process. There is no release of cellular material to the environment, avoiding inflammatory responses [232].

Extrinsic apoptosis

Extrinsic apoptosis (figure 1.11) is also called receptor-mediated apoptosis. In contrast to intrinsic apoptosis, extrinsic apoptosis is triggered by signals outside the cell. These signals are transmitted by cytokines (e.g. TNFα, TRAIL, FasL, Apo3L) and hormones(e.g. Estrogen), which bind to receptors on the cell surface[232, 233]. The receptors mediating cytokine induced extrinsic apoptosis are members of the tumor necrosis factor (TNF) receptor gene superfamily [234]. The TNF receptor family consists of proteins with a cysteine-rich extracellular domain for ligand binding, and a cytoplasmic death domain (DD) responsible for intracellular interactions [235]. The following section focuses on the TNFα and FasL induced extrinsic apoptosis pathways.

TNFα is generated and released upon sensing of diverse stimuli that lead to activation of an innate immune response as described in chapter 1.1.2. Trimeric TNFα binds to the transmembrane TNFα receptor (TNFR)1, which is capable to mediate cell death signaling. After TNFα binding to TNFR1 several adaptor proteins are recruited to form a scaffold which subsequently recruits caspases. The involved adaptor proteins contain different combinations of death domains to bind to TNFR1 and to each other (figure 1.12).

TNFR1 associated death domain (TRADD) directly interacts with TNFR1 through its death domain. Fas associated protein with death domain (FADD) interacts with TRADD through their death domain. Subsequently, initiator pro-caspase-8 is recruited to FADD via its death effector domain. This interactions leads to cleavage of caspase-8 followed by enzymatic processing of the executor caspase-3, -6 and -7, which subsequently mediate cell death by cleaving their appropriate substrates as described above. Additionally, Receptor interacting protein kinase 1 (RIPK1) is recruited to TNFR1 to mediate a signaling cascade activating NF-κB.

Another protein that has the ability to induce cell death is Fas ligand (FasL). It is mostly generated on cytotoxic T cells after repeated activation of antigen receptors [236]. After FasL binds to its receptor Fas, Fas directly interacts with FADD which subsequently recruits caspase-8 [237]. Besides processing of the executer caspases, caspase-8 cleaves BID, too [237]. Truncated BID (tBID) translocates to mitochondria to interact with BAX and subsequently activates the apoptosis pathway [237]. Caspase-8 can be inhibited by FLICE-inhibitory protein (FLIP), which is transcriptionally regulated by NF-κB [238]. FLIP blocks caspase-8 activation by binding FADD and caspase-8 and thereby inhibits apoptosis [239–241]. There are several viral FLIP (v-FLIP) proteins, inhibiting receptor mediated apoptosis, for example in Human Herpesvirus 8 (HHV-8, also named KSHV) and Molluscipoxvirus [242]. Avoiding early apoptosis is of advantage for viral replication.

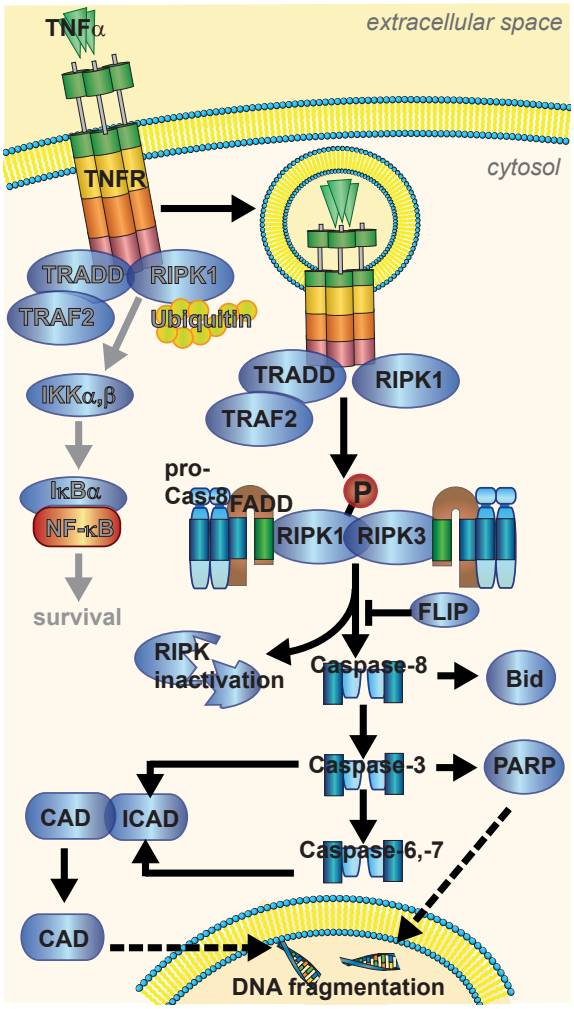

Figure 1.11: Extrinsic apoptosis pathway.
Upon binding of extracellular binding of TNF, the cell has two signaling options: mediating cell survival from membrane bound TNFR1 via ubiquitinylated RIPK1 to activate NF-κB (grey) or inducing cell death via internalized TNFR and caspases. This cell death pathway is called extrinsic apoptosis. Upon internalization TRADD, TRAF2 and RIPK1 bind TNFR1. As RIPK1 is not ubiquitinylated it dissociates from the complex, interacts with RIPK3 which phosphorylates RIPK1. Subsequently, FADD and pro-caspase-8 are binding which inactivate RIPKs and gets activated as caspase-8. Caspase-8 subsequently activates caspase-3, which cleaves its target proteins to induce DNA fragmentation. Caspase-8 can also truncate BID (tBID) which translocates to mitochondria inducing intrinsic apoptosis.

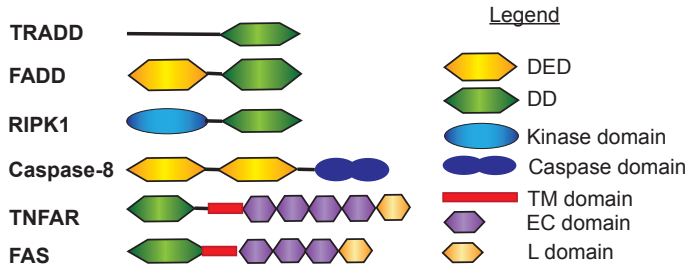

Figure 1.12: Death domain containing proteins.
Abbreviations: DED, Death effector domain; DD, death domain; EC, extracellular; L, ligand binding

Both, intrinsic and extrinsic apoptosis pathways, converge at the point of the execution phase, namely the activation of executer caspase. This point is considered being the final path of apoptosis [232].

Parthanatos

Parthanatos (figure 1.13) is a programmed caspase-independent cell death induced by overactivation of nuclear localized PARP1 and nuclear translocation of mitochondrial resident protein Apoptosis inducing factor, mitochondrial 1 (AIFM1). PARP1 is involved in DNA repair, chromatin function and genomic stability [243]. It has three major domains: an *N*-terminal domain harboring a nuc-

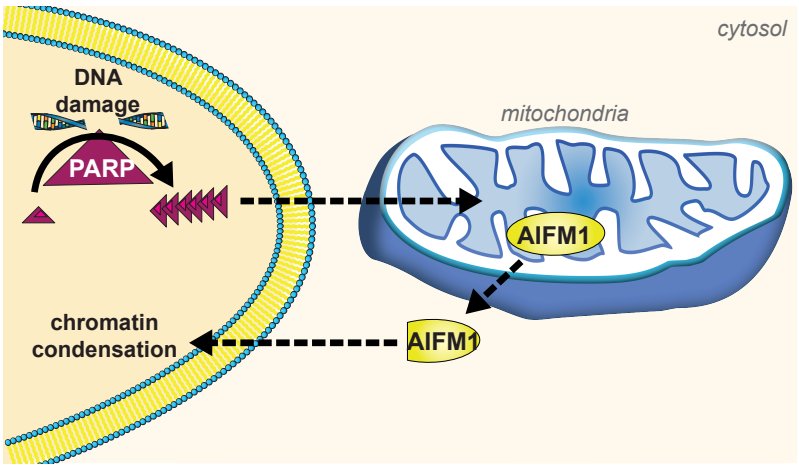

Figure 1.13: Parthanatos cell death pathway.
Upon DNA single strand breaks the DNA is marked and activates PARP1. PARP1 attaches PAR-groups to several proteins for accumulation of DNA damage repair factors. Generation of PARylated modifications require NAD^+. High NAD^+ depletion and increased production of PAR result in not well understood activation of AIFM1, probably by translocation of PAR to mitochondria. Subsequently, AIFM1 transmembrane domain is cleaved and truncated AIFM1 is release and translocate to the nucleus being here involved in chromatin condensation.

lear localization signal and two zinc finger motifs for DNA-binding; a central domain for automodification and a *C*-terminal domain harboring a NAD-binding site and the PAR-synthesizing site [244] Upon DNA strand breaks, induced by ultraviolet (UV) light, ROS or alkylating agents, PARP1 locates to the damaged DNA strand and triggers a suicidal cascade [200, 245]. First, PARP1 binds DNA single-strand breaks and modifies surrounding histones by poly(ADP-ribose) (PAR) [246]. This negatively charged area marks the DNA single-strand breaks for arriving repair enzymes [246]. Synthesis of PAR requires high amounts of NAD^+, resulting in depletion of NADH and ATP. However, if the DNA damage is too severe, PAR polymers accumulate and induce the release of AIFM1 [244]. AIFM1 is protein localized on the inner mitochondrial membrane facing to the intermembrane space. It is nuclear encoded and imported as precursor into the mitochondria, where its mitochondrial localization signal is cleaved off [247]. It is described bearing a oxidoreductase domain and a *C*-terminal domain responsible for cell death mediating activites [247, 248]. The transmembrane domain of AIFM1 is located in the IMM facing with its *C*-terminus to the IMS [247]. After activation by PAR, AIFM1 is cleaved and translocates as truncated AIFM1 (tAIFM1) to the nucleus [249, 250]. Nuclear tAIFM1 mediates large scale DNA fragmentation in cooperation with cyclophilin A, resulting in necrotic like cell death [251].

Necroptosis

Another PCD pathway resulting in necrotic like inflammatory death is necroptosis (figure 1.14). Necroptosis was identified when cells were treated with TNF in the presence of pan-caspase inhibitors [252]. Later it was shown that RIPK1 and RIPK3 are essential for necroptosis [253, 254].

After TNF binding to TNFR1 the extrinsic apoptosis pathway is initiated. However, when caspase-8 is inhibited by host or viral proteins, such as FLIP or viral FLIP (vFLIP), RIPK1 stays associated to RIPK3 and FADD and caspase-8 are released. The resulting complex consisting of one RIPK1 molecule and numerous RIPK3 molecules is called necroptosome [255]. The cytosolic necroptosome recruits Mixed lineage kinase domain-like protein (MLKL), which is phosphorylated by RIPK3 and

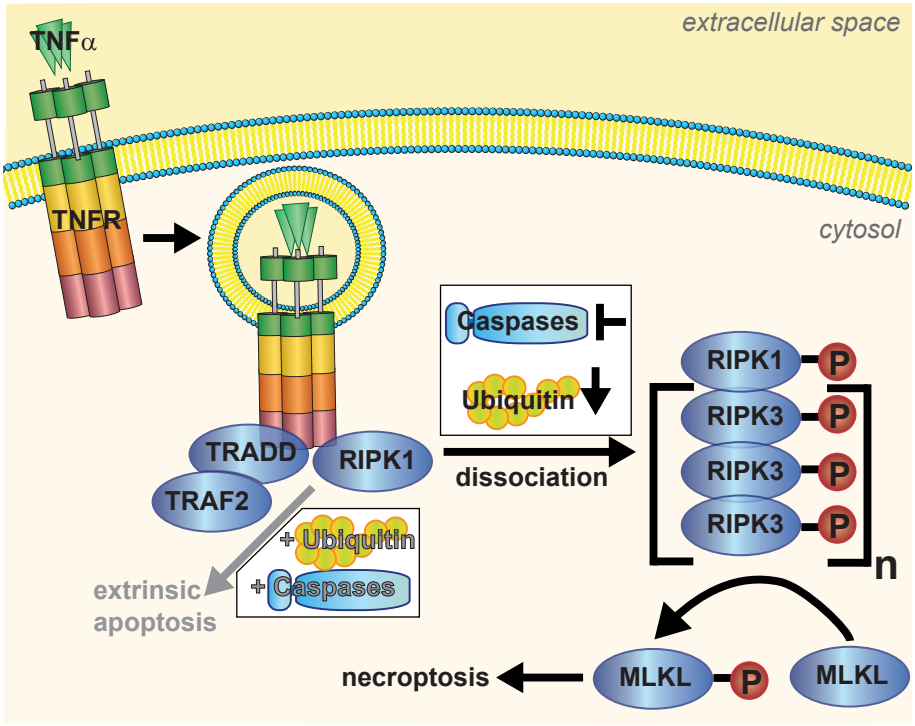

Figure 1.14: Necroptosis cell death pathway.
The general TNF induced cell death pathway involves caspases. However, in certain circumstances caspases are inhibited. In these cases RIPK1 stays associated with RIPK3, but not with FADD and caspase-8. Upon phosphorylation of RIPK1 by RIPK3, a complex with numerous RIPK3 molecules is formed which is responsible for phosphorylation of MLKL. MLKL oligomerize, translocates to the plasma membrane and permeabilize this membrane.

oligomerizes [256]. Phosphorylated MLKL aggregates were shown to translocate to the plasma membrane where it induces plasma membrane lysis resulting in release of damage-associated molecular patterns (DAMPs), a hallmark of necrosis [257]. An essential part for execution of cell death in the necroptosis pathway is an increase of ROS production [252]. Increased ROS is produced in the OxPhos system and by NOX enzymes rather than being a consequence of insufficient ROS scavenging or degradation [252, 258]. Although this pathway mainly operates through TNF-induced cell death, other membrane receptors, such as TLR3 and 4, and intracellular proteins, such as the ALR receptor DAI and the ISG PKR, were identified as triggers for necroptosis [204]. This indicates that necroptosis is a cell death mechanism during viral infections.

1.2.2.2 Necrosis

All forms of cell death mentioned before are tightly controlled. Necrosis is described as a 'more chaotic way of dying' [206]. Apoptotic pathways avoid release of cellular molecules, which would act as DAMPs and trigger inflammatory responses. However, such release of cellular content is a hallmark of necrosis [259, 260]. Morphological characteristics of necrosis are swelling of organelles, disruption of plasma membrane and release of cellular molecules to the extracellular environment [198, 261]. Necrosis can be triggered by tissue injuries due to toxins, cold, heat, osmotic shock and rupture of blood vessels. They result in compromised supply of oxygen and nutrients and subsequently ischemia [262].

To conclude, mitochondria play an essential role in maintaining homeostasis in the cell. Besides their role in ATP production they are required organelles for many cell death pathways. In part these cell death pathways are required for virus inhibition. Many viruses have evolved viral proteins to control various cell death pathways.

1.3 Viruses counteracting the innate immune system

Viruses are acellular pathogens which require a host for replication. By this definition they are no living organisms but infectious agents and are not classified in any kingdom, such as animals and bacteria. The first identified virus was tobacco mosaic virus by Beijerinck in 1898 which infects tobacco plants [263]. Viruses that are released from a cells are called virions. A Virion consist of the viral genetic material, the capsid coated by envelop proteins and in several cases an additional lipid bilayer. Based on their genetic material viruses are classified in eight groups: ssDNA, dsDNA, dsDNA-RT, (+)ssRNA, (-)ssRNA, ambisense ssRNA, dsRNA, ssRNA-RT [264]. In general the viral life cycle consists of three steps: entry, replication and shedding. Herpesviruses and some other viruses have an additional step called latency, which is an established lifelong persistent infection of the host [265, 266]. After viral entry via the endocytotic pathway or direct penetration of the plasma membrane, viruses transport their nucleic acid to the site of replication. Thereby most RNA viruses release their nucleic acid in the cytoplasm, whereas most DNA viruses require cooperation with the nuclear import machinery to release their nucleic acid in the nucleus for replication [264, 267]. However, there are also RNA viruses replicating in the nucleus and DNA viruses replicating in the cytoplasm. By using cellular replication machinery and cellular resources (RNA polymerases, ribosomes, amino acids, nucleotides, etc) viruses produce copies of their genetic material and translate their encoded proteins. When viruses release their genetic material and during the replication process, the host can detect them by numerous nucleic sensing mechanisms mentioned in chapter 1.1.1. Therefore, viruses evolved mechanisms to escape detection by the host's surveillance machinery. These mechanisms include blunting of the innate immune defense system, degradation of inhibiting cellular proteins and impairment of early cell death. This chapter describes mechanisms of some viruses (table 6) to interfere with these three cellular processes. I mostly focus on viruses that are related to my studies.

Table 6: Viruses of different families used in the studies

Virus	full virus name	family	genetic material	resulting disease
HCV	Hepatitis C virus	Flaviviridae	(+)ssRNA	persistent liver infection as hepatitis C (liver disease)
RSV	Respiratory syncytial virus	Paramyxoviridae	(-)ssRNA, non-segmented	acute lung infection
FluAV	Influenza A virus	Orthomyxoviridae	(-)ssRNA, 8 segments	Acute lung infection
LaCV	La Crosse virus	Bunyaviridae	(-)ssRNA, 3 segments	Encephalitis (brain damage)
Rota	Rotavirus A	Reoviridae	dsRNA	severe diarrhoea
HSV-1	Herpes simplex virus	Herpesviridae	dsDNA	Persistent neuronal infection
KSHV	Human herpes virus 8	Herpesviridae	dsDNA	Cancer

1.3.1 Strategies to interfere with the innate immune system

The main aim of viruses is to either overwhelm and thereby disarm the host immune system or to hide from the immune system [268]. However, viruses avoid early death of the host, as the virus would die as well [268]. To achieve this, viruses have several options: to directly attack proteins and cells of the immune system, to avoid detection by the immune system by masking their nucleic acids or escape detection by means of a latency phase during which only limited viral products are expressed.

Impairing PRRs, downstream adaptors and IFN signaling

Disarming the innate immune system can occur by interfering with PRRs and their downstream signaling proteins (see chapter 1.1.2). In this regard, receptors of the TLR, RLR and ALR family with their appropriate cellular adaptor proteins TRIF, MAVS and STING, respectively, are in focus of viral attacks to abolish downstream signaling and influence ISG activation.

DNA viruses, such as HSV and KSHV, predominantly perturb ALR signaling. HSV-1 promote degradation of the DNA sensor IFI16 through its E3-ubiquitin ligase Infected cell protein 0 (ICP0) [269, 270]. Thereby, HSV-1 DNA can not be recognized anymore in the nucleus. Additionally, HSV-1 encodes for ICP27 and Us11 protein inhibiting IRF3 and STAT1 activation as well as production of 2'-5' OAS, respectively [271]. By that, further downstream signaling of various PRRs is disturbed as well as production and function of ISG [271]. KSHV encodes a viral IRF1 that binds STING and prevents its phosphorylation by TBK1 inhibiting further downstream signaling [272]. Furthermore, viral IRF1 interacts with MAVS to abolish downstream signaling after recognition of its viral RNA by RLRs during replication [273]. Viral IRF1 is required for reactivation of KSHV from its latent phase [272]. Another viral protein which is required for reactivation of KSHV is Latency-associated nuclear antigen (LANA). It inhibits cGAS, a cytoplasmic DNA sensor, avoiding generation of cGAMP and subsequent activation of innate immune response [274]. Additionally, ORF52 protein (KicGAS) of KSHV inhibits cGAS through binding to cGAS and DNA [275]. This inhibits the enzymatic activity of cGAS [275] to avoid detection by the innate immune system through recognition of viral DNA.

RNA viruses, such as HCV, FluAV and Rotavirus, interfere mainly with TLR and RLR signaling. For example, HCV encodes for its own serine protease Non-structural (NS)3/4a protein which selectively cleaves MAVS (RLR-pathway) and TRIF (TLR-pathway) to interrupt two different signaling pathways [276, 277]. Cleavage of MAVS results in loss of its ability to dimerize and to signal further downstream. Another protein of HCV, NS4B, binds STING located at MAMs via a STING homology domain and abrogates IFN induction [278, 279]. A commonly studied RNA virus, FluAV, has as well several strategies to inhibit the immune system. The viral transcription process of FluAV leads to accumulation of viral 5'PPP-RNA, which would result in induction of IFN signaling. Therefore, FluAV encodes for NS1 protein which inhibits several host proteins. However, NS1 proteins differ among various FluAV strains resulting in different specificity for host proteins. In general NS1 proteins can act on three different levels of innate immunity signaling. First, NS1 binds TRIM25, the MAVS ubiquitin ligase required for release of the downstream signaling complex [102], inhibiting its multimerization which results in perturbation of RLR signaling [280, 281]. However, inhibition of TRIM25 does not necessarily hinder IRF3 activation [280]. Second, NS1 proteins of highly pathogenic FluAV strains, such as PR8 strain (H1N1) and Ud stain (H3N2), additionally inhibit IRF3 activation which is required for IFN induction [280–282]. Thereby, NS1 protein of PR8 strain inhibits IRF3 by a truncated cytoplasmic localized NS1, whereby NS1 of Ud strain binds Cleavage

and polyadenylation specificity factor (CPSF30), an essential protein for RNA export, and thereby inhibits production of IFNβ [283, 284]. Third, FluAV induces expression of SOCS3 a inhibitor of STAT activation, resulting in reduced expression of IFNβ and cytokines [285]. Rotavirus decreases IFN response by mediating degradation of IRF protein through targeting the IRF association domain which is required for dimerization [286, 287]. Moreover, Rotavirus Viral protein 3 (VP_3) has 2'-5'-phosphodiesterase activity and degrades 2'-5-oligoadenylates [288]. These are required for activation of ISG RNaseL a IFN induced RNA degradation enzyme [288].

Masking viral nucleic acids

Viral nucleic acid is the main viral structure that can be sensed by the innate immune system. Mammalian mRNA is modified on the 5'-end to enable proper RNA processing and translation. mRNA carries a cap-2 which consists of a N7-methylguanosine on the 5'-end and two methylations on the first and second ribose [176]. The cap-2-RNA is always bound to the cap-binding complex and the Eukaryotic translation initiation factor 4F (eIF4F) [289]. These are responsible for processing of RNA, such as splicing and 3'-polyadenylation, nuclear export of RNA and recruitment of the 40S ribosome in order to allow translation [289].

Viruses do not carry a cap-2 on their RNA in general but generate 5'PPP-RNA and are therefore prone to be detected by the innate immune system. Cytoplasmic 5'PPP-RNA activates RIG-I and IFIT proteins resulting in the establishment of an antiviral state in the host. Hence, viruses evolved strategies, such as utilizing cellular capping machinery, 'cap-snatching', capping with virally-encoded enzymes or cap-substitution with viral proteins, to modify their nucleic acid and to avoid detection by the innate immune system [290].

Hijacking the cellular capping machinery occurs when the cellular RNA polymerase II (RNA pol II) is used for mRNA synthesis, a situation for most of the viruses [291]. Cap-snatching occurs for FluAV in the nucleus, its site of replication, and for most other segmented (-)ssRNA viruses, such as bunyaviruses, in the cytoplasm, their site of replication [292]. FluAV cleaves the 5'-end of host mRNA including additional nucleotides by its own polymerase, which possesses endonuclease activity [293, 294]. FluAV uses this capped RNA primer for transcription of its own mRNA [293]. The now capped viral RNA looks like cellular mRNAs, cannot be sensed by PRRs and is translated by cellular ribosomes [293, 295]. Capping with virally-encoded enzymes was first identified in vaccinia virus [296]. Other non-segmented (-)ssRNA viruses encode as well for capping enzymes named L protein, such as RSV, vesicular stomatitis virus (VSV) and Dengue virus (DENV) [297–299]. Additionally, capping of RNA can occur with viral proteins instead of a cap-2. These viral cap proteins directly interacts with eIF4E, the cap-binding protein of the eIF4F complex [289, 291]. However, viral capping is not always identical to host mRNA capping, several viruses, such as RSV and Newcastle disease virus, lack the 2'-O methylation, leaving still an option for detection [297, 300].

Hiding from host detection

Another mechanism to avoid detection is by hiding from the immune system in a dormant state, also called latency [268]. Latency is known to occur during herpes viruses and human immunodeficiency virus 1 (HIV-1) infection in neuronal and T-cells, respectively [266, 301]. During latency the virus remains silent within the host and does not produce infectious particles, however, the virus can be reactivated and than transmitted [266]. To maintain latency viruses keep a small set of viral genes active to keep under the radar of the immune system. Additionally, herpes viruses integrate in the host genome to replicate together with the host cell [265]. Reactivation of HSV-1 can occur by different triggers, such as exposure to ultra violet (UV) light, fever or emotional stress [265].

1.3.2 Strategies to interfere with protein expression levels

Although viruses evolved several strategies to circumvent their host, they have to ensure that unwanted cellular proteins are not produced or immediately degraded. Influences on those steps ensure efficient replication for viruses.

Controlling the host transcription and translation machinery

The before mentioned processes for masking viral nucleic acids still require the host translation machinery. Thus, cellular mRNAs encoding antiviral proteins are transcribed as well. Thus, viruses evolved translation strategies by other means than the conventional cellular translation. Thereby, viruses can inhibiting cellular proteins responsible for initiation of cellular translation, such as eIF4E and poly(A)-binding protein (PABP) [302]. These strategies include the use of internal ribosome entry site (IRES) structures and the before described cap-substitution by viral proteins.

An IRES structure allows translation in the absence of a cap on the 5'-end and can be located everywhere within the mRNA [303]. Viruses like Hepatitis A and C virus as well as KSHV use IRES structures to promote translation of their proteins. There are also host mRNAs carrying IRES structures. This is essential in situation when translation machinery is compromised, such as during mitosis and programmed cell death [304, 305]. These cellular mRNAs include c-myc, p53, XIAP, Bcl-2 and AIFM1 [306, 307]. However, depending on the class of IRES structure (class I-IV) cellular proteins are still required for successful initiation of translation. These proteins include IRES trans-acting factors (ITAFs), eIF4G and eIF4E [290, 305]. If host translation initiation factors are inhibited, viruses need other mechanisms to recruit ribosomes and start translation. HCV circumvents the need of eIF protein through direct recruitment of ribosomes to its IRES [308].

Viruses with (+)ssRNA genome can use cap-substitution. Thereby, Viral proteins genome-linked (VPg) are covalently attached to the 5'-end of (+)ssRNA [290]. These proteins are responsible for 40S ribosome recruitment [290], and allow translation directly after release of (+)ssRNA into the cell [290]. Examples of viruses carrying VPg for translation initiation are Poliovirus and Norwalk virus [309–311].

However, when viruses performed cap-snatching, it is not beneficial to shut down the translation machinery, as viral mRNAs would be similarly affected. These viruses affect the transcription, RNA processing and nuclear export of cellular mRNAs to reduce cellular mRNAs and allow predominantly translation of viral mRNAs. Some examples for perturbing transcription are E7 protein of human papilloma virus (HPV16), which inhibits TATA-binding protein (TBP) and 3C protease of Poliovirus, which cleaves TBP [312, 313]. HSV-1 triggers the loss of serine phosphorylation in the *C*-terminal domain on RNA Pol II to shut off transcription of cellular DNA [314]. FluAV utilizes its protein PA-X to selectively inhibit host mRNA transcribed by RNA Pol II [315]. When targeting nuclear mRNA export viruses either interact with nuclear export factors, such as aforementioned NS1 protein of FluAV [316], or interfere with nuclear mRNA processing mechanisms, such as aforementioned ICP27 protein of HSV-1 [317, 318]. Both strategies aim to restrain cellular mRNAs in the nucleus and therefore avoiding their translation.

Attacking proteasome

Another option to affect protein levels is rapid degradation of unwanted proteins. In this context, proteins have to be labeled for degradation by ubiquitin ligases for the cellular proteasome machinery. KSHV targets TRIF and p53 for proteosomal degradation and thus evades from the

innate immune system [319, 320]. The half-life of TRIF is reduces through contribution of Replication and transcription activator (RTA) protein of KSHV [319]. Additionally, viral IRF1 of KSHV binds cellular Ubiquitin-specific protease 7 (USP7). USP7 inhibits p53 acetylation and results in an increased ubiquitinylation and degradation of p53 and decreases p53-mediated antiviral response [320]. Furthermore, viral IRF3 of KSHV binds the DNA-binding domain of p53 to inhibit its phosphorylation which results in destabilization [321]. By p53 destabilization uncontrolled proliferation and cell growth take place resulting in tumor formation [321].

RNA virus RSV induces ROS upon infection which would subsequently activate the KEAP1-NRF2 pathway resulting in release of NRF2 [322]. However, RSV induces NRF2 degradation via the proteasome avoiding expression of cytoprotective genes resulting in lung damage of children [322]. Furthermore, RSV NS1 protein promotes proteosomal degradation of 2'5'OAS-like protein to avoid activation of RNAseL and subsequent RNA degradation [323].

1.3.3 Strategies to interfere with cell death pathway

An ultimate step for infected cell is to enter a cell death program (suicide) to avoid spreading of the pathogen to neighboring cells [324]. Similar to other host strategies to eliminate viruses, viruses co-evolved programs to inhibit cell death mechanisms (shown in figure 1.15). In this case cells try to label themselves with 'eat me' signals, such as extracellular phosphatidylserine [231, 325], for macrophages, which would result in phagocytic clearance of infected cells. Viruses often try to avoid actively induction of early cell death as this would inhibit their replication. However, some viruses, such as FluAV, Ebola virus and HIV-1, use cell death as a means to leave the cell or to specifically target immune cells in order to weaken the immune response [326]. The induction of cell death is sometimes a matter of time, in the beginning of an infection cell death would not be beneficial as viral replication is not completed. However, it might be beneficial in later phases when viruses already replicated efficiently.

Avoiding cell death

Several viral proteins have been identified to inhibit intrinsic and extrinsic apoptosis. Often, these proteins are homologues to cellular anti-apoptotic proteins. For example, KSHV protein KSBcl-2 is a viral Bcl2-homologs [328, 329]. Additionally, KSHV encodes a vFLIP to inhibit caspase-8 and activate NF-κB and JNK/AP1 pathway [330–332]. Thus, KSHV targets various cell death pathways during infection to avoid host induced cell death and allow persistent infection. These viral proteins are involved in cell death pathways associated to mitochondria (chapter 1.2.2). Furthermore, HCV NS5A protein and KSHV K13 protein activate NF-κB to induce pro-survival genes [329]. Besides various ways to avoid apoptosis viruses evolved strategies to inhibit necroptosis, too. For example, herpes viruses encode for a viral inhibitor of RIP activation (vIRA), which binds the RHIM motif of RIPK3 and thereby inhibits polymerization of RIPK3 [333]. Several viruses, such as RSV, FluAV and KSHV, have been shown to induce increased amounts of ROS after infection which eventually causes cell death [334, 335]. The detailed mechanisms of ROS-induced cell death are largely unknown until now. However, viruses evolved strategies to overcome detrimental amount of ROS by increasing expression of SODs, such as FluAV [336].

Promoting cell death

Viruses promote cell death either to exit cells during cell lysis or to evade the immune system by killing virus-specific T-cells [337]. When inducing cell death, viruses target mitochondrial cell death

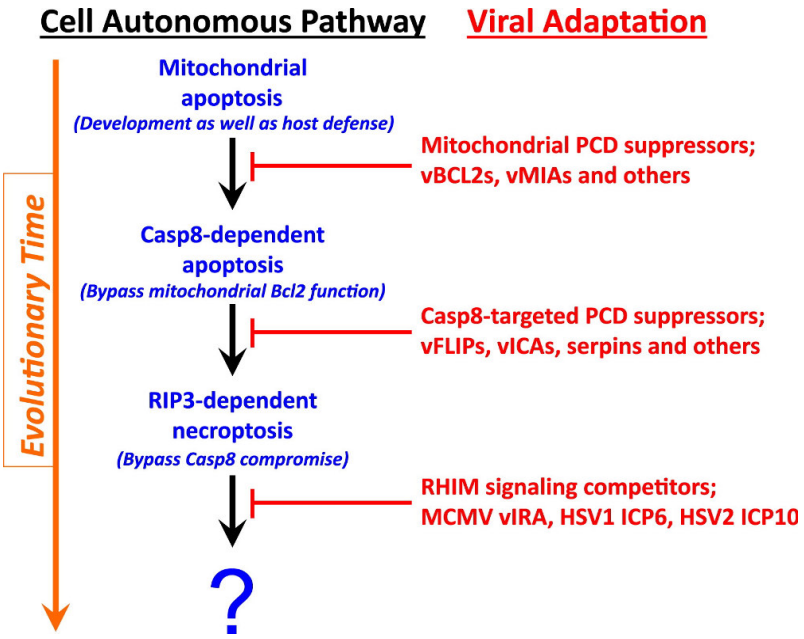

Figure 1.15: Evolutionary relationships in cell autonomous death pathways and virus-encoded countermeasures [327].

processes. For example, the Human immunodeficiency virus 1 (HIV-1) Nef protein activates the cellular pro-apoptotic Bax protein [329]. Targeting of T-cells for apoptosis was mainly shown for HIV and HCV resulting in persistent infections [268]. These viruses avoid clearance of their infected cells by promoting death of cytotoxic T-cells which are responsible cells for clearance of these infected cells.

1.4 Mass spectrometry as tool for interaction studies

Mass spectrometry (MS) is an analytical method applied to a wide range of biological questions in natural sciences. By using MS, different types of molecules can be identified, analyzed and accurately quantified. These molecules range from biomolecules, such as peptides, proteins and oligonucleotides, to chemical compounds in the field of pharmaceuticals and environmental measurements. In this chapter I will focus on the biochemical aspect of analyzing biomolecules in the field of proteins known as proteomics [338]. The main advantage of analyzing proteins instead of cellular RNA or DNA consists in identifying the functional components required for cellular reactions. Not every gene is transcribed to mRNA and not every mRNA is translated to a protein within the cell. Furthermore, increasing mRNA and proteins have different kinetics while regulation. Not only functional cellular reactions have to be understood but also properties of proteins have to be elucidated as displayed in figure 1.16.

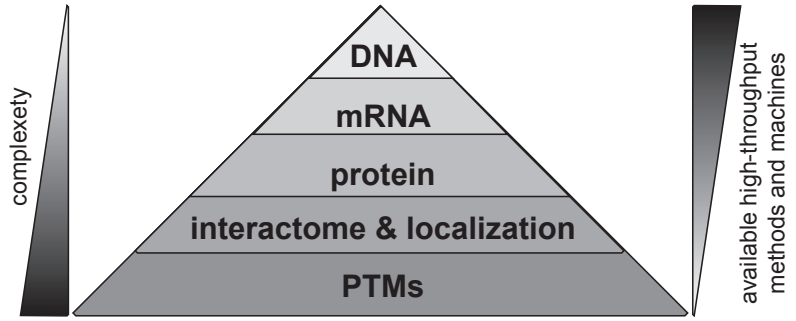

Figure 1.16: Analysis levels of functional cellular signaling networks.
The complexity of molecules increases from DNA to PTMs, whereas the available high throughput methods and machines decrease from DNA to PTM analysis.

Proteomics investigate various protein properties, such as protein-protein interactions, post-translational modifications (PTMs), expression levels, subcellular localization and structural information. The established methods for studying these properties are limited by the availability of antibodies for investigated proteins or genetically tagged proteins. Therefore, these information can nowadays be analyzed by MS with a single machine in an unbiased way. However, technical development of mass spectrometers and improvement of sample preparation are required to gain deeper data sets.

Although it does not yet provide exhaustive information, as every cell type expresses a specific subset of possible proteins and isoforms, the systematic investigation of the human proteome [339–342] represents a major achievement in proteomics. As mentioned above, it is essential to know protein levels available for cellular reactions. However, information on protein expression levels as such does not provide any hint on their functional role within the cell. The investigation of the human interactome provided further insights into cellular signaling networks [343] and has been complemented by studies on post-translational modifications of proteins allowing a much deeper understanding of functional cellular signaling networks [344–347].

The following chapter describes the principle of MS as well as various instrument parts and its experimental application for protein-protein and protein-nucleic acid interaction studies. The last part will describe the analysis of post translational modifications focusing on identification of protein phosphorylation by MS.

1.4.1 Principle of function

MS measures the mass to charge ratio of gas phase charged molecules (ions) which is used to determine the molecular mass of a sample. A mass spectrometer contains three essential parts: an ionization source, an analyzer and a detector. Mostly biological samples are neutral (uncharged) and have to be charged for MS analysis. First, the sample is charged by ionization in the ionization source before being transfered to the gas phase. The analyzer separates the ions by a magnetic or electric field according to their mass to charge ratios (m/z). Separated ions are recorded by the detector and received signals are used to identify and quantify the ions by computational methods. The whole system is kept under vacuum to enable hindrance-free flying of the ions for accurate results. The following section explains the preparation of samples including two MS approaches and the different parts of a mass spectrometer in more detail.

Top-down and bottom-up approach and sample preparation

To analyze proteins by MS two methods are available, the top-down and the bottom-up approach. Top-down approach includes the analysis of samples with simple complexity such as purified proteins. This approach allows analysis of full length proteins covering theoretically the full sequence and splice variants. In comparison, bottom-up approaches are utilized with complex samples such as cell and tissue lysates. To reduce complexity of these samples they are digested by proteases. For easy ionization the protease trypsin is used. It cleaves on the *C*-terminal side of lysine and arginine residues. Both have positive side chains enabling easy ionization and discrimination of at least double charged peptides. High pressure liquid chromatography (HPLC) allows separation of these complex peptide mixtures from cell or tissue lysates during chromatography. The resulting less complex mixtures can be measured by MS [348]. For separation of peptides in the HPLC a reverse phase material such as C18 is used. Peptides bind to C18 based on their inherent hydrophobicity allowing high resolution and reproducibility. Elution of peptides is achieved via an increasing gradient of organic solvents and therefore the analysis of small portions of the complex peptide mixture is achieved with greater resolution [348]. The ionized short peptides can now be analyzed with various analyzers.

Mass spectrometer ionization source

There are different possible ionization sources, the major ones used to analyze biomolecules are matrix assisted laser desorption ionization (MALDI) [349–351] and electrospray ionization (ESI) [352]. While MALDI ionizes samples with the help of a pulsed UV laser beam from a dry crystalline phase, ESI ionizes samples from a liquid phase [349–352]. Both discoveries and developments were recognized by the 2002 Nobel Prize in Chemistry [353]. MALDI-mass spectrometer is mainly used for low complex samples like peptides. ESI instead can be coupled to HPLC [352]. This was one of the major achievement in the MS field as now complex protein mixtures could be separated on HPLC and analyzed stepwise after ESI ionization in mass spectrometers.

Mass spectrometer analyzers and detectors

A mass analyzer is based on the principle that ions accelerate directly after the ion source and are selected and further processed in a magnetic or electric field. There are five commonly used types of mass analyzers which differ in their application: Time-of-flight (TOF), ion trap, Fourier transform ion cyclotron resonance (FT-ICR), quadrupole and orbitrap. Some mass analyzers have a detector already included, such as FT-ICR and orbitrap. The other mass analyzers require a detector. There are various types of detectors, such as continous dynode, electron multiplier and microchannel plate

[354]. Mass analyzers can be coupled together in various combinations to enable high sensitivity, resolution and mass accuracy. Coupled mass analyzers first select specific ions (precursor ions) from the incoming ions, in a second step isolate the most intense ions, fragment these (product ions) and finally analyzed their sequence. As the major MS work in this thesis was performed on a LTQ Orbitrap classic (Thermo), I explain this machine concept in more detail. A LTQ Obitrap classic (Thermo) is based on a linear ion trap analyzer coupled to an orbitrap analyzer (figure 1.17). The Orbitrap has superior mass accuracy [355] and is a major tool for proteomics [356].

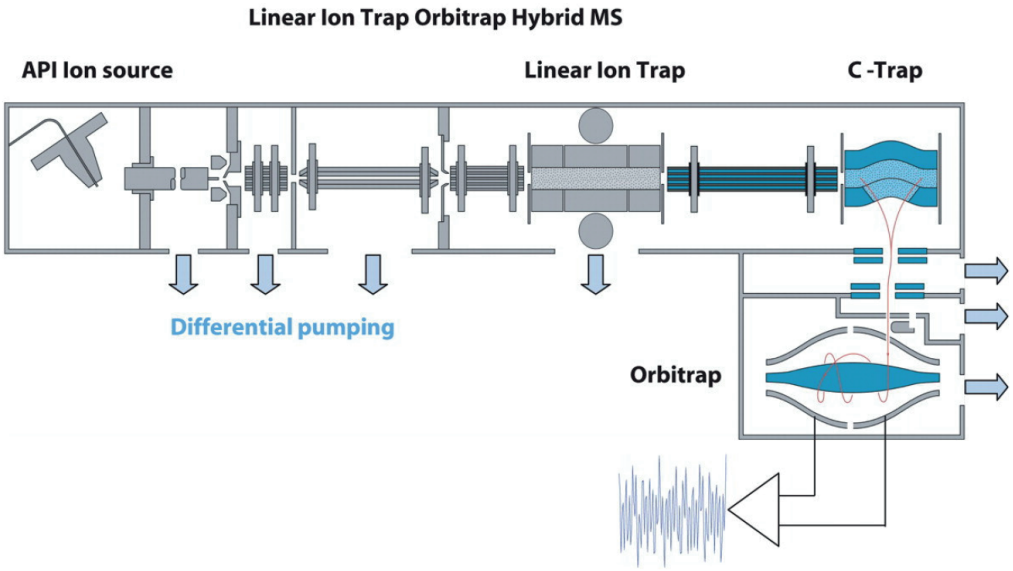

Figure 1.17: LFQ Orbitrap XL mass analyzer (adapted from [357]).

The first step (MS1 analysis) identifies the precursor ions, whereas the second step (MS2) sequences the five to ten most intense ions (TOP5-TOP10). MS1 is carried out in the orbitrap and MS2 in the linear ion trap. Incoming ions are counted within the linear ion trap and collected in a C-trap. When the required number of ions is reached, the C-trap releases these ions into the orbitrap to start the MS1 measurement. The orbitrap consists of a spindle shaped part and a surrounding shell. Within the orbitrap the precursor ions oscillation around an electric field on the spindle shaped part. Depending on their m/z they have specific oscillation tracks. When reaching consistent oscillation tracks, the orbitrap records the signals from the changes in electric current between inner spindle and outer shell. These signals are calculated to m/z by Fourier transformation. The ions are discarded. In a second step, the MS2 ions (TOP5-TOP10 depending on the chosen method) with a selected m/z from the measurement in the orbitrap are analyzed in the linear ion trap. Therefore, a limited amount of ions having a selected m/z is collected in the linear ion trap. By adding inert gas, such as helium or argon, to the highly accelerated precursor ions, these ions are fragmented [358, 359]. Commonly used methods to fragment peptides are collision induced dissociation (CID), higher-energy collisional dissociation (HCD), electron transfer dissociation (ETD) and recently developed electron-transfer and higher-energy collision dissociation (EThcD) [358–361]. Compared to CID, HCD allows recovering of low mass ions, whereas EThcD allows additionally recovering of labile modifications such as some phosphorylation sites [361]. Upon fragmentation, the received product ions are accelerated again by high voltage dynodes and are analyzed by electron multiplier detectors. The recorded signals are analog. The ions analyzed in the orbitrap and linear ion trap are

from the same peak as the peak width is around two seconds and the measurement duration is less than two seconds.

Bioinformatical analysis and quantification

Finally, the recorded m/z values are bioinformatically analyzed [362]. The identification of ions by MS depends on four criteria: (1) The sample preparation has to recover the ions; (2) The peptide has to be reasonable high abundance within the peptide mixture; (3) The ionization ability of the peptide as only ionized peptides may fly and (4) the dispersibility of the ions as only flying ions can be detected. These factors make it difficult to quantify the overall detected proteins. Therefore, several methods were developed to overcome this issue. In earlier times two-dimensional gel electrophoresis (2D gel) coupled to MS was performed whereas the 2D gel was used for quantification and MS for identification. To overcome the time consuming procedure of gels, quantifying MS methods have been developed. Thereby, absolute and relative quantification are differentiated. Absolute quantification determines protein abundance within a sample. Relative quantification compares protein amounts in different samples with each other. For both quantification methods there are labeled and unlabeled methods available. With the focus on applied methods within my thesis, there are labeled and label-free approaches for relative quantification. A labeled approach is Stable Isotope Labeling by Amino Acids in Cell Culture (SILAC) [363]. Label-free approaches are spectral counts [364] and intensity based quantification (LFQ) [365, 366]. SILAC is a metabolic labeling method, enabling the comparison of up to three samples [363]. However, to compare more samples and to avoid disadvantages of labeling, such as costs and impractical handling (animal, primary cells), label-free methods are required. Using spectral counts is very accurate when measuring large changes between proteins, however, less accurate when determining small differences. A more accurate quantification is LFQ. LFQ requires high resolution data, which is achieved by high resolution separation and high accuracy mass analyzer. Both were achieved by introducing nano-scale ultra-high performance liquid chromatography (UHPLC) and Orbitrap [355, 367]. The SILAC approach was applied in this work for measuring translation rates in virus infected mouse embryonic fibroblast (2.3), whereas the spectral count and intensity-based LFQ approach were used in the first virus-host protein interaction study publication (2.1) and in the second protein interaction study publication (2.2), respectively.

1.4.2 MS based interaction studies

The analysis of interaction partners of proteins is an important study field. It helps to elucidate pathways by studying the interaction partners and sites and analyze complexes which are formed or falling apart upon treatment or virus infection. Compared to other methods to study interactions, such as yeast two-hybrid [368, 369], phage display [370] or western blot analysis after co-immunoprecipitation (Co-IP) [371], when applying MS the whole cellular environment can be taken into account. To identify protein interaction partners various methods are established. Based on the kind of bait and the scientific question the optimal method should be chosen. To analyze interactions between cellular proteins affinity purification coupled to MS (AP-MS) or recently described affinity enrichment coupled to MS (AE-MS) can be applied [372, 373]. As modified nucleic acids produced during viral infections are not common in the cell as well as viral proteins, they are introduced into the cellular system, mainly as tagged versions. The workflow for AP-MS with nucleic acids and viral proteins is displayed in figure 1.18.

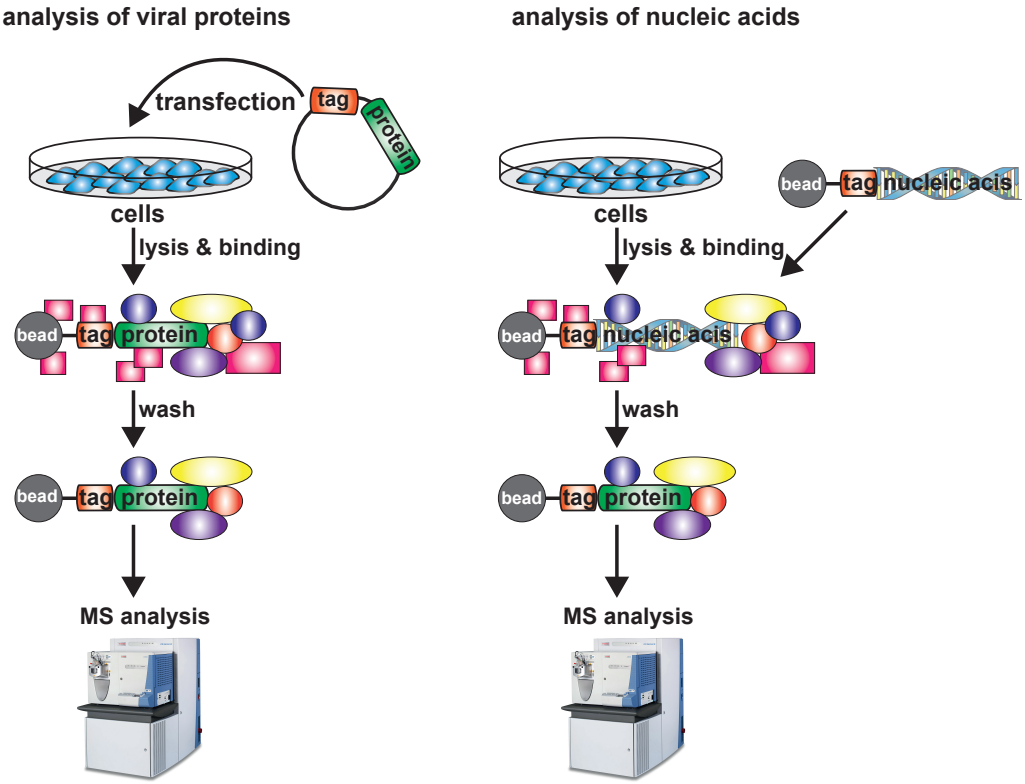

Figure 1.18: AP-MS of viral proteins and nucleic acids.
Description: For analysis of cellular interaction partners for nucleic acids, the nucleic acids are tagged and incubated with an affinity resin. After incubation unbound nucleic acids are washed away and the resin is incubated with cell lysate. Followed by several washing steps, to purify the bound complex on the affinity resin, proteins are digested by proteases, such as Lys-C and trypsin. Digested peptides are used for MS analysis. Compared to nucleic acids, viral proteins mostly can be expressed in the cell and bound after cell lysis to the affinity resin together with probably interacting proteins. This saves the preincubation step with the nucleic acids.

AP has some disadvantages: (1) Highly stringent washing steps result in loss of low affinity interaction partners. (2) The lysis of the whole cell enables proteins to bind to each other which would be normally located in separate compartments. (3) Applying AP to the study of protein-protein interactions with cellular proteins as bait, the overexpression of this bait can modify the interaction schema. (4) The introduced tag can have effects on the interaction by modulating the folding of the protein or covering interaction sites. (5) The lysis conditions have to be adjusted if membrane proteins are analyzed as they require harsher conditions [374]. (6) Finally, bioinformatical analysis after AP-MS relies on negative controls.

Nevertheless, AP has also several advantages: (1) Most importantly, when AP is coupled to MS specific binders have to be distinguishable from unspecific binders as MS is more sensitive [375]. Using tags, especially tandem tags [376], proteins can be purified in two steps eliminating false binders to one tag. (2) Additionally, tags allow high throughput preparations and all samples as well as controls are treated the in same way. (3) When performing tandem purification steps in most cases only strong interactions are recovered, thereby losing transient or weak interactions [377]. Therefore, one should consider using other affinity approaches coupled to MS, such as single purification steps or labeled samples e.g. SILAC [375]. However, single purification steps require more replicates to distinguish between specific and unspecific binders during bioinformatical analysis. To gain an

overview of these background binders the CRAPome was analyzed [378]. However, the CRAPome is not complete yet and differs for utilized mass spectrometers. Moreover it probably requires a large number of measurements to find truly non-specific binder. In the regard of elucidating true from false binders, AE-MS might be a solution. Here the sample itself acts as control.

Detection of cellular targets and influences of pathogens are important to elucidate new targets for fighting diseases. MS gives in this regard the opportunity to analyze more interactions or changes at once. However, in addition to changes of protein-protein interactions also changes of PTMs alter the function or proteins and outcome of signaling pathways.

1.4.3 Phosphorylation - a common post translational modification

PTMs are covalent modifications of proteins carried out by enzymes after protein synthesis [379]. Known PTMs on proteins are addition of phosphate groups, acetate groups, methyl groups, amide groups, ubiquitin-like moieties and carbohydrates groups, formation of disulfides as well as proteolytic cleavage [379]. Many PTMs are highly regulatory and reversible. They can affect the protein folding, stability and activity as well as the cellular localization and interaction partners. The most common experimentally observed PTM is phosphorylation [380] which was also the first described PTM [381]. Addition or removal of phosphate groups can result in alteration of enzymatic activities or binding partners. This chapter elucidates functions of PTMs with focus on phosphorylation and how they can be detected by MS.

Protein phosphorylation in eukaryotes can occur on serine, threonine and tyrosine residues (figure 1.19). These three amino acids have hydroxyl groups. Phosphorylations of protein are generated by protein kinases which are classified in three groups with respect to their substrate specificity: serine/threonine-protein kinases, tyrosine-protein kinases and dual specificity protein kinases [382].

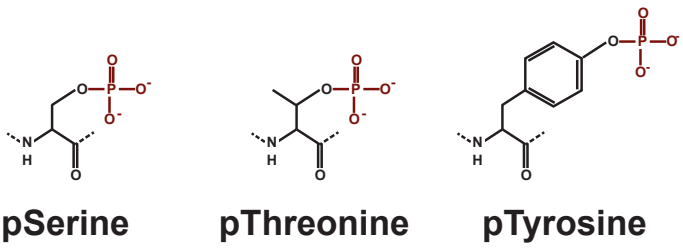

Figure 1.19: Phosphorylated amino acids.

Examples for protein phosphorylation are NF-κB which is phosphorylated by IKK [383] and STATs which are phosphorylated by JAK [384, 385]. Phosphorylation of proteins has to be tightly regulated to avoid e.g. uncontrolled activation of proteins. This activation could result in uncontrolled proliferation and cancer formation [386].

In earlier times phosphorylation of proteins was detected either by radiolabeled phosphates, 2D gels or specifically raised antibodies [387]. However, to detect specific phosphorylation sites in a proteome wide and unbiased way MS is the method of choice [388]. However, the analysis of phosphosites is not easily achieved. The three major disadvantages of MS based analysis are the low stoichiometric abundance of PTMs in general, the liability of attached phosphorylated or glycosylated groups and the modification of more than one residue within a peptide [389]. To overcome the first

issue enrichment of the modification is required for analysis. Enrichment can be achieved by antibodies, such as lysine acetylation [390], arginine methylation [345] and tyrosine phosphorylation [391] or binding to specific domains, such as *N*-glycosylation with lectins [392] and tyrosine phosphorylation with Scr homology 2 (SH2) domains [393]. A recently described method allows analysis of phosphorylated peptides after enrichment with titanium oxide (TiO_2) [394]. The second issue, losing phosphate groups while MS fragmentation could be handled by applying other fragmentation methods such as ETD and EThcD which allows unambiguous localization of phosphosites within a peptide containing more than one phosphorylated residue [360, 361].

To summarize, MS is a mainly unbiased method to start understanding cellular signaling networks by elucidating protein-protein interactions and protein modifications and how they are modified by pathogens. Additionally, MS helps in elucidating cellular components of the innate immune response in recognition of PAMPs.

1.5 Aims of the thesis

Within the last decades a broad range of pattern recognition receptors (PRRs) and downstream signaling pathways have been discovered in the field of innate immunity. Activation of PRRs is critical to successfully protect the infected host from invading pathogens. In case of viruses, PRR activation and signaling often involve mitochondria or mitochondrial associated organelles as signaling hubs. The reason for the involvement of mitochondria is currently not understand but potentially allows integration of various signals that are originating from this organelle. In this regards PRR signaling aiming at sensing of viruses and initiating the antiviral immune response could influence energy metabolism, induction of cell death or the generation/signaling of second messengers such as reactive oxygen species (ROS). It is well known that these cellular processes play an important role in cellular defense within innate immunity.

The aim of my thesis was to understand how viruses interfere with host signaling pathways to achieve their best possible replication. Thereby I took part in the validation of an AP-MS screen, shedding light on global perturbations of viruses on host's signaling pathways. Additionally, viruses produce high amounts of ROS and not much is known on subsequent downstream signaling. Thus, my main project focused on the elucidation of a ROS induced cell death pathway, which I could show was targeted by several viral proteins. I mainly focused on mitochondrial proteins in this process. Further, I investigated the consequences of this ROS signaling pathway on cellular and organismal level. Lastly, I took part in the elucidation of the nucleic sensing selectivity of human IFIT1 protein.

2 Results

This chapter includes the publications I contributed to during my PhD. The first publication elucidates how viral proteins interfere with host signaling pathways to use these pathways either for their own good or perturb them as part of interference with the innate immune signaling. The second publication identifies a new cell death pathway involved in the antiviral defense, which is targeted by several viral proteins partly identified in the first study. The last publication investigates the role of IFIT1 on sequestering viral nucleic acids and inhibit translation of these.

2.1 **Viral interference with host signaling pathways**

For successful replication, viruses have to counteract with the host defense system and utilize parts of the host replication machinery. Therefore, hundreds of studies on single viral proteins were conducted to shed light on virus-host interactions. However, to obtain a systematic view on virus-host interactions and reveal viral perturbation strategies an AP-MS based screen was performed.

By using viral open reading frames (vORFs) encoding for 70 different proteins of 30 different viruses from four taxonomic groups a broad spectrum was covered. The chosen viruses were capable to infect humans and were either (-)ssRNA, (+)ssRNA, dsRNA or dsDNA viruses. The vORFs were expressed from the same genetic locus in HEK293 cells. Bioinformatics analysis was applied to identify common and unique strategies by different viral groups to perturb the human system. Thereby, the focus was not only on virus interaction with one host protein but with the surrounding host signaling network. By this approach we identified that, compared to the average human proteins, vORFs are more connected, more central in the networks, involved in more cellular pathways and are at more central positions within these pathways. Further analysis revealed that viruses were targeting, according to their taxonomic group, pathways specifically needed for their processing and replication. This offers scientist the opportunity to detect pharmaceutical targets to interfere with viral pathogenicity.

Four host proteins targeted by viral proteins were further validated, heterogeneous nuclear ribonucleoprotein U (hnRNP-U), phosphatidylinositol-3-OH kinase (PIK3), the WNK (with-no-lysine) kinase family and ubiquitin-specific peptidase 19 (USP19). Here I contributed to the validation by siRNA based knockdowns and TCID50 measurements. Further validations of viral-host interactions and their downstream effect were also performed by other research groups [395–399]

Pichlmair A, Kandasamy K, Alvisi G, Mulhern O, Sacco R, Habjan M, Binder M, Stefanovic A, Eberle CA, Goncalves A, Bürckstümmer T, Müller AC, Fauster A, **Holze C**, Lindsten K, Goodbourn S, Kochs G, Weber F, Bartenschlager R, Bowie AG, Bennett KL, Colinge J, Superti-Furga G

Viral immune modulators perturb the human molecular network by common and unique strategies

Nature doi:10.1038/nature11289 (2012)

LETTER

doi:10.1038/nature11289

Viral immune modulators perturb the human molecular network by common and unique strategies

Andreas Pichlmair[1,2], Kumaran Kandasamy[1], Gualtiero Alvisi[3], Orla Mulhern[4], Roberto Sacco[1], Matthias Habjan[2,5], Marco Binder[3], Adrijana Stefanovic[1], Carol-Ann Eberle[1], Adriana Goncalves[1], Tilmann Bürckstümmer[1], André C. Müller[1], Astrid Fauster[1], Cathleen Holze[2], Kristina Lindsten[6], Stephen Goodbourn[7], Georg Kochs[5], Friedemann Weber[5,8,9], Ralf Bartenschlager[3], Andrew G. Bowie[4], Keiryn L. Bennett[1], Jacques Colinge[1] & Giulio Superti-Furga[1]

Viruses must enter host cells to replicate, assemble and propagate. Because of the restricted size of their genomes, viruses have had to evolve efficient ways of exploiting host cell processes to promote their own life cycles and also to escape host immune defence mechanisms[1,2]. Many viral open reading frames (viORFs) with immune-modulating functions essential for productive viral growth have been identified across a range of viral classes[3,4]. However, there has been no comprehensive study to identify the host factors with which these viORFs interact for a global perspective of viral perturbation strategies[5–11]. Here we show that different viral perturbation patterns of the host molecular defence network can be deduced from a mass-spectrometry-based host-factor survey in a defined human cellular system by using 70 innate immune-modulating viORFs from 30 viral species. The 579 host proteins targeted by the viORFs mapped to an unexpectedly large number of signalling pathways and cellular processes, suggesting yet unknown mechanisms of antiviral immunity. We further experimentally verified the targets heterogeneous nuclear ribonucleoprotein U, phosphatidylinositol-3-OH kinase, the WNK (with-no-lysine) kinase family and USP19 (ubiquitin-specific peptidase 19) as vulnerable nodes in the host cellular defence system. Evaluation of the impact of viral immune modulators on the host molecular network revealed perturbation strategies used by individual viruses and by viral classes. Our data are also valuable for the design of broad and specific antiviral therapies.

We performed a survey to identify the cellular proteins and associated complexes interacting with 70 viORFs inducibly expressed from an identical genomic locus in a human cell line (HEK293 Flp-In TREx) competent for innate antiviral programs[12,13](Fig. 1a). This set-up allowed us to gauge the expression levels of the viral proteins and to assess the formation of endogenous protein complexes under physiological conditions in human cells[14]. We selected the viORFs to cover four groups of viruses representative of ten different families and checked for their correct expression (Supplementary Figs 1, 2a–c and 3 and Supplementary Table 1)[15] and, in selected cases, immune modulatory activity (Supplementary Fig. 2d, e)[16,17]. We isolated interacting cellular proteins by tandem affinity purification (TAP) and analysed purified proteins by one-dimensional gel-free liquid chromatography tandem mass spectrometry (LC–MS/MS) (Supplementary Fig. 4a, b)[18]. The 70 viORFs specifically interacted with 579 cellular proteins with high confidence, resulting in 1,681 interactions (Fig. 1a, Supplementary Fig. 4c and Supplementary Table 1; see Methods for details). To validate our approach we assessed the impact of viral infection on the identified viORF–host-protein interactions with the use of several cognate viruses and found decreased numbers of co-purifying proteins, probably as a result of decreased cellular viability as well as competition with the tagged viORF (Supplementary Fig. 5). In addition, treatment with type I interferon (IFN) (Supplementary Fig. 4d) to simulate a host immune response had little effect on the interaction pattern of selected viORFs (Supplementary Fig. 5).

Of the 579 cellular proteins identified as interacting with the 70 viORFs, there was a strong enrichment for proteins associated with innate immunity, further validating the approach and potentially revealing additional unknown components of the host antiviral defence network (overlap with InnateDB database[19]; $P < 2.3 \times 10^{-47}$) (Supplementary Fig. 6a and Supplementary Table 2). There was also a strong enrichment for ubiquitously expressed proteins[20] ($P < 2.2 \times 10^{-138}$) and for evolutionarily conserved proteins ($P < 2.2 \times 10^{-16}$) consistent with the coevolution of virus–host relationships (Supplementary Fig. 6b–d and Supplementary Table 3).

To obtain a more comprehensive view of how viORFs influence host cell processes, we used quantitative information from the mass spectrometry data to compute the strength of impact of each viORF on its cellular targets, and used these quantitative parameters in all subsequent analyses. We also incorporated data from the human protein–protein interactome (humPPI) assembled from public databases, to analyse the protein network associated with the viORF-interacting cellular targets. We found that in comparison with an average human

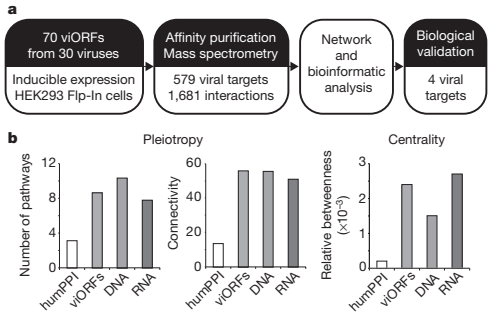

Figure 1 | Host factor survey set-up and general properties of the data set. **a**, Workflow of the host factor survey. **b**, Topological network properties of proteins identified as targets of viral proteins. The histograms compare the average property of proteins in the humPPI with the entire group of viORF interactors, or with viORFs derived from viruses with DNA and RNA genomes, respectively.

[1]CeMM Research Center for Molecular Medicine of the Austrian Academy of Sciences, 1090 Vienna, Austria. [2]Innate Immunity Laboratory, Max Planck Institute of Biochemistry, 82152 Martinsried/Munich, Germany. [3]Department of Infectious Diseases, Molecular Virology, Heidelberg University, 69120 Heidelberg, Germany. [4]School of Biochemistry and Immunology, Trinity Biomedical Sciences Institute, Trinity College Dublin, Dublin 2, Ireland. [5]Department of Virology, University of Freiburg, 79104 Freiburg, Germany. [6]Department of Cell and Molecular Biology, Karolinska Institutet, 17177 Stockholm, Sweden. [7]Division of Basic Medical Sciences, St George's, University of London, London SW17 0RE, UK. [8]Centre for Biological Signalling Studies (BIOSS), Albert-Ludwigs-Universität Freiburg, 79108 Freiburg, Germany. [9]Institute for Virology, Philipps-University Marburg, 35043 Marburg, Germany.

protein, the average viral target was distinct in four ways: it was significantly more connected to other proteins; it was in a more central network position; it participated in more cellular pathways; and it was more likely to be engaged in central positions within these pathways (Fig. 1b and Supplementary Fig. 6d, e). These properties are consistent with a strong influence on pathways and effective control of biological networks[21], which is in line with the parsimonious use of viral genetic material, and coevolution of the virus with the host organism.

Our large host-factor survey using a defined cellular set-up offers the unique opportunity to identify host-cell perturbation strategies pursued by individual viruses, families and groups. On the basis of the humPPI, 70% of the viORF-interacting cellular factors formed a coherent protein–protein interaction network (Supplementary Fig. 7a). When mapped on the entire humPPI, viral targets seemed to occupy central positions (Supplementary Fig. 7b). We also grouped the cellular targets on the basis of their interaction with viORFs from single-stranded (ss) or double-stranded (ds) RNA or DNA viruses and found that about half of the viORF targets linked to a single viral group, and the rest interacted with viruses of more than one group (Fig. 2a). Statistically significant enrichment for individual gene ontology (GO) terms, representing categories of biological processes, could be identified for each subnetwork. Proteins targeted by ssRNA(−) viORFs were enriched for processes related to protection of the viral genome and transcripts from degradation or detection by the host, and for those promoting efficient viral RNA processing (Fig. 2a). This is illustrated by the interaction between NS1 of influenza A virus (FluAV) with the 5′→3′ exoribonuclease XRN2, and among the NSs protein of Rift Valley fever virus, the mRNA export factor RAE1 and the nuclear pore complex protein NUP98. In contrast, dsRNA virus targets were enriched for protein catabolic processes (Fig. 2a) with both rotaviruses and reoviruses (NSP1 and σ3) engaging SKP1–CUL1–F-box protein complexes (containing FBXW11, Cullin-3, and Cullin-7 and Cullin-9, respectively), which mediate protein degradation.

To determine which cellular signalling pathways are targeted by viORFs and to look for differences between DNA and RNA viruses, we used the Kyoto Encyclopedia of Genes and Genomes (KEGG) annotations (Supplementary Table 4). Clear distinctions in preferences were observed between the different viral groups, with viORFs of RNA viruses targeting the JAK–STAT and chemokine signalling pathways, as well as pathways associated with intracellular parasitism, and viORFs of DNA viruses targeting cancer pathways (glioma, acute myeloid leukaemia and prostate cancer) (Supplementary Table 4). Among the viral targets that are involved in multiple cellular pathways were two catalytic and three regulatory subunits of the phosphatidylinositol-3-OH kinase family, identified with the FluAV NS1 protein and with the TLR inhibitory protein A52 of vaccinia virus (VACV) (Supplementary Fig. 8a)[4]. We functionally validated these interactions and identified a critical role for one of the catalytic subunits (PIK3CA) in TRIF-mediated IFN-β promoter activation (Supplementary Fig. 8b–d).

The higher probability of viORFs targeting cellular proteins that link different pathways (Fig. 1b and Supplementary Fig. 6d) prompted us to map which of these pathway connections were preferentially targeted and thus were probably disrupted (Fig. 2b), and to compare the disruption patterns brought about by viORFs from DNA viruses with

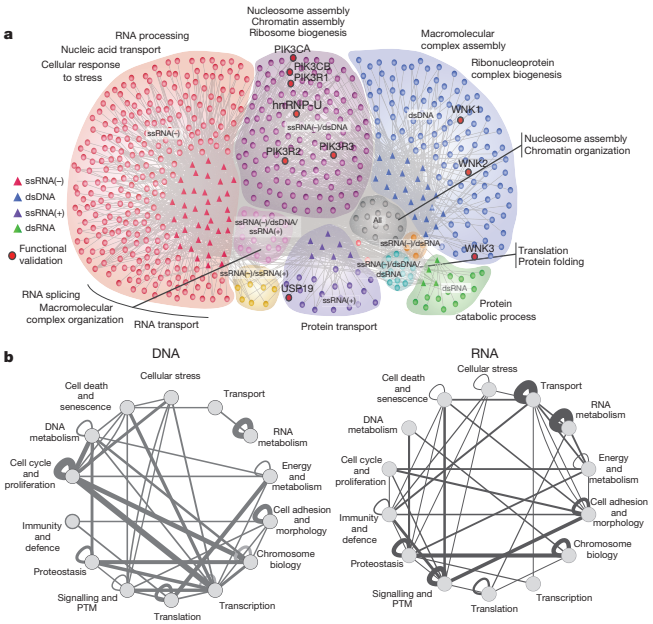

Figure 2 | Network of identified targets and network perturbation induced by viORFs. a, Network representation of all the viORF–target-protein interactions with viral targets grouped according to the genome type of the interacting viORF(s). Proteins identified in the negative control cell line were subtracted as non-specific binders. Triangles represent viORFs; circles represent viral target proteins. Protein interactions functionally validated in detail in the study are marked in dark red. Up to three GO terms significantly enriched in the corresponding viral target subsets are shown around the network to highlight specific functions. **b**, viORFs targeting one or two proteins that physically interact and are involved in one or more biological processes have the potential to perturb communication or synchronization within or between the given process(es). Significant perturbations were determined ($P < 0.001$) using targets of viORFs derived from DNA or RNA viruses; edge thickness represents a normalized perturbation score.

RESEARCH LETTER

those from RNA viruses. About one-third of the connections between specific cellular processes were hit by both viral types, suggesting a similar mechanism of perturbing the host cells. viORFs from DNA viruses preferentially targeted proteins linking the cell cycle with either transcription or chromosome biology, possibly reflecting the necessity of uncoupling viral replication from cellular growth. In contrast, RNA viruses targeted proteins involved in RNA metabolism and also protein and RNA transport, while preferentially disrupting the link between signalling and immunity-related processes (Fig. 2b).

To integrate our viORF–host-protein interaction data sets with intracellular events occurring after viral infection we compared our viORF interaction proteomic profile with the transcriptional profile obtained after infection of the cells with hepatitis C virus (HCV) (Supplementary Table 5). The protein-processing pathway in the endoplasmic reticulum (ER) (Supplementary Fig. 9a) was the most affected process. The HCV viORFs specifically targeted six ER-associated proteins. To analyse the broader implications of this targeting on the cell, we identified the cellular proteins known to bind to these six ER targets and analysed their functions bioinformatically (Supplementary Fig. 9b). Of the 80 cellular protein interactors, 42 were enriched in either cell-cycle or apoptosis functions (Supplementary Fig. 9c). Ubiquitin-specific peptidase 19 (USP19), a deubiquitinating enzyme involved in the unfolded protein response[22], interacted with the viORF NS5A. To study the biological relevance of this interaction, we analysed the localization of USP19 after HCV infection and found that it relocalized to HCV replication compartments in replicon-containing cells, probably disrupting its cellular function (Supplementary Fig. 10a, b). Indeed, NS5A inhibited the ability of USP19 to rescue destabilized green fluorescent protein (GFP) that was degraded by the proteasome (Fig. 3a). In addition, infection of cells with wild-type HCV decreased cell growth[23], whereas infection with recombinant virus lacking the NS5A–USP19 interaction site, which mapped to 50 amino acids in domain III (Supplementary Fig. 10c–g), did not (Fig. 3b and Supplementary Fig. 10h). Thus, the cell-proliferation-inhibitory properties of NS5A are probably mediated by its inhibition of USP19, which is known to promote cell growth[24], and implicates the targeting of ER-resident proteins and proteostasis as an important viral perturbation strategy.

The heterogeneous ribonucleoprotein hnRNP-U was among the most frequently targeted cellular proteins in the analysis (Supplementary Figs 11 and 12a and Supplementary Table 6) and has previously been reported to restrict growth of HIV[25]. Overexpression of hnRNP-U inhibited the polymerase activity of FluAV and the growth of vesicular stomatitis virus (VSV) (Supplementary Fig. 12b and data not shown). This inhibitory effect was alleviated by coexpression of NS1 (FluAV), establishing a functional link to hnRNP-U (Fig. 3c). We mapped the NS1 interaction site on hnRNP-U to the carboxy-terminal Arg-Gly-Gly (RGG) domain (Fig. 3d and Supplementary Fig. 12c)[26]. The RGG domain bound viral RNA in infected cells (Supplementary Fig. 12d), and an hnRNP-U mutant lacking this domain was defective in antiviral polymerase inhibition (Fig. 3e), suggesting that hnRNP-U inhibits the replication of RNA-viruses through viral RNA interaction. Collectively, the analysis highlights hnRNP-U as an important antiviral protein and a hotspot of viral perturbation strategies.

Of the 70 viORFs used in the study, only K7 of VACV[27] interacted with members of the WNK family (Supplementary Figs 11 and 13a–e and Supplementary Table 6), which are regulators of ion transport and are implicated in cancer[28]. Subsequent analyses on the potential role of this protein family in the antiviral immune response revealed that WNK1 and WNK3, but not WNK2 or WNK4, synergized with interleukin-1 (IL-1)-stimulated activation of the p38 kinase (Supplementary Fig. 13f), and activated a NF-κB reporter construct alone or in combination with IL-1 (Fig. 3f), which was inhibited by coexpression of K7 (Fig. 3g). Expression of WNK3 stimulated IL-8 production alone or in combination with IL-1 (Supplementary Fig. 13g). Short interfering RNA (siRNA)-mediated knockdown of various

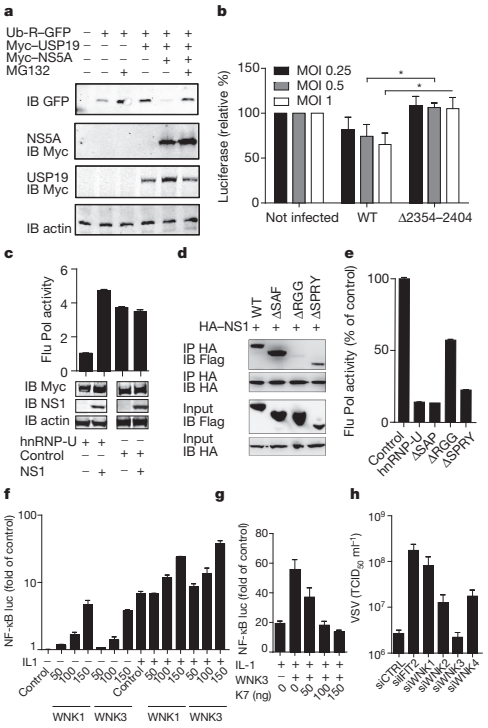

Figure 3 | Functional validation of USP19, hnRNP-U and WNK kinases as viral targets. **a**, 293T cells transfected with GFP fused to a proteasomal degradation signal (Ub-R–GFP), Myc-tagged USP19 and NS5A. MG132 was added for 6 h, and cells were analysed by immunoblotting (IB). **b**, Huh7.5 cells expressing firefly luciferase were infected with wild-type (WT) HCV or HCV lacking the USP19 interaction site (Δ2354–2404). Results are activities after 96 h (means ± s.d. for three independent experiments). Asterisk, $P < 0.025$, Student's *t*-test. MOI, multiplicity of infection. **c**, FluAV minireplicon activity in the presence of 33 ng of Myc–hnRNP-U or GRB2 (control) and 33 ng of NS1 (A/PR/8/34). Results are FluAV polymerase (Pol) activity (means ± s.d. for duplicate measurements, one representative of three). Immunoblots show protein expression (24 h). **d**, Co-immunoprecipitation of Flag–hnRNP-U and indicated mutants with HA–NS1 (A/PR/8/34). **e**, As in **c**, but for 100 ng of GFP (control) and Flag–hnRNP-U mutants (means ± s.d. for duplicate measurements, one representative of three). **f**, **g**, NFκB-luciferase (luc) activity in HEK293 cells in the presence of increasing amounts (in ng) of WNK1 and WNK3 with or without IL-1 (**f**), and K7 (**g**). Results are measurements after 24 h (means ± s.d. for triplicate experiments). **h**, HeLa cells transfected with siRNAs against WNKs and non-silencing control were infected. $TCID_{50}$, 50% tissue culture infective dose (mean ± s.d., $n = 3$).

WNK family members resulted in increased growth of VSV (Fig. 3h and Supplementary Fig. 13h). These results illustrate the value of our proteomics data set by revealing a previously unknown role for WNK kinases in the antiviral immune response.

Proteomic profiling of such a large group of viral regulators of cell function offers the opportunity to explore kinship in their mode of action and, by inference, the perturbation strategy of the viruses that encode them. We defined a notion of kinship distance by incorporating shared targets, proximity in the humPPI of non-shared targets, and their strength of interactions. viORFs from the same viral family had

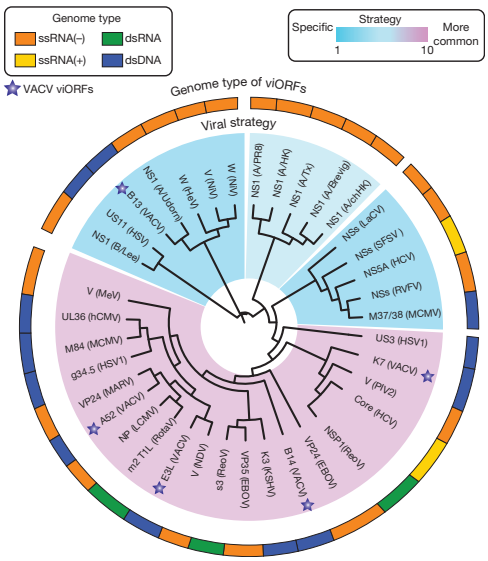

Figure 4 | Similarities of viORF actions. Dendrogram of viORF relationships based on the kinship distance, which integrates the number of shared targets and the network distance in the humPPI of the distinct targets. The virus genotype that the individual viORF derives from is shown in a colour code in the circle around the dendrogram. EBOV, Ebola virus; hCMV, human cytomegalovirus; HCV, hepatitis C virus; HeV, Hendra virus; HSV, herpes simplex virus; HSV1, herpes simplex virus 1; KSHV, Kaposi's sarcoma-associated herpesvirus; LaCV, La Crosse virus; LCMV, lymphochoriomeningitis virus; MARV, Marburg virus; MCMV, murine cytomegalovirus; MeV, measles virus; NDV, Newcastle disease virus; NiV, Nipah virus; PIV2, parainfluenza virus 2; ReoV, reovirus; RotaV, rotavirus; SFSV, sandfly fever sicilian virus. viORFs from VACV are indicated with a star.

short average kinship distances (Supplementary Fig. 14), consistent with their evolutionary relationship. Notable exceptions were viORFs from paramyxoviruses, which had an average distance even larger than randomized viral target profiles, possibly reflecting a particularly pleiotropic mechanism of action. We generated a dendrogram that showed the kinship distance of the individual viORFs as a proxy for the perturbation strategy of the cognate virus (Fig. 4). Roughly half of the viORFs clustered in a central, rather dense part of the tree, reflecting overlapping strategies, whereas the other half was more distant, probably indicating more unique targeting strategies. Many clusters represented viORFs from evolutionarily related viruses, which are more likely to exercise comparable perturbation strategies. For example, most influenza A virus NS1 proteins and all NSs proteins from bunyaviruses clustered together. A few viORFs did not cluster according to their genome group, which was evocative of some degree of evolutionary convergence with the proteins of other viruses on shared pathways, or more distinctive routes of action, possibly as part of a combined attack with another ORF of the same virus. This is best illustrated by the five viORFs from VACV, which were found scattered in the tree and were likely to have evolved to fulfil specific, complementary functions.

Our results demonstrate that viruses have evolved to exploit a variety of cellular mechanisms, and suggest that the host cell relies on the proper homeostatic regulation across these diverse cellular processes to detect, alert to and counteract pathogen interference. In addition, the study provides a rationale for considering or excluding the targeting of specific intracellular pathways for pan-viral or virus-specific antiviral therapy.

METHODS SUMMARY

Complementary DNA of tandem affinity-tagged viORFs was amplified by polymerase chain reaction and cloned into the pTO-SII-HA-GW vector by using Gateway recombination (Invitrogen). The resulting plasmids were used to generate hygromycin-selected stable isogenic HEK293 Flp-In TREx cell lines, and viORF expression was stimulated by doxycycline[12]. Protein complexes isolated by tandem affinity purification using Strep-II and haemagglutinin (HA)-affinity reagents were analysed by LC–MS/MS with an LTQ Orbitrap XL, an LTQ Orbitrap Velos or a QTOF mass spectrometer. The data were searched against the human SwissProt protein database, using Phenyx and Mascot. The humPPI was generated using public interaction databases. Recombinant HCVs (strain JC1) with mutations in domain III of NS5A were generated by transfecting full-length genomic RNA with targeted deletions in the NS5A region. Subcellular localization of proteins was performed on a Leica SP2 confocal microscope. The influenza virus replicon assay was performed as described previously[12].

Full Methods and any associated references are available in the online version of the paper at www.nature.com/nature.

Received 5 September 2011; accepted 7 June 2012.
Published online 18 July 2012.

1. Watanabe, T., Watanabe, S. & Kawaoka, Y. Cellular networks involved in the influenza virus life cycle. *Cell Host Microbe* **7,** 427–439 (2010).
2. Goff, S. P. Host factors exploited by retroviruses. *Nature Rev. Microbiol.* **5,** 253–263 (2007).
3. Finlay, B. B. & McFadden, G. Anti-immunology: evasion of the host immune system by bacterial and viral pathogens. *Cell* **124,** 767–782 (2006).
4. Bowie, A. G. & Unterholzner, L. Viral evasion and subversion of pattern-recognition receptor signalling. *Nature Rev.* **8,** 911–922 (2008).
5. Jager, S. *et al.* Global landscape of HIV–human protein complexes. *Nature* **481,** 365–370 (2012).
6. Shapira, S. D. *et al.* A physical and regulatory map of host–influenza interactions reveals pathways in H1N1 infection. *Cell* **139,** 1255–1267 (2009).
7. Uetz, P. *et al.* Herpesviral protein networks and their interaction with the human proteome. *Science* **311,** 239–242 (2006).
8. Krishnan, M. N. *et al.* RNA interference screen for human genes associated with West Nile virus infection. *Nature* **455,** 242–245 (2008).
9. Brass, A. L. *et al.* Identification of host proteins required for HIV infection through a functional genomic screen. *Science* **319,** 921–926 (2008).
10. Konig, R. *et al.* Human host factors required for influenza virus replication. *Nature* **463,** 813–817 (2010).
11. Karlas, A. *et al.* Genome-wide RNAi screen identifies human host factors crucial for influenza virus replication. *Nature* **463,** 818–822 (2010).
12. Pichlmair, A. *et al.* IFIT1 is an antiviral protein that recognizes 5′-triphosphate RNA. *Nature Immunol.* **12,** 624–630 (2011).
13. Li, S., Wang, L., Berman, M., Kong, Y. Y. & Dorf, M. E. Mapping a dynamic innate immunity protein interaction network regulating type I interferon production. *Immunity* **35,** 426–440 (2011).
14. Cravatt, B. F., Simon, G. M. & Yates, J. R. III. The biological impact of mass-spectrometry-based proteomics. *Nature* **450,** 991–1000 (2007).
15. Randall, R. E. & Goodbourn, S. Interferons and viruses: an interplay between induction, signalling, antiviral responses and virus countermeasures. *J. Gen. Virol.* **89,** 1–47 (2008).
16. Schmolke, M. & Garcia-Sastre, A. Evasion of innate and adaptive immune responses by influenza A virus. *Cell. Microbiol.* **12,** 873–880 (2010).
17. Rodriguez, J. J., Wang, L. F. & Horvath, C. M. Hendra virus V protein inhibits interferon signaling by preventing STAT1 and STAT2 nuclear accumulation. *J. Virol.* **77,** 11842–11845 (2003).
18. Glatter, T., Wepf, A., Aebersold, R. & Gstaiger, M. An integrated workflow for charting the human interaction proteome: insights into the PP2A system. *Mol. Syst. Biol.* **5,** 237 (2009).
19. Lynn, D. J. *et al.* InnateDB: facilitating systems-level analyses of the mammalian innate immune response. *Mol. Syst. Biol.* **4,** 218 (2008).
20. Burkard, T. R. *et al.* Initial characterization of the human central proteome. *BMC Syst. Biol.* **5,** 17 (2011).
21. Albert, R., Jeong, H. & Barabasi, A. L. Error and attack tolerance of complex networks. *Nature* **406,** 378–382 (2000).
22. Hassink, G. C. *et al.* The ER-resident ubiquitin-specific protease 19 participates in the UPR and rescues ERAD substrates. *EMBO Rep.* **10,** 755–761 (2009).
23. Arima, N. *et al.* Modulation of cell growth by the hepatitis C virus nonstructural protein NS5A. *J. Biol. Chem.* **276,** 12675–12684 (2001).
24. Lu, Y. *et al.* USP19 deubiquitinating enzyme supports cell proliferation by stabilizing KPC1, a ubiquitin ligase for $p27^{Kip1}$. *Mol. Cell. Biol.* **29,** 547–558 (2009).
25. Valente, S. T. & Goff, S. P. Inhibition of HIV-1 gene expression by a fragment of hnRNP U. *Mol. Cell* **23,** 597–605 (2006).
26. Hasegawa, Y. *et al.* The matrix protein hnRNP U is required for chromosomal localization of Xist RNA. *Dev. Cell* **19,** 469–476 (2010).

RESEARCH LETTER

27. Schroder, M., Baran, M. & Bowie, A. G. Viral targeting of DEAD box protein 3 reveals its role in TBK1/IKKepsilon-mediated IRF activation. *EMBO J.* **27,** 2147–2157 (2008).
28. Moniz, S. & Jordan, P. Emerging roles for WNK kinases in cancer. *Cell. Mol. Life Sci.* **67,** 1265–1276 (2010).

Supplementary Information is linked to the online version of the paper at www.nature.com/nature.

Acknowledgements We thank C. Basler, A. Bergthaler, K.-K. Conzelmann, A. Garcia-Sastre, M. Hardy, W. Kaiser, E. Mühlberger, R. Randall, B. Roizman, N. Ruggli, B. Sherry and T. Wolf for providing viral ORF cDNAs; P. Jordan for providing WNK expression constructs; S. Nakagawa for Flag-hnRNP-U; M. Sophie-Hiet for GFP-NS5A; M. Zayas for the pFK-Jc1-NS5A-HA expression plasmid; E. Rudashevskaya, A. Stukalov, F. Breitwieser and M. Trippler for support; H. Pickersgill and T. Brummelkamp for critically reading the manuscript; C. Baumann for discussions; and M. Vidal for discussions and for sharing unpublished information. The work was funded by the Austrian Academy of Sciences, an i-FIVE European Research Council grant to G.S.-F., a European Molecular Biology Organization long-term fellowship to A.P. (ATLF 463-2008), Science Foundation Ireland grant 07/IN1/B934 to O.M. and A.G.B., Deutsche Forschungsgemeinschaft grants We 2616/5-2 and SFB 593/B13 to F.W., Ko1579/5-1 to G.K., and FOR1202, TP1 to R.B., and the German Ministry for Education and Research (Suszeptibilität bei Infektionen: HCV; TP1, 01KI 0786) to R.B. J.C. is funded by the Austrian Ministry of Science and Research (GEN-AU/BIN).

Author Contributions A.P., G.A., O.M., R.S., M.H., M.B., A.S., C.A.E., A.G., A.C.M., A.F., C.H., S.G., F.W. and G.K. performed experiments. A.P. and G.S.-F. conceived the study. A.P., G.A., R.B., A.G.B. and G.S.-F. designed experiments. K.K., A.C.M., K.L.B. and J.C. performed mass spectrometry and bioinformatic data analysis. T.B., K.L., S.G., G.K., F.W., R.B. and A.G.B. provided critical material. All authors contributed to the discussion of results and participated in manuscript preparation. A.P., K.K., J.C. and G.S.-F. wrote the manuscript.

Author Information The protein interactions from this publication have been submitted to the IMEx consortium (http://imex.sf.net) through IntAct (identifier IM-17331). Mass spectrometry data are available at http://inhibitomev1.sf.net; microarray data were deposited in ArrayExpress (accession number E-MTAB-1148). Reprints and permissions information is available at www.nature.com/reprints. The authors declare no competing financial interests. Readers are welcome to comment on the online version of this article at www.nature.com/nature. Correspondence and requests for materials should be addressed to G.S.-F. (gsuperti@cemm.oeaw.ac.at).

METHODS

Plasmids, viruses and reagents. Expression constructs were generated by PCR amplification of viORFs followed by Gateway cloning (Invitrogen) into the plasmids pCS2-6myc-GW, pCMV-HA-GW and pTO-SII-HA-GW. pCAGS-Flag-hnRNP-U and mutants thereof were provided by S. Nakagawa. Ub-R–GFP and Myc–USP19 were published previously[22]. pHA-PIK3R2 was from Oliver Hantschel. GFP–NS5A domain mutants were published previously[30]. Recombinant HCV variants with mutations in domain III of NS5A were generated by replacing the NS5A fragment in pFK-Jc1-NS5A-HA, containing the full-length HCV chimaeric Jc1 genome[31] in which a HA tag is inserted in frame within NS5A and in pFK-JcR-2a containing *Renilla* luciferase fused amino-terminally with the 16 N-terminal amino-acid residues of the core protein and C-terminally with the foot-and-mouth disease 2A peptide coding region, enabling direct quantification of viral replication by measuring *Renilla* luciferase activity[32]. All viruses were produced by transient transfection of Huh7.5 cells with RNA transcribed *in vitro*. Recombinant RVFV (Rift valley fever virus)[33] expressing tandem affinity-tagged (GS-TAG) versions of NSs proteins were generated by replacing the RVFV NSs open reading frame with GS-tagged versions of NSs that were generated by PCR amplification. The FluAV minireplicon system to measure FluAV polymerase activity[34], IFN-β–luciferase, NF-κB-luciferase and the *Renilla* luciferase control plasmid (pRL-TK; Promega) were described previously[35].

Streptavidin beads were from IBA (Strep-Tactin agarose); HA–agarose (clone HA7) was from Sigma. Antibody against β-tubulin (anti-β-tubulin; clone DM1A) was from Abcam, anti-β-actin (catalogue number AAN01) was from Cytosceleton. IRDye-conjugated anti-c-Myc (catalogue number 600-432-381) and anti-rabbit (catalogue number 611-732-127) secondary reagents were from Rockland. Alexa Fluor 680-conjugated goat anti-mouse (catalogue number 10524963) were from Molecular Probes. Reagents for quantitative RT–PCR were from Qiagen. Poly(dA)•poly(dT) were from Sigma and transfected with Lipofectamine 2000 (Invitrogen) or Polyfect (Qiagen). Stimulatory PPP-RNA was described previously[12]. MG132 was from Sigma. IFN-β and IFN-α2a were from PBL Interferonsource. Tumour necrosis factor-α and IL-1β were from Pierce. IL-8 was measured by enzyme-linked immunosorbent assay (BD). Lymphochoriomeningitis virus (Armstrong strain), FluAV (A/PR/8/34), VSV (Indiana strain) and VSV-M2 (mutant VSV with M51R substitution of the matrix protein, leading to IFN-α/β induction; originally called AV3) have been described previously[12]. Virus titres were measured by determining the half-maximal infectious dose ($TCID_{50}$) on Vero cells, or on Huh7.5 cells for HCV.

Cells, co-immunoprecipitations and imaging. HEK293 Flp-In TREx cells that allow doxycycline-dependent transgene expression were from Invitrogen. HEK293, 293T, HeLa S3 (ref. 12), Lunet, Lunet-Neo-sgNS5A(RFP), Huh7/5.2 and Huh7.5 cells have been described previously[30]. Highly permissive Huh7.5 or Huh7.5 FLuc, stably expressing firefly luciferase introduced by lentiviral transduction[32], were used for HCV infection experiments. Fibroblasts were kept in DMEM medium (PAA Laboratories) supplemented with 10% (v/v) FCS (Invitrogen) and antibiotics (100 U ml^{-1} penicillin and 100 μg ml^{-1} streptomycin). For inducible transgene expression, HEK293 Flp-In TREx cells were treated for 24–48 h with doxycycline (1 μg ml^{-1}), depending on cellular density to just about reach confluence. For siRNA-mediated knockdown, if not stated otherwise in figure legends, 5 nmol of siRNA pool (Supplementary Table 7) was mixed with HiPerfect (Qiagen) and added to 10^5 HeLa S3 cells. After 48 h, cells were used for experiments. For co-immunoprecipitations 293T cells were transfected with expression plasmids for 24–48 h and lysates were used for affinity purification in TAP buffer[12] using anti-HA–agarose or anti-c-Myc-coated beads. For protein detection in western blot analysis a Li-Cor infrared imager was used. Confocal images were acquired with a Leica SP2 confocal microscope.

Affinity purification, mass spectrometry and transcriptome analysis. HEK293 Flp-In TREx cells and isolation of protein complexes by TAP and peptide analysis by LC–MS/MS have been described previously[18]. Proteins identified by this method can be found in a complex but do not necessarily bind directly to each other. In brief, five subconfluent 15-cm dishes of cells were stimulated with 1 μg ml^{-1} doxycycline for 24–48 h. Protein complexes were isolated by TAP using streptavidin agarose followed by elution with biotin, and a second purification step using HA–agarose beads. Proteins were eluted with 100 mM formic acid, neutralized with triethylammonium bicarbonate (TEAB) and digested with trypsin, and the peptides were analysed by LC–MS/MS [36]. For bunyavirus NSs proteins, recombinant viruses[33] containing GS-tagged NSs proteins were generated. Protein complexes were denatured in Laemmli buffer[37] and separated by one-dimensional SDS–PAGE; entire lanes were excised and digested *in situ* with trypsin and the resultant peptides were analysed by LC–MS/MS. Mass spectrometric analysis was performed for gel-free and gel-based samples, respectively, on a hybrid LTQ Orbitrap XL, an LTQ Orbitrap Velos mass spectrometer (both from ThermoFisher Scientific) or on a quadrupole time-of-flight mass spectrometer (QTOF Premier; Waters) coupled to an 1100/1200 series high-performance liquid chromatography system (Agilent Technologies). Data generated by LC–MS/MS were searched against the human SwissProt protein database (v. 2010.09, plus appended viral bait proteins) with Mascot (v. 2.3.02) and Phenyx (v. 2.6). One missed tryptic cleavage site was allowed. Carbamidomethyl cysteine was set as a fixed modification, and oxidized methionine was set as a variable modification. A false-positive detection rate of less than 1% on the protein groups was imposed (Phenyx *z*-score more than 4.75 for single peptide identifications, *z*-score more than 4.2 for multiple peptide identifications; Mascot single peptide identifications ion score more than 40, multiple peptide identifications ion score more than 14).

To measure gene expression, Huh7/5-2 cells were left uninfected or infected with HCV (strain JC1) at a MOI of 5, and RNA was isolated using Trizol (Invitrogen) after 4, 12, 24, 48 and 72 h. Gene expression analysis was performed in duplicate using an Affymetrix platform (Affymetrix Human Genome U133A 2.0 Array).

Bioinformatic analysis. Data filtering. All proteins identified in the GFP negative controls (51 proteins) were removed.

Data normalization. Affinity-purification MS experiments were performed with two biological replicates and two technical replicates for each; that is, four replicates. We first normalized individual replicates according to the NSAF procedure[29]. The replicates of each viORF normalized data element were then assembled in a table with 0 for missing detection, and each viral target was assigned the average NSAF value across the replicates. On the basis of a robust estimate (MAD) of the coefficient of variation (Supplementary Fig. 15a) we further penalized highly variable targets by applying a reduction factor between 1 (modest variability) and 0.5 (high variability) (Supplementary Fig. 15b). Direct normalization through a division by the standard deviation was excluded because of the limited number of replicates available. For a given viORF *v* and a viral target *p*, the weight given to the interaction *v*–*p* was hence computed as

$$\text{strength}_{v,p} = \text{mean}(\text{NSAF}_{v,p,i})\text{reduction}[\text{CV}(\text{NSAF}_{v,p,i})]$$

where *i* accounts for the replicates. The distribution of strength values is shown in Supplementary Fig. 15c.

Human interactome. We integrated human physical protein–protein interactions (humPPI) obtained from public databases (IntAct, BioGRID, MINT, HPRD and InnateDB[19]) and thereby obtained an interactome (largest connected component) comprising 13,350 proteins and 90,292 interactions.

Human central proteome. A list of commonly expressed human proteins was assembled by merging a previous study[20] with mapped (orthologues) mouse proteins found in the intersection of six mouse tissues[38] and genes expressed in all except four or fewer tissues from SymAtlas. The resulting list included 4,276 proteins and is provided as Supplementary Table 8.

Network topological measures. We retained two classical measures: the connectivity (degree)—that is, the number of interactions of one protein in the PPI—and the relative betweenness centrality, which is equal to the relative number of shortest paths between any two proteins that go through a given protein.

MS-weighted measures. To compute a weighted characteristic of the targeted host proteins, for example connectivity in the human PPI, of one viral modulator *vm* we used

$$\text{weighted\_connectivity}(vm) = \sum_{p \in \text{T}(vm)} \alpha_p \text{connectivity}(p)$$

where T(*vm*) is the set of all human proteins targeted by *vm*; α_p were proportional to the estimated interaction strength, and sum to 1. When the same viral modulator was considered in several viruses (for example NS1 of FluAV), we computed the weights for each interacting protein taking the maximum of the strengths found in different viruses to avoid any bias by over-represented viral modulators; that is, $\alpha_p \propto \max_{v \in \text{NS1\_viruses}} \text{strength}_{v,p}$. Null distributions were generated by assigning actual weights to random proteins 10,000 times, thereby obtaining a histogram of 10,000 random weighted characteristics, which was fitted with a gamma distribution to estimate *P* values (Supplementary Fig. 15d).

Weighted functional annotation analysis. We performed GO and KEGG pathways analysis integrating the interaction strengths of viORF targets by summing all the above normalized (sum equal to 1) α_p weights found in a GO term or a pathway to obtain a score. This score was then compared with a null distribution modelled by a gamma fit on 1,000 random scores to estimate a *P* value. Random scores were obtained by assigning the weights to random proteins and summing those that fell in the GO term or pathway.

Perturbation map and relative position along a pathway. These two computations were performed in accordance with published methods[20]. Pathways were taken from NCI-PID[39], and the perturbation map algorithm (GO fluxes in ref. 20) was modified to use the interaction strengths between viORFs and their targets as weights in scoring interaction between GO terms instead of constant weights. For simplification, GO terms were reduced to 14 categories (Supplementary Table 9).

RESEARCH LETTER

Perturbation map null distributions were obtained with 250 randomized annotated networks that respected the original network connectivity distribution and GO term frequencies.

Distance of viORFs. Given two viORFs x and y, the distance $d(x,y)$ is defined as follows. Let S be the union of all x and y targets, D_x the targets unique to x, and D_y those unique to y. A preliminary distance c is computed by summing all the human interactome shortest path distances from individual targets in D_x and D_y with the targets unique to the other viORF, considering interaction strengths to penalize differences on strong different targets and minimize the impact of weaker distinct targets. Thus,

$$c = \sum_{a \in D_x} \text{strength}_{x,a} \times \text{shortest}(a,D_y) + \sum_{a \in D_y} \text{strength}_{y,b} \times \text{shortest}(b,D_x)$$

Finally, c is normalized to take into account the number of distinct targets compared with the total number of targets: $d(x,y) = c(|D_x \cup D_y|)/|s|$, where $|...|$ denotes set cardinality—that is, the number of elements.

The random distance distributions were obtained as follows: for each viORF, its targets were replaced by a random selection of the same number of proteins from the humPPI such that the same pairs of (random) distances could be computed. The overall procedure was repeated 100 times and in the case of the HEK293 selection the human proteins randomly chosen were restricted to the humPPI and to proteins identified by mass spectrometric analysis of the HEK293 proteome[20].

29. Zybailov, B. *et al.* Statistical analysis of membrane proteome expression changes in *Saccharomyces cerevisiae*. *J. Proteome Res.* **5,** 2339–2347 (2006).
30. Appel, N. *et al.* Essential role of domain III of nonstructural protein 5A for hepatitis C virus infectious particle assembly. *PLoS Pathog.* **4,** e1000035 (2008).
31. Pietschmann, T. *et al.* Construction and characterization of infectious intragenotypic and intergenotypic hepatitis C virus chimeras. *Proc. Natl Acad. Sci. USA* **103,** 7408–7413 (2006).
32. Reiss, S. *et al.* Recruitment and activation of a lipid kinase by hepatitis C virus NS5A is essential for integrity of the membranous replication compartment. *Cell Host Microbe* **9,** 32–45 (2011).
33. Habjan, M., Penski, N., Spiegel, M. & Weber, F. T7 RNA polymerase-dependent and -independent systems for cDNA-based rescue of Rift Valley fever virus. *J. Gen. Virol.* **89,** 2157–2166 (2008).
34. Dittmann, J. *et al.* Influenza A virus strains differ in sensitivity to the antiviral action of Mx-GTPase. *J. Virol.* **82,** 3624–3631 (2008).
35. Keating, S. E., Maloney, G. M., Moran, E. M. & Bowie, A. G. IRAK-2 participates in multiple Toll-like receptor signaling pathways to NFκB via activation of TRAF6 ubiquitination. *J. Biol. Chem.* **282,** 33435–33443 (2007).
36. Haura, E. B. *et al.* Using iTRAQ combined with tandem affinity purification to enhance low-abundance proteins associated with somatically mutated EGFR core complexes in lung cancer. *J. Proteome Res.* **10,** 182–190 (2010).
37. Burckstummer, T. *et al.* An efficient tandem affinity purification procedure for interaction proteomics in mammalian cells. *Nature Methods* **3,** 1013–1019 (2006).
38. Kislinger, T. *et al.* Global survey of organ and organelle protein expression in mouse: combined proteomic and transcriptomic profiling. *Cell* **125,** 173–186 (2006).
39. Schaefer, C. F. *et al.* PID: the Pathway Interaction Database. *Nucleic Acids Res.* **37,** 674–679 (2009).

2.2 Cell death as host response to viral infections

Viruses have been shown to produce increased amount of ROS which can have detrimental effects when reaching a certain threshold. Cells promote their own cell death upon high amounts of ROS to save the organism from DNA mutations and malfunction proteins. However, as viruses require a host for replication they try to avoid its early cell death. Various cell death pathways are inhibited to a certain extent by different viruses. This highlights the importance of cell death for the immune response of an organism to reduce viral load. To elucidate in detail how ROS is sensed by the cell and subsequently induces cell death I investigated the downstream signaling of a known ROS sensor, KEAP1.

By identifying KEAP1 as required protein in ROS mediated cell death I performed AP-MS with KEAP1 as bait to identify interactors involved in cell death. By revealing an interaction between KEAP1 and cell death associated protein PGAM5 as well as between PGAM5 and cell death executing protein AIFM1 I could describe a new cell death pathway which is triggered upon ROS. Additionally, I characterized a new phosphorylation site on AIFM1 serine 116 which was only described in MS based phosphoproteomic approaches before, being targeted by PGAM5 upon ROS and viral infections. The importance of this pathway is highlighted by the fact that this pathway is targeted by at least five viral proteins from viruses of different viral families. Furthermore, one of the proteins, PGAM5, is required for viability upon viral infection of the ROS inducing virus influenza A (strain SC35M) *in vivo*. These mouse experiments were performed in cooperation with Peter Staeheli in Freiburg.

This study reveals that viruses target among the commonly known cell death pathways also this newly identified pathway. This supports not only the investigation in the field of virus based immunology but could also be helpful for further clinical applications in the field of cancer and transplantations, as ROS is induced in both leading either to no cell death or to unwanted cell death, respectively.

Holze C, Haas DA, Hubel P, Benda C, Leung DW, Amarasinghe GK, Staeheli P, Pichlmair A

A ROS-induced cell death pathway through KEAP1, PGAM5 and AIFM1 is involved in antiviral defense

Cell host and microbe submitted manuscript (2016)

A ROS-induced cell death pathway through KEAP1, PGAM5 and AIFM1 is involved in antiviral defense

Cathleen Holze[1], Darya A. Haas[1], Philipp Hubel[1], Christian Benda[2], Daisy W. Leung[3], Gaya K. Amarasinghe[3], Peter Staeheli[4] and Andreas Pichlmair[1]

[1]Innate Immunity Laboratory, [2]Department of Structural Cell Biology, Max-Planck Institute of Biochemistry, Martinsried/Munich, 82152, Germany, [3]Department of Pathology and Immunology, Washington University School of Medicine, St Louis, MO 63110, USA, [4]Institute of Virology, University of Freiburg, Freiburg, Germany

Corresponding author:

Andreas Pichlmair, PhD, DVM
Innate Immunity Laboratory
Max-Planck Institute of Biochemistry
Am Klopferspitz 18
82152 Martinsried/Munich, Germany
Email: apichl@biochem.mpg.de
Telephone: +49 89 8578 2220

Abstract

Reactive oxygen species (ROS) are generated under physiological conditions as well as in the course of infection with pathogens. It is only marginally understood how cells distinguish physiological ROS levels from pathological ROS levels to either initiate protective gene expression or induce cell death, respectively. Here we show that KEAP1 serves as a bi-active regulator that protects cells from low levels of ROS but flips its activity to mediate cell death through a caspase independent mechanism. This cell death pathway involves the serine/threonine protein phosphatase phosphoglycerate mutase family member 5 (PGAM5), which dephosphorylates mitochondrial Apoptosis inducing factor 1 (AIFM1). Proteins derived from distantly related viruses target KEAP1, PGAM5 and AIFM1, suggesting evolutionary convergence of pathogens to modulate this pathway and emphasizing its importance for antiviral immunity. Indeed, cells derived from *Pgam5* deficient mice show impaired cell death induction after infection with influenza A virus. This inability translates into severe disease in *Pgam5* deficient mice challenged with influenza A virus.

Our work shows that besides its life-saving activities, KEAP1 plays a central role in activating a signaling cascade that leads to cell death. This pathway is operational in many cell types and plays a critical role in physiological and pathological conditions. Indeed, this cell death pathway attributes to an antiviral strategy which is targeted by several viruses and proposes that it is constituting an important line of defense against infectious diseases.

Introduction

Reactive nitrogen and oxygen species (RNS and ROS) such as H_2O_2, $.O_2$ and .OH are generated as natural by-products of the normal oxygen metabolism. ROS play an important role in cell signaling by regulating cell proliferation and survival (Nakamura Hajime et al., 1997; Suzuki et al., 1997; Sauer Heinrich et al., 2001). Intracellular ROS are produced during physiological processes, such as oxidative phosphorylation, fatty acid β-oxidation, photorespiration, nucleic acid and polyamine catabolism and ureide metabolism (Sandalio et al., 2013). However, increased protein folding load, elevated fatty acid oxidation and energy metabolism can result in pathological accumulation of ROS in the endoplasmic reticulum, peroxisomes and mitochondria (Shimizu Yuichiro and Hendershot Linda M., 2009; Rosca et al., 2012; Sandalio et al., 2013). Since ROS can cause irreversible conformational changes on proteins and lipids as well as DNA mutations (Lü et al., 2010) several enzymatic and non-enzymatic mechanisms evolved to protect cells from detrimental accumulation of ROS.

A main intracellular sensor that continuously monitors ROS levels is Kelch-like ECH-associated protein 1 (KEAP1), which is primarily known for its ability to regulate expression of cytoprotective genes during oxidative stress (Taguchi et al., 2011). Under physiological conditions KEAP1 ubiquitinates and degrades the transcription factor Nuclear Factor-E2-related factor 2 (NRF2), a regulator of cytoprotective gene expression. Increase of ROS leads to oxidation of cysteine residues in KEAP1, resulting in its conformational change and the inability to mediate NRF2 ubiquitination and degradation. NRF2 accumulates and translocates into the nucleus to regulate expression of genes with promoters containing antioxidant response elements (AREs), such as NAD(P)H dehydrogenase (quinone 1) (NQO1), heme oxygenase (decycling) 1 (HOX1) and thioredoxin (TXN) (Song et al., 2002; Zhang and Hannink, 2003; D'Autréaux and Toledano, 2007; Kaspar et al., 2009; Bryan et al., 2013). Permanent or high oxidative stress levels however, do not induce sufficient expression of cytoprotective proteins and can result in considerable cell damage or cell death (Circu and Aw, 2010).

Exogenous stimuli such as ultraviolet light (UV), heat or inflammatory cytokines have been shown to increase intracellular ROS that contribute to the severity of pathological disorders (Yang Dongli et al., 2007; Uttara et al., 2009; Hroudová et al., 2014). Furthermore, infection with viruses can increase intracellular ROS levels due to perturbation of the cellular metabolism (Li et al., 2007; Ano et al., 2010). However, in case of virus infection, ROS-induced cell death can contribute to limit virus spread and dissemination (Olagnier et al., 2014). In case of persistent virus infection, ROS contribute to organ damage and exacerbate disease progression. Intriguingly, some viruses evolved mechanisms to avoid detrimental ROS functions in order to promote cell survival, thus facilitating viral proliferation. For instance, Dengue virus (DENV) (Olagnier et al., 2014), Human herpes virus 8 (HHV-8) (Bottero et al., 2013) and Encephalomyocarditis virus (EMCV) (Ano et al., 2010) evolved distinct mechanisms to modulate ROS-mediated cell death pathways for their own benefit. Conversely, other viruses, such as Marburg virus (MARV), specifically perturb stress responses by promoting cytoprotective programs (Edwards et al., 2014).

Despite the apparent importance of ROS in physiological and pathological processes, relatively little is known about their sensors and downstream signaling pathways that lead to cell death in response to oxidative stress. It is known that ROS-induced cell death can involve caspase dependent as well as caspase independent mechanisms. We hypothesized on the existence of devoted proteins that link ROS sensing to execution of cell death. Such proteins would be of central importance for a wide range of diseases.

Results

Caspase independent ROS-induced cell death via KEAP1

High levels of ROS are produced by various cellular processes and can be induced by exogenous stimuli such as cytokines and infection with pathogens. To mimic high ROS levels, we exogenously added hydrogen peroxide (H_2O_2) to HeLa or Jurkat T-cells. As expected, this treatment induced cell death. The pan-caspase inhibitor Z-VAD-FMK was not able to rescue the cells, suggesting a caspase independent process (Fig 1A). A dedicated intracellular sensor that directly links H_2O_2 sensing to cell death is currently not known. However, a well-known sensor of ROS is KEAP1, which changes its conformation after ROS engagement and releases NRF2 to regulate expression of cytoprotective genes in order to counterbalance oxidative stress (Kobayashi et al., 2004). We aimed to establish an assay that allows us studying cells with different sensitivity towards ROS treatment. We transiently depleted KEAP1 in HeLa cells and tested cell survival rates upon treatment with cytotoxic doses of H_2O_2. As expected, KEAP1 depleted cells showed significantly less cell death after treatment with high amounts of H_2O_2 as compared to control cells (Fig 1B). Previous studies have shown that KEAP1 depletion triggers increased expression of cytoprotective genes through stabilization of NRF2. Surprisingly, co-depletion of KEAP1 and NRF2, which we expected to increase sensitivity towards H_2O_2 treatment, also rescued cells from H_2O_2 induced cell death (Fig 1B). Control experiments indicated successful depletion of NRF2, ruling out de novo transcription of cytoprotective genes through NRF2 (Fig 1B, C). Indeed, expression of cytoprotective genes was comparable in KEAP1/NRF2 and control knockdown cells (Fig 1C). Altogether these data suggested that KEAP1 plays an active role in a ROS-dependent, caspase-independent cell death pathway and that depletion of KEAP1 protects from ROS-induced cell death in an NRF2-independent manner.

KEAP1 utilizes PGAM5 to induce ROS-induced cell death

We next sought to identify potential interaction partners of KEAP1 that could convey signals leading to cell death. Using affinity purification followed by tandem mass spectrometry (AP-LC-MS/MS) we identified 32 proteins significantly enriched in KEAP1 purifications as compared to an unrelated control protein (Fig 1D). Among these 32 proteins were14 known binding partners of KEAP1 (Fig 1D, brown dots), including NRF2. Only a single protein was previously associated with cell death pathways: mitochondrial serine/threonine protein phosphatase phosphoglycerate mutase family member 5 (PGAM5) (Fig 1D, green dot). PGAM5 has previously been identified as a convergence point of multiple necrotic death pathways and has been shown to be involved in ROS-induced cell death (Wang et al., 2012). PGAM5 bears an *N*-terminal mitochondrial localization signal and a transmembrane domain. Furthermore, PGAM5 interacts with KEAP1to tether it to the mitochondrial membrane (Lo and Hannink, 2006). We validated association of KEAP1 and PGAM5 by co-immunoprecipitation of StrepII-HA-tagged (SII-HA) KEAP1 with endogenous PGAM5 (Fig 1E) and confirmed the amino acids 69 to 89 of PGAM5 as critical residues for its KEAP1 interaction (Supplementary Fig 1) (Lo and Hannink, 2006).

To functionally assess whether PGAM5 is involved in ROS-mediated cell death we next used siRNA-mediated knockdown of PGAM5 and tested for cell survival after graded doses of H_2O_2 treatment. At high levels (0.5mM) of H_2O_2 control cells died, whereas cells lacking PGAM5 showed more than 60% survival (Fig 2A). Depletion of PGAM5 has been reported to result in NRF2-dependent gene expression (Lo and Hannink, 2008), which could lead to protective effects against ROS-induced cell death after PGAM5 knockdown. Interestingly, as already observed for KEAP1 knockdown, co-depletion of PGAM5 and NRF2 also rescued cells from H_2O_2 induced cell death (Fig 2B), suggesting a direct involvement of PGAM5 in ROS-induced cell death, independent of NRF2-driven expression of cytoprotective genes.

KEAP1 releases NRF2 after exposure to ROS. We therefore tested whether the interaction between KEAP1 and PGAM5 may be similarly regulated by ROS levels. Indeed, in the presence of 0.5 mM H_2O_2, binding of KEAP1 to PGAM5 was significantly reduced (Fig 2C). Importantly, low levels of H_2O_2, which do not result in induction of cell death (Fig 1B, 2A), did not affect the interaction between KEAP1 and

PGAM5 (Fig 2C). KEAP1 and PGAM5 localize to mitochondria under steady state conditions (Fig 2D) (Lo and Hannink, 2008). However, in the presence of 0.5 mM H_2O_2, only KEAP1 loses mitochondrial association, whereas PGAM5 remains associated to mitochondrial structures (Fig 2D). Collectively, these data suggest that the ROS sensor KEAP1 is binding to PGAM5 under steady state conditions and that this association is lost in the presence of oxidative stress.

Cell death induction through AIFM1

PGAM5 has previously been proposed to be of central importance to transmit cell death signals (Wang et al., 2012); however both its molecular partners and the mechanistic details governing these interactions are not known. To identify proteins that associate with PGAM5, and may be involved in downstream signaling, we performed AP-LC-MS/MS using PGAM5 as bait. We identified 8 high confidence interactors that showed specific enrichment in PGAM5 as compared to control precipitates (Fig 3A). As expected, PGAM5 associated with KEAP1 (Fig 3A, brown dot). Furthermore, PGAM5 co-precipitated proteins of the Translocase of the inner membrane (TIM) complex (TIMM50, TIMM8A and TIMM13) which facilitates the transport of proteins to the inner mitochondrial membrane (Ceh-Pavia et al., 2013). Only HCLS1-associated protein X-1 (HAX1) and Apoptosis inducing factor 1 mitochondrial (AIFM1) were previously associated with cell death pathways (Fig 3A, green dots). While HAX1 was shown to inhibit caspase-3 and -9 and has been involved in activation of pro-survival, cytoprotective programs (Simmen, 2011), AIFM1 has previously been implicated in caspase-independent cell death (Susin et al., 1999). Thus, AIFM1 represented an ideal effector to mediate ROS-induced cell death downstream of PGAM5. We validated the PGAM5 - AIFM1 interaction by co-precipitation followed by western blotting and LUMIER assays (Fig 3B, C). AIFM1 mutants that lacked the *N*-terminal MLS and TM domain (AIFM1 Δ2-103) lost PGAM5 association while *C*-terminal truncations of AIFM1 did not affect PGAM5 binding (Fig 3C). Intriguingly, binding of AIFM1 to PGAM5 was reduced when cells were treated with H_2O_2 (Fig 3D). Binding could be rescued by the ROS-scavenger N-acetylcysteine (NAC) (Fig 3D), suggesting involvement of this interaction in ROS-modulated cellular processes.

To test whether AIFM1 serves as a downstream target of PGAM5, we depleted HeLa cells for AIFM1 or PGAM5 and monitored for cell survival after stimulation with H_2O_2 or the mitochondrial ROS-inducer tert-Butylhydroquinone (tBHQ). As expected, control cells were highly sensitive to H_2O_2 and tBHQ treatment. Notably, cells that were depleted for AIFM1 or PGAM5 exhibited superior survival rates after H_2O_2 and tBHQ treatment (Fig 3E). Similar results were obtained upon H_2O_2 treatment in the neuroblastoma cell line SKN-BE2 (Fig 3F), suggesting that PGAM5-AIFM1-dependent signaling is operating in multiple cell types.

PGAM5 dephosphorylates AIFM1 on S116

PGAM5 was previously reported to possess serine/threonine-protein phosphatase activity (Wang et al., 2012), and several studies have shown that processed substrates often lose interactions with their modifying enzymes (Carpino et al., 2004; Lo and Hannink, 2006; Mikhailik et al., 2007; Sadatomi et al., 2013). To identify the molecular mechanism regulating PGAM5-AIFM1 interaction, we initially assessed whether the phosphorylation status of AIFM1 itself was critically required for PGAM5 binding. To this end, we repeated the AIFM1-PGAM5 co-precipitation and intentionally omitted phosphatase inhibitors during the whole affinity purification procedure. Notably, binding between PGAM5 and AIFM1 was significantly reduced in the absence of phosphatase inhibitors, hinting towards a requirement of phosphorylated residues for efficient interaction (Fig 4A). To decipher further the functional implications of PGAM5 enzymatic activity on PGAM5-AIFM1 interaction, we next performed structure-guided mutagenesis of PGAM5 (Chaikuad, A., Alfano, I., Picaud, S., Filippakopoulos, P., Barr, A., von Delft, F., Arrowsmith, C.H., Edwards, A.M., Weigelt, J., Bountra, C., Takeda, K., Ichijo, H., Knapp, S., 2010), Supplementary Fig S2A) to generate a phenylalanine 244 to aspartic acid mutant (F244D) that cannot dimerize (Supplementary Fig S2B) and is therefore predicted to lose phosphatase activity (Wilkins et al., 2014). SII-HA-tagged wt PGAM5 and a transmembrane domain deleted version (PGAM5Δ2-29) precipitated from HEK293T cells showed phosphatase activity when incubated with a phospho-serine peptide (Fig 4B). However, precipitated PGAM5[F244D] was inactive in this assay (Fig 4B). Based on

these results, we generated highly purified His-tagged PGAM5Δ2-28 and PGAM5Δ2-28[F244D] for further functional experiments (Fig 4C) and verified integrity of the recombinant proteins (Supplementary Fig S2C-E). Size exclusion chromatography confirmed homodimer formation of PGAM5Δ2-28 in a F244D dependent manner (Fig 4D). We tested both recombinant proteins for their ability to dephosphorylate peptides bearing phosphorylated threonine and serine residues. PGAM5Δ2-28 was able to release phosphates from phospho-serine but not when phospho-threonine peptides were used as a substrate (Fig 4E). PGAM5Δ2-28[F244D] was inactive (Fig 4E), confirming specificity in this assay. Additional evidence for specific phosphatase activity was obtained through phosphatase inhibitors. PGAM5-dependent dephosphorylation could be inhibited by the phosphatase inhibitor sodium orthovanadate (Van), but not by sodium fluoride (NaF) (Fig 4E). Collectively these data suggest that PGAM5 preferentially dephosphorylates serine residues.

To identify residues in AIFM1 that may be a target of PGAM5 and are required for the interaction between both proteins, we selected one threonine and three serine residues in the *N*-terminal region of AIFM1 that were reported three or more times at phosphosite.org. We mutated these residues to alanine and tested the ability of the resulting constructs to co-precipitate with endogenous PGAM5. Mutation of AIFM1 serine 116 to alanine (S116A) impaired binding to PGAM5, whereas other residues did not affect PGAM5 association (Fig 4F). Sequence alignment analysis revealed a remarkable conservation for AIFM1 S116 and surrounding amino acid residues within mammals (Fig 4G, Supplementary Fig S3A). Particularly interesting in this region are two glutamic acid residues located three and five amino acids *C*-terminal of S116 which contribute negative charges to this region (Fig 4G, Supplementary Fig S3A). Such contribution of negative charges has been reported to support binding of substrates to the positively charged phosphatase active site of PGAM5 (Wilkins et al., 2014), further pointing to AIFM1 phospho (p) S116 as potential target of PGAM5 phosphatase activity. A custom raised antibody against pS116 of AIFM1, indicated that AIFM1 S116 is phosphorylated under steady state conditions (Fig 4H, Supplementary Fig S3B). Strikingly, treatment of cells with H_2O_2 led to pS116 dephosphorylation,

indicating that a dynamic regulation of pS116-AIFM1 during oxidative stress (Fig 4H). Moreover, recombinant PGAM5Δ2-28 spiked into cell lysates led to AIFM1 pS116 dephosphorylation, suggesting that PGAM5 directly targets AIFM1 S116 (Fig 4I). In agreement with the phosphatase inhibitor sensitivity of PGAM5 (Fig 4E), this process could be inhibited with vanadate, while sodium fluoride had no effect. Additionally, the PGAM5Δ2-28[F244D] mutant protein did not exhibit dephosphorylation activity on AIFM1 pS116, further confirming pS116 as a specific PGAM5 substrate (Fig 4I).

In sum, these data indicate that AIFM1 pS116 is dephosphorylated during oxidative stress and that PGAM5 has the ability to mediate this dephosphorylation.

Virus interference with KEAP1-PGAM5-AIFM1 pathway

Induction of cell death is an effective mechanism to limit virus spread and is an essential part of the cellular defense system against viruses. However, premature induction of cell death is not in the interest of viral pathogens and many viruses therefore actively interfere with cell death pathways. Recently, we conducted a mass spectrometry based interaction screen using as baits viral proteins that are associated with viral pathogenicity (Pichlmair et al., 2012). Mining this dataset revealed four viral proteins from segmented (La Crosse Virus (LaCV) and non-segmented negative strand (-)ssRNA viruses (Marburg virus, Measles virus) and a DNA virus (Human Herpes virus-8 (HHV-8)) that interacted with either KEAP1, PGAM5 or AIFM1 (Fig 5A). In additional AP-LC-MS/MS experiments using the Non-structural protein 2 (NS2) of Respiratory syncytial virus (RSV) (non-segmented (-)ssRNA virus) as bait we identified AIFM1 as a cellular target (Fig 5A, B). These interactions are functionally relevant, as evidenced by recent studies that showed that VP24 of Marburg virus disrupts KEAP1-NRF2 binding to initiate transcription of NRF2 regulated genes (Edwards et al., 2014; Page et al., 2014). We proceeded to also functionally test interactors of K3 (HHV-8) and PGAM5. AP-LC-MS/MS and co-immunoprecipitation experiments using K3 as bait confirmed the interaction between PGAM5 and K3 (Fig 5C, D). Binding of PGAM5 to K3 required amino acids 29-69 in PGAM5 (Supplementary Fig S4A), a region that has previously been identified to be important for full PGAM5 functionality (Wilkins et al.,

2014). This prompted us to test the activity of PGAM5 in the presence of K3. Precipitates of PGAM5 from cells co-expressing K3 showed reduced phosphatase activity (Fig 5E), confirming a functional interaction between PGAM5 and K3. We further validated interactions between viral proteins and AIFM1 by co-immunoprecipitation and LUMIER assay. AIFM1 co-precipitated with Non-structural protein small (NSs) of LaCV (Fig 5A, F, G) and NS2 of RSV (Fig 5A, B, H). Further analysis of the binding region in AIFM1 needed for interaction with NS2 revealed requirement of amino acids 2-55 (Supplementary Fig 4B), which are also mandatory for PGAM5 interaction (see Fig 3C). Collectively, these data indicate that distantly related viruses, such as DNA and ssRNA viruses, share their ability to bind KEAP1, PGAM5 or AIFM1, suggesting evolutionary pressure to target this pathway.

Influenza A virus infection triggers PGAM5-dependent cell death

Viruses are well known for their ability to induce elevated levels of ROS (Gonzalez-Dosal et al., 2011; Bottero et al., 2013), which could lead to ROS-mediated cell death. We used influenza A virus as model virus that, to our knowledge, does not modulate the activity of KEAP1, PGAM5 and AIFM1. HeLa cells infected with Influenza A virus (FluAV; strain SC35M) induced accumulation of intracellular ROS (Fig 6A) and expression of cytoprotective genes that are under control of the transcription factor NRF2 (Fig 6B). FluAV infection led to reduced AIFM1 pS116 levels as compared to uninfected cells (Fig 6C), indicating activation of PGAM5 after virus infection.

To study the involvement of PGAM5 in virus induced cell death we used mouse embryonic fibroblasts (MEF) generated from *Pgam5* deficient mice (Fig 6D). To first establish that PGAM5 is also required for ROS-induced cell death in mice, we treated MEFs with H_2O_2 and studied cell survival. As expected, H_2O_2 treatment led to cell death of wild-type ($Pgam5^{+/+}$) and heterozygous ($Pgam5^{+/-}$) MEFs (Fig 6E). However, Pgam5 knockout MEFs ($Pgam5^{-/-}$) showed higher resistance to H_2O_2 (Fig 6E). To analyze the involvement of PGAM5 in cell death after treatment with a ROS inducing pathogen, we infected MEFs with FluAV. Remarkably, *Pgam5* deficient cells showed superior survival after infection with FluAV, compared to wt and heterozygous control cells (Fig 6F).

Altogether these data demonstrate that the KEAP1-PGAM5-AIFM1 signaling pathway is conserved among species and leads to a cell death process initiated in response to virus infections.

Lack of Pgam5 *in vivo* renders mice highly susceptible to FluAV infection

Targeting of KEAP1-PGAM5-AIFM1 by viral pathogenicity factors and the dynamic regulation of AIFM1 S116 phosphorylation during virus infection suggested that these cellular proteins play an important role in antiviral immunity. To test this, we used *Pgam5* deficient mice to study virus pathogenicity in the absence of this pathway *in vivo*. *Pgam5* knockout mice bred to normal Mendelian ratio and, unlike suggested recently (Moriwaki et al., 2016), showed no sex-dependent weight differences (data not shown). We infected wild-type (wt, $Pgam5^{+/+}$), heterozygous ($Pgam5^{+/-}$) and homozygous ($Pgam5^{-/-}$) knockout mice with 1,500 pfu of FluAV. Infections at this dose of FluAV only caused 10% mortality in wt and heterozygous ($Pgam5^{+/-}$) mice (Fig 6G). In contrast, *Pgam5* deficient mice showed a markedly increased mortality rate since 78% of animals succumbed to FluAV infection until the end of the experiment at 14 days after infection (Fig 6G).

Collectively, these experiments suggest that PGAM5 is important to protect from virus infection *in vivo* and highlights sensing of ROS as protective antiviral strategy.

Discussion

Frequently cells have to make critical decisions how to respond to physiological and pathological levels of ROS. Increased levels of ROS initiate protective mechanisms that aim to minimize damage induced by oxidative stress. Pathogens, inflammatory cytokines and other environmental cues can raise ROS levels to pathological concentrations, which is eventually detrimental to cells (Medvedev et al., 2016; Ren et al., 2016).

It is well established that oxidative stress can critically contribute to cell death via RIP3 kinase signaling or caspase-dependent pathways (Shindo et al., 2013; Alfonso-Loeches et al., 2014; Okinaga et al., 2015). In the presence of caspase inhibitors or in RIP3 kinase deficient systems, oxidative stress still induces cell death suggesting the existence of additional caspase independent pathways. However, it is currently not clear how intracellular ROS levels are sensed in the cell and at what stage a decision whether to live or die is made. A well-established ROS sensor is KEAP1 that mediates ubiquitination and degradation of the transcription factor NRF2, a known regulator of cytoprotective genes. After ROS-mediated oxidation of cysteine residues in KEAP1, NRF2 is released and mediates expression of a cytoprotective transcriptional program. Surprisingly, KEAP1 and NRF2 co-depletion renders cells more resistant to ROS treatment suggesting the existence of a cell death pathway regulated by KEAP1. Using AP-LC-MS/MS approaches we identified PGAM5 as only cell-death related protein binding to KEAP1. PGAM5 has been proposed to function on a convergence point of multiple caspase-independent cell death pathways (Wang et al., 2012). Notably, cell death stimuli reported to signal through PGAM5, such as TNF-α, H_2O_2, t-butyl hydroxide (TBH) and A23187, have all been shown to generate intracellular ROS (Kajitani Noriko et al., 2007; Blaser et al., 2016). Therefore, the ability of PGAM5 to integrate many diverse cell death signals may to large extend be attributed to its involvement in ROS-dependent cell death signaling. After oxidative stress, KEAP1 loses its mitochondrial localization and its ability to interact with PGAM5, which resides in the mitochondria after ROS treatment. Therefore, similar to the regulation of NRF2 activity, PGAM5 appears to be released from KEAP1 upon reaching a specific oxidative stress threshold. ROS levels

required to perturb the interaction between PGAM5 and KEAP1 are much higher than those required to perturb NRF2 and KEAP1. This difference likely explains the dual character of KEAP1 to regulate cell protection at low levels of ROS, through the release of NRF2 followed by expression of cytoprotective genes, while mediating the induction of cell death, through the release of PGAM5 at high levels of oxidative stress. Such threshold models are well known as regulatory mechanisms in biology and are essential to regulate diverse cellular functions ranging from cell cycle progression to neurotransmission (Edgar et al., 2014; Olson et al., 2016).

Signaling downstream of PGAM5 to induce cell death remained enigmatic. AP-LC-MS/MS analysis identified AIFM1 as a PGAM5 binding partner. Although AIFM1 has been linked to ROS-dependent cell death induction, its regulation has so far remained unclear (Joza et al., 2001). We identified S116 in AIFM1 as critical residue that is changing its phosphorylation status upon treatment with H_2O_2 or after virus infection. Here we show that recombinant PGAM5 is able to dephosphorylate AIFM1 pS116 in cell lysates, indicating a functional role for this protein-protein interaction.

Based on these data we propose the existence of a caspase-independent cell death pathway that consists of KEAP1-PGAM5-AIFM1 and is relevant for ROS-induced cell death. KEAP1 has been reported to be tethered to the outer membrane of mitochondria through PGAM5 engagement (Lo and Hannink, 2008). Conversely, the same mechanism could mediate retention of PGAM5 at the outer mitochondrial membrane in order to spatially dissociate it from its phosphatase target AIFM1, which is localized in mitochondria. PGAM5 translocation into mitochondria could be mediated through the engagement of TIMM8/-13 that are known to be involved in regulating protein import into mitochondria. Release of PGAM5 by KEAP1 during oxidative stress may be part of an activation process that allows internalization of PGAM5 into the mitochondria in order to dephosphorylate its target AIFM1. However, additional signals are required to induce cell death since KEAP1 depletion alone is not detrimental to cells.

Imbalanced ROS levels have been linked to various diseases such as viral infections. Indeed, FluAV induces ROS and cell death through PGAM5 *in vitro*. On organismal level, PGAM5 is important to control pathogenicity of influenza virus, since *Pgam5* deficient mice are highly susceptible to FluAV infection. This clearly indicates a prominent protective function of PGAM5 in antiviral immunity against fulminant virus infections. However, PGAM5 activation may be disadvantageous during persistent virus infection. In this case, virus induced cytokines mediate increased ROS levels followed by liver damage (Bhattacharya et al., 2015), a pathway likely operating through PGAM5. Additional evidence for PGAM5 being involved in antiviral immunity comes from multiple distinct viruses that evolved mechanisms to target KEAP1, PGAM5 or AIFM1 (Fig 5A). This pathway may not only be important for antiviral immunity but could also be involved in other diseases, such as cancer. Cancer cells are known for their high basal levels of ROS (Szatrowski and Nathan, 1991). Additional stimulation by ROS-inducing agents or viral infection, such as used in oncolytic viral therapy, may fuel this ROS-dependent cell death pathway. Notably, it has been shown that treatment of tumors with ROS-inducing agents such as BZL101, an extract of the plant *Scutellaria barbatae*, induces cell death in an AIFM1-dependent manner (Marconett et al., 2010). HHV-8 as the causative agent for Karposi's sarcoma could, in principle, impair the ability to execute such a cell death program through the activity of its K3 protein.

Our study identified a cell death pathway that is of central importance for multiple diseases that are functionally related by their involvement with altered ROS levels. Similar to viral interference with KEAP1, PGAM5, or AIFM1, we propose that targeting this pathway through therapeutic intervention may constitute a means to modulate disease progression.

Author Contributions

C.H. conducted the experiments, C.B. performed structural analysis, D.A.H. and P.H. were analyzing data, P.S. designed and conducted the mouse infections. A.P. and C.H. designed the experiments and wrote the paper.

Acknowledgements

We want to acknowledge the innate immunity laboratory for critical discussions and suggestions, Angelika Mann for technical assistance, the MPI-B core facility for technical assistance with protein purification, analysis and imaging. We further thank Mark Wilson and ECM bioscience for raising the AIFM1 pS116 antibody, Korbinian Mayr, Igor Paron and Gaby Sowa for maintaining mass spectrometers, Silvana Kaphengst and the MPI-B animal facility for breeding mice. This work was supported by the Max-Planck Free Floater program to AP, the German research foundation (PI 1084/2) to AP and an ERC starting grant (ERC-StG iVIP, 311339) to AP.

Figure legends

Figure 1. ROS induced cell death induction through KEAP1

(A) Viability of HeLa and Jurkat cells after hydrogen peroxide (H_2O_2) treatment. Cells were left untreated or treated with 20 μM Z-VAD-FMK for 2 h, followed by 21 h treatment with 0.5 mM hydrogen peroxide (H_2O_2). Cell titers were determined by Resazurin-based cell viability assay. The plot shows the mean ± S.D. of six individual treatments. One representative experiment of three is shown. **(B)** as in (A) but HeLa cells were transfected with siRNAs against KEAP1, KEAP1 and NRF2 or control (siScr). The plot shows the mean ± S.D. of four individual treatments. One representative experiment of six is shown. Knockdown efficiency was confirmed by western blotting against indicated proteins (right panel). **(C)** Expression of NRF2 regulated target genes after siRNA mediated knockdown of KEAP1, KEAP1 and NRF or siScr in HeLa cells 48 h after siRNA treatment. **(D)** Proteins enriched by affinity purification using as baits SII-HA-tagged KEAP1 and THYN1 as control (ctrl) expressed in HeLa FlpIn cells. Associated proteins were analyzed by LC-MS/MS. Volcano plots show the average degree of enrichment by KEAP1 over control (ratio of label-free quantitation (LFQ) log 2 transformed protein intensities; x-axis) and –log 10 transformed p-values (t-test; y-axis) for each identified protein. Significantly enriched proteins (FDR < 0.00001, s0 100) are separated from background proteins by a hyperbolic curve (dotted line). Red dot: KEAP1, brown dots: known KEAP1 interactors (based on Biogrid), green dot: protein associated with cell death. Four independent affinity purifications (AP) were performed for both baits. **(E)** Binding of PGAM5 to KEAP1. Western blot analysis of precipitates after affinity purification (AP) with SII-HA-KEAP1 or SII-HA-THYN1 (ctrl).

Figure 2. Functional interaction of KEAP1 and PGAM5 during oxidative stress

(A, B) Viability of PGAM5 knockdown in HeLa cells after H_2O_2 treatment. Cells were treated with siPGAM5 or siScr for 48 h, followed by 21 h treatment with the indicated concentrations of H_2O_2. Cell titre was determined by Resazurin-based viability assay. The plot shows the mean ± S.D. of four

individual treatments. One representative experiment of six is shown. Knockdown efficiency was confirmed by western blotting against indicated proteins 48 h after knockdown (right panel). **(B)** as in (A) but siRNAs against PGAM5, NRF2 and control have been used. The plot shows the mean ± S.D. of four individual treatments. One representative experiment of six is shown. Knockdown efficiency was confirmed by western blotting against indicated proteins (right panel). **(C)** SII-HA-KEAP1 expressing HeLa Flp-In cells were treated with H_2O_2 for 8 h followed by SII affinity purification (AP) and western blotting. **(D)** Representative confocal images of HeLa cells left untreated or treated for 12 h with 0.5 mM H_2O_2 and stained for DAPI (blue), the mitochondrial marker COX IV (green) and PGAM5 or KEAP1 (red), respectively. Overlays are shown in yellow.

Figure 3. PGAM5 interacts with AIFM1

(A) Proteins enriched with SII-HA-PGAM5 and THYN1 (ctrl) from HeLa FlpIn cells were analyzed by LC-MS/MS. Volcano plots show the average degrees of enrichment by KEAP1 over control (ratio of label-free quantitation (LFQ) protein intensities; x-axis) and p-values (t-test; y-axis) for each protein. Significantly enriched proteins (FDR 0.001, s0.2) are separated from background proteins by a hyperbolic curve (dotted line). Red dot: PGAM5, green dots: proteins known to be involved in cell death. Four independent affinity purifications were performed for both baits. **(B)** Binding of endogenous AIFM1 to PGAM5. Western blot analysis of SII-HA-PGAM5 or SII-HA-ctrl precipitates and input lysate. **(C)** Top panel: domain structure of AIFM1 including MLS (2-55), TM domain (55–103) and *C*-terminal domain (480-613). Bottom panel: AP of indicated Renilla-tagged AIFM1 deletion mutants with SII-HA-PGAM5 followed by Renilla assay. Western blot shows precipitated SII-HA-PGAM5. **(D)** AIFM1-SII-HA Hela FlpIn cells were treated for 1 h with 2 mM N-Acetylcysteine (NAC) followed by 10 h 0.5 mM H_2O_2 treatment. Western blot analysis of precipitates after SII-AP. **(E, F)** Viability of HeLa (e) and SKN (f) cells treated with siRNA against PGAM5, AIFM1 and siScr after 21 h H_2O_2 or tert-Butylhydroquinone (tBHQ) treatment. Cell titers were determined by Resazurin-based viability assay. The plot shows the mean ± S.D. of four individual treatments. One representative experiment of two is shown.

Figure 4. PGAM5 dephosphorylates AIFM1

(A) PGAM5 precipitated with SII-HA-AIFM1 in the presence or absence of phosphatase inhibitors (Phosinh) followed by western blotting. **(B)** Phosphatase activity of PGAM5 and PGAM5 mutants carrying an N-terminal (N) or C-terminal (C) tag precipitated from cell lysates. The plot shows the mean ± S.D. of one AP with three independent measurements. One representative experiment of three is shown. **(C)** Coomassie gel of purified recombinant proteins. **(D)** Size exclusion chromatography analysis of His-PGAM5 Δ2-28 wt and [F244D] mutant for dimer and monomer formation. **(E)** Phosphatase activity of recombinant PGAM5 and PGAM5 mutants. The plot shows the mean ± S.D. of three independent measurements. One representative experiment of three is shown. **(F)** Binding of PGAM5 to the indicated AIFM1-SII-HA mutant proteins expressed in HEK293R1 AIFM1 knockout cells. Western blot analysis of precipitates after AP with SII-beads. **(G)** Sequence logo of AIFM1 S116 and surrounding amino acids in 13 mammalian species. **(H)** Western blot analysis of Jurkat cells that were left untreated or were treated with 0.5 mM H_2O_2 for 2 h. **(I)** HeLa cell lysate was treated with 11 µg recombinant His-PGAM5Δ2-28 or His-tagged PGAM5[F244D]Δ2-28 mutant for 30 min at 30°C and subjected to western blot analysis. (H, I) one representative experiment of three is shown.

Figure 5. Virus proteins interfere with KEAP1-PGAM5-AIFM1 signaling pathway

(A) Schematic representation of viral proteins identified in [33] to bind KEAP1, PGAM5 or AIFM1. **(B, C)** AP-LC-MS/MS experiments using SII-HA-tagged Non-structural protein 2 (NS2) of respiratory syncytial virus (RSV) or non-expressing controls **(B)** or K3 of Human Herpes virus 8 (HHV-8) and SII-HA-THYN1 (ctrl) **(C)** as baits. Volcano plots show the average degrees of enrichment (ratio of label-free quantitation (LFQ) protein intensities; x-axis) and p-value (t-test; y-axis) for each identified protein. Significantly enriched proteins (FDR: 0.01, S0=1) are separated from background proteins by a hyperbolic curve (dotted line). Baits are marked in red, AIFM1 and PGAM5 are highlighted in green. Four independent APs were performed for all baits. **(D)** Ren-K3 or Ren-ctrl were co-transfected with SII-

HA-PGAM5 into HEK293T cells and Renilla activity measured in input lysate or after SII precipitation. **(E)** HEK293R1 PGAM5 knockout cells were co-transfected with the indicated plasmids for 24 h and phosphatase activity of SII-precipitated proteins measured. **(F)** AP of Ren-AIFM1 using Flag tagged Non-structural protein S (NSs) of La Crosse virus (LaCV) or Flag-(ctrl) (ΔMx) as baits followed by Renilla assay. **(G)** AP of endogenous AIFM1 in HEK cells using transfected Flag-NSs or Flag-ctrl (ΔMx) as baits followed by western blot analysis. **(H)** AP of Ren-NS2 (RSV) and Ren-ctrl (THYN1) using SII-HA-AIFM1 as bait followed by Renilla assay. **(D-H)** Representative of experiments of at least 3 independent replicates. Histograms show mean +/-SD of triplicate measurements.

Figure 6. KEAP1-PGAM5-AIFM1 pathway is involved in antiviral defense

(A) HeLa cells were treated with 0.5 mM H_2O_2 (3h) or infected with FluAV (strain SC35M) MOI 3 for 3 h and 24 h. Abundance of mitochondrial ROS was examined by staining with CM-H2DCFDA followed by FACS analysis. **(B**) Influence of FluAV infection on NRF2 regulated gene transcription in HeLa cells tested by RT-qPCR. **(C)** Western blot analysis for indicated proteins of Jurkat cells infected with FluAV for 24 h. **(D)** Characterization of *Pgam5* knockout MEFs by genotyping (PCR) (bottom) and quantification of Pgam5 mRNA levels by RT-qPCR (top). **(E)** Viability of MEF with the indicated genotypes after H_2O_2 treatment for 21 h by Resazurin-based viability assay. The plot shows the mean ± S.D. of six individual treatments. One representative experiment of three is shown. **(F)** Viability of MEF cells after infection with FluAV (MOI 3) for 21 h tested by Resazurin-based viability assay. The plot shows the mean ± S.D. of three individual treatments. One representative experiment of two is shown. **(G)** Survival of littermate $Pgam5^{(+/+)}$ (n=9), $Pgam5^{(+/-)}$ (n=42) and $Pgam5^{(-/-)}$ (n=20) mice infected with FluAV ($1.5x10^3$ pfu/animal). Mice were monitored for 14 days and euthanized when they lost >25% of their initial body weight. Kaplan Meier curve shows pooled data from two independent experiments.

Supplementary Figure S1. PGAM5 and KEAP interaction

Binding of endogenous KEAP1 to PGAM5 deletion mutants. Expression of SII-HA-tagged PGAM5 wild-type (wt) and deletion mutants lacking MLS and TM domain (Δ2-29), lacking MLS, TM domain and phosphatase activity modulating region (PAMR) (Δ2-69) and lacking MLS, TM domain, PAMR and KEAP1 binding site (Δ2-89) in HEK293T cells. Western blot analysis of input lysates and SII-AP.

Supplementary Figure S2. Characterization of recombinant PGAM5

(A) Zoom of crystal structure of PGAM5 dimer interface (PDB 3MXO). One monomer is highlighted in black, the other in grey. Left panel shows the wild-type (wt) protein, right panel shows the modeled mutant PGAM5[F244D]. Side chains of Phenylalanine (F) 244 and, after mutation, aspartic acid (D) 244 are highlighted in purple (carbon) and red (oxygen). **(B)** Binding of Ren-PGAM5, Ren-PGAM5[F244D] or Ren-ctrl (THYN1) to SII-HA-PGAM5 in HEK293T cells. Renilla assay of cell lysates or SII precipitates. **(C)** MS analysis of recombinant His-tagged PGAM5Δ2-28 and His-PGAM5[F244D]Δ2-28. **(D)** Dynamic light scattering (DLS) analysis of recombinant His-tagged PGAM5Δ2-28 and His-PGAM5[F244D]Δ2-28 to test sample homogeneity and globular size. **(E)** CD spectroscopy of His-PGAM5Δ2-28 and His-PGAM5[F244D]Δ2-28 to test comparability of secondary structures and overall integrity of both recombinant proteins.

Supplementary Figure 3. S116 in AIFM and characterization of AIFM1-pS116 antibody

(A) Sequence alignment of AIFM1 amino acids 109-122 of the indicated species. **(B)** Selectivity of AIFM1 pS116 antibody. HeLa cell lysates were treated for 15 min with or without calf intestine alkaline phosphatase (CIAP) and subjected to western blot stained for AIFM1 pS116 and AIFM1.

Supplementary Figure 4. Binding of K3 to PGAM5 and NS2 to AIFM1

(A) AP of Ren-K3 with SII-HA-PGAM5 mutant proteins. 293R1 PGAM5 knockout cells were co-transfected with the indicated SII-HA-tagged PGAM5 constructs or SII-HA-ctrl (THYN1) and Renilla-tagged K3. After 24h Renilla activity was measured in lysate and SII precipitates. Western blot shows

expression of bait proteins in cell lysates. **(B)** Interaction of SII-HA-AIFM1 and AIFM1 mutant proteins and SII-HA-ctrl (THYN1) with co-expressed Ren-NS2 in HEK293T cells. Renilla activity was tested in cell lysates and after SII precipitation.

Supplementary Table 1. AP-LC-MS/MS experiments

HeLa FlpIn cells were genetically engineered to stably express **(A)** KEAP1, **(B)** PGAM5, **(C)** K3 (HHV-8) and **(D)** NS2 (RSV) and were used for AP LC-MS/MS experiments as described in material and methods. Table contains log2 transformed label-free quantification (LFQ) intensities of all identified proteins. Missing values were imputed as described in material and methods. Significantly enriched proteins, p values and mean differences from t-test based analyses are indicated.

Methods

Plasmids

Expression constructs were generated by PCR amplification of plasmids from ImaGenes cDNA Library (MPI core Facility) and a cDNA library obtained from HeLa cells followed by Gateway cloning (Invitrogen) into the plasmids pcDNA3-Ren-GW and pTO-SII-HA-GW (Pichlmair et al., 2012; Habjan et al., 2013). Mutations and truncations were introduced by PCR, respectively. pI.18_3xFlag_NSs (LaCV) and pI.18_3xFlag_DMx_1xFlag were kindly provided by Friedemann Weber. Sequences were verified by Sanger sequencing.

Cells, reagents and viruses

HeLa S3 (CCL-2.2) and Vero E6 cells (CRL-1586) were purchased from ATCC. Jurkat cells were a gift from Felix Meissner (MPI of Biochemistry, Munich). SKN-BE2 cells were kindly provided by Rüdiger Klein (MPI of Neurobiology, Munich). HeLa FlpIn cells (a gift from Andrea Musacchio, MPI of Cell Biology, Dresden) stably expressing SII-HA-tagged human PGAM5, AIFM1, KEAP1 K3, NS2 and THYN1 under control of the same promoter were generated by hygromycin selection. MEFs were isolated from 13.5 day old Embryos from a heterozygous breeding pair.

All cell lines were maintained in DMEM (PAA Laboratories) containing 10% fetal calf serum (GE Healthcare) and antibiotics (100 U/ml penicillin, 100 µg/ml streptomycin). Streptavidin-agarose beads were obtained from Novagen. Resazurin, Sodium Fluoride, Malachite green and N-Acetylcysteine were from Sigma, Polyethylenimine linear MW 25.000 from Polysciences, ortho-Vanadate from Alfa Aesar. Primary antibodies used in this study were as follows: PGAM5, HA-tag (Sigma: HPA036978, H6533), Renilla-tag (Millipore: MAB4410), and KEAP1, AIFM1, NRF2 (Cell Signaling: 8047, 5318, 12721). Antibodies against actin (Santa Cruz; sc-47778), His-tag (Santa Cruz; sc-8036), and secondary antibodies detecting mouse or rabbit IgG (Jackson ImmunoResearch, Dako) were horseradish peroxidase (HRP)-coupled. CM-H2DCFDA, 4',6-diamidino-2-phenylindole (DAPI) and secondary antibodies used for

immunofluorescence were purchased from Invitrogen. Recombinant influenza virus (Flu SC35M wt) described previously (REF).

RNAi-mediated knockdown

Duplex siRNAs were transfected using the Neon Transfection System (Invitrogen). Transfection was performed according to the manufacturer´s instructions for HeLa and SKN-BE2 cells. Briefly, we transfected 1 nmol of siRNA per 1×10^6 cells. Duplex siRNAs were either purchased from Qiagen, Dharmacon or synthesized by the Core Facility at the MPI of Biochemistry. siRNA target sequences were as follows: human PGAM5 [#1: 5`-CCCGCCCGTGTCTCATTGGAA-3`, #2: 5`-TCCAAGCTGGACCACTACAAA-3`, #3: 5`-CTCGGCCGTGGCGGTAGGGAA-3`], human AIFM1 [#1: 5`-GAACATCTTTAACCGAATG-3`; #2: 5`-GCATGAAGATCTCAATGAA-3`; #3: 5`-CAAGGAAGATCATTAAGGA-3`; #4: 5`-GGTAGAAACTGACCACATA-3`], human KEAP1 [#1: 5`-GGACAAACCGCCTTAATTC-3`; #2: 5`-CAGCAGAACTGTACCTGTT-3`; #3: 5`-GGGCGTGGCTGTCCTCAAT-3`; #4: 5`-CGAATGATCACAGCAATGA-3`], human NFE2L2 [#1: 5`-TAAAGTGGCTGCTGAGAAT-3`; #2: 5`-GAGTTACAGTGTCTTAATA-3`; #3: 5`-TGGAGTAAGTCGAGAAGTA-3`; #4: 5`-CACCTTATATCTCGAAGTT-3`] and scrambled [5`-AAGGTAATTGCGCGTGCAACT-3].

Cell viability assay

To test cell viability a Resazurin-based cell viability assay was used. Resazurin (100 µg/mL) was dissolved in PBS and added to each well of a 96well plate. Cells were incubated 30 min @37°C, followed by measurement of fluorescence (535/590 nm) using an Infinite 200 PRO series micro plate reader (Tecan).

Immunofluorescence

For immunofluorescence, HeLa cells were grown on coverslips and fixed with 4% (w/v) paraformaldehyde for 10 minutes, permeabilized with 0.1% (v/v) Triton X-100 for 7 minutes and washed three times with blocking buffer (1 × PBS containing 0.1% fetal calf serum (w/v)). Immunofluorescense analysis was performed as described previously (Habjan et al., 2013). Confocal imaging was performed using a LSM780 confocal laser scanning microscope (ZEISS, Jena, Germany) equipped with a Plan-APO 63x/NA1.46 oil immersion objective (ZEISS).

Affinity purifications and quantitative LC-MS/MS

Cell lysates were prepared by lysing cells for 5 min on ice in TAP lysis buffer (50 mM Tris pH 7.5, 100 mM NaCl, 5% (v/v) glycerol, 0.2 % (v/v) Nonidet-P40, 1.5 mM $MgCl_2$ and protease inhibitor cocktail (EDTA-free, cOmplete; Roche)) or Cell Signaling IP buffer (20 mM TrisHCl pH 7.5, 150 mM NaCl, 1 mM Na_2EDTA, 1 mM EGTA, 1 % Triton and protease inhibitor cocktail (EDTA-free, cOmplete; Roche). Were indicated, phosphatase inhibitor cocktail (PhosSTOP; Roche) or NaF and Van were added. For affinity-purification with HA-SII-tagged proteins, streptavidin affinity resin was incubated with cell lysate in either TAP lysis buffer or CellSignaling IP buffer for 60 min at 4°C on a rotary wheel. Beads were washed four times with TAP lysis buffer, followed by two times with TAP wash buffer [lacking 0.2 % (v/v) Nonidet-P40] or five times with Cell Signaling IP buffer, boiled in 2x Cell Signaling SDS buffer for 5 min at 95°C and subjected to SDS-PAGE and Western Blot analysis. For LUMIER experiments cell lysates (1:10 diluted in TAP wash buffer) or beads were resuspended in TAP wash buffer and transferred in 4x 20 µL aliquots to white well plate (Nunc) and mixed with 2x Renilla reagent (100 mM K_3PO_4, 500 mM NaCl, 1 mM EDTA, 25 mM Thiourea, freshly added 30 µM Coelenterazine) and luminescence was measured using an Infinite 200 PRO series micro plate reader (Tecan).

To detect and quantify proteins bound to HA-SII-tagged bait proteins by affinity purification and mass spectrometry, samples were prepared as described above. After the final four washes in TAP lysis buffer, samples were in addition washed four times with TAP wash buffer to remove residual detergent. Four

independent affinity purifications were performed for each bait. Sample preparations and LC-MS/MS analysis was performed as described previously (Habjan et al., 2013). Briefly, samples were sequentially digested with LysC (Wako Chemicals USA) and Trypsin (Promega), acidified with 0.1% TFA, desalted with C18 stage tips and analyzed by liquid chromatography coupled to mass spectrometry on an Orbitrap XL platform (Thermo Fisher Scientific).

For analysis of interaction proteomics data, mass spectrometry raw files were processed with MaxQuant version 1.3.0.5 or 1.4.0.6 (Cox and Mann, 2008) using the built-in Andromeda engine to search against human proteome (UniprotKB, release 2012_06) containing forward and reverse sequences. In MaxQuant the label-free quantitation (LFQ) algorithm (Cox et al., 2014) and Match Between Runs option were used as described previously (Habjan et al., 2013). Only proteins identified on the basis of at least two peptides and a minimum of three quantitation events in at least one experimental group were considered. LFQ protein intensity values were log-transformed and missing values filled by imputation. Specific enrichment was determined by multiple equal variance t-tests with permutation-based false discovery rate (FDR) statistics, performing 250 permutations. FDR thresholds and S_0 parameters were empirically set to separate background from specifically enriched proteins. Results were plotted using R (www.R-project.org).

***In vivo* experiments using *Pgam5* knockout mice**

Heterozygous mice were obtained from the European Mouse Mutant Archive (EMMA). Mice were bred at the MPI of Biochemistry animal facility. All animal experiments have been performed according to animal welfare regulations and have been approved by the responsible authorities (Freiburg, G-12/46). Primer sequences for genotyping were as follow L3f_6764 5'-AGGCTGGATCACTATAAGGC-3' and L3r_6765 5'-CTGGAGACATTGTGACCATC-3'.

Real-time RT-PCR

RNA was reverse transcribed with PrimeScript™ RT Master Mix (TAKARA) and quantified by real-time RT-PCR using the QuantiFast SYBR Green RT-PCR Kit (Qiagen) and a CFX96 Touch Real-Time PCR Detection System (BioRad). Each cycle consisted of 10 sec at 95°C and 30 sec at 60°C, followed by melting curve analysis. Primer sequences were as follows: huGAPDH (5'-GATTCCACCCATGGCAAATTC-3' and 5'-AGCATCGCCCCACTTGATT-3'), hTBP (5'-GTTCTGAATAGGCTGTGGGG-3' and 5'-ACAACAGCCTGCCACCTTAC-3'), KEAP1 (5'-GCTGATGAGGGTCACCAGTT-3' and 5'-CCAACTTCGCTGAGCAGATT-3'), NRF2 (5'-GCTCATACTCTTTCCGTCGC-3' and 5'- ATCATGATGGACTTGGAGCTG-3'), NQO1 (5'-GCATAGAGGTCCGACTCCAC-3' and 5'-GGACTGCACCAGAGCCAT-3'), TXN (5'-AATGTTGGCATGCATTTGAC-3' and 5'-CCTTGCAAAATGATCAAGCC-3'),

Cloning and expression of recombinant proteins

N-terminal His-tagged PGAM5 (pNIC28-Bsa4-PGAM5(D2-28)) was a kindly provided by Apirat Chaikuad and Stefan Knapp. For solubility reasons the recombinant protein carried a deletion from amino acid 2-28. Mutation F244D in PGAM5 was introduced by site directed mutagenesis. Sequences of all cloning primers are available on request. Expression of recombinant proteins was induced over night at 18°C in *E. coli* strain Rosetta(DE3) using 0.5 mM IPTG (Thermo). Cells were lysed in lysis buffer (50 mM Tris-HCl pH 8.5, 500 mM NaCl, 10% glycerol, 40 mM imidazole, 1 mM DTT and protease inhibitor cocktail (EDTA-free, cOmplete; Roche)) using an Emulsiflex-C3 homogenizer and cleared lysate was used for protein purification using a HisTrap HP column (GE Healthcare; 17-5247-01) and further purified by gel filtration (mobile phase: 30 mM Tris-HCl pH 8.5, 300 mM NaCl, 10% glycerol, 1 mM DTT). Identity of recombinant PGAM5 and mutant PGAM5 was confirmed by mass spectrometry. Far ultraviolet (UV) circular dichroism (CD) spectra of wild type and a mutant version of PGAM5 were recorded on a Jasco J-810 CD-Photometer at room temperature in 20 mM sodium phosphate buffer pH 7.4 and 50 mM NaF. For each sample and the buffer (baseline), four scans were recorded and averaged.

The averaged baseline spectrum was subtracted from the averaged sample spectra and the resulting spectra were smoothed using an FFT filter (as part of the software package). Measurements were only made down to wavelengths where the instrument dynode voltage indicated the detector was still in its linear range (190 nm). Spectra are shown as the mean residue elipticity. Secondary structure compositions were estimated using the CONTINLL program (Provencher and Glockner, 1981).

Phosphatase assay

Proteins were incubated in PGAM5 phosphatase buffer (50 mM imidazole pH 7.2, 0.2 mM EGTA, 0.02 % β-mercaptoethanol, 0.1 mg/ml BSA) and 50 µM phosphorylated peptide (peptide sequences: RRA(pT)VA and AAL(pS)ASE) for 20 minutes at 30°C. The reaction was stopped by addition of Malachite Green Reagent as described before (Sherwood et al., 2013). After 15 minutes incubation at room temperature absorbance at 630 nm was measured using an Infinite 200 PRO series micro plate reader (Tecan).

FACS analysis

The production of H_2O_2 was detected by CM-H2DCFDA staining assay. Cells were treated as indicated and 30 min prior analysis cells were incubated with 1 µM CM-H2DCFDA in the dark. Cells were fixed and analyzed by FACS machine.

Generation of Sequence logo

Sequence logo was generated with WebLogo, a web based application (Crooks et al., 2004). List of sequences used (starting all at amino acid 109 from *N*-terminus): *Homo sapiens* (Human, O95831) KQKKAALSASEGEE; *Macaca mulatte* (Rhesus macaque, F7C7I3) KQKKAALSASEGEE; *Bos taurus*

(Bovine, E1BJA2) KQKRATSSALEGEP; *Cavia porcellus* (Guinea pig, H0VP14) KQRRAALSASAGEQ; *Equus caballus* (Horse, F6WXF6) KQKRATSSAPEGEP; *Myotis lucifugus* (Little brown bat, G1PCN7) KQKRAALSAPEGEP; *Oryctolagus cuniculus* (Rabbit, G1SIM3) KQKRATASAPEGEP; *Pan troglodytes* (Chimpanzee, K7BTY6) KQKKAALSASEGEE; *Sus scrofa* (Pig, A0A068CA64) KQKRATSSAPEGEP; *Ovis Aries* (Sheep, W5Q1F6) KQKRATSSALEGEP; *Ictidomys tridecemlineatus* (Thirteen-lined ground squirrel, I3MBI5) KQRRATSSAPEGEP; *Mus musculus* (Mouse, Q9Z0X1) KQRRAIASATEGGS; *Rattus norvegicus* (Rat, Q9JM53) KQRRAIASAAEGGS

References

Alfonso-Loeches, S., Urena-Peralta, J.R., Morillo-Bargues, M.J., Oliver-De La Cruz, Jorge, and Guerri, C. (2014). Role of mitochondria ROS generation in ethanol-induced NLRP3 inflammasome activation and cell death in astroglial cells. Frontiers in cellular neuroscience *8*, 216.

Ano, Y., Sakudo, A., Kimata, T., Uraki, R., Sugiura, K., and Onodera, T. (2010). Oxidative damage to neurons caused by the induction of microglial NADPH oxidase in encephalomyocarditis virus infection. Neuroscience letters *469*, 39-43.

Bhattacharya, A., Hegazy, A.N., Deigendesch, N., Kosack, L., Cupovic, J., Kandasamy, R.K., Hildebrandt, A., Merkler, D., Kuhl, A.A., and Vilagos, B., et al. (2015). Superoxide Dismutase 1 Protects Hepatocytes from Type I Interferon-Driven Oxidative Damage. Immunity *43*, 974-986.

Blaser, H., Dostert, C., Mak, T.W., and Brenner, D. (2016). TNF and ROS Crosstalk in Inflammation. Trends in cell biology *26*, 249-261.

Bottero, V., Chakraborty, S., and Chandran, B. (2013). Reactive oxygen species are induced by Kaposi's sarcoma-associated herpesvirus early during primary infection of endothelial cells to promote virus entry. Journal of virology *87*, 1733-1749.

Bryan, H.K., Olayanju, A., Goldring, C.E., and Park, B.K. (2013). The Nrf2 cell defence pathway: Keap1-dependent and -independent mechanisms of regulation. Biochemical pharmacology *85*, 705-717.

Carpino, N., Turner, S., Mekala, D., Takahashi, Y., Zang, H., Geiger, T.L., Doherty, P., and Ihle, J.N. (2004). Regulation of ZAP-70 activation and TCR signaling by two related proteins, Sts-1 and Sts-2. Immunity *20*, 37-46.

Ceh-Pavia, E., Spiller, M.P., and Lu, H. (2013). Folding and biogenesis of mitochondrial small Tim proteins. International journal of molecular sciences *14*, 16685-16705.

Chaikuad, A., Alfano, I., Picaud, S., Filippakopoulos, P., Barr, A., von Delft, F., Arrowsmith, C.H., Edwards, A.M., Weigelt, J., Bountra, C., Takeda, K., Ichijo, H., Knapp, S. (2010). 3MXO. Crystal structure oh human phosphoglycerate mutase family member 5 (PGAM5).

Circu, M.L., and Aw, T.Y. (2010). Reactive oxygen species, cellular redox systems, and apoptosis. Free radical biology & medicine *48*, 749-762.

Cox, J., Hein, M.Y., Luber, C.A., Paron, I., Nagaraj, N., and Mann, M. (2014). Accurate proteome-wide label-free quantification by delayed normalization and maximal peptide ratio extraction, termed MaxLFQ. Molecular & cellular proteomics : MCP *13*, 2513-2526.

Cox, J., and Mann, M. (2008). MaxQuant enables high peptide identification rates, individualized p.p.b.-range mass accuracies and proteome-wide protein quantification. Nature biotechnology *26*, 1367-1372.

Crooks, G.E., Hon, G., Chandonia, J.-M., and Brenner, S.E. (2004). WebLogo: a sequence logo generator. Genome research *14*, 1188-1190.

D'Autréaux, B., and Toledano, M.B. (2007). ROS as signalling molecules: mechanisms that generate specificity in ROS homeostasis. Nature reviews. Molecular cell biology *8*, 813-824.

Edgar, B.A., Zielke, N., and Gutierrez, C. (2014). Endocycles: a recurrent evolutionary innovation for post-mitotic cell growth. Nature reviews. Molecular cell biology *15*, 197-210.

Edwards, M.R., Johnson, B., Mire, C.E., Xu, W., Shabman, R.S., Speller, L.N., Leung, D.W., Geisbert, T.W., Amarasinghe, G.K., and Basler, C.F. (2014). The Marburg virus VP24 protein interacts with Keap1 to activate the cytoprotective antioxidant response pathway. Cell reports *6*, 1017-1025.

Gonzalez-Dosal, R., Horan, K.A., Rahbek, S.H., Ichijo, H., Chen, Z.J., Mieyal, J.J., Hartmann, R., and Paludan, S.R. (2011). HSV infection induces production of ROS, which potentiate signaling from pattern recognition receptors: role for S-glutathionylation of TRAF3 and 6. PLoS pathogens *7*, e1002250.

Habjan, M., Hubel, P., Lacerda, L., Benda, C., Holze, C., Eberl, C.H., Mann, A., Kindler, E., Gil-Cruz, C., and Ziebuhr, J., et al. (2013). Sequestration by IFIT1 impairs translation of 2'O-unmethylated capped RNA. PLoS pathogens *9*, e1003663.

Hroudová, J., Singh, N., and Fišar, Z. (2014). Mitochondrial dysfunctions in neurodegenerative diseases: relevance to Alzheimer's disease. BioMed research international *2014*, 175062.

Joza, N., Susin, S.A., Daugas, E., Stanford, W.L., Cho, S.K., Li, C.Y., Sasaki, T., Elia, A.J., Cheng, H.Y., and Ravagnan, L., et al. (2001). Essential role of the mitochondrial apoptosis-inducing factor in programmed cell death. Nature *410*, 549-554.

Kajitani Noriko, Kobuchi Hirotsugu, Fujita Hirofumi, Yano Hiromi, Fujiwara Takuzo, Yasuda Tatsuji, and Utsumi Kozo (2007). Mechanism of A23187-Induced Apoptosis in HL-60 Cells: Dependency on Mitochondrial Permeability Transition but Not on NADPH Oxidase. Biosci. Biotechnol. Biochem., 2701-2711.

Kaspar, J.W., Niture, S.K., and Jaiswal, A.K. (2009). Nrf2:INrf2 (Keap1) signaling in oxidative stress. Free radical biology & medicine *47*, 1304-1309.

Kobayashi, A., Kang, M.-I., Okawa, H., Ohtsuji, M., Zenke, Y., Chiba, T., Igarashi, K., and Yamamoto, M. (2004). Oxidative stress sensor Keap1 functions as an adaptor for Cul3-based E3 ligase to regulate proteasomal degradation of Nrf2. Molecular and Cellular Biology *24*, 7130-7139.

Li, Y., Boehning, D.F., Qian, T., Popov, V.L., and Weinman, S.A. (2007). Hepatitis C virus core protein increases mitochondrial ROS production by stimulation of Ca2+ uniporter activity. FASEB journal : official publication of the Federation of American Societies for Experimental Biology *21*, 2474-2485.

Lo, S.-C., and Hannink, M. (2006). PGAM5, a Bcl-XL-interacting protein, is a novel substrate for the redox-regulated Keap1-dependent ubiquitin ligase complex. The Journal of biological chemistry *281*, 37893-37903.

Lo, S.-C., and Hannink, M. (2008). PGAM5 tethers a ternary complex containing Keap1 and Nrf2 to mitochondria. Experimental cell research *314*, 1789-1803.

Lü, J.-M., Lin, P.H., Yao, Q., and Chen, C. (2010). Chemical and molecular mechanisms of antioxidants: experimental approaches and model systems. Journal of cellular and molecular medicine *14*, 840-860.

Marconett, C.N., Morgenstern, T.J., San Roman, Adrianna K, Sundar, S.N., Singhal, A.K., and Firestone, G.L. (2010). BZL101, a phytochemical extract from the Scutellaria barbata plant, disrupts proliferation of human breast and prostate cancer cells through distinct mechanisms dependent on the cancer cell phenotype. Cancer biology & therapy *10*, 397-405.

Medvedev, R., Ploen, D., and Hildt, E. (2016). HCV and Oxidative Stress: Implications for HCV Life Cycle and HCV-Associated Pathogenesis. Oxidative medicine and cellular longevity *2016*, 9012580.

Mikhailik, A., Ford, B., Keller, J., Chen, Y., Nassar, N., and Carpino, N. (2007). A phosphatase activity of Sts-1 contributes to the suppression of TCR signaling. Molecular cell *27*, 486-497.

Moriwaki, K., Farias Luz, N., Balaji, S., De Rosa, Maria Jose, O'Donnell, C.L., Gough, P.J., Bertin, J., Welsh, R.M., and Chan, F.K.-M. (2016). The Mitochondrial Phosphatase PGAM5 Is Dispensable for Necroptosis but Promotes Inflammasome Activation in Macrophages. Journal of immunology (Baltimore, Md. : 1950) *196*, 407-415.

Nakamura Hajime, Nakamura Kazuhiro, and Yodoi Junji (1997). Redox Regulation of Cellular Activation. Ann. Rev. Immunol., 351-369.

Okinaga, T., Ariyoshi, W., and Nishihara, T. (2015). Aggregatibacter actinomycetemcomitans Invasion Induces Interleukin-1beta Production Through Reactive Oxygen Species and Cathepsin B. Journal of interferon & cytokine research : the official journal of the International Society for Interferon and Cytokine Research *35*, 431-440.

Olagnier, D., Peri, S., Steel, C., van Montfoort, N., Chiang, C., Beljanski, V., Slifker, M., He, Z., Nichols, C.N., and Lin, R., et al. (2014). Cellular oxidative stress response controls the antiviral and apoptotic programs in dengue virus-infected dendritic cells. PLoS pathogens *10*, e1004566.

Olson, W., Dong, P., Fleming, M., and Luo, W. (2016). The specification and wiring of mammalian cutaneous low-threshold mechanoreceptors. Wiley interdisciplinary reviews. Developmental biology.

Page, A., Volchkova, V.A., Reid, S.P., Mateo, M., Bagnaud-Baule, A., Nemirov, K., Shurtleff, A.C., Lawrence, P., Reynard, O., and Ottmann, M., et al. (2014). Marburgvirus hijacks nrf2-dependent pathway by targeting nrf2-negative regulator keap1. Cell reports *6*, 1026-1036.

Pichlmair, A., Kandasamy, K., Alvisi, G., Mulhern, O., Sacco, R., Habjan, M., Binder, M., Stefanovic, A., Eberle, C.-A., and Goncalves, A., et al. (2012). Viral immune modulators perturb the human molecular network by common and unique strategies. Nature *487*, 486-490.

Provencher, S.W., and Glockner, J. (1981). Estimation of globular protein secondary structure from circular dichroism. Biochemistry *20*, 33-37.

Ren, J.-H., Chen, X., Zhou, L., Tao, N.-N., Zhou, H.-Z., Liu, B., Li, W.-Y., Huang, A.-L., and Chen, J. (2016). Protective Role of Sirtuin3 (SIRT3) in Oxidative Stress Mediated by Hepatitis B Virus X Protein Expression. PloS one *11*, e0150961.

Rosca, M.G., Vazquez, E.J., Chen, Q., Kerner, J., Kern, T.S., and Hoppel, C.L. (2012). Oxidation of fatty acids is the source of increased mitochondrial reactive oxygen species production in kidney cortical tubules in early diabetes. Diabetes *61*, 2074-2083.

Sadatomi, D., Tanimura, S., Ozaki, K.-I., and Takeda, K. (2013). Atypical protein phosphatases: emerging players in cellular signaling. International journal of molecular sciences *14*, 4596-4612.

Sandalio, L.M., Rodriguez-Serrano, M., Romero-Puertas, M.C., and del Rio, Luis A (2013). Role of peroxisomes as a source of reactive oxygen species (ROS) signaling molecules. Sub-cellular biochemistry *69*, 231-255.

Sauer Heinrich, Wartenberg Maria, and Hescheler Jürgen (2001). Reactive Oxygen Species as Intracellular Messengers During Cell Growth and Differentiation. cellular physiology and Biochemistry, 173-186.

Sherwood, A.R., Paasch, B.C., Worby, C.A., and Gentry, M.S. (2013). A malachite green-based assay to assess glucan phosphatase activity. Analytical biochemistry *435*, 54-56.

Shimizu Yuichiro, and Hendershot Linda M. (2009). Oxidative Folding: Cellular Strategies for Dealing with the Resultant Equimolar Production of Reactive Oxygen Species. Antioxidants & redox signaling, 2317-2331.

Shindo, R., Kakehashi, H., Okumura, K., Kumagai, Y., and Nakano, H. (2013). Critical contribution of oxidative stress to TNFalpha-induced necroptosis downstream of RIPK1 activation. Biochemical and biophysical research communications *436*, 212-216.

Simmen, T. (2011). Hax-1: a regulator of calcium signaling and apoptosis progression with multiple roles in human disease. Expert opinion on therapeutic targets *15*, 741-751.

Song, J.J., Rhee, J.G., Suntharalingam, M., Walsh, S.A., Spitz, D.R., and Lee, Y.J. (2002). Role of glutaredoxin in metabolic oxidative stress. Glutaredoxin as a sensor of oxidative stress mediated by H2O2. The Journal of biological chemistry *277*, 46566-46575.

Susin, S.A., Lorenzo, H.K., Zamzami, N., Marzo, I., Snow, B.E., Brothers, G.M., Mangion, J., Jacotot, E., Costantini, P., and Loeffler, M., et al. (1999). Molecular characterization of mitochondrial apoptosis-inducing factor. Nature *397*, 441-446.

Suzuki, Y.J., Forman, H.J., and Sevanian, A. (1997). Oxidants as Stimulators of Signal Transduction. Free Radical Biology and Medicine *22*, 269-285.

Szatrowski, T.P., and Nathan, C.F. (1991). Production of large amounts of hydrogen peroxide by human tumor cells. Cancer research *51*, 794-798.

Taguchi, K., Motohashi, H., and Yamamoto, M. (2011). Molecular mechanisms of the Keap1–Nrf2 pathway in stress response and cancer evolution. Genes to cells : devoted to molecular & cellular mechanisms *16*, 123-140.

Uttara, B., Singh, A.V., Zamboni, P., and Mahajan, R.T. (2009). Oxidative stress and neurodegenerative diseases: a review of upstream and downstream antioxidant therapeutic options. Current neuropharmacology *7*, 65-74.

Wang, Z., Jiang, H., Chen, S., Du, F., and Wang, X. (2012). The mitochondrial phosphatase PGAM5 functions at the convergence point of multiple necrotic death pathways. Cell *148*, 228-243.

Wilkins, J.M., McConnell, C., Tipton, P.A., and Hannink, M. (2014). A conserved motif mediates both multimer formation and allosteric activation of phosphoglycerate mutase 5. The Journal of biological chemistry *289*, 25137-25148.

Yang Dongli, Elner Susan G., Bian Zong-Mei, Till Gerd O., Petty Howard R., and Elner Victor M. (2007). Pro-inflammatory Cytokines Increase Reactive Oxygen Species through Mitochondria and NADPH Oxidase in Cultured RPE Cells. Exp Eye Res, 462-472.

Zhang, D.D., and Hannink, M. (2003). Distinct Cysteine Residues in Keap1 Are Required for Keap1-Dependent Ubiquitination of Nrf2 and for Stabilization of Nrf2 by Chemopreventive Agents and Oxidative Stress. Molecular and Cellular Biology *23*, 8137-8151.

Figure 1

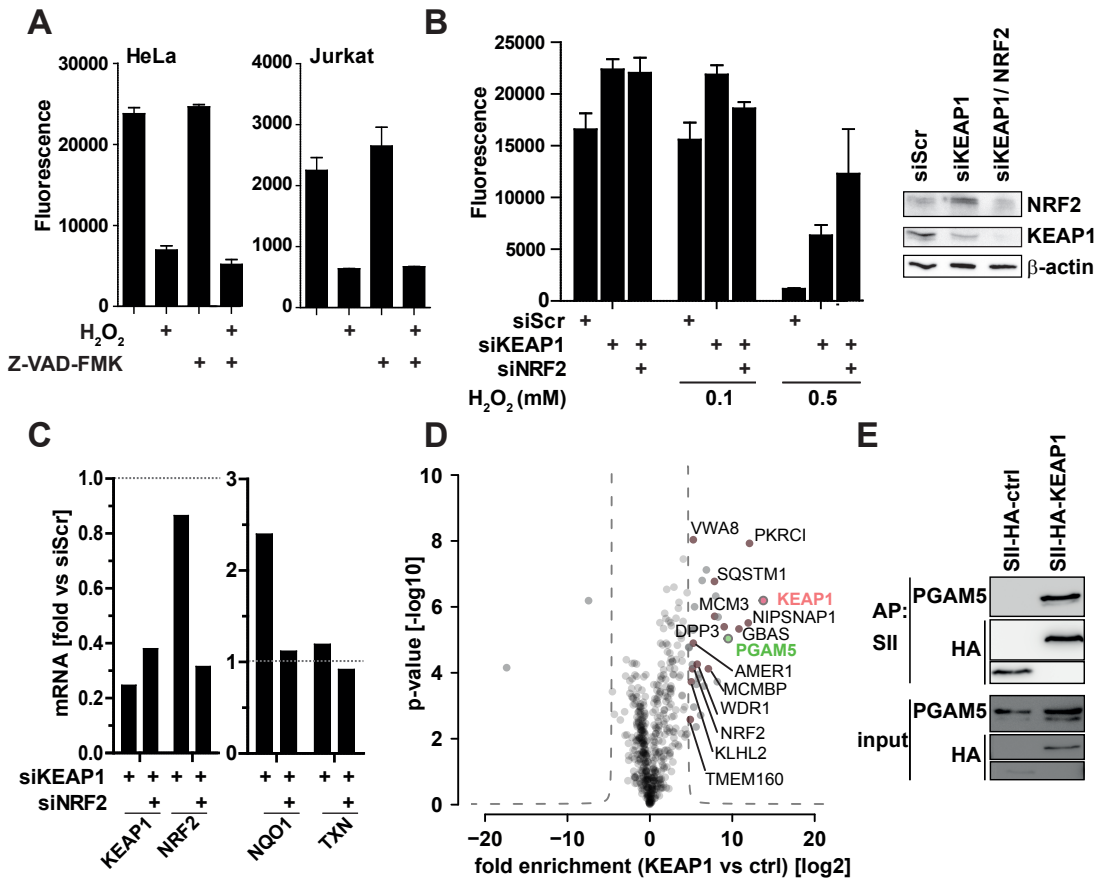
A
HeLa
Jurkat
Fluorescence
H2O2
Z-VAD-FMK
B
Fluorescence
siScr
siKEAP1
siNRF2
H2O2 (mM)
0.1
0.5
siScr
siKEAP1
siKEAP1/ NRF2
NRF2
KEAP1
β-actin
C
mRNA [fold vs siScr]
siKEAP1
siNRF2
KEAP1
NRF2
NQO1
TXN
D
p-value [-log10]
fold enrichment (KEAP1 vs ctrl) [log2]
VWA8
PKRCI
SQSTM1
MCM3
KEAP1
NIPSNAP1
DPP3
GBAS
PGAM5
AMER1
MCMBP
WDR1
NRF2
KLHL2
TMEM160
E
SII-HA-ctrl
SII-HA-KEAP1
AP: SII
PGAM5
HA
input
PGAM5
HA

Figure 2

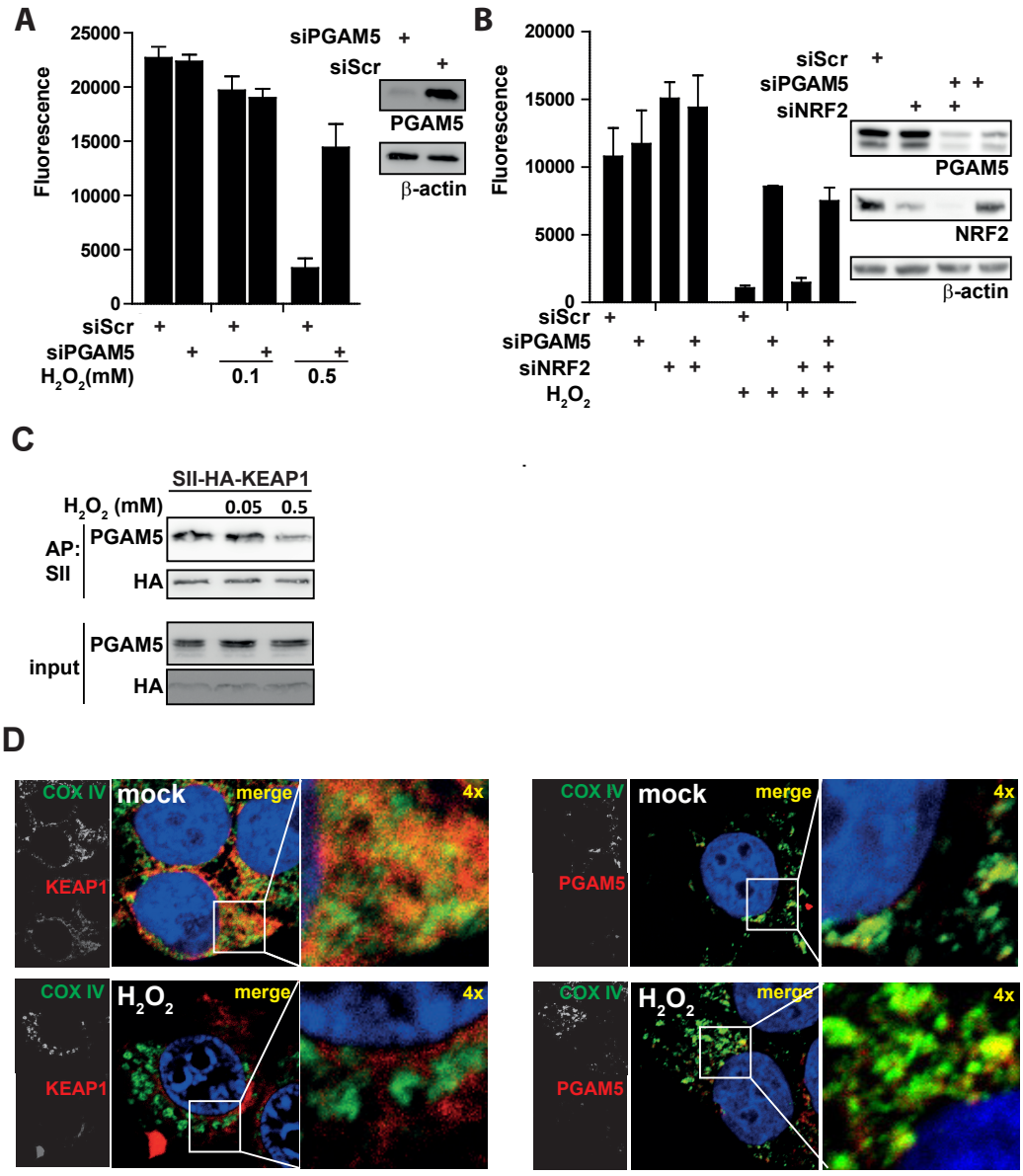
A
Fluorescence
25000
20000
15000
10000
5000
0
siPGAM5 +
siScr +
PGAM5
β-actin
siScr + + +
siPGAM5 + + +
H2O2(mM) 0.1 0.5
B
Fluorescence
20000
15000
10000
5000
0
siScr +
siPGAM5 + +
siNRF2 + +
PGAM5
NRF2
β-actin
siScr + +
siPGAM5 + + +
siNRF2 + + + +
H2O2 + + + +
C
SII-HA-KEAP1
H2O2 (mM) 0.05 0.5
AP: SII
PGAM5
HA
input
PGAM5
HA
D
COX IV
KEAP1
mock
merge
4x
COX IV
PGAM5
mock
merge
4x
COX IV
KEAP1
H2O2
merge
4x
COX IV
PGAM5
H2O2
merge
4x

Figure 3

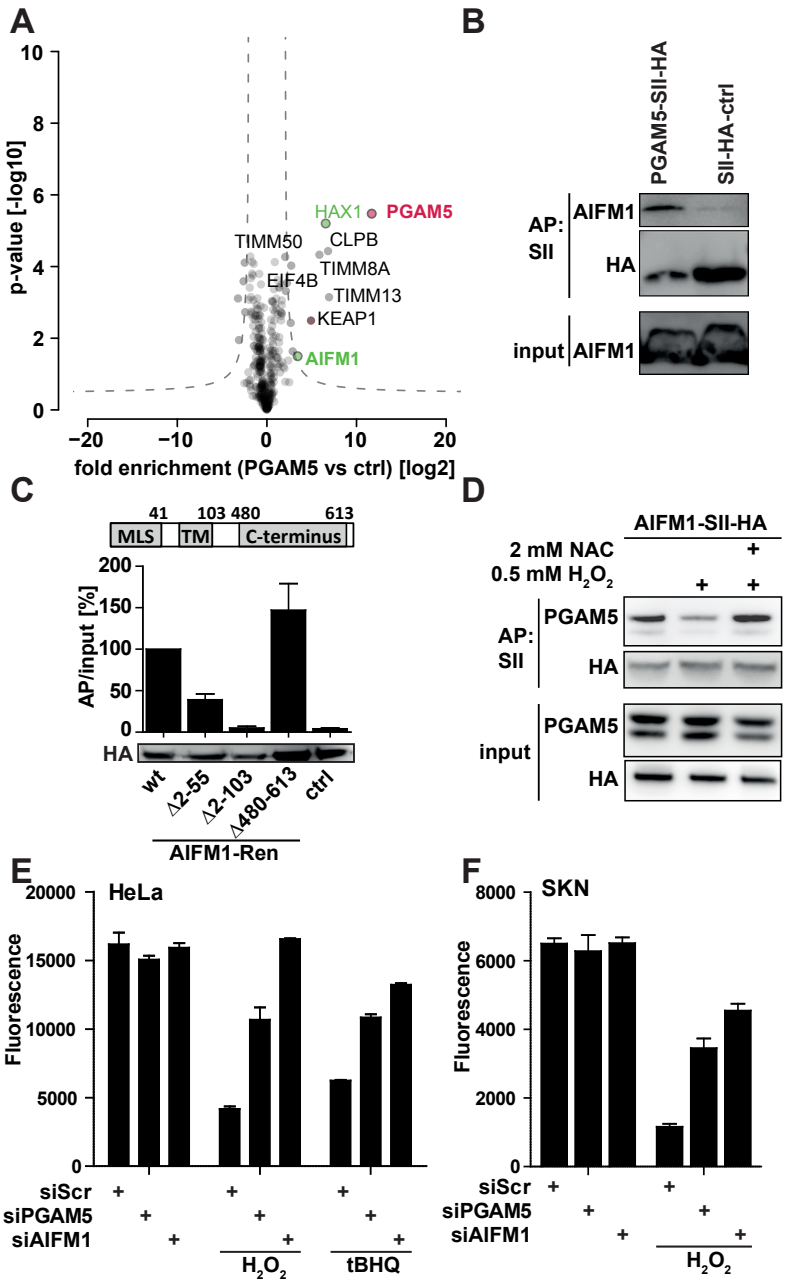
A
p-value [-log10]
fold enrichment (PGAM5 vs ctrl) [log2]
HAX1
PGAM5
TIMM50
CLPB
TIMM8A
EIF4B
TIMM13
KEAP1
AIFM1
B
PGAM5-SII-HA
SII-HA-ctrl
AP: SII
AIFM1
HA
input
AIFM1
C
MLS
TM
C-terminus
41
103 480
613
AP/input [%]
HA
wt
Δ2-55
Δ2-103
Δ480-613
ctrl
AIFM1-Ren
D
AIFM1-SII-HA
2 mM NAC
0.5 mM H2O2
AP: SII
PGAM5
HA
input
PGAM5
HA
E
HeLa
Fluorescence
siScr
siPGAM5
siAIFM1
H2O2
tBHQ
F
SKN
Fluorescence
siScr
siPGAM5
siAIFM1
H2O2

Figure 4

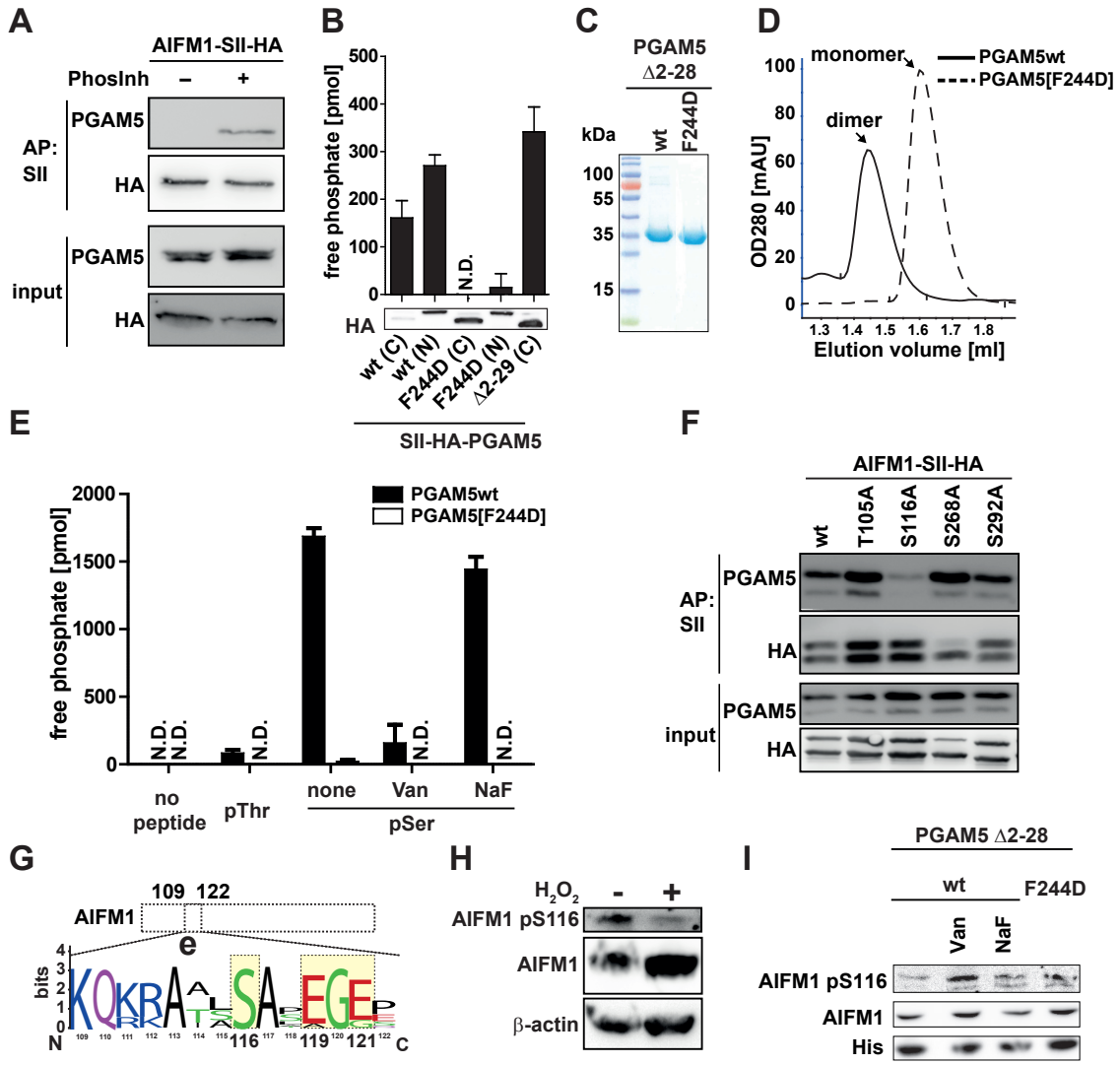
A
AIFM1-SII-HA
PhosInh – +
AP: SII
PGAM5
HA
input
PGAM5
HA
B
free phosphate [pmol]
500
400
300
200
100
0
N.D.
HA
wt (C)
wt (N)
F244D (C)
F244D (N)
Δ2-29 (C)
SII-HA-PGAM5
C
PGAM5 Δ2-28
kDa
wt
F244D
100
55
35
15
D
monomer
dimer
PGAM5wt
PGAM5[F244D]
OD280 [mAU]
100
80
60
40
20
0
1.3 1.4 1.5 1.6 1.7 1.8
Elution volume [ml]
E
free phosphate [pmol]
2000
1500
1000
500
0
PGAM5wt
PGAM5[F244D]
N.D.
N.D.
N.D.
N.D.
N.D.
N.D.
no peptide
pThr
none
Van
NaF
pSer
F
AIFM1-SII-HA
wt
T105A
S116A
S268A
S292A
AP: SII
PGAM5
HA
input
PGAM5
HA
G
109 122
AIFM1
bits
4
3
2
1
0
N
116
119
121
C
H
H2O2 - +
AIFM1 pS116
AIFM1
β-actin
I
PGAM5 Δ2-28
wt
F244D
Van
NaF
AIFM1 pS116
AIFM1
His

Figure 5

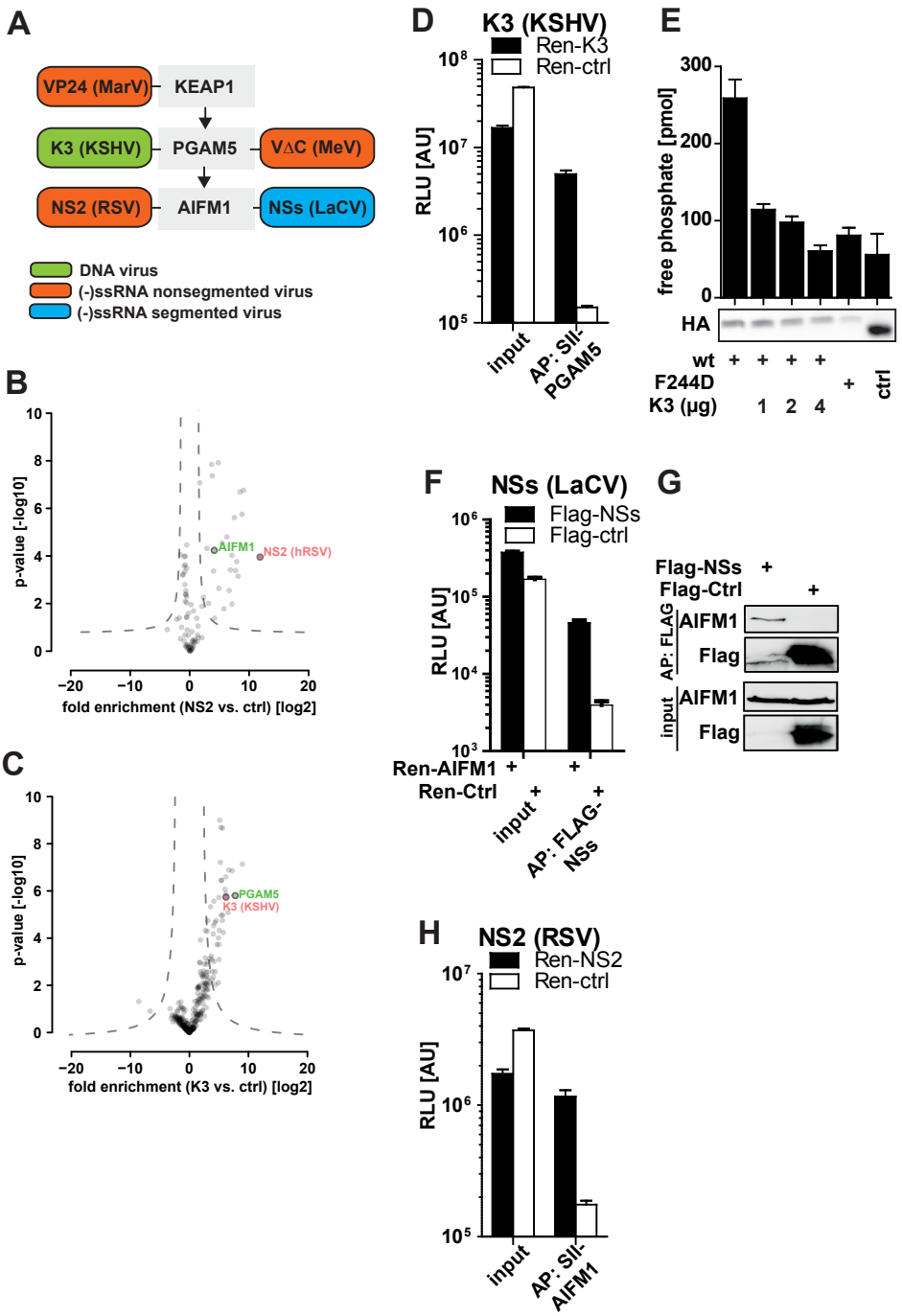
A
VP24 (MarV)
KEAP1
K3 (KSHV)
PGAM5
VΔC (MeV)
NS2 (RSV)
AIFM1
NSs (LaCV)
DNA virus
(-)ssRNA nonsegmented virus
(-)ssRNA segmented virus
B
p-value [-log10]
AIFM1
NS2 (hRSV)
fold enrichment (NS2 vs. ctrl) [log2]
C
p-value [-log10]
PGAM5
K3 (KSHV)
fold enrichment (K3 vs. ctrl) [log2]
D
K3 (KSHV)
Ren-K3
Ren-ctrl
RLU [AU]
input
AP: SII-PGAM5
E
free phosphate [pmol]
HA
wt
F244D
K3 (μg)
ctrl
F
NSs (LaCV)
Flag-NSs
Flag-ctrl
RLU [AU]
Ren-AIFM1
Ren-Ctrl
input
AP: FLAG-NSs
G
Flag-NSs
Flag-Ctrl
AP: FLAG
AIFM1
Flag
input
H
NS2 (RSV)
Ren-NS2
Ren-ctrl
RLU [AU]
input
AP: SII-AIFM1

Figure 6

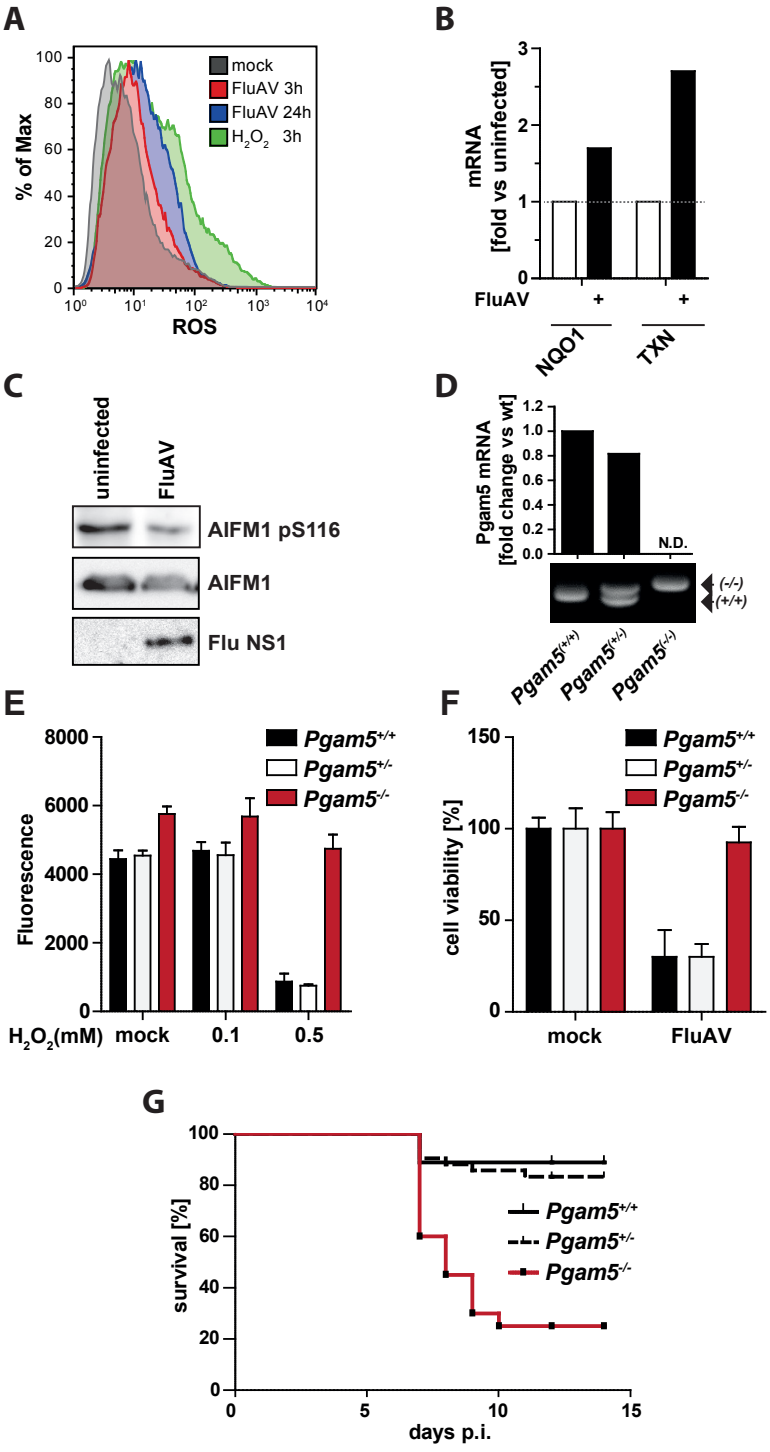
A
mock
FluAV 3h
FluAV 24h
H2O2 3h
% of Max
ROS
B
mRNA [fold vs uninfected]
FluAV
NQO1
TXN
C
uninfected
FluAV
AIFM1 pS116
AIFM1
Flu NS1
D
Pgam5 mRNA [fold change vs wt]
N.D.
(-/-)
(+/+)
Pgam5(+/+)
Pgam5(+/-)
Pgam5(-/-)
E
Pgam5+/+
Pgam5+/-
Pgam5-/-
Fluorescence
H2O2(mM) mock 0.1 0.5
F
cell viability [%]
mock
FluAV
G
survival [%]
days p.i.

Supplementary Figure S1

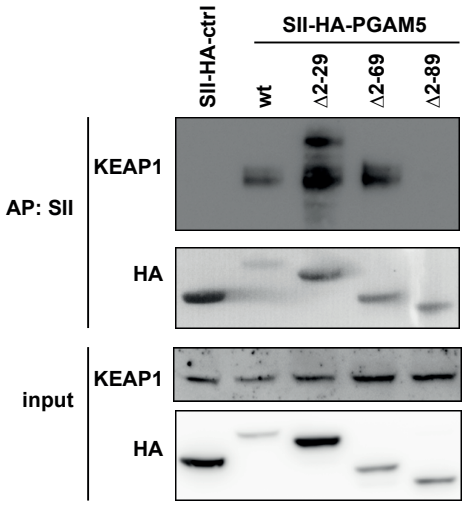

Supplementary Figure S2

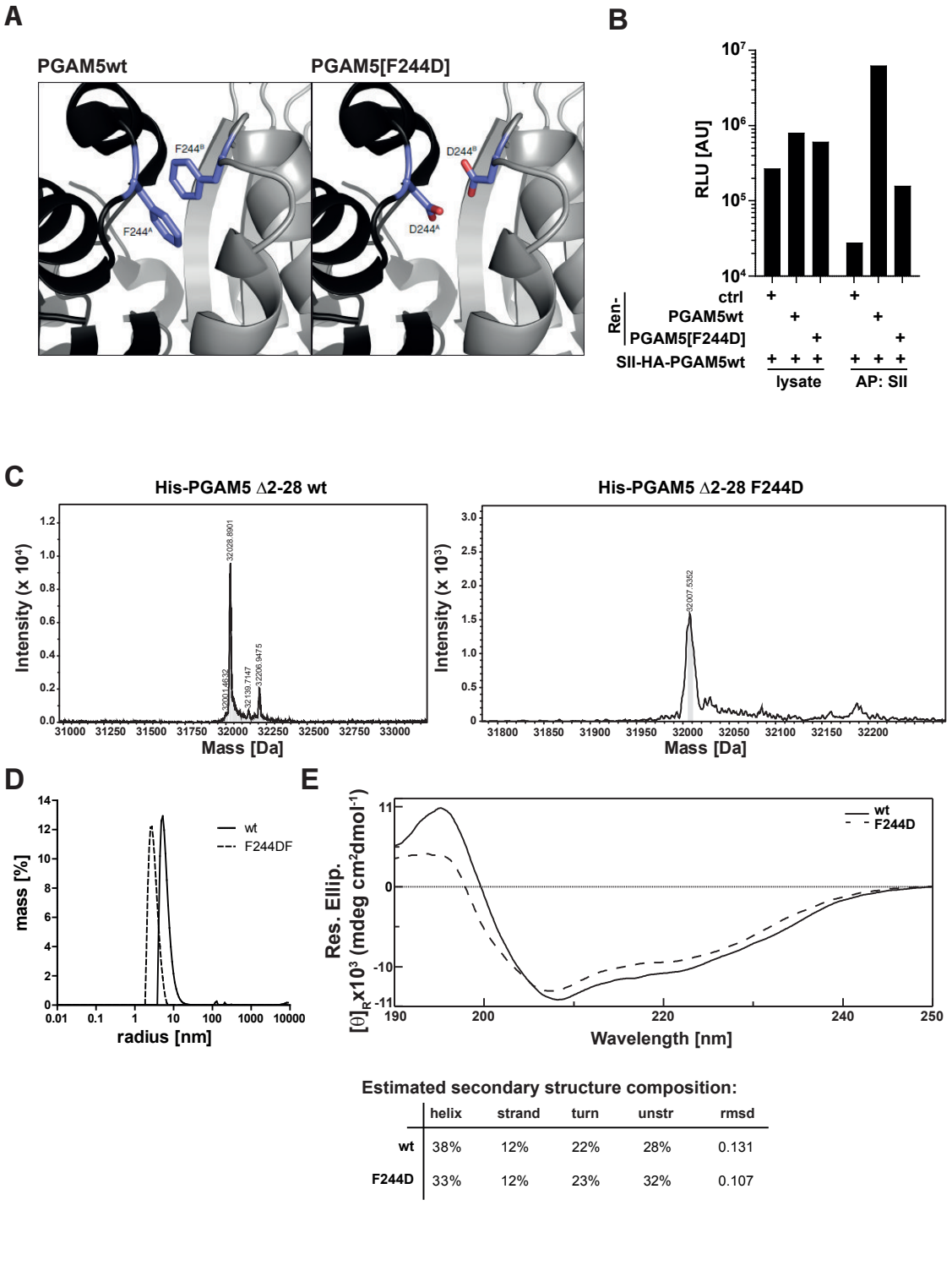

Estimated secondary structure composition:

	helix	strand	turn	unstr	rmsd
wt	38%	12%	22%	28%	0.131
F244D	33%	12%	23%	32%	0.107

Supplementary Figure S3

A

Mus musculus	Mouse	Q9Z0X1	KQRRAIAS ATEGGS
Rattus norvegicus	Rat	Q9JM53	KQRRAIAS AAEGGS
Cavia porcellus	Guinea pig	H0VP14	KQRRAALS ASAGEQ
Homo sapiens	Human	O95831	KQKKAALS ASEGEE
Pan troglodytes	Chimpanzee	K7BTY6	KQKKAALS ASEGEE
Macaca mulatte	Rhesus macaque	F7C7I3	KQKKAALS ASEGEE
Myotis lucifugus	Little brown bat	G1PCN7	KQKRAALS APEGEP
Ictidomys tridecemlineatus	Thirteen-lined ground squirrel	I3MBI5	KQRRATSS APEGEP
Oryctolagus cuniculus	Rabbit	G1SIM3	KQKRATAS APEGEP
Bos taurus	Bovine	E1BJA2	KQKRATSS ALEGEP
Ovis Aries	Sheep	W5Q1F6	KQKRATSS ALEGEP
Equus caballus	Horse	F6WXF6	KQKRATSS APEGEP
Sus scrofa	Pig	A0A068CA64	KQKRATSS APEGEP

S116

B

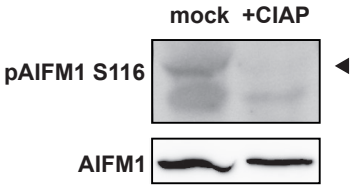

Supplementary Figure S4

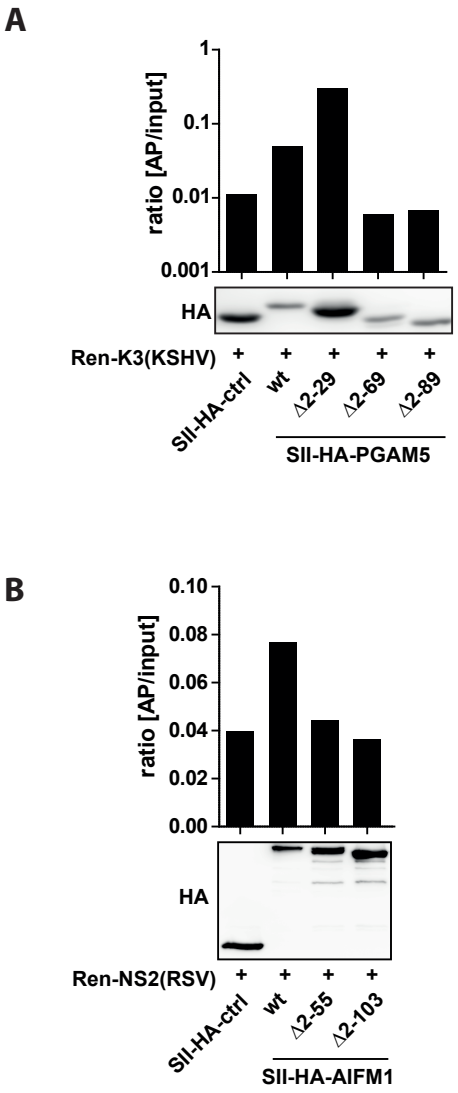

2.3 Host immune response to viral nucleic acids

By recognition of microbial structures such as unusual viral nucleic acids the innate immune system is activated. Upon viral infection, activation of IFN signaling increases the expression of ISGs and thereby plays a pivotal role. Daffis et al showed that viruses producing 2'O unmethylated capped RNA (cap-RNA) are sensitive to IFN and showed nearly no effect on IFIT1-/- mice [400]. This gave hints that IFIT1 might be involved in binding of Cap-RNA besides its role in binding 5'triphosphorylated-RNA (5'PPP-RNA) [160].

By using AP-MS with 2'O-unmethylated cap-RNA as bait we could identify the big IFIT complex (IFIT1, 2 and 3), which also is identified when using PPP-RNA as bait. By performing affinity purification with cap-RNA and Renilla-tagged cellular expressed IFIT proteins and His-tagged recombinant IFIT proteins, we could show that IFIT1 binds directly to cap-RNA. As IFIT1 reduction increased virulence of viruses lacking 2'O methyltransferase we tested if this binding affects replication of viruses. By assaying transcription and translation rates of viral RNAs and proteins we elucidated that IFIT1 binding to cap-RNA inhibits viruses on transcriptional and subsequently translational level without affecting cellular protein levels.

My part in this project was the synthesis and modification of various RNAs by in vitro transcription. Additionally, I performed translation assays in cell culture with HeLa and mouse cells depleted in IFIT1. In addition, I established affinity purification with Renilla-tagged proteins in the lab to quantify relatively interactions of proteins to nucleic acids or other proteins.

This study underlines the importance to identify inhibitors for viral 2'-O methyltransferases. These inhibitors would allow IFIT1 detection of viral nucleic acids and subsequently inhibition of viral replication and reduction in viral load by the innate immune system.

Habjan M, Hubel P, Lacerda L, Benda C, **Holze C**, Eberl CH, Mann A, Kindler E, Gil-Cruz C, Ziebuhr J, Thiel V, Pichlmair A

Sequestration by IFIT1 impairs translation of 2'O-unmethylated capped RNA

PLoS Pathogen doi: 10.1371/journal.ppat.1003663 (2013)

OPEN ACCESS Freely available online

PLOS | PATHOGENS

Sequestration by IFIT1 Impairs Translation of 2′O-unmethylated Capped RNA

Matthias Habjan[1☯], Philipp Hubel[1☯], Livia Lacerda[1], Christian Benda[2], Cathleen Holze[1], Christian H. Eberl[3], Angelika Mann[1], Eveline Kindler[4], Cristina Gil-Cruz[4], John Ziebuhr[5], Volker Thiel[4,6], Andreas Pichlmair[1]*

1 Innate Immunity Laboratory, Max-Planck Institute of Biochemistry, Martinsried/Munich, Germany, **2** Department of Structural Cell Biology, Max-Planck Institute of Biochemistry, Martinsried/Munich, Germany, **3** Department of Proteomics and Signal Transduction, Max-Planck Institute of Biochemistry, Martinsried/Munich, Germany, **4** Institute of Immunobiology, Kantonspital St. Gallen, St. Gallen, Switzerland, **5** Institute of Medical Virology, Justus Liebig University, Giessen, Germany, **6** Vetsuisse Faculty, University of Zürich, Zürich, Switzerland

Abstract

Viruses that generate capped RNA lacking 2′O methylation on the first ribose are severely affected by the antiviral activity of Type I interferons. We used proteome-wide affinity purification coupled to mass spectrometry to identify human and mouse proteins specifically binding to capped RNA with different methylation states. This analysis, complemented with functional validation experiments, revealed that IFIT1 is the sole interferon-induced protein displaying higher affinity for unmethylated than for methylated capped RNA. IFIT1 tethers a species-specific protein complex consisting of other IFITs to RNA. Pulsed stable isotope labelling with amino acids in cell culture coupled to mass spectrometry as well as *in vitro* competition assays indicate that IFIT1 sequesters 2′O-unmethylated capped RNA and thereby impairs binding of eukaryotic translation initiation factors to 2′O-unmethylated RNA template, which results in inhibition of translation. The specificity of IFIT1 for 2′O-unmethylated RNA serves as potent antiviral mechanism against viruses lacking 2′O-methyltransferase activity and at the same time allows unperturbed progression of the antiviral program in infected cells.

Citation: Habjan M, Hubel P, Lacerda L, Benda C, Holze C, et al. (2013) Sequestration by IFIT1 Impairs Translation of 2′O-unmethylated Capped RNA. PLoS Pathog 9(10): e1003663. doi:10.1371/journal.ppat.1003663

Editor: Michael S. Diamond, Washington University School of Medicine, United States of America

Received April 4, 2013; **Accepted** August 12, 2013; **Published** October 3, 2013

Funding: This work was supported by the Max Planck Society Free-Floater program to AP, the European Research Council (iViP)to AP, the Humboldt Research Fellowship to MH, and the German Research Society (DFG; SFB1022) to JZ. The funders had no role in study design, data collection and analysis, decision to publish, or preparation of the manuscript.

Competing Interests: The authors have declared that no competing interests exist.

* E-mail: apichl@biochem.mpg.de

☯ These authors contributed equally to this work.

Introduction

Effective control of viral infection by host organisms requires sensing of pathogens and activation of appropriate defence mechanisms [1–3]. One component commonly sensed by the host is viral genetic material, whether DNA delivered to the cytoplasm through viral infection or viral RNA bearing motifs not commonly found on eukaryotic RNAs [4,5]. Most cellular cytoplasmic RNAs are single-stranded, and bear a 5′monophosphate (rRNAs and tRNAs), or an N7 methylated guanosine cap (mRNAs) linked via a 5′-to-5′ triphosphate bridge to the first base. In higher eukaryotes, mRNA is further methylated at the 2′O position of the first ribose [6,7]. Viruses, in contrast, can form long double-stranded RNA (dsRNA) and generate RNAs bearing 5′triphosphosphates (PPP-RNA) or RNAs lacking methylation [8–10]. All these distinct features of viral as opposed to cellular RNAs have been shown to activate the innate immune system and elicit synthesis of antiviral cytokines including Type I interferons (IFN-α/β), which ultimately restrict virus growth [11–14]. Among the proteins that sense viral RNA and are linked to IFN-α/β synthesis are retinoic acid-inducible gene I (RIG-I) and melanoma differentiation-associated gene 5 (Mda-5), which form the family of RIG-like receptors (RLRs) [5]. A further set of host proteins appears to bind virus-derived RNAs to directly inhibit virus production [8]. Several of these proteins are highly expressed upon stimulation of cells with cytokines like IFN-α/β and their antiviral effects become apparent only after binding to virus-derived nucleic acid. Prominent examples for such proteins are dsRNA binding proteins such as dsRNA-activated protein kinase R and 2′-5′ oligoadenylate synthetase, and proteins that bind PPP-RNA, like interferon-induced proteins with tetratricopeptide repeats (IFIT) 1 and -5 [3,15,16]. Little is known about the repertoire of cellular proteins that recognise unmethylated cap structures, although replication of viruses with inactive RNA 2′O methyltransferase is strongly inhibited by IFN-α/β *in vitro* and *in vivo* [11,15]. Some of this antiviral activity has been genetically linked to Ifit1 and -2 in mice [17–19]. Here, we used an unbiased mass-spectrometry-based approach to identify cellular proteins that bind to 5′ unmethylated and methylated capped RNA, and explored their contribution to antiviral host responses.

Results

Identification of human and mouse proteins that bind capped RNA

To identify proteins that interact with 5′ capped RNA we used a proteomics approach based on affinity purification and mass

Author Summary

Cellular messenger RNAs of higher eukaryotes are capped with a methylated guanine and, in addition, methylated at the 2′O position of the first ribose. Viruses unable to methylate their RNA at the 2′O position of the cap and viruses generating uncapped RNA with 5′ triphosphate groups are inhibited by an antiviral complex of different IFIT proteins. How IFIT proteins restrict viruses lacking 2′O methylation at the RNA cap remained unclear. We used a mass spectrometry-based approach to identify proteins binding to capped RNA with different methylation states. We found that IFIT1 directly binds to capped RNA and that this binding was dependent on the methylation state of the cap. Having identified IFIT1 as being central for recognition of 2′O-unmethylated viral RNA we further examined the mode of action of IFITs *in vitro* and *in vivo*. Our experiments clearly show that the antiviral mechanism of IFIT1 is based on sequestration of viral RNA lacking cap 2′O methylation, thereby selectively preventing translation of viral RNA. Our data establish IFIT1 as a general sensor for RNA 5′ end structures and provide an important missing link in our understanding of the antiviral activity of IFIT proteins.

spectrometry (AP-MS) [16]. RNA bearing terminal 5′ hydroxyl (OH-RNA), 5′ triphosphate (PPP-RNA), an unmethylated cap (CAP-RNA), a guanosine-N7 methylated cap (CAP0-RNA), or a guanosine-N7 methylated cap and a ribose-2′O methylated first nucleotide (CAP1-RNA) was coupled to agarose beads. The beads were then incubated with lysates of naïve HeLa cells or HeLa cells treated with IFN-α to increase the abundance of antiviral proteins (Fig. 1a, Fig. S1). By employing liquid-chromatography coupled to tandem mass spectrometry (LC-MS/MS) followed by quantitative interaction proteomics analysis, we identified 528 proteins that interacted with unmodified or RNA-coated beads (Fig. S2a, Table S1). While a large number of proteins were equally well represented in the bound fractions obtained with all RNAs (Fig. S2a), 68 proteins were found to be significantly enriched in samples recovered with 5′modified RNA compared to OH-RNA (Fig. S2b). As expected, the PPP-RNA binding proteins RIG-I (DDX-58), the IFIT1, -2, -3 complex and IFIT5 were enriched in PPP-RNA affinity purifications of IFN-α-treated HeLa cell lysate (Fig. 1b), validating the approach and confirming previous data [16]. Using unmethylated CAP-RNA as bait, we significantly enriched for proteins known to associate with cellular capped RNA (12 of 16 proteins) (Fig. 1c, Fig. S2b, Table S1). However, an important feature of cellular mRNAs is methylation on the N7 position of the guanosine cap and the ribose-2′O position of the first nucleotide (CAP1). N7 methylation is known to increase the affinity of the cap structure for proteins such as EIF4E and other cap-binding proteins [6,7]. A methylation-dependent increase in protein binding was also evident in our AP-MS analysis when unmethylated CAP-RNA and methylated CAP1-RNA were used as baits (16 vs. 27 identified proteins), as the latter captured a higher number of significantly enriched proteins and, overall, these were enriched to a greater degree, as measured by label-free quantification (Fig. 1c–d, Table S1). Notably, we identified IFIT1, -2 and -3 among the uncharacterised CAP-RNA binding proteins, suggesting that the IFIT complex binds to RNA in a cap-dependent manner (Fig. 1c). IFIT5, which shows 57.2% aminoacid sequence identity and 75.6% similarity to IFIT1 and has recently been shown to form a tight binding pocket that specifically accommodates PPP-RNA [20], was not detected in fractions that bound capped RNA. When we compared our AP-MS dataset with transcriptome data of interferon-stimulated cells [21], IFITs were the only interferon-induced proteins found to be specifically enriched in CAP-RNA purifications, suggesting a predominant role of IFITs in innate immune responses directed against CAP-RNA (Fig. 1c, Fig. S2b). To analyse whether the set of proteins that binds to 5′modified RNA is conserved in other species, we performed the same AP-MS analysis on lysates of naïve and IFN-α-treated mouse embryonic fibroblasts (MEFs) (Fig. S3a, b, Table S2). Surprisingly, although PPP-RNA specifically enriched for Ifit1, the abundance of Ifit2 and Ifit3 was not increased (Fig. 1e). Instead we found enrichment of Ifit1c (also known as Gm14446), an uncharacterised IFIT protein that is strongly induced by IFN-α/β or virus infection (Fig. S4), suggesting that the architecture of the murine IFIT complex differs from that of its human counterpart. Significant enrichment for Ifit1 and Ifit1c could also be achieved with unmethylated CAP-RNA, but not with methylated CAP1-RNA, despite the fact that the latter bait captured more proteins with higher enrichment scores (Fig. 1f, g). We concluded from these analyses that, in both human and mouse, the IFIT complex is the only IFN-induced component that shows significant affinity for capped RNA.

IFIT1 is the only IFIT that binds capped RNA

Since human IFIT1, -2 and -3 associate with each other to form a multiprotein complex, we wished to determine which of them was responsible for tethering the IFIT complex to unmethylated CAP-RNA. We overexpressed each of the IFIT proteins, tagged with *Renilla* luciferase, in 293T cells and performed affinity purifications using OH-RNA, PPP-RNA and CAP-RNA. Remarkably, only human and murine IFIT1 were detected when CAP-RNA was used as bait (Fig. 2a, b), suggesting that IFIT1 mediates binding of the IFIT complex to CAP-RNA. Consistent with the MS analysis, IFIT5 exclusively bound to PPP-RNA but not to CAP-RNA. To exclude contribution of cellular factors to the interaction between IFIT1 and CAP-RNA we used recombinant human IFIT proteins for RNA precipitations which confirmed a direct interaction of IFIT1 with capped RNA (Fig. 2c). A structure-based modelling approach using IFIT5 [20] as template suggested that the RNA-binding cavity of IFIT1 is ~700 $Å^3$ larger than that of IFIT5 (Fig. S5) – implying that IFIT1 has slightly different RNA-binding properties. However, a lysine at position 151 and an arginine at position 255 of IFIT1, two residues involved in binding the terminal 5′ triphosphate group on PPP-RNA by IFIT5 and IFIT1 [20], were also required for binding of IFIT1 to capped RNA (Fig. 2d), indicating an overall similar mode of binding.

To provide additional evidence that binding of IFIT1 is indeed responsible for associating the IFIT complex to CAP-RNA, we performed AP-MS experiments on wild-type ($Ifit1^{+/+}$) and mutant, Ifit1-deficient ($Ifit1^{-/-}$) MEFs. The overall precipitation efficiency was comparable in both cell types, as evidenced by equal enrichment of the RNA-binding protein Syncrip and the cap-binding protein Ncbp1 (Fig. 2e and Fig. S4b). Ifit1c was not enriched in precipitates from $Ifit1^{-/-}$ MEFs, which is consistent with the notion that the murine Ifit complex binds to CAP-RNA through Ifit1. These results show that the specific binding properties of IFIT1 are essential for recruitment of the human and murine IFIT complexes to their RNA targets.

IFIT1 binding depends on the methylation status of the RNA cap

To identify proteins that bind capped RNA in a methylation-dependent manner we used unmethylated CAP-RNA and fully

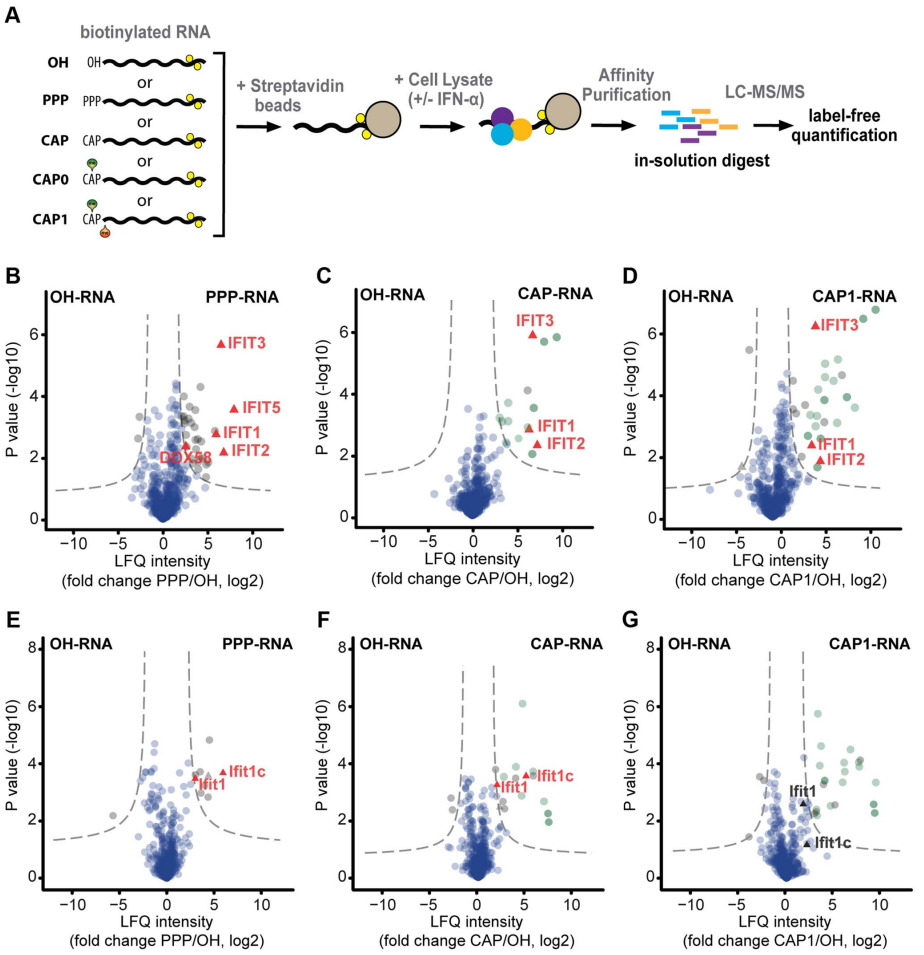

Figure 1. Mass spectrometry-based identification of human and murine interactors of capped RNA. (**a**) Schematic depiction of the experimental approach used for mass spectrometry (MS)-based identification of cellular RNA binding proteins. Biotinylated RNA with different 5′ end structures (OH, PPP, CAP, CAP0, CAP1) was coupled to streptavidin beads, and incubated with lysates obtained from cells that had been left untreated or treated with 1000 U/ml IFN-α for 16 h. Bound proteins were denatured, alkylated and directly digested with trypsin. The resulting peptides were subjected to shotgun liquid chromatography-tandem MS (LC-MS/MS). Three independent experiments were performed for each RNA bait, and the data were analysed with the MaxQuant software [37] using the label-free quantification algorithm [38]. (**b–d**) Proteins obtained from lysates of IFN-α-treated HeLa cells using the indicated biotinylated RNA baits were analysed by LC-MS/MS. Volcano plots show the degrees of enrichment (ratio of label-free quantitation (LFQ) protein intensities; x-axis) and p-values (t-test; y-axis) by PPP-RNA (**b**), CAP-RNA (**c**), and CAP1-RNA (**d**) baits as compared to OH-RNA. Significantly enriched interactors (see Materials and Methods) are separated by a hyperbolic curve (dotted line) from background proteins (blue dots), known cap-binding proteins (dark-green), and proteins known to associate with capped RNA (light green). Interferon-induced proteins [21] detected in the significantly enriched fractions (IFIT1-3 and 5, DDX58) are highlighted (red triangles). (**e–g**) As in (**b–d**) but for lysates of IFN-α-treated mouse embryo fibroblasts (MEFs). The interferon-induced proteins Ifit1 and Ifit1c [42] in significantly enriched and non-enriched fractions are highlighted.
doi:10.1371/journal.ppat.1003663.g001

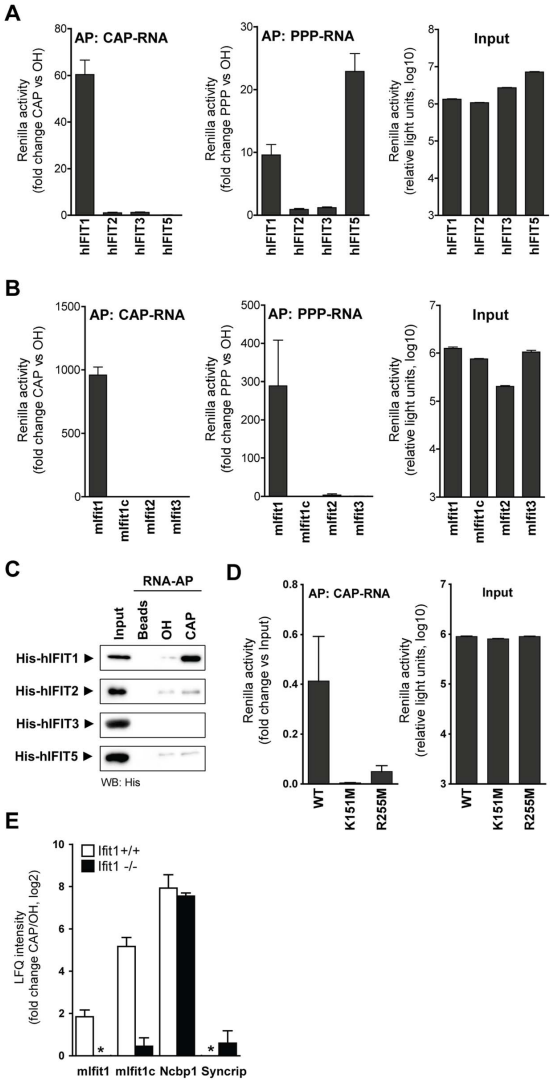

Figure 2. Human and mouse IFIT1 bind directly to unmethylated capped RNA. (**a**) Isolation of luciferase-tagged human IFIT (hIFIT) proteins from transfected 293T cells with beads coated with 250 ng RNA bearing 5′ OH, PPP or CAP. The graphs show luciferase activity after affinity purification (AP) with PPP-RNA and CAP-RNA (normalized to OH-RNA) and the activity of 10% of the input lysates. (**b**) Data obtained (as in **a**) for luciferase-tagged murine Ifit (mIfit) proteins affinity purified with PPP-RNA and CAP-RNA. (**c**) Recombinant His-tagged hIFIT1, -2, -3, and -5 were incubated with beads only or beads coated with OH-RNA or CAP-RNA. Bound proteins were detected by western blotting. Input shows $1/10^{th}$ of the amount incubated with beads. (**d**) Purification of luciferase-tagged wild-type (WT) and hIFIT1 mutants with CAP-RNA-coated beads. The graphs show luciferase activity after affinity purification and the activity of 10% of the input lysates. (**e**) Ratios of LFQ intensities of proteins identified by mass spectrometry in precipitates of CAP-RNA vs. OH-RNA in IFN-α-treated MEFs from wild-type ($Ifit1^{+/+}$, grey bars) and Ifit1-deficient ($Ifit1^{-/-}$, black bars) C57BL/6 mice. Error bars indicate means (±SD) from three independent affinity purifications. Asterisks indicate ratios with negative values.
doi:10.1371/journal.ppat.1003663.g002

methylated CAP1-RNA as baits with IFN-treated HeLa cell lysates and quantified the captured proteins by LC-MS/MS. As expected [6,7], most cellular proteins were significantly enriched in the CAP1-RNA bound fraction (Fig. 3a, Fig. S2c). The most notable exceptions were IFITs and the cellular 2′O-methyltransferase FTSJD2, both of which clearly favoured CAP-RNA (Fig. 3a, Fig. S2c and Fig. 1 c, d and f, g). We confirmed the MS data by a series of RNA precipitations followed by western blotting for endogenous proteins. Proteins associating to RNA in a 5′ independent manner, such as ILF3, precipitated similarly well regardless of the RNA used (Fig. 3b). Cap N7 methylation increased the association of EIF4E to RNA and methylation of the 2′O position did not impair precipitation efficiency. In accordance with the MS results, IFIT1 bound well to unmethylated CAP-RNA and CAP0-RNA (N7 methylated cap) but revealed reduced binding to CAP1-RNA (N7 methylated cap and 2′O methylated first ribos).

We next tested the contributions of individual cap methylation sites to IFIT1 binding. To this end, we measured binding of luciferase-tagged human and murine IFIT1 with either CAP-, CAP0- or CAP1-RNA. The unmethylated CAP-RNA bait captured more human or murine IFIT1 than either of the methylated RNAs (Fig. 3c). Furthermore, the analysis suggested that N7 methylation on the cap and 2′O methylation of the first ribose both contributed to the reduced binding of IFIT1 to RNA. Similarly, the precipitation efficiency of recombinant human and murine IFIT1 was reduced when capped *in vitro* transcribed RNAs were enzymatically methylated at the N7 and 2′O position (Fig. 3d) or when chemically synthesised RNAs with the same modifications were used (Fig. 3e). This was in contrast to EIF4E that showed prominent binding when CAP0- or CAP1-RNA was used (Fig. 3d, e). Collectively, these data suggest that human and murine IFIT1 have the capability to directly sense the methylation state of capped RNA.

Antiviral activity of IFIT1 against 2′O methyltransferase-deficient viruses

Having established that IFIT1 binds directly to capped RNA and that methylation on the 2′O position of the first ribose markedly reduces binding, we tested the impact of IFIT1 on virus replication. Probably as a result of evolutionary pressure, most viruses that infect higher eukaryotes have evolved mechanisms to generate RNA that is methylated on both the N7 position of the guanosine cap and the 2′O position of the first ribose [9]. We therefore used wild-type human coronavirus (HCoV) 229E (229E-WT), which generates CAP1-RNA, and a mutant variant that has a single amino acid substitution (D129A) in the viral 2′O methyltransferase that is part of non-structural protein 16 (229E-DA), and consequently only produces CAP0-RNA [11]. IFN-α-treated HeLa cells infected with the 229E-DA mutant expressed significantly reduced levels of viral RNA and protein relative to those exposed to 229E-WT (Fig. 4a, b). Moreover, this effect was strictly dependent on IFIT1, since the two viruses replicated equally well in HeLa cells treated with siRNA against IFIT1 (Fig. 4a, b). Similar effects were observed in an analogous mouse model. Thus, when IFN-α treated macrophages (MΦs) from C57BL/6 (Ifit $^{+/+}$) mice were infected with a wild-type murine coronavirus (mouse hepatitis virus strain A59; MHV-WT) and a mutant strain carrying the equivalent amino acid substitution (D130A) in its 2′O methyltransferase [11,17] (MHV-DA), the latter produced 100-fold less viral RNA and comparably reduced levels of viral protein (Fig. 4c, d). In contrast, when Ifit1-deficient MΦs were infected, no significant virus-dependent differences were observed, again pointing to a critical role for Ifit1 in restricting replication of MHV-DA. Note that the presence of Ifit1 itself did not increase IFN-α/β production (Fig. S6), suggesting a direct antiviral effect of Ifit1. We next assessed the impact of Ifit1 on virus growth *in vivo*. MHV-WT grew to high titres in the spleens of infected Ifit1$^{+/+}$ mice, whereas no viral replication could be detected upon infection with MHV-DA (Fig. 4e). In agreement with the *in vitro* data, growth of MHV-DA was partially restored in Ifit1-deficient animals. These data suggest that IFIT1 has a central role in restraining the growth of 2′O methyltransferase-deficient coronaviruses *in vitro* and *in vivo*, which is compatible with the greater affinity of IFIT1 for non-2′O-methylated RNA cap structures. The data further imply that this role is conserved in mouse and human.

IFIT1 specifically regulates the translation of 2′O unmethylated capped viral RNA

RNA capping is essential for a variety of cellular functions. The presence of a 5′ cap regulates mRNA export from the nucleus, protects RNAs from degradation and is necessary for efficient translation [7,22]. An involvement of IFIT1 in nuclear-cytoplasmic transport is unlikely, given the exclusively cytoplasmic localisation of IFIT proteins and their negative effect on coronaviruses, which replicate in the cytoplasm. We therefore measured the stability of the RNAs generated by MHV-WT or MHV-DA in MΦs that had been stimulated with IFN-α. Since MHV-WT replicates significantly better than the mutant virus, we blocked virus replication by adding cycloheximide (CHX) shortly after infecting MΦs with the two viruses (Fig. 5a). CHX inhibits de novo synthesis of the viral polymerase, a prerequisite for transcription of viral RNA and thereby allows to normalise for viral transcripts in coronavirus infected cells. The abundance of viral transcripts 4 h and 8 h after infection was indistinguishable in CHX treated cells infected with MHV-WT and MHV-DA (Fig. 5b), suggesting that 2′O methylation of the first ribose does not affect the stability of the viral RNA within the timeframe of this experiment.

Many cellular antiviral defence mechanisms generally block translation of mRNA, thereby also severely inhibiting virus growth. To assess the global impact of Ifit1 on the translation machinery, we used pulsed stable isotope labelling in cell culture (SILAC) [23]. In pulsed SILAC, unlabelled cells are transferred to SILAC growth medium containing ^{13}C- and ^{15}N-labelled arginine (Arg10) and lysine (Lys8). Newly synthesized proteins incorporate the heavy label and pre-existing proteins remain in the light form, which allows to measure relative changes in the translation of individual proteins, regardless of the absolute amount of RNA present. We pulsed Ifit1$^{+/+}$ and Ifit1$^{-/-}$ MΦs infected for 5½ h with either MHV-WT or MHV-DA for 2 h with SILAC medium (Fig. 5c) and analysed infected cells by whole-proteome shotgun LC-MS/MS. We could reliably quantify 721 proteins in terms of heavy/light ratios in all three biological replicates tested. Heavy/light ratios of cellular proteins were comparable in Ifit1$^{+/+}$ and Ifit1$^{-/-}$ MΦs, irrespective of the virus used for infection (Fig. 5d, boxes), suggesting that neither the presence of Ifit1 nor infection with MHV-DA affected the overall rate of translation in the cells. The expression profiles of individual proteins known to be important in innate immune responses against viruses, such as the pattern recognition receptor RIG-I (DDX58), signalling molecules (STAT1, -2, -3), interferon-induced proteins (Ifi205b, Ifi35, Gvin1) and components of the major histocompatibility complex (H2-K1, H2-D1, Cd74), were similar in both cell types infected with either virus (Fig. S7). However, translation of viral nucleocapsid and membrane proteins was selectively reduced in Ifit1$^{+/+}$ MΦs infected with MHV-DA (Fig. 5d and Fig. S7).

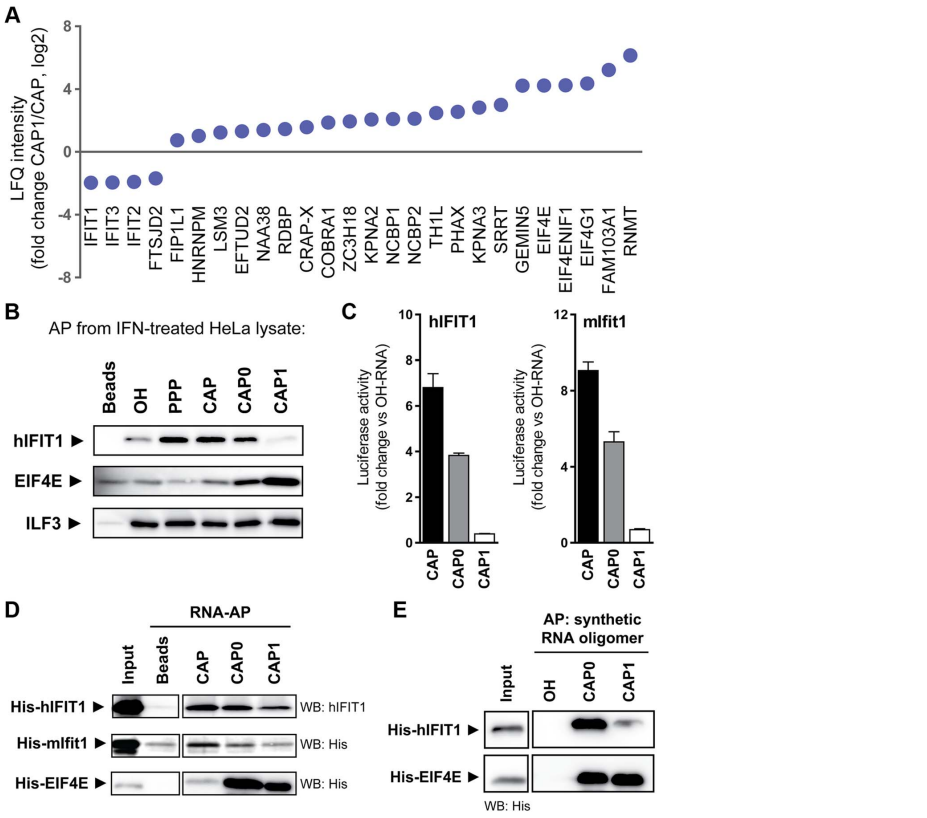

Figure 3. IFIT1 binds capped RNA in a methylation state-dependent manner. (**a**) Ratio of LFQ intensities of proteins identified by LC-MS/MS as significantly enriched in CAP1-RNA relative to CAP-RNA affinity purifications from IFN-treated HeLa cells, after filtering against the set of proteins that showed enrichment relative to 5′ OH-RNA(see Fig. S2b). Error bars indicate means (±SD) from three independent affinity purifications. (**b**) Precipitation of endogenous proteins from lysates of IFN-α treated HeLa cells with biotinylated RNA bearing 5′ OH, PPP, CAP, CAP0 or CAP1 structures. Human IFIT1 (hIFIT1), EIF4E and ILF3 in precipitates were detected by western blotting. Input shows 1/10th (mIFIT1, EIF4E) and 1/30th (hIFIT1) of the amount incubated with beads. (**c**) Affinity purification of luciferase-tagged human (hIFIT1) and murine (mIfit1) IFIT1 expressed in 293T cells on beads bearing 5′ OH, CAP, CAP0, or CAP1 RNA. (**d**) Binding of recombinant IFIT1 to capped RNAs. As in (**c**), but RNA-coated beads were incubated with recombinant His-tagged mouse Ifit1 (His-mIfit1), human His-hIFIT1 or human His-EIF4E and bound protein was quantified by western blotting. (**e**) Binding of recombinant His-tagged hIFIT1 and EIF4E to chemically synthesized, biotinylated RNA oligomers. Synthetic triphosphorylated RNAs with (CAP1) or without (CAP0) 2′O-methyl group on the first ribose were capped in vitro using recombinant vaccinia virus capping enzyme (see Materials and Methods). As control we used a synthetic RNA harbouring a 5′ hydroxyl group (OH). Synthetic RNAs were coupled to beads, incubated with recombinant proteins and bound proteins detected by western blotting. Input shows 1/10th of the amount incubated with beads.
doi:10.1371/journal.ppat.1003663.g003

Variation in large datasets can be best evaluated by principal-component analysis, which computes the variable with the greatest effect in a given dataset. This analysis revealed that Ifit1$^{+/+}$ MΦs infected with MHV-DA showed the highest variation (Component 1 accounting for 55.9% of variation) as compared to all other conditions tested (Fig. 5e), and among all identified proteins, MHV proteins were mainly responsible for this variation (Fig. 5f). Taken together, these data indicate that synthesis of proteins encoded by viral RNAs lacking 2′O methylation on the first ribose is specifically inhibited by IFIT1. Expression of proteins encoded by fully methylated RNA, such as cellular mRNA or 2′O methylated viral RNA, is not affected by the activity of IFIT1.

IFIT1 and translation factors compete for mRNA templates

Translation of cellular capped mRNA requires binding of the cap-binding protein EIF4E, which has a high affinity for

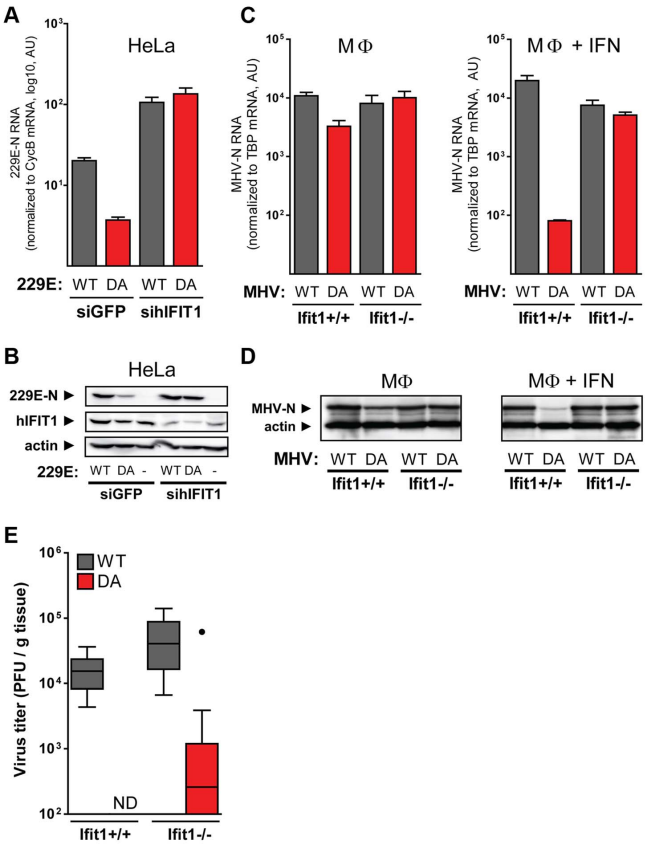

Figure 4. IFIT1 inhibits viral RNA and protein synthesis in cells infected with 2′O methyltransferase-deficient coronavirus. (**a–b**) HeLa cells were cotransfected for 48 h with an expression construct for the HCoV-229E receptor, human aminopeptidase N, and siRNAs targeting IFIT1 or the green fluorescent protein (GFP). Cells were then treated with 20 U IFN-α and infected with wild-type HCoV-229E (229E-WT; grey bars) or the 2′O methyltransferase-deficient HCoV-229E (D129A) mutant (229E-DA; red bars). Total RNA and protein were harvested 24 h post infection and analysed by quantitative RT-PCR (**a**) and western blotting (**b**), respectively. Quantitative RT-PCR data are from one of three representative experiments showing means ±SD for HCoV-229E nucleoprotein (229E-N) RNA after normalization to cyclin B (CycB) mRNA. (**c–d**) Bone marrow-derived macrophages (Mϕ) derived from C57BL/6 (Ifit1$^{+/+}$) and Ifit1-deficient (Ifit1$^{-/-}$) mice were treated or not with 50 U of IFN-α for 2 h and infected with wild-type MHV (WT; grey bars) or 2′O methyltransferase-deficient MHV (DA; red bars). RNA and protein were harvested 8 h post infection and analysed by quantitative RT-PCR (**c**) and western blotting (**d**). Quantitative RT-PCR results are from one of three representative experiments, showing means ±SD for MHV nucleoprotein (MHV-N) RNA after normalization to the TATA-binding protein (TBP) mRNA. (**e**) Ifit1$^{+/+}$ and Ifit1$^{-/-}$ mice were infected intraperitoneally with 5,000 plaque-forming units of MHV WT (grey bars) or DA (red bars). Viral titers in the spleens of 12 mice per condition were measured 48 h after infection. Data are shown as Tukey box-whisker plots (ND, not detectable; outlier indicated as black dot).
doi:10.1371/journal.ppat.1003663.g004

methylated cap structures [7,22]. Therefore, we tested whether IFIT1 could compete with EIF4E for binding to RNA template. We coupled limiting amounts of unmethylated CAP-RNA, N7-methylated CAP0-RNA and fully methylated CAP1-RNA to beads and tested whether the binding ability of recombinant EIF4E is altered by the presence of recombinant IFIT1. When we used CAP-RNA or CAP0-RNA, EIF4E binding to the beads was reduced by addition of IFIT1, suggesting that the two proteins compete for the RNA target (Fig. 6a). In contrast, when methylated CAP1-RNA was used the amount of EIF4E recovered was not affected by the presence of IFIT1. Competition between Eif4e and Ifit1 for capped RNA was also seen when total lysates of IFN-α-stimulated MEFs were used as inputs for experiments. Unmethylated CAP-RNA captured considerably more Eif4e from

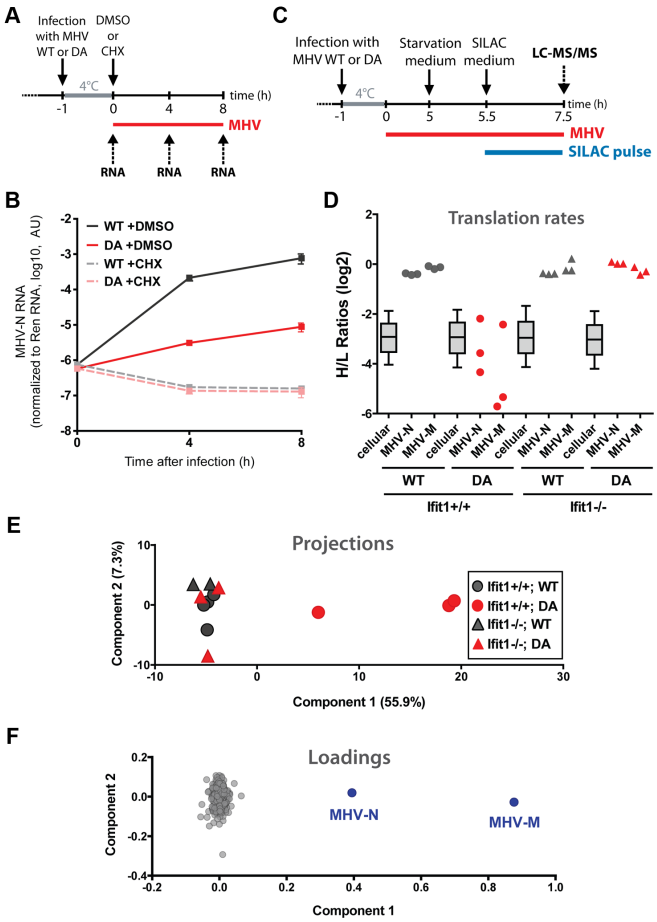

Figure 5. IFIT1 specifically blocks translation of 2′-O-unmethylated capped viral RNA. (**a**) Experimental design used to assess the stability of MHV RNA in infected cells. Bone marrow-derived macrophages (Mϕ) from C57/BL6 mice were treated with 50 U of IFN-α for 2 h prior to infection with wild-type MHV (WT) or 2′O methyltransferase-deficient MHV (DA) at 4°C for 1 h. Directly after infection, cells were treated with 100 μg/ml cycloheximide (CHX) or DMSO. Total RNA was harvested at 0, 4, and 8 h post infection and analysed by quantitative RT-PCR. (**b**) MHV nucleoprotein (MHV-N) RNA in cells infected with MHV WT (grey) or DA mutant (red), treated with DMSO (solid lines) or CHX (dashed lines). Data from one representative experiment of three are depicted, showing means ±SD after normalization to a known amount of in vitro transcribed *Renilla* luciferase RNA (Ren) added to cell lysates. (**c**) Experimental design for pulsed SILAC coupled to mass spectrometry to determine relative changes in protein translation during infection. Macrophages from C75/BL6 (Ifit1$^{+/+}$) and Ifit1-deficient (Ifit1$^{-/-}$) mice grown in normal growth medium containing light (L) amino acids were infected at 4°C for 1 h with wild-type MHV (WT) or 2′O methyltransferase-deficient MHV (DA). Five hours post infection cells were incubated with starvation medium (lacking Lys and Arg) for 30 min, then SILAC medium containing heavy (H) labelled amino acids (Lys8, Arg10) was added, and 2 h later total protein lysate was prepared and subjected to LC-MS/MS analysis. (**d**) Translation rates for 721 cellular proteins, as determined by heavy (H) to light (L) ratios from LC-MS/MS, were plotted as box-whisker plots (whiskers from 10th to 90th percentile). Individual ratios for the MHV nucleoprotein (MHV-N) and membrane protein (MHV-M) in WT- (grey) and DA-infected (red) Ifit1$^{+/+}$ (circles) and Ifit1$^{-/-}$ (triangles) macrophages are plotted separately. Data are from three independent experiments. (**e,f**) Principal Component Analysis based on valid H/L ratios of all measurements from (**d**) showing clustering of the individual samples of the entire dataset (**e**). Panel (**f**) shows all proteins plotted for their contribution to the variation in components 1 and 2. MHV proteins are indicated in blue.
doi:10.1371/journal.ppat.1003663.g005

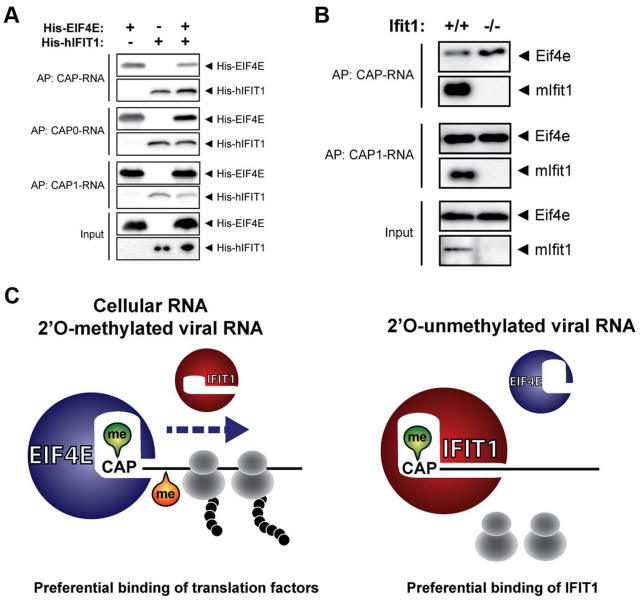

Figure 6. Competition between IFIT1 and translation factor EIF4E for mRNA templates. (**a**) Recovery of recombinant human EIF4E based on RNA affinity binding in the presence or absence of IFIT1. Streptavidin beads were coupled to 250 ng of the indicated RNA and mixed with 5 µg of recombinant His-tagged hIFIT1 and/or His-tagged EIF4E, as indicated. Bound proteins were analysed by western blotting with antibodies directed against the His-tag. (**b**) As in (**a**), except that RNA-coated beads were incubated with lysates of interferon-treated Ifit1$^{+/+}$ and Ifit1$^{-/-}$ mouse embryo fibroblasts. Bound proteins were analysed by western blotting with antibodies directed against murine Eif4e and mIfit1. (**c**) Proposed model for IFIT1-mediated translational inhibition of 2′O-unmethylated viral RNA. Capped and 2′O-methylated cellular and viral RNA is bound by EIF4E to initiate translation. Viral mRNA lacking 2′O methylation at the first ribose is recognized by IFIT1 which prevents binding of cellular factors required for efficient translation. The model is based on data presented here and elsewhere [16,17,19,20].
doi:10.1371/journal.ppat.1003663.g006

lysates of IFN-α treated Ifit1$^{-/-}$ MEFs than from lysates of Ifit1$^{+/+}$ MEFs (Fig. 6b). This difference disappeared when methylated CAP1-RNA was used as bait (Fig. 6b). We therefore conclude that IFIT1 competes with cellular translation initiation factors for mRNA, thereby selectively regulating translation based on the 5′ methylation status of the RNA templates present (Fig. 6c).

Discussion

We previously identified IFIT1 as a nucleic acid-binding protein that recognises the 5′triphosphosphate present on genomes and transcripts of most negative-strand RNA viruses [16]. Here we show that, in addition, IFIT1 binds mRNAs that lack 2′O methylation on the first ribose, such as those produced by RNA viruses that replicate in the cytoplasm and are deficient in RNA cap-specific ribose-2′-O methyltransferase activity. This suggests that IFIT1 has a unique ability to recognize 5′ RNA modifications that are present on viral nucleic acids. Co-purification experiments with human IFIT proteins clearly show formation of a multi-protein complex comprising IFIT1, -2 and -3. Overexpression of single IFIT proteins, including IFIT1, only marginally affects viral growth [16,17], suggesting that the cooperative action of IFIT proteins is required for full antiviral action. This is supported by loss-of-function experiments in cell culture and *in vivo* that show a requirement for Ifit2, which by itself does not bind CAP-RNA, to restrict viruses lacking 2′O methyltransferase activity [17,18]. IFIT2 is known to bind to components of the cytoskeleton [24], which could allow intracellular trafficking of the IFIT complex to its sites of action. While some IFITs possess conserved biological activities in different species, e.g. human and murine IFIT1 which bind to PPP-RNA and unmethylated CAP-RNA, others appear to have evolved in a species-specific manner. We showed here that the yet uncharacterised murine interferon-induced Ifit1c binds to RNA-coated beads in an Ifit1-dependent manner, and we therefore propose that a corresponding Ifit complex with a different protein composition exists in mice.

Residues previously identified to be important for binding of the triphosphate moiety are also required for binding of unmethylated CAP-RNA by IFIT1, suggesting a conserved mechanism of RNA binding. In this context it is of interest to note that crystallographic analysis indicates that PPP-RNA binding to IFIT5, which shows high similarity to IFIT1, occurs in a fashion that is reminiscent of CAP-RNA binding by cap-binding proteins, in that the first two nucleotides are stacked by an aromatic phenylalanine [20]. However, the higher affinity of IFIT1 for unmethylated relative to fully methylated capped RNA is unusual among cellular

proteins since 5′ methylation has so far been reported to increase the affinity of cellular proteins for RNA [7], a notion clearly supported by our RNA AP-MS data. Like its specific antiviral activity, this property of IFIT1 may only become apparent during infections with viruses that produce non-methylated RNA 5′ ends [25,26]. We propose that IFIT1 acts as a molecular switch that allows selective translation based on the 5′ methylation state of the mRNA. The phenomenon of translational control by IFIT1 based on its differential affinity for the capped RNA is reminiscent of the 4E homologous protein (4EHP) in Drosophila and mice, which has been found to control translation by competing with EIF4E for the RNA cap structure, thereby regulating development-specific gene expression [27,28]. Similarly, in our hands, IFIT1 does not associate directly with the translation machinery ([16] and data not shown), which again suggests that it perturbs translation through sequestration of viral RNA. Such a model is consistent with the high expression levels of IFIT proteins resulting from infections with viruses or treatment with IFN-α/β.

Rather than mediating general inhibition of translation, IFIT1 shows high selectivity for mRNAs that lack 5′ methylation. This is supported by pulsed SILAC experiments showing specific, IFIT1-dependent inhibition of translation of capped RNAs lacking 2′O methylation at the first ribose, such as those generated by MHV and HCoV mutants expressing inactive 2′O methyltransferase. Lower eukaryotes and viruses that infect them lack 2′O methylated CAP RNA [29–31], and the latter should be susceptible to the antiviral activity of IFITs. Consequently, the IFIT defence system is likely to contribute to a species barrier that puts selective pressure on viruses to generate 5′ methylated RNA. Our data provide a mechanistic rationale for why most viruses make considerable effort and dedicate part of their coding capacity to produce genomic and subgenomic RNAs with 5′-terminal ends that perfectly mimic those of cellular mRNAs, including fully methylated 5′-cap structures [9,31–33]. Other viruses have evolved specific mechanisms to hide their uncapped/unmethylated 5′ ends, for example, by covalent binding of viral proteins to the 5′ end of viral RNAs and use of alternative strategies for translation initiation, thereby escaping IFIT1-based surveillance, which is centred on RNA 5′ end structures. Despite these viral strategies to generate host-like mRNAs, IFIT1 remains active against viruses that generate 5′ triphosphate RNA, most likely through translation-independent mechanisms. The ability of IFIT1 to target viral RNAs selectively allows the cell to specifically fight virus infections while pursuing an antiviral program aimed at destroying the intruding pathogen.

Materials and Methods

Ethics statement

All animal experiments were performed in accordance with Swiss federal legislation on animal protection and with the approval of the Animal Studies Committee of the Cantonal Veterinary Office (St. Gallen, Switzerland), license nr. SG 11/03.

Reagents, cells and viruses

Interferon-α (IFN-α A/D) was a kind gift from Peter Stäheli. Expression constructs for human and murine IFIT proteins [16,20] and the human aminopeptidase N (APN) were described previously. Products tagged with *Renilla* luciferase were expressed from constructs obtained by Gateway cloning into pCDNA-REN-NT-GW (a kind gift from Albrecht v. Brunn). For expression in bacteria, human EIF4E cDNA was cloned into pETG10A-GW [16]. Recombinant IFIT proteins and human EIF4E were expressed in *E. coli* and purified using HisPur Ni-NTA resin (Thermo Scientific). Streptavidin-agarose beads were obtained from Novagen. Polyclonal antibodies directed against human and mouse IFIT1 were described previously [16]. The antibody against MHV nucleoprotein (MHV-N556) was kindly donated by Stuart Siddell. Primary antibodies against ILF-3 (Sigma; HPA001897), the nucleoprotein of HCoV-229E (Ingenasa; mAb 1H11) and EIF4E (Cell Signaling; C46H6) were obtained from commercial sources. For western blot analysis we used horseradish peroxidase (HRP)-coupled antibodies specific for actin (Santa Cruz; sc-47778), the His-tag (Santa Cruz; sc-8036) or the c-Myc-tag (Roche; 1667149), and HRP-coupled secondary antibodies (Jackson ImmunoResearch). All cell lines used (293T, HeLa, Vero-E6, Huh7, L929, 17Clone1, and $Ifit1^{+/+}$ and $Ifit1^{-/-}$ mouse embryonic fibroblasts) were described previously [11,16], and were maintained in DMEM (PAA Laboratories) containing 10% fetal calf serum (PAA Laboratories) and antibiotics (100 U/ml penicillin, 100 µg/ml streptomycin). DMEM medium containing antibiotics, 10 mM L-glutamine, 10% dialyzed fetal calf serum (PAA Laboratories) and 84 mg/L $^{13}C_6$ $^{15}N_4$ L-arginine and 146 mg/L $^{13}C_6$ $^{15}N_2$ lysine (Cambridge Isotope Laboratories) was used for SILAC experiments. Murine bone marrow-derived macrophages were generated *in vitro* by cultivating bone marrow from mouse femur and tibia in DMEM supplemented with 10% (v/v) fetal calf serum, 5% (v/v) horse serum, 10 mM HEPES pH 7.4, 1 mM sodium pyruvate, 10 mM L-glutamine and 20% (v/v) L929 cell-conditioned medium (containing macrophage colony-stimulating factor) for 6 days. Reagents for transfection with plasmid DNA (Nanofectin) or siRNA duplexes (siRNA Prime) were obtained from PAA Laboratories. Wild-type and 2′-O-methyltransferase-deficient recombinant coronaviruses [mouse hepatitis virus strain A59 (MHV) and human coronavirus 229E (HCoV-229E) [11]], Sendai virus, RVFV Clone13 [34] and VSV-M2 (mutant VSV with the M51R substitution in the matrix protein) [35] have been described previously. Duplex siRNAs targeting human IFIT1 [sense#1: r(CAUGGGAGUUAUCCAUUGA)dTdT; antisense#1: r(UCAAUGGAUAACUCCCAUG)dTdA; sense#2: r(CCUUGGGUUCGUCUACAAA)dTdT, antisense#2: r(UUUGUAGACGAACCCAAGG)dAdG] and the green fluorescent protein [sense: 5′ r(AAGCAGCACGACUUCUUCAAGU)dT 3′; antisense 5′ r(CUUGAAGAAGUCGUGCUGCUUU)dT 3′] were synthesized by the Core Facility at the MPI of Biochemistry.

Capping and methylation of in vitro transcribed RNA

Triphosphorylated PPP-RNA was synthesized by in vitro transcription with SP6 or T7 polymerase (RiboMAX Large Scale RNA Production Systems; Promega), in the presence or absence of biotin-16-UTP (Enzo), from plasmids encoding antisense 7SK RNA (7SK-as) [13] or *Renilla* luciferase (pRL-SV40; Promega), and purified by ammonium-acetate isopropanol precipitation. Aliquots of PPP-RNA were then mock-treated, dephosphorylated with alkaline phosphatase (FastAP; Fermentas), or modified with different 5′ cap structures using the ScriptCap 2′-O-Methyltransferase and m7G Capping System (CellScript) according to the manufacturer's instructions. Briefly, 20-µg samples of RNA were heat-denatured at 65°C for 5 min, cooled on ice, then incubated with ScriptCap Buffer in the presence of 500 µM GTP, 100 µM SAM, 100 U 2′-O-methyltransferase (VP39), 10 U Vaccinia Capping Enzyme (VCE) and 40 U RNase inhibitor for 1 h at 37°C. Capped RNAs were further treated with FastAP to dephosphorylate any residual PPP-RNA, and then column-purified using the NucleoSpin RNA II kit (Macherey-Nagel). To add radioactively labelled methyl groups to in vitro transcribed RNA, 500 ng of each RNA was incubated with 100 U 2′-O-

methyltransferase or 10 U of VCE in 0.5 µM S-adenosylmethionine and 1.4 µM S-[^{3}H-methyl]-adenosylmethionine (78 Ci/mmol; Perkin-Elmer) for 1 h at 37°C. Reactions were purified on SigmaSpin Post-Reaction Clean-Up columns (Sigma) and eluates were mixed with 2 ml Ultima Gold scintillation fluid for measurement of ^{3}H incorporation with a Packard Tri-Carb liquid scintillation counter (Perkin Elmer).

Generation and capping of chemically synthesized RNA oligomers

Capped m7Gppp-oligoribonucleotides matching the first 22 nucleotides of the 5′ untranslated region of Severe Acute Respiratory Syndrome Coronavirus HKU-39849 were prepared by adding N7-methylated cap structures to chemically synthesized RNA oligomers with a 3′-terminal C6 amino linker. A triphosphorylated RNA oligomer [PPP-r(AUAUUAGGUUUUUACCUACCC)-NH_2) and a corresponding 2′O-ribose methylated RNA-oligomer [PPP-r(AmUAUUAGGUUUUUACCUACCC)-NH_2] were ordered from ChemGenes Corporation (Wilmington, MA, USA) and capped as described above using the m7G Capping System (CellScript). Capped RNA oligomers were then HPLC-purified, biotinylated with biotin-N-hydroxysuccinimide ester (Epicentre) according to the manufacturer's instructions and again HPLC-purified. As control we used a corresponding 3′-terminal biotinylated and HPLC-purified oligoribonucleotide harbouring a 5′ hydroxyl group [OH-r(AUAUUAGGUUUUUACCUACCCU)-biotin].

Identification and quantitation of RNA-binding proteins

For quantitative purification of RNA-binding proteins, streptavidin affinity resin was first incubated with 1-µg aliquots of biotin-labelled OH-RNA, PPP-RNA, CAP-RNA, CAP0-RNA or CAP1-RNA (all 7SK-antisense) in TAP buffer [50 mM Tris pH 7.5, 100 mM NaCl, 5% (v/v) glycerol, 0.2% (v/v) Nonidet-P40, 1.5 mM $MgCl_2$ and protease inhibitor cocktail (EDTA-free, cOmplete; Roche)] in the presence of 40 U RNase inhibitor (Fermentas) for 60 min at 4°C on a rotary wheel. Control or RNA-coated beads were then incubated with 2-mg samples of HeLa cell lysate for 60 min, washed three times with TAP buffer, and twice with TAP buffer lacking Nonidet-P40 to remove residual detergent. Three independent affinity purifications were performed for each RNA. Bound proteins were dentatured by incubation in 6 M urea-2 M thiourea with 1 mM DTT (Sigma) for 30 min and alkylated with 5.5 mM iodoacetamide (Sigma) for 20 min. After digestion with 1 µg LysC (WAKO Chemicals USA) at room temperature for 3 h, the suspension was diluted in 50 mM ammonium bicarbonate buffer (pH 8). The beads were removed by filtration through 96-well multiscreen filter plates (Millipore, MSBVN1210), and the protein solution was digested with trypsin (Promega) overnight at room temperature. Peptides were purified on stage tips with three C18 Empore filter discs (3M) and analyzed by mass spectrometry as described previously [36]. Briefly, peptides were eluted from stage tips and separated on a C18 reversed-phase column (Reprosil-Pur 120 C18-AQ, 3 µM, 150×0.075 mm; Dr. Maisch) by applying a 5% to 30% acetonitrile gradient in 0.5% acetic acid at a flow rate of 250 nl/min over a period of 95 min, using an EASY-nanoLC system (Proxeon Biosystems). The nanoLC system was directly coupled to the electrospray ion source of an LTQ-Orbitrap XL mass spectrometer (Thermo Fisher Scientific) operated in a data dependent mode with a full scan in the Orbitrap cell at a resolution of 60,000 with concomitant isolation and fragmentation of the ten most abundant ions in the linear ion trap.

Affinity purification of luciferase-tagged and recombinant proteins

N-terminally *Renilla* luciferase-tagged proteins were transiently expressed in 293T cells. Three micrograms of each construct were transfected into 6×10^6 cells using 9.6 µl nanofectin (PAA Laboratories) in 10-cm dishes according to the manufacturer's instructions. After 24 h, the medium was removed, and cells were lysed in ice-cold TAP lysis buffer. An aliquot (10%) of the lysate was removed to determine input luciferase activity. The rest was added to streptavidin-agarose beads coated with 250 ng of RNA as described above, and incubated on a rotary wheel at 4°C for 60 min. Beads were washed three times and resuspended in 50 µl TAP buffer. Luciferase activities present in the suspension and in the input lysate were assayed in Renilla reaction buffer (100 mM K_3PO_4, 500 mM NaCl, 1 mM EDTA, 25 mM thiourea) containing 10 µM coelenterazine as substrate. The reactions were performed in triplicate and results were quantified using an Infinite 200 PRO series microplate reader (Tecan). For affinity purification of recombinant proteins with different RNAs, 50 to 250 ng of biotinylated RNA were coupled to streptavidin-agarose beads for 60 min at 4°C. Beads were washed three times with TAP buffer and incubated with recombinant His-tagged proteins for 60 min at 4°C. After three washes beads were boiled in Laemmli buffer for 10 min at 95°C and subjected to SDS-PAGE and Western Blot analysis.

Real-time RT-PCR

Total RNA was isolated using the NucleoSpin RNA II kit (Macherey-Nagel), including on-column DNase digestion, and 200 to 500 ng of RNA was reverse transcribed with the RevertAid H Minus First Strand cDNA Synthesis Kit (Fermentas). RNA levels were then quantified by real-time RT-PCR using the QuantiTect SYBR Green RT-PCR kit (Qiagen) and a CFX96 Touch Real-Time PCR Detection System (BioRad). Each cycle consisted of 15 sec at 95°C, 30 sec at 50°C and 30 sec at 72°C, followed by melting curve analysis. Primer sequences were as follows: *Renilla* luciferase (5′-CGAAAGTTTATGATCCAGAAC-3′ and 5′-AATCATAATAATTAATAAATG-3′), hCycB (5′-CAGCAAGTTCCATCGTGTCATCAAGG-3′ and 5′-GGAAGCGCTCACCATAGATGCTC-3′), mTBP (5′-CCTTCACCAATGACTCCTATGAC-3′ and 5′- CAAGTTTACAGCCAAGATTCA-3′), mIFN-β (5′-ATGGTGGTCCGAGCAGAGAT-3′ and 5′-CCACCACTCATTCTGAGGCA-3′), MHV-N (5′-GCCTCGCCAAAAGAGGACT-3′ and 5′- GGGCCTCTCTTTTCCAAAACAC-3′), 229E-N (5′-CAGTCAAATGGGCTGATGCA-3′ and 5′- AAAGGGCTATAAAGAGAATAAGGTATTCT-3′), mIfit1 (5′- CCATAGCGGAGGTGAATATC-3′ and 5′- GGCAGGACAATGTGCAAGAA-3′), mIfit1c (5′-AATCAGAAGAGGCAGCCATC-3′ and 5′-CATGGCTTCACTTGTGTTCC-3′), mIfit2 (5′-TCAGCACCTGCTTCATCCAA-3′ and 5′-CACCTTCGGTATGGCAACTT-3′), and mIfit3 (5′-GCTGCGAGGTCTTCAGACTT-3′ and 5′-TGGTCATGTGCCGTTACAGG-3′).

Virus infection experiments in cell culture and in vivo

C57BL/6 mice were obtained from Charles River Laboratories (Sulzfeld, Germany), and *Ifit1*$^{-/-}$ mice have been described [16,17]. Mice were maintained in individually ventilated cages and used at 6 to 9 weeks of age. All animal experiments were performed in accordance with Swiss federal legislation on animal protection and with the approval of the Animal Studies Committee of the Cantonal Veterinary Office (St. Gallen, Switzerland). Wild-type and *Ifit1*$^{-/-}$ mice (kindly provided by

Michael Diamond) were injected intraperitoneally with 5,000 plaque-forming units of MHV. Virus titers in samples of spleens removed and frozen 48 h post infection were assessed by standard plaque assay on L929 cells. Bone marrow-derived macrophages or mouse embryo fibroblasts (1 to 5×10^5 cells) were treated or not with IFN-α and infected with the indicated viruses at a multiplicity of infection (MOI) of 5. For synchronised infection, cells were infected with virus on ice and pre-warmed DMEM growth medium was added 1 h later. To quantify the effects of siRNA-mediated knockdown of IFIT1, aliquots of 10^5 HeLa cells that had been transfected for 48 h with 15 pmol siRNA and 500 ng expression plasmid for human APN using the siRNA Prime reagent (PAA Laboratories) according to the manufacturer's instructions, were pretreated with IFN-α as indicated and infected with HCoV-229E at an MOI of 1 for 24 h.

Pulsed SILAC and mass spectrometry

For pulsed SILAC, mouse macrophages labelled with heavy isotopes (see above) were lysed in SDS lysis buffer (50 mM Tris pH 7.5, 4% sodium dodecyl sulfate). The lysate was then heated for 5 min at 95°C, sonicated for 15 min with a Bioruptor (Diagenode) and centrifuged for 5 min at 16,000× *g* at room temperature. Protein concentration was determined by Lowry assay (DC Protein Assay, BioRAD), and 50-µg aliquots were reduced with 10 mM DTT for 30 min, alkylated with 55 mM IAA for 20 min at room temperature, and precipitated with 80% acetone for 3 h at −20°C. After centrifugation for 15 min at 16,000× *g* at 4°C, pellets were washed with 80% acetone, dried for 30 min at room temperature and dissolved in 6 M urea-2 M thiourea. Proteins were digested with LysC and trypsin at room temperature and peptides were purified on stage tips and analysed by LC-MS/MS using a Easy nano LC system coupled to a Q Exactive mass spectrometer (Thermo Fisher Scientific). Peptide separation was achieved on a C18-reversed phase column (Reprosil-Pur 120 C18-AQ, 1.9 µM, 200×0.075 mm; Dr. Maisch) using a 95-min linear gradient of 2 to 30% acetonitrile in 0.1% formic acid. The mass spectrometer was set up to run a Top10 method, with a full scan followed by isolation, HCD fragmentation and detection of the ten most abundant ions per scan in the Orbitrap cell.

Bioinformatic analysis

Raw mass-spectrometry data were processed with MaxQuant software versions 1.2.7.4 and version 1.3.0.5 [37] using the built-in Andromeda search engine to search against human and mouse proteomes (UniprotKB, release 2012_01) containing forward and reverse sequences, and the label-free quantitation algorithm as described previously [36,38]. In MaxQuant, carbamidomethylation was set as fixed and methionine oxidation and N-acetylation as variable modifications, using an initial mass tolerance of 6 ppm for the precursor ion and 0.5 Da for the fragment ions. For SILAC samples, multiplicity was set to 2 and Arg10 and Lys8 were set as heavy label parameters. Search results were filtered with a false discovery rate (FDR) of 0.01 for peptide and protein identifications. Protein tables were filtered to eliminate the identifications from the reverse database and common contaminants.

In analyzing mass spectrometry data from RNA affinity purifications, only proteins identified on the basis of at least two peptides and a minimum of three quantitation events in at least one experimental group were considered. Label-free quantitation (LFQ) protein intensity values were log-transformed and missing values filled by imputation with random numbers drawn from a normal distribution, whose mean and standard deviation were chosen to best simulate low abundance values. Significant interactors of RNAs with different 5′ end structures were determined by multiple equal variance t-tests with permutation-based false discovery rate statistics [39]. We performed 250 permutations and the FDR threshold was set between 0.02 and 0.1. The parameter S_0 was empirically set between 0.2 and 1, to separate background from specifically enriched interactors.

For data analysis from pulsed SILAC experiments, we used log-transformed heavy to light protein ratios. Only proteins with valid values were considered for analysis, and normalized by dividing by the row median. Profile plots were generated using LFQ intensities of log-transformed heavy-labelled protein intensities. We excluded proteins containing less than 10 valid values in all 12 measurements, and missing values were filled by imputation. LFQ intensities were then normalized by dividing by the row median.

Results were plotted using R (www.R-project.org) and GraphPad Prism version 5.02. Multiple sequence alignments were generated with ClustalW (http://www.ebi.ac.uk/Tools/msa/clustalw2/).

Structural modelling

A homology model of human IFIT1 was obtained with MODELLER [40] using the X-ray structure of human IFIT5 (4HOQ) as a structural template [20]. A pairwise sequence alignment was generated with ClustalW (http://www.ebi.ac.uk/Tools/msa/clustalw2/) and further refined with MODELLERs align2d. Human IFIT1 and IFIT5 share approximately 75.6% sequence similarity, with 57.2% of all residues being identical. Cavity volumes in both structures were calculated in a two-step process with the rolling probe method using 3V [41]. First, a solvent-excluded volume was calculated for each structure using a probe radius of 1.5 Å (corresponding to water). A larger probe size of 5 Å was used to calculate so-called "shell volumes". The solvent-accessible cavity volumes were obtained by subtraction of each solvent-excluded volume from the corresponding shell volume.

Supporting Information

Figure S1 Generation of 5′end modified in-vitro transcribed RNA. (**a**) Schematic overview of synthesis of the biotinylated RNA used in this study. 5′ triphosphorylated (PPP-) 7SK-antisense RNA obtained by in vitro transcription with SP6 polymerase was modified enzymatically at the 5′ end by incubating with alkaline phosphatase (AP) to remove 5′ phosphates (OH-RNA), with recombinant Vaccinia virus capping enzyme (VCE) to produce unmethylated capped RNA (CAP-RNA), with VCE in the presence of S-adenosyl methionine (SAM) to generate N7-methylated capped RNA (CAP0-RNA), or with VCE and recombinant Vaccinia virus 2′O methyltransferase (VP39) in the presence of SAM to generate N7-methylated capped RNA methylated at the 2′O position of the first ribose (CAP1-RNA) [43],[44]. (**b**) Agarose gel image showing 200 ng of in vitro transcribed, biotinylated RNA following the enzymatic treatments depicted in (**a**). (**c**) Evaluation of the N7- and 2′O-methylation efficiency of recombinant Vaccinia virus enzymes. Capped RNAs produced as in (**a**) were incubated either with VCE or VP39 in the presence of ^{3}H-labeled SAM, and the incorporation efficiency was measured by scintillation counting. ^{3}H-labeled methyl groups were transferred from SAM only if the RNA had not previously been methylated (N7-methylation of CAP-RNA, and 2′O methylation of CAP0-RNA), showing that methylation of RNA by both VCE and VP39 was maximally efficient.
(TIF)

Figure S2 RNA affinity purifications from HeLa cell lysates. (**a**) Heatmap of all proteins identified in RNA affinity purifications from HeLa cell lysates. Hierarchical clustering of proteins was performed on logarithmic LFQ protein intensities using Euclidean distances. The colour code represents LFQ intensities in rainbow colours (see colour scale). (**b**) Heatmap showing hierarchical clustering (Euclidean distances) of interactors that were significantly enriched (see Materials and Methods) in fractions bound by at least one RNA with a modified 5′ end structure (compared to OH-RNA). The plot shows means of Z-score transformed logarithmic LFQ intensities. Blue colours indicate Z-score <0, red colours indicate Z-score >0, white indicates Z-score = 0. The saturation threshold is set at -2.25 and +2.25. Asterisks indicate the IFIT complex. (**c**) Volcano plots showing enrichment (ratio of LFQ protein intensities; x-axis) and p-values (t-test; y-axis) of CAP1-RNA to CAP-RNA. Data are from three independent affinity purifications. Significantly enriched interactors (see Materials and Methods) are separated from background proteins (blue dots) by a hyperbolic curve (dotted line). Among the significant interactors, IFIT proteins and FTSJD2 (red) are highlighted.
(TIF)

Figure S3 RNA affinity purifications from lysates of mouse embryo fibroblasts. (**a–b**) As in Fig. S2, but showing proteins identified in RNA affinity purifications from mouse embryo fibroblasts. In (**b**) the saturation threshold is set at −1. 5 and +1. 5. The asterisk indicates the Ifit complex.
(TIF)

Figure S4 Characterisation of the murine IFIT complex. (**a**) Expression of Ifit genes in wild-type ($Ifit1^{+/+}$) and Ifit1-deficient ($Ifit1^{-/-}$) mouse embryonic fibroblasts (MEFs). MEFs were left untreated, treated with 1000 U/ml IFN-α, or infected with Rift Valley fever virus Clone13 or a mutant version of vesicular stomatitis virus (VSV-M2) at a multiplicity of infection of 1 or 0.01, respectively. Sixteen hours later RNA was analysed by quantitative RT-PCR for mIfit1, mIfit1c, mIfit2 and mIfit3. In each case, one representative experiment of three is shown, with means ±SD after normalization to the TATA-binding protein (TBP) mRNA. (**b**) Heatmap of selected proteins identified in RNA affinity purifications from cell lysates of $Ifit1^{+/+}$ and $Ifit1^{-/-}$ MEFs. The plot shows the means of log-transformed label-free quantitation protein intensities in rainbow colours (see colour scale). (**c**) Alignment of murine and human IFIT proteins using ClustalW. (**d**) Matrix showing amino acid similarity (based on ClustalW alignment) of all murine and human IFIT proteins. Percent similarity is indicated as color coded from white to red, and the exact similarity is shown within each element of the matrix.
(TIF)

Figure S5 Comparison of the RNA binding cavities of IFIT5 and IFIT1. Sections of surface representations of the solvent-accessible surfaces of IFIT5 (top) and IFIT1 (bottom) are shown, with PPP-RNA bound as in IFIT5 (stick representation, superimposed on IFIT1), and the corresponding cavity volumes V calculated as described in Materials and Methods. In our calcuations, the main RNA-binding cavity in IFIT5 has volume of 11881 $Å^3$. The calculated volume of the corresponding cavity of the modelled IFIT1, at 12627 $Å^3$, is about 700 $Å^3$ larger.
(TIF)

Figure S6 Induction of interferon-β in wild-type and Ifit1-deficient mouse cells. Interferon-stimulated bone marrow-derived macrophages (MΦs) from C57/BL6 ($Ifit1^{+/+}$) or Ifit1-deficient ($Ifit1^{-/-}$) mice were left untreated, or infected with wild-type MHV (WT), 2′O-methyltransferase-deficient MHV (DA), or Sendai virus (SeV). Twelve hours later total RNA was harvested and analysed by quantitative RT-PCR for interferon β (IFN-β) mRNA. Data from three independent experiments showing fold change relative to untreated cells (mean ±SD) after normalization to the TATA-binding protein (TBP) mRNA.
(TIF)

Figure S7 Translation profiles of individual proteins in MHV-infected macrophages. Translation profiles based on pulsed SILAC of macrophages from C75/BL6 ($Ifit1^{+/+}$) and Ifit1-deficient ($Ifit1^{-/-}$) mice infected with wild-type MHV (WT) or 2′O methyltransferase-deficient MHV (DA) as shown in Fig. 5. The profile plot shows normalized LFQ intensities of heavy proteins, representing a total number of 451 proteins labelled during the 2 h pulse period. Data show average LFQ intensities from three independent replicates. Selected profiles are coloured and represent MHV proteins and cellular proteins involved in immune responses.
(TIF)

Table S1 Quantitative MS data from RNA affinity purifications with HeLa cell lysates. Proteins identified by LC-MS/MS from lysates of HeLa cells upon affinity purification with different RNA baits. Table contains log-transformed and imputed label-free quantification (LFQ) intensities of all identified proteins. Significantly enriched proteins, p values and mean differences from t-test based analyses are indicated.
(XLSX)

Table S2 Quantitative MS data from RNA affinity purifications with MEF lysates. Proteins identified by LC-MS/MS from lysates of mouse embryo fibroblasts (MEF) upon affinity purification with different RNA baits. Table contains log-transformed and imputed label-free quantification (LFQ) intensities of all identified proteins. Significantly enriched proteins, p values and mean differences from t-test based analyses are indicated.
(XLSX)

Acknowledgments

We thank Matthias Mann, Felix Meissner, Korbinian Mayer, Igor Paron, Gabi Sowa, Falk Butter, Jürgen Cox, and Bernd Haas and Stephan Übel (MPI of Biochemistry Core Facility) for technical support, Albrecht von Brunn for the Lumier plasmids, and Elena Conti for scientific input and critical reading of the manuscript. We further want to thank Giulio Superti-Furga for providing reagents.

Author Contributions

Conceived and designed the experiments: MH PH VT AP. Performed the experiments: MH PH LL CH AM EK CGC AP. Analyzed the data: MH PH CB CHE VT AP. Contributed reagents/materials/analysis tools: JZ VT. Wrote the paper: MH PH AP.

References

1. Versteeg GA, Garcia-Sastre A (2010) Viral tricks to grid-lock the type I interferon system. Curr Opin Microbiol 13: 508–516.
2. Iwasaki A, Medzhitov R (2010) Regulation of adaptive immunity by the innate immune system. Science 327: 291–295.

3. Sadler AJ, Williams BR (2008) Interferon-inducible antiviral effectors. Nat Rev Immunol 8: 559–568.
4. Hornung V, Latz E (2010) Intracellular DNA recognition. Nat Rev Immunol 10: 123–130.
5. Kato H, Takahasi K, Fujita T (2011) RIG-I-like receptors: cytoplasmic sensors for non-self RNA. Immunol Rev 243: 91–98.
6. Gebauer F, Hentze MW (2004) Molecular mechanisms of translational control. Nat Rev Mol Cell Biol 5: 827–835.
7. Topisirovic I, Svitkin YV, Sonenberg N, Shatkin AJ (2011) Cap and cap-binding proteins in the control of gene expression. Wiley Interdiscip Rev RNA 2: 277–298.
8. Pichlmair A, Reis e Sousa C (2007) Innate Recognition of Viruses. Immunity 27: 370–383.
9. Decroly E, Ferron F, Lescar J, Canard B (2012) Conventional and unconventional mechanisms for capping viral mRNA. Nat Rev Microbiol 10: 51–65.
10. Colonno RJ, Stone HO (1976) Newcastle disease virus mRNA lacks 2′-O-methylated nucleotides. Nature 261: 611–614.
11. Zust R, Cervantes-Barragan L, Habjan M, Maier R, Neuman BW, et al. (2011) Ribose 2′-O-methylation provides a molecular signature for the distinction of self and non-self mRNA dependent on the RNA sensor Mda5. Nat Immunol 12: 137–143.
12. Hornung V, Ellegast J, Kim S, Brzozka K, Jung A, et al. (2006) 5′-Triphosphate RNA is the ligand for RIG-I. Science 314: 994–997.
13. Pichlmair A, Schulz O, Tan CP, Naslund TI, Liljestrom P, et al. (2006) RIG-I-mediated antiviral responses to single-stranded RNA bearing 5′-phosphates. Science 314: 997–1001.
14. Kato H, Takeuchi O, Mikamo-Satoh E, Hirai R, Kawai T, et al. (2008) Length-dependent recognition of double-stranded ribonucleic acids by retinoic acid-inducible gene-I and melanoma differentiation-associated gene 5. J Exp Med 205: 1601–1610.
15. Diamond MS, Farzan M (2013) The broad-spectrum antiviral functions of IFIT and IFITM proteins. Nat Rev Immunol 13: 46–57.
16. Pichlmair A, Lassnig C, Eberle CA, Gorna MW, Baumann CL, et al. (2011) IFIT1 is an antiviral protein that recognizes 5′-triphosphate RNA. Nat Immunol 12:624–630.
17. Daffis S, Szretter KJ, Schriewer J, Li J, Youn S, et al. (2010) 2′-O methylation of the viral mRNA cap evades host restriction by IFIT family members. Nature 468: 452–456.
18. Fensterl V, Wetzel JL, Ramachandran S, Ogino T, Stohlman SA, et al. (2012) Interferon-induced Ifit2/ISG54 protects mice from lethal VSV neuropathogenesis. PLoS Pathog 8: e1002712.
19. Szretter KJ, Daniels BP, Cho H, Gainey MD, Yokoyama WM, et al. (2012) 2′-O methylation of the viral mRNA cap by West Nile virus evades ifit1-dependent and -independent mechanisms of host restriction in vivo. PLoS Pathog 8: e1002698.
20. Abbas YM, Pichlmair A, Gorna MW, Superti-Furga G, Nagar B (2013) Structural basis for viral 5′-PPP-RNA recognition by human IFIT proteins. Nature 494: 60–64.
21. Shapira SD, Gat-Viks I, Shum BO, Dricot A, de Grace MM, et al. (2009) A physical and regulatory map of host-influenza interactions reveals pathways in H1N1 infection. Cell 139: 1255–1267.
22. Furuichi Y, Shatkin AJ (2001) Caps on Eukaryotic mRNAs. eLS. doi: 10.1038/npg.els.0000891
23. Schwanhausser B, Busse D, Li N, Dittmar G, Schuchhardt J, et al. (2011) Global quantification of mammalian gene expression control. Nature 473: 337–342.
24. Saha S, Sugumar P, Bhandari P, Rangarajan PN (2006) Identification of Japanese encephalitis virus-inducible genes in mouse brain and characterization of GARG39/IFIT2 as a microtubule-associated protein. J Gen Virol 87: 3285–3289.
25. Li J, Fontaine-Rodriguez EC, Whelan SP (2005) Amino acid residues within conserved domain VI of the vesicular stomatitis virus large polymerase protein essential for mRNA cap methyltransferase activity. J Virol 79: 13373–13384.
26. Li J, Wang JT, Whelan SP (2006) A unique strategy for mRNA cap methylation used by vesicular stomatitis virus. Proc Natl Acad Sci U S A 103: 8493–8498.
27. Morita M, Ler LW, Fabian MR, Siddiqui N, Mullin M, et al. (2012) A novel 4EHP-GIGYF2 translational repressor complex is essential for mammalian development. Mol Cell Biol 32: 3585–3593.
28. Cho PF, Poulin F, Cho-Park YA, Cho-Park IB, Chicoine JD, et al. (2005) A new paradigm for translational control: inhibition via 5′-3′ mRNA tethering by Bicoid and the eIF4E cognate 4EHP. Cell 121: 411–423.
29. Sripati CE, Groner Y, Warner JR (1976) Methylated, blocked 5′ termini of yeast mRNA. J Biol Chem 251: 2898–2904.
30. Zimmern D (1975) The 5′ end group of tobacco mosaic virus RNA is m7G5′ppp5′ Gp. Nucleic Acids Res 2: 1189–1201.
31. Bouloy M, Plotch SJ, Krug RM (1980) Both the 7-methyl and the 2′-O-methyl groups in the cap of mRNA strongly influence its ability to act as primer for influenza virus RNA transcription. Proc Natl Acad Sci U S A 77: 3952–3956.
32. Fechter P, Brownlee GG (2005) Recognition of mRNA cap structures by viral and cellular proteins. J Gen Virol 86: 1239–1249.
33. Ruigrok RW, Crepin T, Hart DJ, Cusack S (2010) Towards an atomic resolution understanding of the influenza virus replication machinery. Curr Opin Struct Biol 20: 104–113.
34. Muller R, Saluzzo JF, Lopez N, Dreier T, Turell M, et al. (1995) Characterization of clone 13, a naturally attenuated avirulent isolate of Rift Valley fever virus, which is altered in the small segment. Am J Trop Med Hyg 53: 405–411.
35. Stojdl DF, Lichty BD, tenOever BR, Paterson JM, Power AT, et al. (2003) VSV strains with defects in their ability to shutdown innate immunity are potent systemic anti-cancer agents. Cancer Cell 4: 263–275.
36. Hubner NC, Bird AW, Cox J, Splettstoesser B, Bandilla P, et al. (2010) Quantitative proteomics combined with BAC TransgeneOmics reveals in vivo protein interactions. J Cell Biol 189: 739–754.
37. Cox J, Mann M (2008) MaxQuant enables high peptide identification rates, individualized p.p.b.-range mass accuracies and proteome-wide protein quantification. Nat Biotechnol 26: 1367–1372.
38. Luber CA, Cox J, Lauterbach H, Fancke B, Selbach M, et al. (2010) Quantitative proteomics reveals subset-specific viral recognition in dendritic cells. Immunity 32: 279–289.
39. Tusher VG, Tibshirani R, Chu G (2001) Significance analysis of microarrays applied to the ionizing radiation response. Proc Natl Acad Sci U S A 98: 5116–5121.
40. Eswar N, Webb B, Marti-Renom MA, Madhusudhan MS, Eramian D, et al. (2006) Comparative protein structure modeling using Modeller. Curr Protoc Bioinformatics Chapter 5: Unit 5 6.
41. Voss NR, Gerstein M (2010) 3V: cavity, channel and cleft volume calculator and extractor. Nucleic Acids Res 38: W555–562.
42. Liu SY, Sanchez DJ, Aliyari R, Lu S, Cheng G (2012) Systematic identification of type I and type II interferon-induced antiviral factors. Proc Natl Acad Sci U S A 109: 4239–4244.
43. Martin SA, Moss B (1975) Modification of RNA by mRNA guanylyltransferase and mRNA (guanine-7-)methyltransferase from vaccinia virions. J Biol Chem 250: 9330–9335.
44. Barbosa E, Moss B (1978) mRNA(nucleoside-2′-)-methyltransferase from vaccinia virus. Characteristics and substrate specificity. J Biol Chem 253: 7698–7702.

3 Concluding remarks and outlook

The battle between viruses and hosts led to the co-evolution of sophisticated and effective viral attack strategies and host defense mechanisms. Since virus lack own replication mechanisms, they are strictly depend on the host and evolved strategies to modulate cellular pathways to serve its needs. However, the host evolved numerous defense mechanisms to detect and clear viruses. As main barrier for viruses, hosts make use of the innate immune system. The full repertoire of the innate immune system is not yet known, thus additional information could reveal novel therapeutic approaches for antiviral treatments. In this thesis, I identified novel aspects of the ancient battle between viruses and their hosts.

In the first project of my thesis we set out to gain a global picture of the influence of viral proteins on the host signaling network. We applied affinity-purification coupled to mass spectrometry (AP-MS) based analysis of viral proteins to identify interacting host proteins. We revealed novel host targets clearly showing that viruses from different classes target the host immune defense by various signaling pathways. My second and main project focused on the identification of a cell death pathway which is activated upon ROS. By studying protein-protein interactions I could identify a pathway that link viral ROS production to caspase-independent cell death. Functional experiments support the notion that cell death is a powerful tool to clear virus infections. Additional data from the first project and new interaction data revealed a number of viral proteins targeting this cell death pathway. The third project elucidates cellular proteins which binds RNA, which is normally not common in the host, such as viral RNA lacking 2'O-methylation. By AP-MS experiments and work with recombinant proteins, IFIT1 was identified as direct interactor of this viral RNA. Further analysis revealed a selective inhibitory function of IFIT1 on translation of this type of viral RNA. Thus, IFIT1 inhibits viruses lacking mechanisms or enzymes that mediate 2'O methylation of their RNA. Such viruses are commonly found in lower eukaryotes and thus the IFIT1 system may contribute to protect us from a wide variety of different viruses that could cross the species barrier.

Those studies all together revealed new virus-host interactions and partly their particular function for the host to clear viral infections. By investigating how viruses modulate the host by their viral proteins and avoid detection by adapting their viral nucleic acid to host nucleic acids, we can identify potential proteins that could be therapeutically exploited to modulate viral replication.

Within the following chapter I briefly touch the future potential of AP-MS in the field of virus infection research and therapeutic studies. Furthermore, I am going to focus on the conclusions and possible future questions which can be derived from my main project, the ROS-induced cell death pathway and its role in antiviral defense.

Applications for interaction studies and optimized methods

AP-MS can be applied in a wide range of biological applications. It can be used as tool to identify potential host targets of viral proteins. These targets can be further analyzed by biochemical methods, which help to gain a faster and broader overview on possible interactions. Furthermore, by identifying essential residues or peptides for interactions new targets of peptide based drugs can be elucidated. Peptide based drugs are a new emerging field for modulation of a wide range of diseases [401, 402]. Additionally, the binding of peptide based drugs could be analyzed by AP-MS, to study at an early stage on unwanted interaction with other cellular proteins. More recent developments, such as BAC-aided recombination and CRISPR-technology, now allow expression of tagged cellular proteins under their own promoter. Thereby side effects, such as diversity in cellular localization

due to overexpression, may be reduced. Another option that will further help identifying interactors, is crosslinking coupled to MS (XL-MS) [403]. Thereby, interacting proteins are covalently bound by chemical crosslinks [404, 405]. XL-MS could allow detection of transient interactions, such as kinases or phosphatases with their substrate. However, this method is used with purified protein complexes [404, 406] and was applied recently as well in vivo to investigate the global membrane protein interactome [407]. In the future, conditions, such as viral-host interactions, could be analyzed during different time points after infection. This could shed light on different steps while a viral infection. Another interaction study method, named BioID [408], could as well help to identify new targets of enzymes while various infection phases in the cell. By tagging the protein of interest with a biotin ligase, the close interactors of this protein are biotinylated by this ligase and can be analyzed after AP-MS. However, the tag could still interfere with physiological interactions. A tag-free option could be a technique called protein correlation profiling (PCP) [409]. By size exclusion chromatography (SEC) protein complexes can be separated and the different fractions analyzed by MS, which could reveal protein complexes co-elution in the same fraction [410].

All those methods give options to study viral components and infections in a cellular context, but still leave a broad field for further optimization. In addition to the knowledge of interaction between viral and host proteins it would be of interest if these interactions also modulate post-translational modifications of the host proteins. This could help to understand the global picture of viruses modulating their host and hosts dealing with viral attacks.

Importance of ROS induced cell death pathways

Viral and host strategies to fight each other co-evolved over many million years. Viruses often target the host replication machinery to utilize it and the immune system to perturb it. One major viral target in the host innate immune system is the IFN response to avoid an antiviral state in cells, which could eliminate the virus. Another major viral target are processes related to programmed cell death (PCD). PCD utilized in most cases mitochondrial proteins, highlighting the function of mitochondria for the innate immune system. Focusing on my main project, I revealed a novel cell death pathway, which involves mitochondrial localized proteins. Additionally, it is targeted by several viral proteins, emphasizing its role in antiviral immunity. PCD is a central option for individual cells to save the whole organism from virus spreading. Elucidating PCD pathways in particular are of importance to identify pathways that may support the host to help aid antiviral defense [411]. The focus on ROS as cell death inducer is emphasized by the increasing number of known pathogenic viruses to produce ROS during infection [336, 412, 413]. ROS production and scavenging is of great importance for viruses. This is evidenced by a large number of studies on mechanisms of how ROS-inducing viruses influence expression levels of ROS scavenging pathways and enzymes, such as KEAP1-NRF2 and the superoxide dismutase (SOD) family [322, 414].

Upon release from KEAP1, NRF2 translocates to the nucleus and induces the expression of cytoprotective genes [415–417]. Activation of NRF2 is beneficial for the host against several viruses, such as RSV, HIV and influenza virus [418–420]. Many viruses, resulting in persistent infections, induce NRF2 activation [421–423]. In these cases an activation of the KEAP1-PGAM5-AIFM1 cell death pathway would be beneficial for the host. This could be accomplished by either inhibition of NRF2 or direct activation of PGAM5. KSHV (HHV-8) induces ROS and activates NRF2 during initial infection [424]. In addition, to allow a persistent infection, KSHV probably avoids early cell death by inhibiting PGAM5 phosphatase activity by K3 protein, as shown in the second part of this thesis (2.2). Viruses leading to pathogenic and acute infections may activate in addition to the novel KEAP1-PGAM5-AIFM1 cell death pathway other cell death pathways resulting in death

of the organism. We were using influenza A virus (FluAV, strain SC35M) [425], which induced ROS but failed to inhibit NRF2. We hypothesize that this in sum, resulting in viability of the whole organism, probably due to selective death of infected cells. This was impaired in the Pgam5 deficient mice. ROS-mediated cell death is regulated by viruses. For instance by controlling ROS scavenging via SOD enzymes [322]. Viruses target SODs again with the aim to either save the cell by inducing SODs, or promoting cell death by inhibiting SOD enzymes. The SOD family contains three members, the cytosolic SOD1 (Cu, Zn-SOD), the mitochondrial SOD2 (Mn-SOD) and the extracellular SOD3 (Cu, Zn-SOD). ROS induction can increase the expression levels of SOD1 and SOD2, latter seems to be a target gene of the KEAP1-NRF2 pathway [426]. Examples for viruses influencing SODs are highly pathogenic influenza A virus strains, which decrease cytosolic SOD1 [336] and Zika virus, which upregulates mitochondrial SOD2 [427]. In addition, it was shown that LCMV, another ROS inducing virus [428], had detrimental effects in cells and mice depleted for SOD1 [429]. The importance of ROS for the innate immune signaling and its tight control was shown by Dengue virus infection. A lack of ROS induction lead to dampened innate immune response [335]. This points out, how central the level of oxidative stress is to control antiviral and cell death response in the host [335]. A switch, such as KEAP1, could decide if a cell should survive or die. It was already shown for SOD1, being a ROS sensor, to directly modulate cancer signaling [430]. This fact supports the hypothesis of KEAP1 acting as well as sensing and signaling protein within the cell. Moreover, this is emphasized by the fact that viruses not only target scavenging pathways but as well cell death pathways such as this new ROS-induced KEAP1-PGAM5-AIFM1 cell death pathway with the aim to either avoid or promote cell death upon increased ROS.

All together several publications reveal that viruses produce ROS most likely by different mechanisms. It would be of common interest, which mechanisms viruses use to induce ROS and if they do it either on purpose or accidentally. Additionally, in many cases viruses try to control ROS amounts to prevent recognition by the innate immune system, establishment of an antiviral state and early cell death. Therefore, viruses can control mitochondrial or cytosolic produced ROS and this ROS-induced cell death pathway. A mitochondrial anchored protein facing to the cytosol, such as KEAP1, is a perfectly located sensor for cytosolic ROS and ROS leaking from mitochondria. By linking ROS sensing with mitochondrial related cell death mechanisms I could shed light on the complex cell death system involved in the innate immune defense. Further steps should elucidate detailed mechanisms how those viral proteins, K3 (KSHV), NSs (LaCV) and NS2 (RSV), influence the KEAP1-PGAM5-AIFM1 cell death pathway. In addition further studies on related viral proteins from the initial virus-host-interactom study (2.1) would emphasize the role of this ROS-induced cell death pathway for antiviral immunity. Viral proteins, which have connecting signaling pathways to the already tested proteins, are VP35 (EBOV), S3 (ReoV), A52 (VACV) and NSs proteins (SFSV, HCV, RVFV, MCMV).

Further roles of PGAM5 and AIFM1 in programmed cell death

Besides their role in the here described PCD pathway, PGAM5 and AIFM1 are involved in other cellular processes related to cell death and oxidative processes. PGAM5 was described being involved in two other cell death related processes. One is mitochondrial fission required for intrinsic apoptosis [431, 432] and the other one is necroptosis [141]. Mitochondrial fission is required for cytochrom c release during intrinsic apoptosis and is dependent on DRP1 [219]. DRP1 is a substrate of PGAM5 phosphatase activity [432]. Necroptosis requires RIP kinase 3 (RIPK3) and ROS both are essential to fulfill cell death [204]. However, it was shown that TNF-induced necroptosis does not directly require PGAM5 [433], indicating that PGAM5 is most likely essential for ROS-induced

cell death, which could have similar molecular characteristics as necroptosis. Most assays in my studies were performed in cells naturally deficient in RIPK3 [434], excluding influence of RIPK3 on the here described ROS-induced cell death pathway. AIFM1 has two functional domains, one associated with caspase-independent PCD, called parthanatos, and the other bearing oxidoreductase activity [247]. The latter is described to affect complex I in the OxPhos system [435]. Keeping in mind that KEAP1 is a cytosolic ROS sensor, PGAM5 dephosphorylation of AIFM1 is probably no effect of mitochondrial ROS increase or an effect of AIFM1 on complex I activity. This underlines the influence of AIFM1 on the proposed novel caspase-independent PCD pathway.

Application in clinical settings

Besides the antiviral aspect of this ROS-induced cell death pathway, it probably plays as well a significant role in oxidative stress induced neurodegenerative diseases. Oxidative stress is important in the pathogenicity of neurodegenerative diseases, such as Alzheimer's disease, Parkinson's disease, Huntington's disease and amyotrophic lateral sclerosis [436]. Here again, the influence of ROS-induced PCD is emphasized by the fact, that mice deficient in Pgam5 or reduced Aifm1 levels show signs of neurodegenerative diseases. In particular Pgam5 deficient mice have Parkinson's disease like moving disorders after 12 month of age [437]. Harlekin mice, reduced in Aifm1, show neurodegenerative disorders probably due to an impaired OxPhos system [438]. It has not been shown whether ROS is specifically invovled in pathogenicity in these mouse models. However, the connection between PGAM5 and AIFM1 may suggest ROS-induced programmed cell death pathways [439, 440]. This newly identified PCD pathway may not only play an essential role in antiviral immunity, but as well in the field of cancer and transplantations. ROS is induced in both of these situations, leading either to no cell death or to unwanted cell death, respectively. Further research of this PCD pathway in the field of cancer and transplantation could elucidate new therapeutic opportunities. Especially, when elucidating the mechanisms of viral proteins on the pathway. Bioactive peptides of these viral proteins could serve as novel pharmaceuticals to treat ROS-associated diseases.

Together, the presented studies in my thesis demonstrate how MS can support the identification of new cellular targets of viruses and how MS can be used to elucidate cellular pathways. Both aspects may help to develop successful treatments in the future. Additionally, I could show the critical control of ROS levels within the cell to regulate antiviral immunity by programmed cell death.

References

[1] Akira, S., Uematsu, S., & Takeuchi, O. Pathogen recognition and innate immunity. *Cell* **124**(4), 783–801 (2006). (↑ pp. 1, 2, 3, and 9)

[2] Medzhitov, R. Recognition of microorganisms and activation of the immune response. *Nature* **449**(7164), 819–826 (2007). (↑ p. 1)

[3] Clark, R. & Kupper, T. Old meets new: the interaction between innate and adaptive immunity. *The Journal of investigative dermatology* **125**(4), 629–637 (2005). (↑ p. 2)

[4] Hotchkiss, R. S., Monneret, G., & Payen, D. Sepsis-induced immunosuppression: from cellular dysfunctions to immunotherapy. *Nature reviews. Immunology* **13**(12), 862–874 (2013). (↑ p. 2)

[5] Kawasaki, T., Kawai, T., & Akira, S. Recognition of nucleic acids by pattern-recognition receptors and its relevance in autoimmunity. *Immunological reviews* **243**(1), 61–73 (2011). (↑ p. 2)

[6] Janeway, C. A. J. & Medzhitov, R. Innate immune recognition. *Annual review of immunology* **20**, 197–216 (2002). (↑ pp. 2 and 3)

[7] Medzhitov, R. & Janeway, C. J. Innate immunity. *The New England journal of medicine* **343**(5), 338–344 (2000). (↑ p. 2)

[8] Medzhitov, R. & Janeway, C A Jr. An ancient system of host defense. *Current opinion in immunology* **10**(1), 12–15 (1998). (↑ p. 3)

[9] Rubartelli, A. & Lotze, M. T. Inside, outside, upside down: damage-associated molecular-pattern molecules (DAMPs) and redox. *Trends in immunology* **28**(10), 429–436 (2007). (↑ p. 3)

[10] Jensen, S. & Thomsen, A. R. Sensing of RNA viruses: a review of innate immune receptors involved in recognizing RNA virus invasion. *Journal of virology* **86**(6), 2900–2910 (2012). (↑ pp. 3 and 5)

[11] Unterholzner, L., Keating, S. E., Baran, M., *et al.* IFI16 is an innate immune sensor for intracellular DNA. *Nature immunology* **11**(11), 997–1004 (2010). (↑ pp. 3 and 6)

[12] Brubaker, S. W., Bonham, K. S., Zanoni, I., & Kagan, J. C. Innate immune pattern recognition: a cell biological perspective. *Annual review of immunology* **33**, 257–290 (2015). (↑ pp. 3 and 6)

[13] Medzhitov, R. Toll-like receptors and innate immunity. *Nature reviews. Immunology* **1**(2), 135–145 (2001). (↑ p. 3)

[14] Anderson, K. V., Jurgens, G., & Nusslein-Volhard, C. Establishment of dorsal-ventral polarity in the Drosophila embryo: genetic studies on the role of the Toll gene product. *Cell* **42**(3), 779–789 (1985). (↑ p. 3)

[15] Lemaitre, B., Nicolas, E., Michaut, L., Reichhart, J. M., & Hoffmann, J. A. The dorsoventral regulatory gene cassette spatzle/Toll/cactus controls the potent antifungal response in Drosophila adults. *Cell* **86**(6), 973–983 (1996). (↑ p. 3)

[16] Medzhitov, R., Preston-Hurlburt, P., & Janeway, C A Jr. A human homologue of the Drosophila Toll protein signals activation of adaptive immunity. *Nature* (388), 394–397 (1997). (↑ p. 3)

[17] Akira, S. & Takeda, K. Toll-like receptor signalling. *Nature reviews. Immunology* **4**(7), 499–511 (2004). (↑ pp. 3 and 4)

[18] Nishiya, T. & DeFranco, A. L. Ligand-regulated chimeric receptor approach reveals distinctive subcellular localization and signaling properties of the Toll-like receptors. *The Journal of biological chemistry* **279**(18), 19008–19017 (2004). (↑ p. 3)

[19] Botos, I., Segal, D. M., & Davies, D. R. The structural biology of Toll-like receptors. *Structure (London, England : 1993)* **19**(4), 447–459 (2011). (↑ p. 3)

[20] Uematsu, S. & Akira, S. Toll-Like receptors (TLRs) and their ligands. *Handbook of experimental pharmacology* (183), 1–20 (2008). (↑ p. 4)

[21] Broz, P. & Monack, D. M. Newly described pattern recognition receptors team up against intracellular pathogens. *Nature reviews. Immunology* **13**(8), 551–565 (2013). (↑ pp. 5 and 6)

[22] Takeuchi, O. & Akira, S. Pattern recognition receptors and inflammation. *Cell* **140**(6), 805–820 (2010). (↑ p. 4)

[23] Schmidt, A., Rothenfusser, S., & Hopfner, K.-P. Sensing of viral nucleic acids by RIG-I: from translocation to translation. *European journal of cell biology* **91**(1), 78–85 (2012). (↑ pp. 4 and 5)

[24] Kato, H., Takeuchi, O., Sato, S., *et al.* Differential roles of MDA5 and RIG-I helicases in the recognition of RNA viruses. *Nature* **441**(7089), 101–105 (2006). (↑ p. 4)

[25] Hornung, V., Ellegast, J., Kim, S., *et al.* 5'-Triphosphate RNA is the ligand for RIG-I. *Science (New York, N.Y.)* **314**(5801), 994–997 (2006). (↑ pp. 4 and 5)

[26] Pichlmair, A., Schulz, O., Tan, C. P., *et al.* RIG-I-mediated antiviral responses to single-stranded RNA bearing 5'-phosphates. *Science (New York, N.Y.)* **314**(5801), 997–1001 (2006).

[27] Saito, T., Owen, D. M., Jiang, F., Marcotrigiano, J., & Gale, M. J. Innate immunity induced by composition-dependent RIG-I recognition of hepatitis C virus RNA. *Nature* **454**(7203), 523–527 (2008).

[28] Schmidt, A., Schwerd, T., Hamm, W., *et al.* 5'-triphosphate RNA requires base-paired structures to activate antiviral signaling via RIG-I. *Proceedings of the National Academy of Sciences of the United States of America* **106**(29), 12067–12072 (2009). (↑ p. 4)

[29] Kato, H., Takeuchi, O., Mikamo-Satoh, E., *et al.* Length-dependent recognition of double-stranded ribonucleic acids by retinoic acid-inducible gene-I and melanoma differentiation-associated gene 5. *The Journal of experimental medicine* **205**(7), 1601–1610 (2008). (↑ p. 4)

[30] Pippig, D. A., Hellmuth, J. C., Cui, S., *et al.* The regulatory domain of the RIG-I family ATPase LGP2 senses double-stranded RNA. *Nucleic acids research* **37**(6), 2014–2025 (2009). (↑ p. 4)

[31] Bruns, A. M. & Horvath, C. M. LGP2 synergy with MDA5 in RLR-mediated RNA recognition and antiviral signaling. *Cytokine* **74**(2), 198–206 (2015). (↑ p. 4)

[32] Cui, S., Eisenächer, K., Kirchhofer, A., *et al.* The C-terminal regulatory domain is the RNA 5'-triphosphate sensor of RIG-I. *Molecular cell* **29**(2), 169–179 (2008). (↑ p. 5)

[33] Peisley, A., Wu, B., Xu, H., Chen, Z. J., & Hur, S. Structural basis for ubiquitin-mediated antiviral signal activation by RIG-I. *Nature* **509**(7498), 110–114 (2014). (↑ p. 5)

[34] Yoneyama, M., Kikuchi, M., Natsukawa, T., *et al.* The RNA helicase RIG-I has an essential function in double-stranded RNA-induced innate antiviral responses. *Nature immunology* **5**(7), 730–737 (2004). (↑ p. 5)

[35] Au, W.-C., Moore, P. A., Lowther, W., Juang, Y.-T., & Pitha, P. M. Identification of a member of the interferon regulatory factor family that binds to the interferon-stimulated response element and activates expression of interferon-induced genes. *Proceedings of the National Academy of Sciences of the United States of America* (92), 11657–11661 (1995). (↑ pp. 5 and 8)

[36] Satoh, T., Kato, H., Kumagai, Y., *et al.* LGP2 is a positive regulator of RIG-I- and MDA5-mediated antiviral responses. *Proceedings of the National Academy of Sciences of the United States of America* **107**(4), 1512–1517 (2010). (↑ p. 5)

[37] Saito, T., Hirai R, Loo YM, *et al.* Regulation of innate antiviral defenses through a shared repressor domain in RIG-I and LGP2. *Proceedings of the National Academy of Sciences of the United States of America* (104), 582–587 (2007). (↑ p. 5)

[38] Yao, H., Dittmann, M., Peisley, A., *et al.* ATP-dependent effector-like functions of RIG-I-like receptors. *Molecular cell* **58**(3), 541–548 (2015). (↑ p. 5)

[39] Pollpeter, D., Komuro, A., Barber, G. N., & Horvath, C. M. Impaired cellular responses to cytosolic DNA or infection with Listeria monocytogenes and vaccinia virus in the absence of the murine LGP2 protein. *PloS one* **6**(4), e18842 (2011). (↑ p. 5)

[40] Stetson, D. B. & Medzhitov, R. Recognition of cytosolic DNA activates an IRF3-dependent innate immune response. *Immunity* **24**(1), 93–103 (2006). (↑ p. 6)

[41] Takaoka, A., Wang, Z., Choi, M. K., *et al.* DAI (DLM-1/ZBP1) is a cytosolic DNA sensor and an activator of innate immune response. *Nature* **448**(7152), 501–505 (2007). (↑ p. 6)

[42] Ishii, K. J., Kawagoe, T., Koyama, S., *et al.* TANK-binding kinase-1 delineates innate and adaptive immune responses to DNA vaccines. *Nature* **451**(7179), 725–729 (2008). (↑ p. 6)

[43] Bürckstümmer, T., Baumann, C., Blüml, S., *et al.* An orthogonal proteomic-genomic screen identifies AIM2 as a cytoplasmic DNA sensor for the inflammasome. *Nature immunology* **10**(3), 266–272 (2009). (↑ p. 6)

[44] Hornung, V., Ablasser, A., Charrel-Dennis, M., *et al.* AIM2 recognizes cytosolic dsDNA and forms a caspase-1-activating inflammasome with ASC. *Nature* **458**(7237), 514–518 (2009). (↑ p. 6)

[45] Fernandes-Alnemri, T., Yu, J.-W., Datta, P., Wu, J., & Alnemri, E. S. AIM2 activates the inflammasome and cell death in response to cytoplasmic DNA. *Nature* **458**(7237), 509–513 (2009).

[46] Kerur, N., Veettil, M. V., Sharma-Walia, N., *et al.* IFI16 acts as a nuclear pathogen sensor to induce the inflammasome in response to Kaposi Sarcoma-associated herpesvirus infection. *Cell host & microbe* **9**(5), 363–375 (2011). (↑ p. 6)

[47] Sun, L., Wu, J., Du, F., Chen, X., & Chen, Z. J. Cyclic GMP-AMP synthase is a cytosolic DNA sensor that activates the type I interferon pathway. *Science (New York, N.Y.)* **339**(6121), 786–791 (2013). (↑ pp. 6 and 10)

[48] Liang, Q., Seo, G. J., Choi, Y. J., *et al.* Crosstalk between the cGAS DNA sensor and Beclin-1 autophagy protein shapes innate antimicrobial immune responses. *Cell host & microbe* **15**(2), 228–238 (2014). (↑ p. 6)

[49] Ansari, M. A., Singh, V. V., Dutta, S., *et al.* Constitutive interferon-inducible protein 16-inflammasome activation during Epstein-Barr

virus latency I, II, and III in B and epithelial cells. *Journal of virology* **87**(15), 8606–8623 (2013). (↑ p. 6)

[50] Dutta, D., Dutta, S., Veettil, M. V., *et al.* BRCA1 Regulates IFI16 Mediated Nuclear Innate Sensing of Herpes Viral DNA and Subsequent Induction of the Innate Inflammasome and Interferon-beta Responses. *PLoS pathogens* **11**(6), e1005030 (2015). (↑ p. 6)

[51] Wu, X., Wu, F.-H., Wang, X., *et al.* Molecular evolutionary and structural analysis of the cytosolic DNA sensor cGAS and STING. *Nucleic acids research* **42**(13), 8243–8257 (2014). (↑ p. 6)

[52] Ablasser, A., Goldeck, M., Cavlar, T., *et al.* cGAS produces a 2'-5'-linked cyclic dinucleotide second messenger that activates STING. *Nature* **498**(7454), 380–384 (2013). (↑ p. 10)

[53] Mankan, A. K., Schmidt, T., Chauhan, D., *et al.* Cytosolic RNA:DNA hybrids activate the cGAS-STING axis. *The EMBO journal* **33**(24), 2937–2946 (2014). (↑ pp. 6 and 10)

[54] Ablasser, A. & Hornung, V. DNA sensing unchained. *Cell research* **23**(5), 585–587 (2013). (↑ p. 6)

[55] Unterholzner, L. The interferon response to intracellular DNA: why so many receptors? *Immunobiology* **218**(11), 1312–1321 (2013). (↑ p. 6)

[56] Kagan, J. C. Signaling organelles of the innate immune system. *Cell* **151**(6), 1168–1178 (2012). (↑ pp. 7 and 10)

[57] Lee, M. S. & Kim, Y.-J. Signaling pathways downstream of pattern-recognition receptors and their cross talk. *Annual review of biochemistry* **76**, 447–480 (2007). (↑ p. 7)

[58] Latz, E., Verma, A., Visintin, A., *et al.* Ligand-induced conformational changes allosterically activate Toll-like receptor 9. *Nature immunology* **8**(7), 772–779 (2007). (↑ p. 7)

[59] O'Neill, Luke A J & Bowie, A. G. The family of five: TIR-domain-containing adaptors in Toll-like receptor signalling. *Nature reviews. Immunology* **7**(5), 353–364 (2007). (↑ pp. 7 and 9)

[60] Carty, M., Goodbody, R., Schröder, M., *et al.* The human adaptor SARM negatively regulates adaptor protein TRIF-dependent Toll-like receptor signaling. *Nature immunology* **7**(10), 1074–1081 (2006). (↑ pp. 7 and 9)

[61] Carlsson, E., Ding, J. L., & Byrne, B. SARM modulates MyD88-mediated TLR activation through BB-loop dependent TIR-TIR interactions. *Biochimica et biophysica acta* **1863**(2), 244–253 (2016). (↑ p. 7)

[62] Moynagh, P. N. TLR signalling and activation of IRFs: revisiting old friends from the NF-kappaB pathway. *Trends in immunology* **26**(9), 469–476 (2005). (↑ p. 7)

[63] Ewald, S. E., Lee, B. L., Lau, L., *et al.* The ectodomain of Toll-like receptor 9 is cleaved to generate a functional receptor. *Nature* **456**(7222), 658–662 (2008). (↑ p. 7)

[64] Park, B., Brinkmann, M. M., Spooner, E., *et al.* Proteolytic cleavage in an endolysosomal compartment is required for activation of Toll-like receptor 9. *Nature immunology* **9**(12), 1407–1414 (2008). (↑ p. 7)

[65] Ewald, S. E., Engel, A., Lee, J., *et al.* Nucleic acid recognition by Toll-like receptors is coupled to stepwise processing by cathepsins and asparagine endopeptidase. *The Journal of experimental medicine* **208**(4), 643–651 (2011). (↑ p. 7)

[66] Yamamoto, M., Sato, S., Mori, K., *et al.* Cutting edge: a novel Toll/IL-1 receptor domain-containing adapter that preferentially activates the IFN-beta promoter in the Toll-like receptor signaling. *Journal of immunology (Baltimore, Md. : 1950)* **169**(12), 6668–6672 (2002). (↑ p. 7)

[67] Oshiumi, H., Matsumoto, M., Funami, K., Akazawa, T., & Seya, T. TICAM-1, an adaptor molecule that participates in Toll-like receptor 3-mediated interferon-beta induction. *Nature immunology* **4**(2), 161–167 (2003). (↑ p. 7)

[68] Yamashita, M., Chattopadhyay, S., Fensterl, V., *et al.* Epidermal growth factor receptor is essential for Toll-like receptor 3 signaling. *Science signaling* **5**(233), ra50 (2012). (↑ p. 7)

[69] Häcker, H., Redecke, V., Blagoev, B., *et al.* Specificity in Toll-like receptor signalling through distinct effector functions of TRAF3 and TRAF6. *Nature* **439**(7073), 204–207 (2006). (↑ p. 8)

[70] Oganesyan, G., Saha, S. K., Guo, B., *et al.* Critical role of TRAF3 in the Toll-like receptor-dependent and -independent antiviral response. *Nature* **439**(7073), 208–211 (2006). (↑ p. 8)

[71] PÃ©rez de Diego, Rebeca, Sancho-Shimizu, V., Lorenzo, L., *et al.* Human TRAF3 adaptor molecule deficiency leads to impaired Toll-like receptor 3 response and susceptibility to herpes simplex encephalitis. *Immunity* **33**(3), 400–411 (2010).

[72] Gay, N. J., Symmons, M. F., Gangloff, M., & Bryant, C. E. Assembly and localization of Toll-like receptor signalling complexes. *Nature reviews. Immunology* **14**(8), 546–558 (2014). (↑ p. 8)

[73] Schafer, S. L., Lin, R., Moore, P. A., Hiscott, J., & Pitha, P. M. Regulation of Type I Interferon Gene Expression by Interferon Regulatory Factor-3. *Journal of biological chemistry* (273), 2714–2720 (1998). (↑ p. 8)

[74] Sato, M., Tanaka, N., Hata, N., Oda, E., & Taniguchi, T. Involvement of the IRF family transcription factor IRF-3 in virus-induced activation of the IFN-

beta gene. *FEBS letters* **425**(1), 112–116 (1998). (↑ p. 8)

[75] Han, K.-J., Su, X., Xu, L.-G., *et al.* Mechanisms of the TRIF-induced interferon-stimulated response element and NF-kappaB activation and apoptosis pathways. *The Journal of biological chemistry* **279**(15), 15652–15661 (2004). (↑ p. 8)

[76] Jiang, Z., Zamanian-Daryoush, M., Nie, H., *et al.* Poly(I-C)-induced Toll-like receptor 3 (TLR3)-mediated activation of NFkappa B and MAP kinase is through an interleukin-1 receptor-associated kinase (IRAK)-independent pathway employing the signaling components TLR3-TRAF6-TAK1-TAB2-PKR. *The Journal of biological chemistry* **278**(19), 16713–16719 (2003). (↑ p. 8)

[77] Pahl, H. L. Activators and target genes of Rel/NF-kappaB transcription factors. *Oncogene* **18**(49), 6853–6866 (1999). (↑ p. 8)

[78] Mitchell, S., Vargas, J., & Hoffmann, A. Signaling via the NFκB system. *Wiley interdisciplinary reviews. Systems biology and medicine* (2016). (↑ p. 8)

[79] Kaiser, W. J. & Offermann, M. K. Apoptosis Induced by the Toll-Like Receptor Adaptor TRIF Is Dependent on Its Receptor Interacting Protein Homotypic Interaction Motif. *The Journal of Immunology* **174**(8), 4942–4952 (2005). (↑ p. 9)

[80] Estornes, Y., Toscano, F., Virard, F., *et al.* dsRNA induces apoptosis through an atypical death complex associating TLR3 to caspase-8. *Cell death and differentiation* **19**(9), 1482–1494 (2012). (↑ p. 9)

[81] Kaiser, W. J., Sridharan, H., Huang, C., *et al.* Toll-like receptor 3-mediated necrosis via TRIF, RIP3, and MLKL. *The Journal of biological chemistry* **288**(43), 31268–31279 (2013). (↑ p. 9)

[82] Ahmed, S., Maratha, A., Butt, A. Q., Shevlin, E., & Miggin, S. M. TRIF-mediated TLR3 and TLR4 signaling is negatively regulated by ADAM15. *Journal of immunology (Baltimore, Md. : 1950)* **190**(5), 2217–2228 (2013). (↑ p. 9)

[83] Chang, L. & Karin, M. Mammalian MAP kinase signalling cascades. *Nature* **410**(6824), 37–40 (2001). (↑ p. 9)

[84] Karin, M. The regulation of AP-1 activity by mitogen-activated protein kinases. *The Journal of biological chemistry* **270**(28), 16483–16486 (1995). (↑ p. 9)

[85] Johnson, K. D., Norton, J. E., & Bresnick, E. H. Requirements for utilization of CREB binding protein by hypersensitive site two of the beta-globin locus control region. *Nucleic acids research* **30**(7), 1522–1530 (2002). (↑ p. 9)

[86] Gack, M. U., Kirchhofer, A., Shin, Y. C., *et al.* Roles of RIG-I N-terminal tandem CARD and splice variant in TRIM25-mediated antiviral signal transduction. *Proceedings of the National Academy of Sciences of the United States of America* **105**(43), 16743–16748 (2008). (↑ p. 9)

[87] Liu, H. M., Loo, Y.-M., Horner, S. M., *et al.* The mitochondrial targeting chaperone 14-3-3ε regulates a RIG-I translocon that mediates membrane association and innate antiviral immunity. *Cell host & microbe* **11**(5), 528–537 (2012). (↑ p. 9)

[88] Seth, R. B., Sun, L., Ea, C.-K., & Chen, Z. J. Identification and characterization of MAVS, a mitochondrial antiviral signaling protein that activates NF-kappaB and IRF 3. *Cell* **122**(5), 669–682 (2005). (↑ p. 9)

[89] Kawai, T., Takahashi, K., Sato, S., *et al.* IPS-1, an adaptor triggering RIG-I- and Mda5-mediated type I interferon induction. *Nature immunology* **6**(10), 981–988 (2005).

[90] Xu, L.-G., Wang, Y.-Y., Han, K.-J., *et al.* VISA is an adapter protein required for virus-triggered IFN-beta signaling. *Molecular cell* **19**(6), 727–740 (2005).

[91] Meylan, E., Curran, J., Hofmann, K., *et al.* Cardif is an adaptor protein in the RIG-I antiviral pathway and is targeted by hepatitis C virus. *Nature* **437**(7062), 1167–1172 (2005). (↑ p. 9)

[92] Dixit, E., Boulant, S., Zhang, Y., *et al.* Peroxisomes are signaling platforms for antiviral innate immunity. *Cell* **141**(4), 668–681 (2010). (↑ p. 9)

[93] Horner, S. M., Liu, H. M., Park, H. S., Briley, J., & Gale, M. Mitochondrial-associated endoplasmic reticulum membranes (MAM) form innate immune synapses and are targeted by hepatitis C virus. *Proceedings of the National Academy of Sciences of the United States of America* **108**(35), 14590–14595 (2011). (↑ p. 9)

[94] Tang, E. D. & Wang, C.-Y. MAVS self-association mediates antiviral innate immune signaling. *Journal of virology* **83**(8), 3420–3428 (2009). (↑ p. 9)

[95] Hou, F., Sun, L., Zheng, H., *et al.* MAVS forms functional prion-like aggregates to activate and propagate antiviral innate immune response. *Cell* **146**(3), 448–461 (2011). (↑ p. 9)

[96] Saha, S. K., Pietras, E. M., He, J. Q., *et al.* Regulation of antiviral responses by a direct and specific interaction between TRAF3 and Cardif. *The EMBO journal* **25**(14), 3257–3263 (2006). (↑ p. 9)

[97] Paz, S., Vilasco, M., Werden, S. J., *et al.* A functional C-terminal TRAF3-binding site in MAVS participates in positive and negative regulation of the IFN antiviral response. *Cell research* **21**(6), 895–910 (2011).

[98] Tang, E. D. & Wang, C.-Y. TRAF5 is a downstream target of MAVS in antiviral innate immune signaling. *PloS one* **5**(2), e9172 (2010).

[99] Liu, S., Chen, J., Cai, X., *et al.* MAVS recruits multiple ubiquitin E3 ligases to activate antiviral signaling cascades. *eLife* **2**, e00785 (2013).

[100] Shi, Z., Zhang, Z., Zhang, Z., *et al.* Structural Insights into mitochondrial antiviral signaling protein (MAVS)-tumor necrosis factor receptor-associated factor 6 (TRAF6) signaling. *The Journal of biological chemistry* **290**(44), 26811–26820 (2015). (↑ p. 9)

[101] Zhao, T., Yang, L., Sun, Q., *et al.* The NEMO adaptor bridges the nuclear factor-kappaB and interferon regulatory factor signaling pathways. *Nature immunology* **8**(6), 592–600 (2007). (↑ p. 9)

[102] Castanier, C. & Arnoult, D. Mitochondrial localization of viral proteins as a means to subvert host defense. *Biochimica et biophysica acta* **1813**(4), 575–583 (2011). (↑ pp. 9 and 28)

[103] Lei, Y., Moore, C. B., Liesman, R. M., *et al.* MAVS-mediated apoptosis and its inhibition by viral proteins. *PloS one* **4**(5), e5466 (2009). (↑ p. 9)

[104] Rebsamen, M., Meylan, E., Curran, J., & Tschopp, J. The antiviral adaptor proteins Cardif and Trif are processed and inactivated by caspases. *Cell death and differentiation* **15**(11), 1804–1811 (2008). (↑ p. 9)

[105] Scott, I. Mitochondrial factors in the regulation of innate immunity. *Microbes and infection / Institut Pasteur* **11**(8-9), 729–736 (2009).

[106] Yu, C.-Y., Chiang, R.-L., Chang, T.-H., Liao, C.-L., & Lin, Y.-L. The interferon stimulator mitochondrial antiviral signaling protein facilitates cell death by disrupting the mitochondrial membrane potential and by activating caspases. *Journal of virology* **84**(5), 2421–2431 (2010). (↑ p. 9)

[107] Guan, K., Zheng, Z., Song, T., *et al.* MAVS regulates apoptotic cell death by decreasing K48-linked ubiquitination of voltage-dependent anion channel 1. *Molecular and cellular biology* **33**(16), 3137–3149 (2013). (↑ p. 9)

[108] Civril, F., Deimling, T., de Oliveira Mann, Carina C, *et al.* Structural mechanism of cytosolic DNA sensing by cGAS. *Nature* **498**(7454), 332–337 (2013). (↑ p. 10)

[109] Zhang, X., Wu, J., Du, F., *et al.* The cytosolic DNA sensor cGAS forms an oligomeric complex with DNA and undergoes switch-like conformational changes in the activation loop. *Cell reports* **6**(3), 421–430 (2014). (↑ p. 10)

[110] Li, X.-D., Wu, J., Gao, D., *et al.* Pivotal roles of cGAS-cGAMP signaling in antiviral defense and immune adjuvant effects. *Science (New York, N.Y.)* **341**(6152), 1390–1394 (2013). (↑ p. 10)

[111] Ishikawa, H. & Barber, G. N. STING is an endoplasmic reticulum adaptor that facilitates innate immune signalling. *Nature* **455**(7213), 674–678 (2008). (↑ p. 10)

[112] Ishikawa, H., Ma, Z., & Barber, G. N. STING regulates intracellular DNA-mediated, type I interferon-dependent innate immunity. *Nature* **461**(7265), 788–792 (2009). (↑ p. 10)

[113] Suzuki, T., Oshiumi, H., Miyashita, M., *et al.* Cell type-specific subcellular localization of phospho-TBK1 in response to cytoplasmic viral DNA. *PloS one* **8**(12), e83639 (2013).

[114] Dobbs, N., Burnaevskiy, N., Chen, D., *et al.* STING Activation by Translocation from the ER Is Associated with Infection and Autoinflammatory Disease. *Cell host & microbe* **18**(2), 157–168 (2015). (↑ p. 10)

[115] Zhong, B., Yang, Y., Li, S., *et al.* The adaptor protein MITA links virus-sensing receptors to IRF3 transcription factor activation. *Immunity* **29**(4), 538–550 (2008). (↑ p. 10)

[116] Abe, T. & Barber, G. N. Cytosolic-DNA-mediated, STING-dependent proinflammatory gene induction necessitates canonical NF-κB activation through TBK1. *Journal of virology* **88**(10), 5328–5341 (2014). (↑ p. 10)

[117] Ablasser, A., Schmid-Burgk, J. L., Hemmerling, I., *et al.* Cell intrinsic immunity spreads to bystander cells via the intercellular transfer of cGAMP. *Nature* **503**(7477), 530–534 (2013). (↑ p. 10)

[118] Mogensen, T. H. Pathogen recognition and inflammatory signaling in innate immune defenses. *Clinical microbiology reviews* **22**(2), 240–73, Table of Contents (2009). (↑ p. 10)

[119] Isaacs, A. & LINDENMANN, J. Virus interference. I. The interferon. *Proceedings of the Royal Society of London. Series B, Biological sciences* **147**(927), 258–267 (1957). (↑ p. 10)

[120] Martal, J. L., Chene, N. M., Huynh, L. P., *et al.* IFN-tau: a novel subtype I IFN1. Structural characteristics, non-ubiquitous expression, structure-function relationships, a pregnancy hormonal embryonic signal and cross-species therapeutic potentialities. *Biochimie* **80**(8-9), 755–777 (1998). (↑ p. 11)

[121] Lefevre, F., Guillomot, M., D'Andrea, S., Battegay, S., & La Bonnardiere, C. Interferon-delta: the first member of a novel type I interferon family. *Biochimie* **80**(8-9), 779–788 (1998). (↑ p. 11)

[122] Ivashkiv, L. B. & Donlin, L. T. Regulation of type I interferon responses. *Nature reviews. Immunology* **14**(1), 36–49 (2014). (↑ p. 11)

[123] Honda, K., Yanai, H., Negishi, H., *et al.* IRF-7 is the master regulator of type-I interferon-dependent immune responses. *Nature* **434**(7034), 772–777 (2005). (↑ p. 11)

[124] Haller, O., Kochs, G., & Weber, F. The interferon response circuit: induction and suppression by patho-

genic viruses. *Virology* **344**(1), 119–130 (2006). (↑ p. 11)

[125] Valente, G., Ozmen, L., Novelli, F., *et al.* Distribution of interferon-gamma receptor in human tissues. *European journal of immunology* **22**(9), 2403–2412 (1992). (↑ p. 11)

[126] Walter, M. R., Windsor, W. T., Nagabhushan, T. L., *et al.* Crystal structure of a complex between interferon-gamma and its soluble high-affinity receptor. *Nature* **376**(6537), 230–235 (1995). (↑ p. 11)

[127] Chan, S. H., Perussia, B., Gupta, J. W., *et al.* Induction of interferon gamma production by natural killer cell stimulatory factor: characterization of the responder cells and synergy with other inducers. *The Journal of experimental medicine* **173**(4), 869–879 (1991). (↑ p. 11)

[128] Trinchieri, G. Interleukin-12 and the regulation of innate resistance and adaptive immunity. *Nature reviews. Immunology* **3**(2), 133–146 (2003).

[129] Wang, L., Wang, K., & Zou, Z.-Q. Crosstalk between innate and adaptive immunity in hepatitis B virus infection. *World journal of hepatology* **7**(30), 2980–2991 (2015). (↑ p. 11)

[130] Kotenko, S. V., Gallagher, G., Baurin, V. V., *et al.* IFN-lambdas mediate antiviral protection through a distinct class II cytokine receptor complex. *Nature immunology* **4**(1), 69–77 (2003). (↑ p. 11)

[131] Sheppard, P., Kindsvogel, W., Xu, W., *et al.* IL-28, IL-29 and their class II cytokine receptor IL-28R. *Nature immunology* **4**(1), 63–68 (2003).

[132] Prokunina-Olsson, L., Muchmore, B., Tang, W., *et al.* A variant upstream of IFNL3 (IL28B) creating a new interferon gene IFNL4 is associated with impaired clearance of hepatitis C virus. *Nature genetics* **45**(2), 164–171 (2013).

[133] Hamming, O. J., Terczynska-Dyla, E., Vieyres, G., *et al.* Interferon lambda 4 signals via the IFNlambda receptor to regulate antiviral activity against HCV and coronaviruses. *The EMBO journal* **32**(23), 3055–3065 (2013). (↑ p. 11)

[134] Ank, N., West, H., & Paludan, S. R. IFN-λ: Novel Antiviral Cytokines. *Journal of interferon & cytokine research : the official journal of the International Society for Interferon and Cytokine Research* (26), 373–379 (2006). (↑ p. 11)

[135] Akdis, M., Burgler, S., Crameri, R., *et al.* Interleukins, from 1 to 37, and interferon-γ: receptors, functions, and roles in diseases. *The Journal of allergy and clinical immunology* **127**(3), 701–21.e1–70 (2011). (↑ p. 11)

[136] Zheng, C., Zhou, X.-W., & Wang, J.-Z. The dual roles of cytokines in Alzheimer's disease: update on interleukins, TNF-alpha, TGF-beta and IFN-gamma. *Translational neurodegeneration* **5**, 7 (2016).

[137] Doan, T. *Immunology*. Lippincott's illustrated reviews. Wolters Kluwer Health/Lippincott Williams & Wilkins, Philadelphia, (2008). (↑ p. 11)

[138] Palomino, Diana Carolina Torres & Marti, L. C. Chemokines and immunity. *Einstein (São Paulo, Brazil)* **13**(3), 469–473 (2015). (↑ p. 11)

[139] Matikainen, S., Ronni, T., Lehtonen, A., *et al.* Retinoic acid induces signal transducer and activator of transcription (STAT) 1, STAT2, and p48 expression in myeloid leukemia cells and enhances their responsiveness to interferons. *Cell growth & differentiation : the molecular biology journal of the American Association for Cancer Research* **8**(6), 687–698 (1997). (↑ p. 12)

[140] Uddin, S., Majchrzak, B., Wang, P. C., *et al.* Interferon-dependent activation of the serine kinase PI 3'-kinase requires engagement of the IRS pathway but not the Stat pathway. *Biochemical and biophysical research communications* **270**(1), 158–162 (2000). (↑ p. 12)

[141] Wang, B. X. & Fish, E. N. The yin and yang of viruses and interferons. *Trends in immunology* **33**(4), 190–197 (2012). (↑ pp. 12 and 111)

[142] Li, Y., Sassano, A., Majchrzak, B., *et al.* Role of p38alpha Map kinase in Type I interferon signaling. *The Journal of biological chemistry* **279**(2), 970–979 (2004). (↑ p. 12)

[143] Soloaga, A., Thomson, S., Wiggin, G. R., *et al.* MSK2 and MSK1 mediate the mitogen- and stress-induced phosphorylation of histone H3 and HMG-14. *The EMBO journal* **22**(11), 2788–2797 (2003). (↑ p. 12)

[144] Song, M. M. & Shuai, K. The suppressor of cytokine signaling (SOCS) 1 and SOCS3 but not SOCS2 proteins inhibit interferon-mediated antiviral and antiproliferative activities. *The Journal of biological chemistry* **273**(52), 35056–35062 (1998). (↑ p. 12)

[145] Kubo, M., Hanada, T., & Yoshimura, A. Suppressors of cytokine signaling and immunity. *Nature immunology* **4**(12), 1169–1176 (2003). (↑ p. 12)

[146] Shuai, K. & Liu, B. Regulation of gene-activation pathways by PIAS proteins in the immune system. *Nature reviews. Immunology* **5**(8), 593–605 (2005). (↑ p. 12)

[147] Decker T, Kovarik P, & Meinke A. GAS Elements: A Few Nucleotides with a Major Impact on Cytokine-Induced Gene Expression. *Journal of interferon & cytokine research : the official journal of the International Society for Interferon and Cytokine Research* (17), 121–134 (1997). (↑ p. 12)

[148] Schneider, W. M., Chevillotte, M. D., & Rice, C. M. Interferon-stimulated genes: a complex web of host defenses. *Annual review of immunology* **32**, 513–545

(2014). (↑ p. 12)

[149] Rusinova, I., Forster, S., Yu, S., *et al.* Interferome v2.0: an updated database of annotated interferon-regulated genes. *Nucleic acids research* **41**(Database issue), D1040–6 (2013). (↑ p. 12)

[150] Hovanessian, A. G. The double stranded RNA-activated protein kinase induced by interferon: dsRNA-PK. *Journal of interferon research* **9**(6), 641–647 (1989). (↑ p. 12)

[151] Garcia, M. A., Meurs, E. F., & Esteban, M. The dsRNA protein kinase PKR: virus and cell control. *Biochimie* **89**(6-7), 799–811 (2007). (↑ p. 12)

[152] Galabru, J. & Hovanessian, A. Autophosphorylation of the protein kinase dependent on double-stranded RNA. *The Journal of biological chemistry* **262**(32), 15538–15544 (1987). (↑ p. 12)

[153] Garcia, M. A., Gil, J., Ventoso, I., *et al.* Impact of protein kinase PKR in cell biology: from antiviral to antiproliferative action. *Microbiology and molecular biology reviews : MMBR* **70**(4), 1032–1060 (2006). (↑ p. 12)

[154] Lee, S. B. & Esteban, M. The interferon-induced double-stranded RNA-activated protein kinase induces apoptosis. *Virology* **199**(2), 491–496 (1994). (↑ p. 12)

[155] Kumar, A., Haque, J., Lacoste, J., Hiscott, J., & Williams, B. R. Double-stranded RNA-dependent protein kinase activates transcription factor NF-kappa B by phosphorylating I kappa B. *Proceedings of the National Academy of Sciences of the United States of America* **91**(14), 6288–6292 (1994). (↑ p. 13)

[156] Koromilas, A. E., Cantin, C., Craig, A. W., *et al.* The interferon-inducible protein kinase PKR modulates the transcriptional activation of immunoglobulin kappa gene. *The Journal of biological chemistry* **270**(43), 25426–25434 (1995). (↑ p. 13)

[157] Gil, J. & Esteban, M. Induction of apoptosis by the dsRNA-dependent protein kinase (PKR): mechanism of action. *Apoptosis : an international journal on programmed cell death* **5**(2), 107–114 (2000). (↑ p. 13)

[158] Gil, J., Alcami, J., & Esteban, M. Induction of apoptosis by double-stranded-RNA-dependent protein kinase (PKR) involves the alpha subunit of eukaryotic translation initiation factor 2 and NF-kappaB. *Molecular and cellular biology* **19**(7), 4653–4663 (1999). (↑ p. 13)

[159] Liu, Y., Zhang, Y.-B., Liu, T.-K., & Gui, J.-F. Lineage-specific expansion of IFIT gene family: an insight into coevolution with IFN gene family. *PloS one* **8**(6), e66859 (2013). (↑ p. 13)

[160] Pichlmair, A., Lassnig, C., Eberle, C.-A., *et al.* IFIT1 is an antiviral protein that recognizes 5'-triphosphate RNA. *Nature immunology* **12**(7), 624–630 (2011). (↑ pp. 13, 14, and 94)

[161] Stawowczyk, M., van Scoy, S., Kumar, K. P., & Reich, N. C. The interferon stimulated gene 54 promotes apoptosis. *The Journal of biological chemistry* **286**(9), 7257–7266 (2011).

[162] Habjan, M., Hubel, P., Lacerda, L., *et al.* Sequestration by IFIT1 impairs translation of 2'O-unmethylated capped RNA. *PLoS pathogens* **9**(10), e1003663 (2013). (↑ pp. 13 and 14)

[163] Fensterl, V. & Sen, G. C. Interferon-induced Ifit proteins: their role in viral pathogenesis. *Journal of virology* **89**(5), 2462–2468 (2015). (↑ p. 13)

[164] Abbas, Y. M., Pichlmair, A., Gorna, M. W., Superti-Furga, G., & Nagar, B. Structural basis for viral 5'-PPP-RNA recognition by human IFIT proteins. *Nature* **494**(7435), 60–64 (2013). (↑ p. 14)

[165] Kimura, T., Katoh, H., Kayama, H., *et al.* Ifit1 inhibits Japanese encephalitis virus replication through binding to 5' capped 2'-O unmethylated RNA. *Journal of virology* **87**(18), 9997–10003 (2013).

[166] Kumar, P., Sweeney, T. R., Skabkin, M. A., *et al.* Inhibition of translation by IFIT family members is determined by their ability to interact selectively with the 5'-terminal regions of cap0-, cap1- and 5'ppp-mRNAs. *Nucleic acids research* **42**(5), 3228–3245 (2014). (↑ p. 14)

[167] Weber, M., Gawanbacht, A., Habjan, M., *et al.* Incoming RNA virus nucleocapsids containing a 5'-triphosphorylated genome activate RIG-I and antiviral signaling. *Cell host & microbe* **13**(3), 336–346 (2013). (↑ p. 14)

[168] Hyde, J. L. & Diamond, M. S. Innate immune restriction and antagonism of viral RNA lacking 2'-O methylation. *Virology* **479-480**, 66–74 (2015). (↑ p. 14)

[169] Ashwell, M. & Work, T. S. The biogenesis of mitochondria. *Annual review of biochemistry* **39**, 251–290 (1970). (↑ p. 15)

[170] Mayr, J. A. Lipid metabolism in mitochondrial membranes. *Journal of inherited metabolic disease* **38**(1), 137–144 (2015). (↑ p. 15)

[171] Taanman, J.-W. The mitochondrial genome: structure, transcription, translation and replication. *Biochimica et Biophysica Acta (BBA) - Bioenergetics* **1410**(2), 103–123 (1999). (↑ p. 15)

[172] Pagliarini, D. J., Calvo, S. E., Chang, B., *et al.* A mitochondrial protein compendium elucidates complex I disease biology. *Cell* **134**(1), 112–123 (2008). (↑ p. 15)

[173] Dickinson, A., Yeung, K. Y., Donoghue, J., *et al.* The regulation of mitochondrial DNA copy number in glioblastoma cells. *Cell death and differentiation* **20**(12), 1644–1653 (2013). (↑ p. 15)

[174] Liesa, M. & Shirihai, O. S. Mitochondrial dynamics in the regulation of nutrient utilization and energy expenditure. *Cell metabolism* **17**(4), 491–506 (2013). (↑ p. 15)

[175] Tsang, W. Y. & Lemire, B. D. The role of mitochondria in the life of the nematode, Caenorhabditis elegans. *Biochimica et Biophysica Acta (BBA) - Molecular Basis of Disease* **1638**(2), 91–105 (2003). (↑ p. 15)

[176] Lehninger, A. L., Nelson, D. L., & Cox, M. M. *Lehninger principles of biochemistry*. W.H. Freeman, New York, 4th ed edition, (2005). (↑ pp. 16 and 29)

[177] Brand, M. D. The sites and topology of mitochondrial superoxide production. *Experimental gerontology* **45**(7-8), 466–472 (2010). (↑ p. 16)

[178] Quinlan, C. L., Perevoshchikova, I. V., Hey-Mogensen, M., Orr, A. L., & Brand, M. D. Sites of reactive oxygen species generation by mitochondria oxidizing different substrates. *Redox biology* **1**, 304–312 (2013). (↑ p. 16)

[179] Zelko, I. N., Mariani, T. J., & Folz, R. J. Superoxide dismutase multigene family: a comparison of the CuZn-SOD (SOD1), Mn-SOD (SOD2), and EC-SOD (SOD3) gene structures, evolution, and expression. *Free radical biology & medicine* **33**(3), 337–349 (2002). (↑ p. 16)

[180] Marklund, S. L., Holme, E., & Hellner, L. Superoxide dismutase in extracellular fluids. *Clinica chimica acta; international journal of clinical chemistry* **126**(1), 41–51 (1982). (↑ p. 16)

[181] Marklund, S. L., Bjelle, A., & Elmqvist, L. G. Superoxide dismutase isoenzymes of the synovial fluid in rheumatoid arthritis and in reactive arthritides. *Annals of the rheumatic diseases* **45**(10), 847–851 (1986).

[182] Levin, E. D. Extracellular superoxide dismutase (EC-SOD) quenches free radicals and attenuates age-related cognitive decline: opportunities for novel drug development in aging. *Current Alzheimer research* **2**(2), 191–196 (2005). (↑ p. 16)

[183] Gravel, M., Beland, L.-C., Soucy, G., *et al.* IL-10 Controls Early Microglial Phenotypes and Disease Onset in ALS Caused by Misfolded Superoxide Dismutase 1. *The Journal of neuroscience : the official journal of the Society for Neuroscience* **36**(3), 1031–1048 (2016). (↑ p. 16)

[184] McCord, J. M. & Edeas, M. A. SOD, oxidative stress and human pathologies: a brief history and a future vision. *Biomedicine & pharmacotherapy = Biomedecine & pharmacotherapie* **59**(4), 139–142 (2005). (↑ p. 16)

[185] Chandel, N. S. Mitochondria as signaling organelles. *BMC biology* **12**, 34 (2014). (↑ pp. 17 and 18)

[186] Itoh, K., Wakabayashi, N., Katoh, Y., *et al.* Keap1 represses nuclear activation of antioxidant responsive elements by Nrf2 through binding to the amino-terminal Neh2 domain. *Genes & development* **13**(1), 76–86 (1999). (↑ p. 18)

[187] Itoh, K., Wakabayashi, N., Katoh, Y., *et al.* Keap1 regulates both cytoplasmic-nuclear shuttling and degradation of Nrf2 in response to electrophiles. *Genes to cells : devoted to molecular & cellular mechanisms* **8**(4), 379–391 (2003).

[188] Itoh, K., Tong, K. I., & Yamamoto, M. Molecular mechanism activating Nrf2-Keap1 pathway in regulation of adaptive response to electrophiles. *Free radical biology & medicine* **36**(10), 1208–1213 (2004). (↑ p. 18)

[189] Kobayashi, A., Kang, M.-I., Okawa, H., *et al.* Oxidative stress sensor Keap1 functions as an adaptor for Cul3-based E3 ligase to regulate proteasomal degradation of Nrf2. *Molecular and cellular biology* **24**(16), 7130–7139 (2004). (↑ p. 18)

[190] Sekhar, K. R., Yan, X. X., & Freeman, M. L. Nrf2 degradation by the ubiquitin proteasome pathway is inhibited by KIAA0132, the human homolog to INrf2. *Oncogene* **21**(44), 6829–6834 (2002). (↑ p. 18)

[191] Taguchi, K., Motohashi, H., & Yamamoto, M. Molecular mechanisms of the Keap1–Nrf2 pathway in stress response and cancer evolution. *Genes to cells : devoted to molecular & cellular mechanisms* **16**(2), 123–140 (2011). (↑ p. 18)

[192] Itoh, K., Chiba, T., Takahashi, S., *et al.* An Nrf2/small Maf heterodimer mediates the induction of phase II detoxifying enzyme genes through antioxidant response elements. *Biochemical and biophysical research communications* **236**(2), 313–322 (1997). (↑ p. 18)

[193] Motohashi, H. & Yamamoto, M. Nrf2-Keap1 defines a physiologically important stress response mechanism. *Trends in molecular medicine* **10**(11), 549–557 (2004).

[194] Thimmulappa, R. K., Mai, K. H., Srisuma, S., *et al.* Identification of Nrf2-regulated genes induced by the chemopreventive agent sulforaphane by oligonucleotide microarray. *Cancer research* **62**(18), 5196–5203 (2002).

[195] Chorley, B. N., Campbell, M. R., Wang, X., *et al.* Identification of novel NRF2-regulated genes by ChIP-Seq: influence on retinoid X receptor alpha. *Nucleic acids research* **40**(15), 7416–7429 (2012). (↑ p. 18)

[196] Trachootham, D., Alexandre, J., & Huang, P. Targeting cancer cells by ROS-mediated mechanisms: a radical therapeutic approach? *Nature reviews. Drug discovery* **8**(7), 579–591 (2009). (↑ p. 19)

[197] Nathan, C. & Cunningham-Bussel, A. Beyond oxidative stress: an immunologist's guide to reactive oxygen species. *Nature reviews. Immunology* **13**(5), 349–361 (2013). (↑ p. 19)

[198] Degterev, A. & Yuan, J. Expansion and evolution of cell death programmes. *Nature reviews. Molecular cell biology* **9**(5), 378–390 (2008). (↑ pp. 19, 20, 21, and 25)

[199] Jackson, S. P. & Schoenwaelder, S. M. Procoagulant platelets: are they necrotic? *Blood* **116**(12), 2011–2018 (2010). (↑ p. 19)

[200] Vanden Berghe, T., Linkermann, A., Jouan-Lanhouet, S., Walczak, H., & Vandenabeele, P. Regulated necrosis: the expanding network of non-apoptotic cell death pathways. *Nature reviews. Molecular cell biology* **15**(2), 135–147 (2014). (↑ pp. 20 and 24)

[201] Meier, P., Finch, A., & Evan, G. Apoptosis in development. *Nature* (407), 796–801 (2000). (↑ p. 20)

[202] Bergsbaken, T., Fink, S. L., & Cookson, B. T. Pyroptosis: host cell death and inflammation. *Nature reviews. Microbiology* **7**(2), 99–109 (2009). (↑ p. 20)

[203] Davidovich, P., Kearney, C. J., & Martin, S. J. Inflammatory outcomes of apoptosis, necrosis and necroptosis. *Biological chemistry* **395**(10), 1163–1171 (2014).

[204] Linkermann, A. & Green, D. R. Necroptosis. *The New England journal of medicine* **370**(5), 455–465 (2014). (↑ pp. 20, 25, and 111)

[205] Taylor, R. C., Cullen, S. P., & Martin, S. J. Apoptosis: controlled demolition at the cellular level. *Nature reviews. Molecular cell biology* **9**(3), 231–241 (2008). (↑ p. 20)

[206] Bröker, L. E. & Kruyt, Frank A.E. and Giaccone, Giuseppe. Cell Death Independent of Caspases: AReview. *Clinical cancer research* (11), 3155–3162 (2005). (↑ pp. 20 and 25)

[207] Vandenabeele, P., Orrenius, S., & Zhivotovsky, B. Serine proteases and calpains fulfill important supporting roles in the apoptotic tragedy of the cellular opera. *Cell death and differentiation* **12**(9), 1219–1224 (2005). (↑ p. 20)

[208] Lockshin, R. A. & Zakeri, Z. Caspase-independent cell deaths. *Current opinion in cell biology* **14**(6), 727–733 (2002). (↑ p. 20)

[209] Sanfilippo, C. M. & Blaho, J. A. The facts of death. *International reviews of immunology* **22**(5-6), 327–340 (2003). (↑ p. 20)

[210] Youle, R. J. & Strasser, A. The BCL-2 protein family: opposing activities that mediate cell death. *Nature reviews. Molecular cell biology* **9**(1), 47–59 (2008). (↑ p. 21)

[211] Chipuk, J. E., Moldoveanu, T., Llambi, F., Parsons, M. J., & Green, D. R. The BCL-2 family reunion. *Molecular cell* **37**(3), 299–310 (2010). (↑ p. 21)

[212] Oda, E., Ohki, R., Murasawa, H., *et al.* Noxa, a BH3-only member of the Bcl-2 family and candidate mediator of p53-induced apoptosis. *Science (New York, N.Y.)* **288**(5468), 1053–1058 (2000).

[213] Nakano, K. & Vousden, K. H. PUMA, a novel proapoptotic gene, is induced by p53. *Molecular cell* **7**(3), 683–694 (2001). (↑ p. 21)

[214] Puthalakath, H. & Strasser, A. Keeping killers on a tight leash: transcriptional and post-translational control of the pro-apoptotic activity of BH3-only proteins. *Cell death and differentiation* **9**(5), 505–512 (2002). (↑ p. 21)

[215] Michalak, E. M., Villunger, A., Adams, J. M., & Strasser, A. In several cell types tumour suppressor p53 induces apoptosis largely via Puma but Noxa can contribute. *Cell death and differentiation* **15**(6), 1019–1029 (2008). (↑ p. 21)

[216] Kim, H., Rafiuddin-Shah, M., Tu, H.-C., *et al.* Hierarchical regulation of mitochondrion-dependent apoptosis by BCL-2 subfamilies. *Nature cell biology* **8**(12), 1348–1358 (2006). (↑ p. 21)

[217] Oltvai, Z. N., Milliman, C. L., & Korsmeyer, S. J. Bcl-2 heterodimerizes in vivo with a conserved homolog, Bax, that accelerates programmed cell death. *Cell* **74**(4), 609–619 (1993). (↑ p. 21)

[218] Gottschalk, A. R., Boise, L. H., Oltvai, Z. N., *et al.* The ability of Bcl-x(L) and Bcl-2 to prevent apoptosis can be differentially regulated. *Cell death and differentiation* **3**(1), 113–118 (1996). (↑ p. 21)

[219] Grosse, L., Wurm, C. A., Bruser, C., *et al.* Bax assembles into large ring-like structures remodeling the mitochondrial outer membrane in apoptosis. *The EMBO journal* **35**(4), 402–413 (2016). (↑ pp. 21 and 111)

[220] Salvador-Gallego, R., Mund, M., Cosentino, K., *et al.* Bax assembly into rings and arcs in apoptotic mitochondria is linked to membrane pores. *The EMBO journal* **35**(4), 389–401 (2016). (↑ p. 21)

[221] Green, D. R. & Reed, J. C. Mitochondria and apoptosis. *Science (New York, N.Y.)* **281**(5381), 1309–1312 (1998). (↑ p. 21)

[222] Du, C., Fang, M., Li, Y., Li, L., & Wang, X. Smac, a mitochondrial protein that promotes cytochrome c-dependent caspase activation by eliminating IAP inhibition. *Cell* **102**(1), 33–42 (2000).

[223] Suzuki, Y., Imai, Y., Nakayama, H., *et al.* A serine protease, HtrA2, is released from the mitochondria and interacts with XIAP, inducing cell death. *Molecular cell* **8**(3), 613–621 (2001). (↑ p. 21)

[224] Zou, H., Henzel, W. J., Liu, X., Lutschg, A., & Wang, X. Apaf-1, a human protein homologous to C. elegans CED-4, participates in cytochrome c-dependent activation of caspase-3. *Cell* **90**(3), 405–413 (1997). (↑ p. 21)

[225] Li, P., Nijhawan, D., Budihardjo, I., *et al.* Cytochrome c and dATP-dependent formation of Apaf-1/caspase-9 complex initiates an apoptotic protease cascade. *Cell* **91**(4), 479–489 (1997). (↑ p. 21)

[226] Srinivasula, S. M., Hegde, R., Saleh, A., *et al.* A conserved XIAP-interaction motif in caspase-9 and Smac/DIABLO regulates caspase activity and apoptosis. *Nature* **410**(6824), 112–116 (2001). (↑ p. 21)

[227] Nicholson, D. W., Ali, A., Thornberry, N. A., *et al.* Identification and inhibition of the ICE/CED-3 protease necessary for mammalian apoptosis. *Nature* **376**(6535), 37–43 (1995). (↑ p. 21)

[228] Slee, E. A., Adrain, C., & Martin, S. J. Executioner caspase-3, -6, and -7 perform distinct, non-redundant roles during the demolition phase of apoptosis. *The Journal of biological chemistry* **276**(10), 7320–7326 (2001). (↑ p. 22)

[229] Sakahira, H., Enari, M., & Nagata, S. Cleavage of CAD inhibitor in CAD activation and DNA degradation during apoptosis. *Nature* **391**(6662), 96–99 (1998). (↑ p. 22)

[230] Kerr, J. F., Wyllie, A. H., & Currie, A. R. Apoptosis: a basic biological phenomenon with wide-ranging implications in tissue kinetics. *British journal of cancer* **26**(4), 239–257 (1972). (↑ p. 22)

[231] Fadok, V. A., Cathelineau, A. d., Daleke, D. L., Henson, P. M., & Bratton, D. L. Loss of phospholipid asymmetry and surface exposure of phosphatidylserine is required for phagocytosis of apoptotic cells by macrophages and fibroblasts. *The Journal of biological chemistry* **276**(2), 1071–1077 (2001). (↑ pp. 22 and 31)

[232] Elmore, S. Apoptosis: a review of programmed cell death. *Toxicologic pathology* **35**(4), 495–516 (2007). (↑ pp. 22 and 23)

[233] Lewis-Wambi, J. S. & Jordan, V. C. Estrogen regulation of apoptosis: how can one hormone stimulate and inhibit? *Breast cancer research : BCR* **11**(3), 206 (2009). (↑ p. 22)

[234] Locksley, R. M., Killeen, N., & Lenardo, M. J. The TNF and TNF receptor superfamilies: integrating mammalian biology. *Cell* **104**(4), 487–501 (2001). (↑ p. 22)

[235] Ashkenazi, A. & Dixit, V. M. Death receptors: signaling and modulation. *Science (New York, N.Y.)* **281**(5381), 1305–1308 (1998). (↑ p. 22)

[236] Huang, D. C., Hahne, M., Schroeter, M., *et al.* Activation of Fas by FasL induces apoptosis by a mechanism that cannot be blocked by Bcl-2 or Bcl-x(L). *Proceedings of the National Academy of Sciences of the United States of America* **96**(26), 14871–14876 (1999). (↑ p. 22)

[237] Wang, K., Yin, X. M., Chao, D. T., Milliman, C. L., & Korsmeyer, S. J. BID: a novel BH3 domain-only death agonist. *Genes & development* **10**(22), 2859–2869 (1996). (↑ p. 22)

[238] Moujalled, D. M., Cook, W. D., Lluis, J. M., *et al.* In mouse embryonic fibroblasts, neither caspase-8 nor cellular FLICE-inhibitory protein (FLIP) is necessary for TNF to activate NF-kappaB, but caspase-8 is required for TNF to cause cell death, and induction of FLIP by NF-kappaB is required to prevent it. *Cell death and differentiation* **19**(5), 808–815 (2012). (↑ p. 22)

[239] Irmler, M., Thome, M., Hahne, M., *et al.* Inhibition of death receptor signals by cellular FLIP. *Nature* **388**(6638), 190–195 (1997). (↑ p. 22)

[240] Kataoka, T., Schroter, M., Hahne, M., *et al.* FLIP prevents apoptosis induced by death receptors but not by perforin/granzyme B, chemotherapeutic drugs, and gamma irradiation. *Journal of immunology (Baltimore, Md. : 1950)* **161**(8), 3936–3942 (1998).

[241] Scaffidi, C., Fulda, S., Srinivasan, A., *et al.* Two CD95 (APO-1/Fas) signaling pathways. *The EMBO journal* **17**(6), 1675–1687 (1998). (↑ p. 22)

[242] Thome, M., Schneider, P., Hofmann, K., *et al.* Viral FLICE-inhibitory proteins (FLIPs) prevent apoptosis induced by death receptors. *Nature* (386), 517–521 (1997). (↑ p. 22)

[243] Herceg, Z. & Wang, Z.-Q. Functions of poly(ADP-ribose) polymerase (PARP) in DNA repair, genomic integrity and cell death. *Mutation Research/Fundamental and Molecular Mechanisms of Mutagenesis* **477**(1-2), 97–110 (2001). (↑ p. 23)

[244] Fatokun, A. A., Dawson, V. L., & Dawson, T. M. Parthanatos: mitochondrial-linked mechanisms and therapeutic opportunities. *British journal of pharmacology* **171**(8), 2000–2016 (2014). (↑ p. 24)

[245] Devalaraja-Narashimha, K., Singaravelu, K., & Padanilam, B. J. Poly(ADP-ribose) polymerase-mediated cell injury in acute renal failure. *Pharmacological research* **52**(1), 44–59 (2005). (↑ p. 24)

[246] Javle, M. & Curtin, N. J. The role of PARP in DNA repair and its therapeutic exploitation. *British journal of cancer* **105**(8), 1114–1122 (2011). (↑ p. 24)

[247] Susin, S. A., Lorenzo, H. K., Zamzami, N., *et al.* Molecular characterization of mitochondrial apoptosis-inducing factor. *Nature* **397**(6718), 441–446 (1999). (↑ pp. 24 and 112)

[248] Wang, Y., Dawson, V. L., & Dawson, T. M. Poly(ADP-ribose) signals to mitochondrial AIF: a key event in parthanatos. *Experimental neurology* **218**(2), 193–202 (2009). (↑ p. 24)

[249] Polster, B. M., Basañez, G., Etxebarria, A., Hardwick, J. M., & Nicholls, D. G. Calpain I induces cleavage and release of apoptosis-inducing factor from isolated mitochondria. *The Journal of biological chemistry* **280**(8), 6447–6454 (2005). (↑ p. 24)

[250] Wang, Y., Kim, N. S., Li, X., *et al.* Calpain activation is not required for AIF translocation in PARP-1-dependent cell death (parthanatos). *Journal of neurochemistry* **110**(2), 687–696 (2009). (↑ p. 24)

[251] Cande, C., Vahsen, N., Kouranti, I., *et al.* AIF and cyclophilin A cooperate in apoptosis-associated chromatinolysis. *Oncogene* **23**(8), 1514–1521 (2004). (↑ p. 24)

[252] Vercammen, D., Beyaert, R., Denecker, G., *et al.* Inhibition of Caspases Increases the Sensitivity of L929 Cells to Necrosis Mediated by Tumor Necrosis Factor. *Journal of experimental medicine* (187), 1477–1485 (1998). (↑ pp. 24 and 25)

[253] Duprez, L., Takahashi, N., van Hauwermeiren, F., *et al.* RIP kinase-dependent necrosis drives lethal systemic inflammatory response syndrome. *Immunity* **35**(6), 908–918 (2011). (↑ p. 24)

[254] Rickard, J. A., O'Donnell, J. A., Evans, J. M., *et al.* RIPK1 regulates RIPK3-MLKL-driven systemic inflammation and emergency hematopoiesis. *Cell* **157**(5), 1175–1188 (2014). (↑ p. 24)

[255] Silke, J., Rickard, J. A., & Gerlic, M. The diverse role of RIP kinases in necroptosis and inflammation. *Nature immunology* **16**(7), 689–697 (2015). (↑ p. 24)

[256] Rodriguez, D. A., Weinlich, R., Brown, S., *et al.* Characterization of RIPK3-mediated phosphorylation of the activation loop of MLKL during necroptosis. *Cell death and differentiation* **23**(1), 76–88 (2016). (↑ p. 25)

[257] Kaczmarek, A., Vandenabeele, P., & Krysko, D. V. Necroptosis: the release of damage-associated molecular patterns and its physiological relevance. *Immunity* **38**(2), 209–223 (2013). (↑ p. 25)

[258] Babu, D., Leclercq, G., Goossens, V., *et al.* Mitochondria and NADPH oxidases are the major sources of TNF-α/cycloheximide-induced oxidative stress in murine intestinal epithelial MODE-K cells. *Cellular signalling* **27**(6), 1141–1158 (2015). (↑ p. 25)

[259] Krysko, D. V., Berghe, T. V., Parthoens, E., D'Herde, K., & Vandenabeele, P. Chapter 16 Methods for Distinguishing Apoptotic from Necrotic Cells and Measuring Their Clearance. In *Programmed Cell Death,General Principles forStudying Cell Death, Part A*, volume 442 of *Methods in Enzymology*, 307–341. Elsevier (2008). (↑ p. 25)

[260] Vanden Berghe, T., Vanlangenakker, N., Parthoens, E., *et al.* Necroptosis, necrosis and secondary necrosis converge on similar cellular disintegration features. *Cell death and differentiation* **17**(6), 922–930 (2010). (↑ p. 25)

[261] Kroemer, G., Galluzzi, L., Vandenabeele, P., *et al.* Classification of cell death: recommendations of the Nomenclature Committee on Cell Death 2009. *Cell death and differentiation* **16**(1), 3–11 (2009). (↑ p. 25)

[262] Rammos, C., Luedike, P., Hendgen-Cotta, U., & Rassaf, T. Potential of dietary nitrate in angiogenesis. *World journal of cardiology* **7**(10), 652–657 (2015). (↑ p. 25)

[263] Beijerinck, W. M. Ueber ein Contagium vivum fluidum als Ursache der Fleckenkrankheit der Tabaksblätter. *Proceedings* (1), 1–24 (1898). (↑ p. 27)

[264] Fields, B. N. & Knipe, D. M. *Fields virology*. Wolters Kluwer, Lippincott Williams & Wilkins, Philadelphia, Pa. [u.a.], 6. ed edition, (2013). (↑ p. 27)

[265] Wilson, A. C. & Mohr, I. A cultured affair: HSV latency and reactivation in neurons. *Trends in microbiology* **20**(12), 604–611 (2012). (↑ pp. 27 and 29)

[266] Nicoll, M. P., Proença, J. T., & Efstathiou, S. The molecular basis of herpes simplex virus latency. *FEMS microbiology reviews* **36**(3), 684–705 (2012). (↑ pp. 27 and 29)

[267] Whittaker, G. R. Virus nuclear import. *Advanced drug delivery reviews* **55**(6), 733–747 (2003). (↑ p. 27)

[268] Simmons, R. A., Willberg, C. B., & Paul, K. Immune Evasion by Viruses. *eLS* , 1–10 (2013). (↑ pp. 28, 29, and 32)

[269] Cuchet-Lourenço, D., Anderson, G., Sloan, E., Orr, A., & Everett, R. D. The viral ubiquitin ligase ICP0 is neither sufficient nor necessary for degradation of the cellular DNA sensor IFI16 during herpes simplex virus 1 infection. *Journal of virology* **87**(24), 13422–13432 (2013). (↑ p. 28)

[270] Orzalli, M. H., DeLuca, N. A., & Knipe, D. M. Nuclear IFI16 induction of IRF-3 signaling during herpesviral infection and degradation of IFI16 by the viral ICP0 protein. *Proceedings of the National Academy of Sciences of the United States of America* **109**(44), E3008–17 (2012). (↑ p. 28)

[271] Paladino, P. & Mossman, K. L. Mechanisms employed by herpes simplex virus 1 to inhibit the interferon response. *Journal of interferon & cytokine research : the official journal of the International Society for Interferon and Cytokine Research* **29**(9), 599–607 (2009). (↑ p. 28)

[272] Ma, Z., Jacobs, S. R., West, J. A., *et al.* Modulation of the cGAS-STING DNA sensing pathway by gammaherpesviruses. *Proceedings of the National Academy*

of Sciences of the United States of America **112**(31), E4306–15 (2015). (↑ p. 28)

[273] Hwang, K. Y. & Choi, Y. B. Modulation of Mitochondrial Antiviral Signaling by Human Herpesvirus 8 Interferon Regulatory Factor 1. *Journal of virology* **90**(1), 506–520 (2016). (↑ p. 28)

[274] Zhang, G., Chan, B., Samarina, N., *et al.* Cytoplasmic isoforms of Kaposi sarcoma herpesvirus LANA recruit and antagonize the innate immune DNA sensor cGAS. *Proceedings of the National Academy of Sciences of the United States of America* **113**(8), E1034–43 (2016). (↑ p. 28)

[275] Wu, J.-j., Li, W., Shao, Y., *et al.* Inhibition of cGAS DNA Sensing by a Herpesvirus Virion Protein. *Cell host & microbe* **18**(3), 333–344 (2015). (↑ p. 28)

[276] Li, X.-D., Sun, L., Seth, R. B., Pineda, G., & Chen, Z. J. Hepatitis C virus protease NS3/4A cleaves mitochondrial antiviral signaling protein off the mitochondria to evade innate immunity. *Proceedings of the National Academy of Sciences of the United States of America* **102**(49), 17717–17722 (2005). (↑ p. 28)

[277] Li, K., Foy, E., Ferreon, J. C., *et al.* Immune evasion by hepatitis C virus NS3/4A protease-mediated cleavage of the Toll-like receptor 3 adaptor protein TRIF. *Proceedings of the National Academy of Sciences of the United States of America* **102**(8), 2992–2997 (2005). (↑ p. 28)

[278] Nitta, S., Sakamoto, N., Nakagawa, M., *et al.* Hepatitis C virus NS4B protein targets STING and abrogates RIG-I-mediated type I interferon-dependent innate immunity. *Hepatology (Baltimore, Md.)* **57**(1), 46–58 (2013). (↑ p. 28)

[279] Tasaka, M., Sakamoto, N., Itakura, Y., *et al.* Hepatitis C virus non-structural proteins responsible for suppression of the RIG-I/Cardif-induced interferon response. *The Journal of general virology* **88**(Pt 12), 3323–3333 (2007). (↑ p. 28)

[280] Kuo, R.-L., Zhao, C., Malur, M., & Krug, R. M. Influenza A virus strains that circulate in humans differ in the ability of their NS1 proteins to block the activation of IRF3 and interferon-β transcription. *Virology* **408**(2), 146–158 (2010). (↑ p. 28)

[281] Gack, M. U., Albrecht, R. A., Urano, T., *et al.* Influenza A virus NS1 targets the ubiquitin ligase TRIM25 to evade recognition by the host viral RNA sensor RIG-I. *Cell host & microbe* **5**(5), 439–449 (2009). (↑ p. 28)

[282] Kuo, R.-L., Li, L.-H., Lin, S.-J., *et al.* Role of N Terminus-Truncated NS1 Proteins of Influenza A Virus in Inhibiting IRF3 Activation. *Journal of virology* **90**(9), 4696–4705 (2016). (↑ p. 28)

[283] Nemeroff, M. E., Barabino, S. M., Li, Y., Keller, W., & Krug, R. M. Influenza Virus NS1 Protein Interacts with the Cellular 30 kDa Subunit of CPSF and Inhibits 3'End Formation of Cellular Pre-mRNAs. *Molecular cell* (1), 991–1000 (1998). (↑ p. 29)

[284] Noah, D. L., Twu, K. Y., & Krug, R. M. Cellular antiviral responses against influenza A virus are countered at the posttranscriptional level by the viral NS1A protein via its binding to a cellular protein required for the 3′ end processing of cellular pre-mRNAS. *Virology* **307**(2), 386–395 (2003). (↑ p. 29)

[285] Pauli, E.-K., Schmolke, M., Wolff, T., *et al.* Influenza A virus inhibits type I IFN signaling via NF-kappaB-dependent induction of SOCS-3 expression. *PLoS pathogens* **4**(11), e1000196 (2008). (↑ p. 29)

[286] Barro, M. & Patton, J. T. Rotavirus NSP1 inhibits expression of type I interferon by antagonizing the function of interferon regulatory factors IRF3, IRF5, and IRF7. *Journal of virology* **81**(9), 4473–4481 (2007). (↑ p. 29)

[287] Arnold, M. M., Barro, M., & Patton, J. T. Rotavirus NSP1 mediates degradation of interferon regulatory factors through targeting of the dimerization domain. *Journal of virology* **87**(17), 9813–9821 (2013). (↑ p. 29)

[288] Sanchez-Tacuba, L., Rojas, M., Arias, C. F., & Lopez, S. Rotavirus Controls Activation of the 2'-5'-Oligoadenylate Synthetase/RNase L Pathway Using at Least Two Distinct Mechanisms. *Journal of virology* **89**(23), 12145–12153 (2015). (↑ p. 29)

[289] Gonatopoulos-Pournatzis, T. & Cowling, V. H. Cap-binding complex (CBC). *The Biochemical journal* **457**(2), 231–242 (2014). (↑ p. 29)

[290] Walsh, D., Mathews, M. B., & Mohr, I. Tinkering with translation: protein synthesis in virus-infected cells. *Cold Spring Harbor perspectives in biology* **5**(1), a012351 (2013). (↑ pp. 29 and 30)

[291] Decroly, E., Ferron, F., Lescar, J., & Canard, B. Conventional and unconventional mechanisms for capping viral mRNA. *Nature reviews. Microbiology* **10**(1), 51–65 (2012). (↑ p. 29)

[292] Hopkins, K. C., McLane, L. M., Maqbool, T., *et al.* A genome-wide RNAi screen reveals that mRNA decapping restricts bunyaviral replication by limiting the pools of Dcp2-accessible targets for cap-snatching. *Genes & development* **27**(13), 1511–1525 (2013). (↑ p. 29)

[293] Plotch, S. J., Bouloy, M., Ulmanen, I., & Krug, R. M. A unique cap(m7GpppXm)-dependent influenza virion endonuclease cleaves capped RNAs to generate the primers that initiate viral RNA transcription. *Cell* **23**(3), 847–858 (1981). (↑ p. 29)

[294] Guilligay, D., Tarendeau, F., Resa-Infante, P., *et al.* The structural basis for cap binding by influenza

virus polymerase subunit PB2. *Nature structural & molecular biology* **15**(5), 500–506 (2008). (↑ p. 29)

[295] Fujimura, T. & Esteban, R. Cap-snatching mechanism in yeast L-A double-stranded RNA virus. *Proceedings of the National Academy of Sciences of the United States of America* **108**(43), 17667–17671 (2011). (↑ p. 29)

[296] Venkatesan, S., Gershowitz, A., & Moss, B. Modification of the 5' end of mRNA. Association of RNA triphosphatase with the RNA guanylyltransferase-RNA (guanine-7-)methyltransferase complex from vaccinia virus. *The Journal of biological chemistry* **255**(3), 903–908 (1980). (↑ p. 29)

[297] Barik, S. The structure of the 5' terminal cap of the respiratory syncytial virus mRNA. *The Journal of general virology* **74 (Pt 3)**, 485–490 (1993). (↑ p. 29)

[298] Neubauer, J., Ogino, M., Green, T. J., & Ogino, T. Signature motifs of GDP polyribonucleotidyltransferase, a non-segmented negative strand RNA viral mRNA capping enzyme, domain in the L protein are required for covalent enzyme-pRNA intermediate formation. *Nucleic acids research* **44**(1), 330–341 (2016).

[299] Zhao, Y., Soh, T. S., Lim, S. P., *et al.* Molecular basis for specific viral RNA recognition and 2'-O-ribose methylation by the dengue virus nonstructural protein 5 (NS5). *Proceedings of the National Academy of Sciences of the United States of America* **112**(48), 14834–14839 (2015). (↑ p. 29)

[300] Colonno, R. J. & Stone, H. O. Newcastle disease virus mRNA lacks 2'-O-methylated nucleotides. *Nature* **261**(5561), 611–614 (1976). (↑ p. 29)

[301] Siliciano, R. F. & Greene, W. C. HIV latency. *Cold Spring Harbor perspectives in medicine* **1**(1), a007096 (2011). (↑ p. 29)

[302] Walsh, D. & Mohr, I. Viral subversion of the host protein synthesis machinery. *Nature reviews. Microbiology* **9**(12), 860–875 (2011). (↑ p. 30)

[303] Thompson, S. R. Tricks an IRES uses to enslave ribosomes. *Trends in microbiology* **20**(11), 558–566 (2012). (↑ p. 30)

[304] Lewis, S. M. & Holcik, M. For IRES trans-acting factors, it is all about location. *Oncogene* **27**(8), 1033–1035 (2008). (↑ p. 30)

[305] Komar, A. A. & Hatzoglou, M. Cellular IRES-mediated translation: the war of ITAFs in pathophysiological states. *Cell cycle (Georgetown, Tex.)* **10**(2), 229–240 (2011). (↑ p. 30)

[306] Hellen CU, Sarnow P. Internal ribosome entry sites in eukaryotic ll. *Genes & development* (15), 1593–1612 (2001). (↑ p. 30)

[307] Jiang, H., Schwertz, H., Schmid, D. I., *et al.* Different mechanisms preserve translation of programmed cell death 8 and JunB in virus-infected endothelial cells. *Arteriosclerosis, thrombosis, and vascular biology* **32**(4), 997–1004 (2012). (↑ p. 30)

[308] Kieft, J. S., Zhou, K., Jubin, R., & Doudna, J. A. Mechanism of ribosome recruitment by hepatitis C IRES RNA. *RNA (New York, N.Y.)* **7**(2), 194–206 (2001). (↑ p. 30)

[309] Flanegan, J. B., Petterson, R. F., Ambros, V., Hewlett, N. J., & Baltimore, D. Covalent linkage of a protein to a defined nucleotide sequence at the 5'-terminus of virion and replicative intermediate RNAs of poliovirus. *Proceedings of the National Academy of Sciences of the United States of America* **74**(3), 961–965 (1977). (↑ p. 30)

[310] Lee, Y. F., Nomoto, A., Detjen, B. M., & Wimmer, E. A protein covalently linked to poliovirus genome RNA. *Proceedings of the National Academy of Sciences of the United States of America* **74**(1), 59–63 (1977).

[311] Daughenbaugh, K. F., Fraser, C. S., Hershey, John W B, & Hardy, M. E. The genome-linked protein VPg of the Norwalk virus binds eIF3, suggesting its role in translation initiation complex recruitment. *The EMBO journal* **22**(11), 2852–2859 (2003). (↑ p. 30)

[312] Maldonado, E., Cabrejos, M. E., Banks, L., & Allende, J. E. Human papillomavirus-16 E7 protein inhibits the DNA interaction of the TATA binding transcription factor. *Journal of cellular biochemistry* **85**(4), 663–669 (2002). (↑ p. 30)

[313] Kundu, P., Raychaudhuri, S., Tsai, W., & Dasgupta, A. Shutoff of RNA polymerase II transcription by poliovirus involves 3C protease-mediated cleavage of the TATA-binding protein at an alternative site: incomplete shutoff of transcription interferes with efficient viral replication. *Journal of virology* **79**(15), 9702–9713 (2005). (↑ p. 30)

[314] Fraser, K. A. & Rice, S. A. Herpes simplex virus immediate-early protein ICP22 triggers loss of serine 2-phosphorylated RNA polymerase II. *Journal of virology* **81**(10), 5091–5101 (2007). (↑ p. 30)

[315] Khaperskyy, D. A., Schmaling, S., Larkins-Ford, J., McCormick, C., & Gaglia, M. M. Selective Degradation of Host RNA Polymerase II Transcripts by Influenza A Virus PA-X Host Shutoff Protein. *PLoS pathogens* **12**(2), e1005427 (2016). (↑ p. 30)

[316] Qiu, Y. & Krug, R. M. The influenza virus NS1 protein is a poly(A)-binding protein that inhibits nuclear export of mRNAs containing poly(A). *Journal of virology* **68**(4), 2425–2432 (1994). (↑ p. 30)

[317] Hardy, W. R. & Sandri-Goldin, R. M. Herpes simplex virus inhibits host cell splicing, and regulatory protein ICP27 is required for this effect. *Journal of virology* **68**(12), 7790–7799 (1994). (↑ p. 30)

[318] Bryant, H. E., Wadd, S. E., Lamond, A. I., Silverstein, S. J., & Clements, J. B. Herpes simplex virus IE63 (ICP27) protein interacts with spliceosome-associated protein 145 and inhibits splicing prior to the first catalytic step. *Journal of virology* **75**(9), 4376–4385 (2001). (↑ p. 30)

[319] Ahmad, H., Gubbels, R., Ehlers, E., *et al.* Kaposi sarcoma-associated herpesvirus degrades cellular Toll-interleukin-1 receptor domain-containing adaptor-inducing beta-interferon (TRIF). *The Journal of biological chemistry* **286**(10), 7865–7872 (2011). (↑ p. 31)

[320] Chavoshi, S., Egorova, O., Lacdao, I. K., *et al.* Identification of Kaposi Sarcoma Herpesvirus (KSHV) vIRF1 Protein as a Novel Interaction Partner of Human Deubiquitinase USP7. *The Journal of biological chemistry* **291**(12), 6281–6291 (2016). (↑ p. 31)

[321] Baresova, P., Musilova, J., Pitha, P. M., & Lubyova, B. p53 tumor suppressor protein stability and transcriptional activity are targeted by Kaposi's sarcoma-associated herpesvirus-encoded viral interferon regulatory factor 3. *Molecular and cellular biology* **34**(3), 386–399 (2014). (↑ p. 31)

[322] Komaravelli, N., Tian, B., Ivanciuc, T., *et al.* Respiratory syncytial virus infection down-regulates antioxidant enzyme expression by triggering deacetylation-proteasomal degradation of Nrf2. *Free radical biology & medicine* **88**(Pt B), 391–403 (2015). (↑ pp. 31, 110, and 111)

[323] Dhar, J., Cuevas, R. A., Goswami, R., *et al.* 2'-5'-Oligoadenylate Synthetase-Like Protein Inhibits Respiratory Syncytial Virus Replication and Is Targeted by the Viral Nonstructural Protein 1. *Journal of virology* **89**(19), 10115–10119 (2015). (↑ p. 31)

[324] Labbé, K. & Saleh, M. Cell death in the host response to infection. *Cell death and differentiation* **15**(9), 1339–1349 (2008). (↑ p. 31)

[325] Fadok, V. A., Voelker, D. R., Campbell, P. A., *et al.* Exposure of phosphatidylserine on the surface of apoptotic lymphocytes triggers specific recognition and removal by macrophages. *Journal of immunology (Baltimore, Md. : 1950)* **148**(7), 2207–2216 (1992). (↑ p. 31)

[326] Kaminskyy, V. & Zhivotovsky, B. To kill or be killed: how viruses interact with the cell death machinery. *Journal of internal medicine* **267**(5), 473–482 (2010). (↑ p. 31)

[327] Mocarski, E. S., Guo, H., & Kaiser, W. J. Necroptosis: The Trojan horse in cell autonomous antiviral host defense. *Virology* **479-480**, 160–166 (2015). (↑ p. 32)

[328] Cuconati A & White E. Viral homologs of BCL-2: role of apoptosis in the regulation of virus infection. *Genes & development* (16), 2465–2478 (2002). (↑ p. 31)

[329] Galluzzi, L., Brenner, C., Morselli, E., Touat, Z., & Kroemer, G. Viral control of mitochondrial apoptosis. *PLoS pathogens* **4**(5), e1000018 (2008). (↑ pp. 31 and 32)

[330] Liu, L., Eby, M. T., Rathore, N., *et al.* The human herpes virus 8-encoded viral FLICE inhibitory protein physically associates with and persistently activates the Ikappa B kinase complex. *The Journal of biological chemistry* **277**(16), 13745–13751 (2002). (↑ p. 31)

[331] Sun, Q., Matta, H., & Chaudhary, P. M. The human herpes virus 8-encoded viral FLICE inhibitory protein protects against growth factor withdrawal-induced apoptosis via NF-kappa B activation. *Blood* **101**(5), 1956–1961 (2003).

[332] An J & Sun Y, Sun R, Rettig MB. Kaposi's sarcoma-associated herpesvirus encoded vFLIP induces cellular IL-6 expression: the role of the NF-kB and JNK/AP1 pathways. *Oncogene* (22), 3371–3385 (2003). (↑ p. 31)

[333] Huang, Z., Wu, S.-Q., Liang, Y., *et al.* RIP1/RIP3 binding to HSV-1 ICP6 initiates necroptosis to restrict virus propagation in mice. *Cell host & microbe* **17**(2), 229–242 (2015). (↑ p. 31)

[334] Reshi, M. L., Su, Y.-C., & Hong, J.-R. RNA Viruses: ROS-Mediated Cell Death. *International journal of cell biology* **2014**, 467452 (2014). (↑ p. 31)

[335] Olagnier, D., Peri, S., Steel, C., *et al.* Cellular oxidative stress response controls the antiviral and apoptotic programs in dengue virus-infected dendritic cells. *PLoS pathogens* **10**(12), e1004566 (2014). (↑ pp. 31 and 111)

[336] Lin, X., Wang, R., Zou, W., *et al.* The Influenza Virus H5N1 Infection Can Induce ROS Production for Viral Replication and Host Cell Death in A549 Cells Modulated by Human Cu/Zn Superoxide Dismutase (SOD1) Overexpression. *Viruses* **8**(1) (2016). (↑ pp. 31, 110, and 111)

[337] Larrubia, J. R., Lokhande, M. U., Garcia-Garzon, S., *et al.* Role of T cell death in maintaining immune tolerance during persistent viral hepatitis. *World journal of gastroenterology* **19**(12), 1877–1889 (2013). (↑ p. 31)

[338] James, P. Protein identification in the post-genome era: the rapid rise of proteomics. *Quarterly reviews of biophysics* **30**(4), 279–331 (1997). (↑ p. 33)

[339] Nagaraj, N., Wisniewski, J. R., Geiger, T., *et al.* Deep proteome and transcriptome mapping of a human cancer cell line. *Molecular systems biology* **7**, 548 (2011). (↑ p. 33)

[340] Beck, M., Schmidt, A., Malmstroem, J., *et al.* The quantitative proteome of a human cell line. *Molecular systems biology* **7**, 549 (2011).

[341] Kim, M.-S., Pinto, S. M., Getnet, D., *et al.* A draft map of the human proteome. *Nature* **509**(7502), 575–581 (2014).

[342] Wilhelm, M., Schlegl, J., Hahne, H., *et al.* Mass-spectrometry-based draft of the human proteome. *Nature* **509**(7502), 582–587 (2014). (↑ p. 33)

[343] Hein, M. Y., Hubner, N. C., Poser, I., *et al.* A human interactome in three quantitative dimensions organized by stoichiometries and abundances. *Cell* **163**(3), 712–723 (2015). (↑ p. 33)

[344] Sharma, K., D'Souza, Rochelle C J, Tyanova, S., *et al.* Ultradeep human phosphoproteome reveals a distinct regulatory nature of Tyr and Ser/Thr-based signaling. *Cell reports* **8**(5), 1583–1594 (2014). (↑ p. 33)

[345] Ong, S.-E., Mittler, G., & Mann, M. Identifying and quantifying in vivo methylation sites by heavy methyl SILAC. *Nature methods* **1**(2), 119–126 (2004). (↑ p. 39)

[346] Geoghegan, V., Guo, A., Trudgian, D., Thomas, B., & Acuto, O. Comprehensive identification of arginine methylation in primary T cells reveals regulatory roles in cell signalling. *Nature communications* **6**, 6758 (2015).

[347] Carlson, S. M., Moore, K. E., Green, E. M., Martín, G. M., & Gozani, O. Proteome-wide enrichment of proteins modified by lysine methylation. *Nature protocols* **9**(1), 37–50 (2014). (↑ p. 33)

[348] Aebersold, R. & Mann, M. Mass spectrometry-based proteomics. *Nature* **422**(6928), 198–207 (2003). (↑ p. 34)

[349] Karas, M., Bachmann, D., & Hillenkamp, F. Influence of the Wavelength in High-Irradiance Ultraviolet Laser Desorption Mass Spectrometry of Organic Molecules. *Analytical Chemistry* (57), 2935–2939 (1985). (↑ p. 34)

[350] Karas, M. & Hillenkamp, F. Laser Desorption Ionization of Proteins with Molecular Masses Exceeding 10 000 Daltons. *Analytical Chemistry* (60), 2299–2301 (1988).

[351] Tanaka, N., Waki, A., Ido, Y., *et al.* Protein and polymer analyses up to m/z 100 000 by laser ionization time-of-flight mass spectrometry. *Rapid Communications in Mass spectrometry* (2), 151–153 (1988). (↑ p. 34)

[352] Fenn, J. B., Mann, M., Meng, C. K., Wong, S. F., & Whitehouse, C. M. Electrospray Ionization for Mass Spectrometry of Large Biomolecules. *Science (New York, N.Y.)* (246), 64–71 (1989). (↑ p. 34)

[353] Nobelprize.org. The Nobel Prize in Chemistry 2002, (Web. 27 Apr 2016). (↑ p. 34)

[354] Parker, C. E., Warren, M. R., & Mocanu, V. Frontiers in Neuroscience: Mass Spectrometry for Proteomics: Neuroproteomics. In *Frontiers in Neuroscience,* Alzate, O., editor. (2010). (↑ p. 35)

[355] Makarov, A., Denisov, E., Lange, O., & Horning, S. Dynamic range of mass accuracy in LTQ Orbitrap hybrid mass spectrometer. *Journal of the American Society for Mass Spectrometry* **17**(7), 977–982 (2006). (↑ pp. 35 and 36)

[356] Hu, Q., Noll, R. J., Li, H., *et al.* The Orbitrap: a new mass spectrometer. *Journal of mass spectrometry : JMS* **40**(4), 430–443 (2005). (↑ p. 35)

[357] Olsen, J. V., de Godoy, Lyris M F, Li, G., *et al.* Parts per million mass accuracy on an Orbitrap mass spectrometer via lock mass injection into a C-trap. *Molecular & cellular proteomics : MCP* **4**(12), 2010–2021 (2005). (↑ p. 35)

[358] Wells, J. M. & McLuckey, S. A. Collision–Induced Dissociation (CID) of Peptides and Proteins. In *Biological Mass Spectrometry*, volume 402 of *Methods in Enzymology*, 148–185. Elsevier (2005). (↑ p. 35)

[359] Olsen, J. V., Macek, B., Lange, O., *et al.* Higher-energy C-trap dissociation for peptide modification analysis. *Nature methods* **4**(9), 709–712 (2007). (↑ p. 35)

[360] Syka JE, Coon JJ, Schroeder MJ, Shabanowitz J, & Hunt DF. Peptide and protein sequence analysis by electron transfer dissociation mass spectrometry. *Proceedings of the National Academy of Sciences of the United States of America* (101), 9528–9533 (2004). (↑ p. 39)

[361] Frese, C. K., Zhou, H., Taus, T., *et al.* Unambiguous phosphosite localization using electron-transfer/higher-energy collision dissociation (EThcD). *Journal of proteome research* **12**(3), 1520–1525 (2013). (↑ pp. 35 and 39)

[362] Kumar, C. & Mann, M. Bioinformatics analysis of mass spectrometry-based proteomics data sets. *FEBS letters* **583**(11), 1703–1712 (2009). (↑ p. 36)

[363] Ong SE, Blagoev B, Kratchmarova I, Kristensen DB, Steen H, Pandey A, Mann M. Stable Isotope Labeling by Amino Acids in Cell Culture, SILAC, as a Simple and Accurate Approach to Expression Proteomics*. *Molecular & cellular proteomics : MCP* (1), 376–386 (2002). (↑ p. 36)

[364] Liu, H., Sadygov, R. G., & Yates, J. R. A model for random sampling and estimation of relative protein abundance in shotgun proteomics. *Analytical chemistry* **76**(14), 4193–4201 (2004). (↑ p. 36)

[365] Bondarenko, P. V., Chelius, D., & Shaler, T. A. Identification and Relative Quantitation of Protein Mixtures by Enzymatic Digestion Followed by Capillary Reversed-Phase Liquid Chromatography–Tandem Mass Spectrometry. *Analytical Chemistry* **74**(18), 4741–4749 (2002). (↑ p. 36)

[366] Cox, J., Hein, M. Y., Luber, C. A., *et al.* Accurate proteome-wide label-free quantification by delayed normalization and maximal peptide ratio extraction, termed MaxLFQ. *Molecular & cellular proteomics : MCP* **13**(9), 2513–2526 (2014). (↑ p. 36)

[367] Shen, Y., Zhao, R., Berger, S. J., *et al.* High-Efficiency Nanoscale Liquid Chromatography Coupled On-Line with Mass Spectrometry Using Nanoelectrospray Ionization for Proteomics. *Analytical Chemistry* **74**(16), 4235–4249 (2002). (↑ p. 36)

[368] Fields, S. & Song, O. A novel genetic system to detect protein-protein interactions. *Nature* **340**(6230), 245–246 (1989). (↑ p. 36)

[369] Rajagopala, S. V., Sikorski, P., Caufield, J. H., Tovchigrechko, A., & Uetz, P. Studying protein complexes by the yeast two-hybrid system. *Methods (San Diego, Calif.)* **58**(4), 392–399 (2012). (↑ p. 36)

[370] Smith, G. P. Filamentous Fusion Phage: Novel Expression Vectors That Display Cloned Antigens on the Virion Surface. *Science Translational Medicine* (228), 1315–1317 (1985). (↑ p. 36)

[371] Masters, S. C. Co-Immunoprecipitation from Transfected Cells. *Methods in molecular biology (Clifton, N.J.)* (261), 337–348 (2004). (↑ p. 36)

[372] Dunham, W. H., Mullin, M., & Gingras, A.-C. Affinity-purification coupled to mass spectrometry: basic principles and strategies. *Proteomics* **12**(10), 1576–1590 (2012). (↑ p. 36)

[373] Keilhauer, E. C., Hein, M. Y., & Mann, M. Accurate protein complex retrieval by affinity enrichment mass spectrometry (AE-MS) rather than affinity purification mass spectrometry (AP-MS). *Molecular & cellular proteomics : MCP* **14**(1), 120–135 (2015). (↑ p. 36)

[374] Vuckovic, D., Dagley, L. F., Purcell, A. W., & Emili, A. Membrane proteomics by high performance liquid chromatography-tandem mass spectrometry: Analytical approaches and challenges. *Proteomics* **13**(3-4), 404–423 (2013). (↑ p. 37)

[375] Berggård, T., Linse, S., & James, P. Methods for the detection and analysis of protein-protein interactions. *Proteomics* **7**(16), 2833–2842 (2007). (↑ p. 37)

[376] Li, Y. The tandem affinity purification technology: an overview. *Biotechnology letters* **33**(8), 1487–1499 (2011). (↑ p. 37)

[377] Bauch, A. & Superti-Furga, G. Charting protein complexes, signaling pathways, and networks in the immune system. *Immunological reviews* (210), 187–207 (2006). (↑ p. 37)

[378] Mellacheruvu, D., Wright, Z., Couzens, A. L., *et al.* The CRAPome: a contaminant repository for affinity purification-mass spectrometry data. *Nature methods* **10**(8), 730–736 (2013). (↑ p. 38)

[379] Walsh, C. *Posttranslational modification of proteins: Expanding nature's inventory*. Roberts and Co. Publishers, Englewood, Colo., (2006). (↑ p. 38)

[380] Khoury, G. A., Baliban, R. C., & Floudas, C. A. Proteome-wide post-translational modification statistics: frequency analysis and curation of the swiss-prot database. *Scientific reports* **1** (2011). (↑ p. 38)

[381] Fischer, E. H. & Krebs, E. G. Conversion of Phosphorylase b to phosphorylase a in muscle extracts. *Journal of biological chemistry* (216), 121–132 (1955). (↑ p. 38)

[382] Hanks, S. K., Quinn, A. M., & Hunter, T. The Protein Kinase Family: Conserved Features and Deduced Phylogeny of the Catalytic Domains. *Science (New York, N.Y.)* (241), 42–52 (1988). (↑ p. 38)

[383] Heissmeyer, V., Krappmann, D., Wulczyn, F. G., & Scheidereit, C. NF-kappaB p105 is a target of IkappaB kinases and controls signal induction of Bcl-3-p50 complexes. *The EMBO journal* **18**(17), 4766–4778 (1999). (↑ p. 38)

[384] Shuai, K., Ziemiecki, A., Wilks, A. F., *et al.* Polypeptide signalling to the nucleus through tyrosine phosphorylation of Jak and Stat proteins. *Nature* **366**(6455), 580–583 (1993). (↑ p. 38)

[385] Beadling, C., Guschin, D., Witthuhn, B. A., *et al.* Activation of JAK kinases and STAT proteins by interleukin-2 and interferon alpha, but not the T cell antigen receptor, in human T lymphocytes. *The EMBO journal* **13**(23), 5605–5615 (1994). (↑ p. 38)

[386] Chan, L. C., Karhi, K. K., Rayter, S. I., *et al.* A novel abl protein expressed in Philadelphia chromosome positive acute lymphoblastic leukaemia. *Nature* **325**(6105), 635–637 (1987). (↑ p. 38)

[387] Raggiaschi, R., Gotta, S., & Terstappen, G. C. Phosphoproteome analysis. *Bioscience reports* **25**(1-2), 33–44 (2005). (↑ p. 38)

[388] Mann, M., Ong, S. E., Gronborg, M., *et al.* Analysis of protein phosphorylation using mass spectrometry: deciphering the phosphoproteome. *Trends in biotechnology* **20**(6), 261–268 (2002). (↑ p. 38)

[389] Boersema, P. J., Mohammed, S., & Heck, Albert J R. Phosphopeptide fragmentation and analysis by mass spectrometry. *Journal of mass spectrometry : JMS* **44**(6), 861–878 (2009). (↑ p. 38)

[390] Kim, S. C., Sprung, R., Chen, Y., *et al.* Substrate and functional diversity of lysine acetylation revealed by a proteomics survey. *Molecular cell* **23**(4), 607–618 (2006). (↑ p. 39)

[391] Ross, A. H., Baltimore, D., & Eisen, H. N. Phosphotyrosine-containing proteins isolated by affinity chromatography with antibodies to a synthetic hapten. *Nature* **294**(5842), 654–656 (1981). (↑ p. 39)

[392] Cummings, R. D. & Kornfeld, S. Fractionation of asparagine-linked oligosaccharides by serial lectin-Agarose affinity chromatography. A rapid, sensitive, and specific technique. *The Journal of biological chemistry* **257**(19), 11235–11240 (1982). (↑ p. 39)

[393] Machida, K., Mayer, B. J., & Nollau, P. Profiling the global tyrosine phosphorylation state. *Molecular & cellular proteomics : MCP* **2**(4), 215–233 (2003). (↑ p. 39)

[394] Pinkse, Martijn W H, Uitto, P. M., Hilhorst, M. J., Ooms, B., & Heck, Albert J R. Selective isolation at the femtomole level of phosphopeptides from proteolytic digests using 2D-NanoLC-ESI-MS/MS and titanium oxide precolumns. *Analytical chemistry* **76**(14), 3935–3943 (2004). (↑ p. 39)

[395] Eberle, C.-A., Zayas, M., Stukalov, A., *et al.* The lysine methyltransferase SMYD3 interacts with hepatitis C virus NS5A and is a negative regulator of viral particle production. *Virology* **462-463**, 34–41 (2014). (↑ p. 41)

[396] Xu, W., Edwards, M. R., Borek, D. M., *et al.* Ebola virus VP24 targets a unique NLS binding site on karyopherin alpha 5 to selectively compete with nuclear import of phosphorylated STAT1. *Cell host & microbe* **16**(2), 187–200 (2014).

[397] Edwards, M. R., Johnson, B., Mire, C. E., *et al.* The Marburg virus VP24 protein interacts with Keap1 to activate the cytoprotective antioxidant response pathway. *Cell reports* **6**(6), 1017–1025 (2014).

[398] Kainulainen, M., Habjan, M., Hubel, P., *et al.* Virulence factor NSs of rift valley fever virus recruits the F-box protein FBXO3 to degrade subunit p62 of general transcription factor TFIIH. *Journal of virology* **88**(6), 3464–3473 (2014).

[399] Luthra, P., Jordan, D. S., Leung, D. W., Amarasinghe, G. K., & Basler, C. F. Ebola virus VP35 interaction with dynein LC8 regulates viral RNA synthesis. *Journal of virology* **89**(9), 5148–5153 (2015). (↑ p. 41)

[400] Daffis, S., Szretter, K. J., Schriewer, J., *et al.* 2'-O methylation of the viral mRNA cap evades host restriction by IFIT family members. *Nature* **468**(7322), 452–456 (2010). (↑ p. 94)

[401] Craik, D. J., Fairlie, D. P., Liras, S., & Price, D. The future of peptide-based drugs. *Chemical biology & drug design* **81**(1), 136–147 (2013). (↑ p. 109)

[402] Fosgerau, K. & Hoffmann, T. Peptide therapeutics: current status and future directions. *Drug discovery today* **20**(1), 122–128 (2015). (↑ p. 109)

[403] Herzog, F., Kahraman, A., Boehringer, D., *et al.* Structural probing of a protein phosphatase 2A network by chemical cross-linking and mass spectrometry. *Science (New York, N.Y.)* **337**(6100), 1348–1352 (2012). (↑ p. 110)

[404] Kao, A., Randall, A., Yang, Y., *et al.* Mapping the structural topology of the yeast 19S proteasomal regulatory particle using chemical cross-linking and probabilistic modeling. *Molecular & cellular proteomics : MCP* **11**(12), 1566–1577 (2012). (↑ p. 110)

[405] Soderblom, E. J. & Goshe, M. B. Collision-induced dissociative chemical cross-linking reagents and methodology: Applications to protein structural characterization using tandem mass spectrometry analysis. *Analytical chemistry* **78**(23), 8059–8068 (2006). (↑ p. 110)

[406] Zybailov, B., Gokulan, K., Wiese, J., *et al.* Analysis of Protein-protein Interaction Interface between Yeast Mitochondrial Proteins Rim1 and Pif1 Using Chemical Cross-linking Mass Spectrometry. *Journal of proteomics & bioinformatics* **8**(11), 243–252 (2015). (↑ p. 110)

[407] Larance, M., Kirkwood, K. J., Tinti, M., *et al.* Global Membrane Protein Interactome Analysis using In vivo Crosslinking and MS-based Protein Correlation Profiling. *Molecular & cellular proteomics : MCP* (2016). (↑ p. 110)

[408] Roux, K. J., Kim, D. I., Raida, M., & Burke, B. A promiscuous biotin ligase fusion protein identifies proximal and interacting proteins in mammalian cells. *The Journal of cell biology* **196**(6), 801–810 (2012). (↑ p. 110)

[409] Andersen, J. S., Wilkinson, C. J., Mayor, T., *et al.* Proteomic characterization of the human centrosome by protein correlation profiling. *Nature* **426**(6966), 570–574 (2003). (↑ p. 110)

[410] Kristensen, A. R. & Foster, L. J. Protein correlation profiling-SILAC to study protein-protein interactions. *Methods in molecular biology (Clifton, N.J.)* **1188**, 263–270 (2014). (↑ p. 110)

[411] Le-Trilling, V T K & Trilling, M. Attack, parry and riposte: molecular fencing between the innate immune system and human herpesviruses. *Tissue antigens* **86**(1), 1–13 (2015). (↑ p. 110)

[412] Reshi, L., Wu, J.-L., Wang, H.-V., & Hong, J.-R. Aquatic viruses induce host cell death pathways and its application. *Virus research* **211**, 133–144 (2016). (↑ p. 110)

[413] Tsukiyama-Kohara, K. Role of oxidative stress in hepatocarcinogenesis induced by hepatitis C virus. *International journal of molecular sciences* **13**(11), 15271–15278 (2012). (↑ p. 110)

[414] Hosakote, Y. M., Jantzi, P. D., Esham, D. L., *et al.* Viral-mediated inhibition of antioxidant enzymes contributes to the pathogenesis of severe respiratory syncytial virus bronchiolitis. *American journal of respiratory and critical care medicine* **183**(11), 1550–1560 (2011). (↑ p. 110)

[415] Nioi, P., McMahon, M., Itoh, K., Yamamoto, M., & Hayes, J. D. Identification of a novel Nrf2-regulated antioxidant response element (ARE) in the mouse NAD(P)H:quinone oxidoreductase 1 gene: reassessment of the ARE consensus sequence. *The Biochemical journal* **374**(Pt 2), 337–348 (2003). (↑ p. 110)

[416] Inamdar, N. M., Ahn, Y. I., & Alam, J. The heme-responsive element of the mouse heme oxygenase-1 gene is an extended AP-1 binding site that resembles the recognition sequences for MAF and NF-E2 transcription factors. *Biochemical and biophysical research communications* **221**(3), 570–576 (1996).

[417] Gorrini, C., Harris, I. S., & Mak, T. W. Modulation of oxidative stress as an anticancer strategy. *Nature reviews. Drug discovery* **12**(12), 931–947 (2013). (↑ p. 110)

[418] Cho, H.-Y., Imani, F., Miller-DeGraff, L., *et al.* Antiviral activity of Nrf2 in a murine model of respiratory syncytial virus disease. *American journal of respiratory and critical care medicine* **179**(2), 138–150 (2009). (↑ p. 110)

[419] Furuya, Andrea Kinga Marias, Sharifi, H. J., Jellinger, R. M., *et al.* Sulforaphane Inhibits HIV Infection of Macrophages through Nrf2. *PLoS pathogens* **12**(4), e1005581 (2016).

[420] Kosmider, B., Messier, E. M., Janssen, W. J., *et al.* Nrf2 protects human alveolar epithelial cells against injury induced by influenza A virus. *Respiratory research* **13**, 43 (2012). (↑ p. 110)

[421] Burdette, D., Olivarez, M., & Waris, G. Activation of transcription factor Nrf2 by hepatitis C virus induces the cell-survival pathway. *The Journal of general virology* **91**(Pt 3), 681–690 (2010). (↑ p. 110)

[422] Schaedler, S., Krause, J., Himmelsbach, K., *et al.* Hepatitis B virus induces expression of antioxidant response element-regulated genes by activation of Nrf2. *The Journal of biological chemistry* **285**(52), 41074–41086 (2010).

[423] Lee, J., Koh, K., Kim, Y.-E., Ahn, J.-H., & Kim, S. Upregulation of Nrf2 expression by human cytomegalovirus infection protects host cells from oxidative stress. *The Journal of general virology* **94**(Pt 7), 1658–1668 (2013). (↑ p. 110)

[424] Gjyshi, O., Bottero, V., Veettil, M. V., *et al.* Kaposi's sarcoma-associated herpesvirus induces Nrf2 during de novo infection of endothelial cells to create a microenvironment conducive to infection. *PLoS pathogens* **10**(10), e1004460 (2014). (↑ p. 110)

[425] Werner, O., Starick, E., & Grund, C. H. Isolation and characterization of a low-pathogenicity H7N7 influenza virus from a turkey in a small mixed free-range poultry flock in Germany. *Avian diseases* **47**(3 Suppl), 1104–1106 (2003). (↑ p. 111)

[426] Sun, J., Ren, X., & Simpkins, J. W. Sequential Upregulation of Superoxide Dismutase 2 and Heme Oxygenase 1 by tert-Butylhydroquinone Protects Mitochondria during Oxidative Stress. *Molecular pharmacology* **88**(3), 437–449 (2015). (↑ p. 111)

[427] Frumence, E., Roche, M., Krejbich-Trotot, P., *et al.* The South Pacific epidemic strain of Zika virus replicates efficiently in human epithelial A549 cells leading to IFN-beta production and apoptosis induction. *Virology* **493**, 217–226 (2016). (↑ p. 111)

[428] Lang, P. A., Xu, H. C., Grusdat, M., *et al.* Reactive oxygen species delay control of lymphocytic choriomeningitis virus. *Cell death and differentiation* **20**(4), 649–658 (2013). (↑ p. 111)

[429] Bhattacharya, A., Hegazy, A. N., Deigendesch, N., *et al.* Superoxide Dismutase 1 Protects Hepatocytes from Type I Interferon-Driven Oxidative Damage. *Immunity* **43**(5), 974–986 (2015). (↑ p. 111)

[430] Young, B., Purcell, C., Kuang, Y.-Q., Charette, N., & Dupre, D. J. Superoxide Dismutase 1 Regulation of CXCR4-Mediated Signaling in Prostate Cancer Cells is Dependent on Cellular Oxidative State. *Cellular physiology and biochemistry : international journal of experimental cellular physiology, biochemistry, and pharmacology* **37**(6), 2071–2084 (2015). (↑ p. 111)

[431] Lin, H.-Y., Lai, R.-H., Lin, S.-T., *et al.* Suppressor of cytokine signaling 6 (SOCS6) promotes mitochondrial fission via regulating DRP1 translocation. *Cell death and differentiation* **20**(1), 139–153 (2013). (↑ p. 111)

[432] Xu, W., Jing, L., Wang, Q., *et al.* Bax-PGAM5L-Drp1 complex is required for intrinsic apoptosis execution. *Oncotarget* **6**(30), 30017–30034 (2015). (↑ p. 111)

[433] Remijsen, Q., Goossens, V., Grootjans, S., *et al.* Depletion of RIPK3 or MLKL blocks TNF-driven necroptosis and switches towards a delayed RIPK1 kinase-dependent apoptosis. *Cell death & disease* **5**, e1004 (2014). (↑ p. 111)

[434] He, S., Wang, L., Miao, L., *et al.* Receptor interacting protein kinase-3 determines cellular necrotic response to TNF-alpha. *Cell* **137**(6), 1100–1111 (2009). (↑ p. 112)

[435] Delettre, C., Yuste, V. J., Moubarak, R. S., *et al.* Identification and characterization of AIFsh2, a mitochondrial apoptosis-inducing factor (AIF) isoform with NADH oxidase activity. *The Journal of biological chemistry* **281**(27), 18507–18518 (2006). (↑ p. 112)

[436] Radi, E., Formichi, P., Battisti, C., & Federico, A. Apoptosis and oxidative stress in neurodegenerative diseases. *Journal of Alzheimer's disease : JAD* **42 Suppl 3**, S125–52 (2014). (↑ p. 112)

[437] Lu, W., Karuppagounder, S. S., Springer, D. A., *et al.* Genetic deficiency of the mitochondrial protein PGAM5 causes a Parkinson's-like movement disorder. *Nature communications* **5**, 4930 (2014). (↑ p. 112)

[438] Vahsen, N., Cande, C., Briere, J.-J., *et al.* AIF deficiency compromises oxidative phosphorylation. *The EMBO journal* **23**(23), 4679–4689 (2004). (↑ p. 112)

[439] Johnson, J. A., Johnson, D. A., Kraft, A. D., *et al.* The Nrf2-ARE pathway: an indicator and modulator of oxidative stress in neurodegeneration. *Annals of the New York Academy of Sciences* **1147**, 61–69 (2008). (↑ p. 112)

[440] de Vries, Helga E, Witte, M., Hondius, D., *et al.* Nrf2-induced antioxidant protection: a promising target to counteract ROS-mediated damage in neurodegenerative disease? *Free radical biology & medicine* **45**(10), 1375–1383 (2008). (↑ p. 112)

Acknowledgements

When applying to Dr. Andreas Pichlmair's new lab, I didn't think about starting a PhD, but suddenly I did. I thank you very much, Andreas, for giving me the unexpected opportunity to work in your lab and broaden my knowledge in natural science and leadership. My special thanks goes to Prof. Matthias Mann for taking the responsibility as my official doctoral advisor, for all the support during TAC meetings and for running a great department including the Christmas parties, barbeques and Happy Hours.

Thanks to the members of my defense committee: Prof. Matthias Mann, Prof. Karl-Peter Hopfner, Prof. Klaus Förstemann, Prof. Karl-Klaus Conzelmann, PD Dr. Dietmar Martin, Prof. Barbara Conradt.

I also would thank the group of Prof. Matthias Mann for the great atmosphere, especially Eva Keilhauer, Martin Steger, Daniel Hornburg and Steven Dewitz for support, great conversations and organization of Careers for PhD, it was a great time for me.

Thank you Igor, Korbi Philipp G. as well as Philipp H. for explaining the mass spectrometry with such a patients. Thank you Marco for the great LaTeX script and support! Thank you Alexey for helping me a lot modifying the LaTeX script and debugging my system!

Many thanks go to all members within my years of the Innate Immunity Lab (Angelika, Anna, Bea, Darya, Hannah, Livia, Matthias H., Philipp H., Alexey and Arno) for fruitful discussions, helpful hands in the lab, an open ear for all issues and for proof-reading of this thesis. Thank you for the really cool retreats, the nice bike tour and eating all the cakes. Thank you for getting to know you!

Thank you Darya for the nice time and conversation in the lab and outside the lab and for the wonderful walks together with you and Dominik.

Additionally, I want to thank Silvana Kaphengst from the MPI for taking care of the Pgam5 mice in the mouse house. And thanks to Prof. Dr. Peter Staeheli for performing the mouse experiments in Freiburg. Thanks to Fee and Kiri, who passed away, but rescued me from mouse work.

Thank you Linda, Marlen and Franzi for the great time during our studies, for listening to issues during our training and PhD, thank you for being there.

My deepest thanks go to my family, especially to the three persons for being essential part of my life: my parents and my boyfriend Helge. Danke Mama und Papa für eure Unterstützung in jeglicher Hinsicht. DafÃ¼r dass ihr stets an mich geglaubt habt, auch wenn ihr zwischenzeitlich nicht damit gerechnet habt, dass ich doch einen Master mache und jetzt dann doch tatsächlich meine Doktorarbeit korrigieren konntet. Danke, dass ihr mir nahezu alle Möglichkeiten gegeben habt um mein Leben zu genießen und etwas ganz Tolles daraus zu machen.

Vielen Dank Helge, dass du immer da bist, dir meine Hochs und Tiefs anhörst, mich wieder aufbaust und auch auf den Boden der Tatsachen zurück holst. Und danke, dass du wenigstens versuchst zu verstehen, was in so kleinen Zellen passiert und wieso die manchmal sterben.